

**LONG-TERM MEASUREMENTS OF SPATIALLY-
AVERAGED SENSIBLE HEAT FLUX FOR A MIXED
GRASSLAND COMMUNITY, USING SURFACE LAYER
SCINTILLOMETRY**

by

GEORGE O. ODHIAMBO

B. Env. Sc. (Hons), Kenyatta University

M. Sc. (Nuclear Science), University of Nairobi


**Thesis submitted in fulfilment of the requirement for
the award of degree of
PhD**

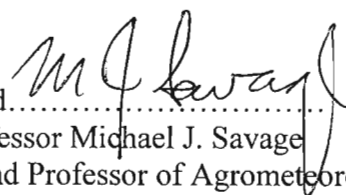
**in Agrometeorology,
SPAC Research Unit
School of Environmental Sciences
Faculty of Science and Agriculture
University of KwaZulu-Natal
Pietermaritzburg Campus
South Africa**

July 2007

DECLARATION

I hereby declare that the research work reported in this thesis is the result of my own original investigations except where acknowledged.

 2/7/2007
Signed.....
George Odhiambo


Signed.....
Professor Michael J. Savage
Supervisor and Professor of Agrometeorology

ACKNOWLEDGEMENTS

I would like to acknowledge the encouragement, support, suggestions and criticisms of all individuals who directly and indirectly contributed to the completion of this thesis.

My first sincere gratitude is to my supervisor Prof. Michael J. Savage for accepting me as his student thereby giving me an opportunity to participate in the Water Research Commission (WRC) project on the application of scintillometer technique in evaporation estimations. His support, guidance, valuable suggestions and concern for my welfare were of immense importance to this research. I would also like to sincerely thank Dr. C. S. Everson of the Council for Scientific and Industrial Research (CSIR) for his assistance in the early stages of this project.

Special thanks to all the staff members of the Agrometeorology discipline, University of KwaZulu-Natal (UKZN), and more specifically to Jothimala Manickum and Peter Dovey for having facilitated the necessary activities related to administrative and field operations, respectively, which made my program run smoothly without any hitches.

I am also grateful to Agrometeorology, UKZN for the financial support to enable me pursue my PhD research studies. Your gracious financial support that enabled me to stay in Pietermaritzburg and complete my studies can never be forgotten. I am equally grateful to the WRC and UKZN for funding the research project on which this thesis is based. My gratitude also goes to the owner and workers of the Bellevue farm where this study was carried out. This research was made possible due to their cooperation.

Last but not least, I would like to extend my special thanks to my colleagues, Michael Mengistu and Michael Abraha for their discussions and suggestions on various issues of the research studies, all my friends and Kenyan colleagues in Pietermaritzburg for their moral support when needed most. Your company, friendship, support and encouragement in times of need was invaluable in my stay, study and research at UKZN. To Jesus be all the glory and honour!

ABSTRACT

Evapotranspiration by vegetation cover is an important component of the water budget and energy balance in any ecosystem. A key to more improved water management therefore lies in improving our understanding of evapotranspiration, the process that drives water use by plants.

Estimations of the turbulent fluxes are required for various applications in micrometeorology, hydrology, environmental studies and agriculture. Numerous methods for estimation of turbulent fluxes have been developed and tested. Direct measurements of fluxes are usually achieved by the eddy covariance (EC) method, which is considered as the most reliable. However, the application of the EC method is often problematic. The necessary sensors for wind, temperature and humidity must respond very fast (resolution of 10 Hz or better) and at the same time must not show noticeable drift. This makes them delicate, expensive and difficult to calibrate among other problems associated with the method.

Due to their ability to integrate atmospheric processes along a path length that may range between a few hundred metres to a few kilometres, optical methods based on the analysis of scintillation appear to be an alternative and possible supplement to classical micrometeorological methods such as the EC method, which may provide local fluxes typically at the scale of 100 m. The use of the scintillometry technique in surface flux measurements is therefore gaining in popularity.

The accuracy of the measurements obtained by one method is judged by comparison of the measurements obtained by those of another method considered as the standard. For turbulent flux measurements, the EC method is taken as the standard method for the determination of sensible heat fluxes.

This research presents the measurement of sensible heat fluxes using the surface layer scintillometer (SLS). The SLS system used has a dual-beam and a recommended path length of between 50 and 250 m. The method was tested against the EC method for different Bowen ratio (β) values, as required by the theory, under different atmospheric stability conditions, as well as for different wind directions relative to the SLS beam path and slanting beam path orientation. Also presented is an analysis of the different forms of the Monin-Obukhov Similarity (MOST) functions used in micrometeorology and suggested by various authors, done by comparing the

resulting sensible heat flux measured by the SLS method with the ones calculated through an iterative determination of the Monin-Obukhov parameters.

A comparison of the structure function parameter of temperature (C_T^2) corrected for β and those measured (using SLS) was carried out, with the results showing very good correspondence between the corrected and uncorrected C_T^2 values, indicating that not correcting for β for SLS measured C_T^2 does not result in significant error in the resulting C_T^2 values, and hence sensible heat flux estimates. A comparison of the sensible heat flux F_h obtained using EC and SLS methods for $\beta < 0.6$ and $\beta > 0.6$ followed and the results also show good correspondence between the values obtained using the EC and SLS methods, although the agreement is slightly improved for cases when $\beta > 0.6$. A sensitivity analysis indicates that both the EC- and SLS-measurements of F_h are influenced by β values. A sensitivity analysis on the influence of β on F_h measurements by both the EC and SLS methods further indicates that the influence of β on F_h measurements is not large enough to warrant correcting F_h measurements for β . The F_h measurements by the EC method appears to be influenced more by β especially for β values less than 0.74. A comparison of the various methods for computing the empirical similarity functions used by MOST was also carried out and the results show a significant difference in the F_h computed following the various methods suggested by different researchers.

As for the agreement between the EC and SLS methods determination of F_h for the different atmospheric stability conditions, there seems to be a better agreement in the F_h measurements as noted by correlation coefficients closer to 1 and greater t -values obtained during unstable atmospheric conditions in the colder months of June and August while reduced agreement in the values is recorded in the warmer summer period from November to December. Also noted is a slight difference in the EC measurements compared to the SLS measurement of F_h . The difference in the measurements is noticed for unstable atmospheric conditions. Also noted is that EC and SLS measurements of F_h differ slightly when the atmospheric condition is near-neutral. However the agreement between the F_h values measured by the two measurement methods is still good.

To test the scintillometry method for non-ideal (heterogeneous) surfaces, the SLS was set up in an inclined position, with the receiver set at 0.68 m above the ground level and transmitter at 1.68 m, resulting in an effective height difference of 1.00 m. There was generally good agreement in the 2-min measurements of F_h by the two methods for the SLS set up in inclined position, with the 30-min data resulting in even better agreements. The findings confirm that the SLS set up does not impair its performance in measuring sensible heat fluxes. This also shows that the SLS would also work well in non-ideal (heterogeneous) conditions which the inclined optical beam path mimics. For those days when wind direction was mainly approximately perpendicular to the beam, the F_h values obtained by SLS and EC methods are more in agreement than when the wind direction was either irregular or parallel to the SLS beam path. Wind speed also seems to influence the F_h estimates by the two methods since the agreement in the F_h values obtained by the two methods is greater when wind speed is higher compared to times of the day when the wind speed is reduced.

The atmospheric stability influences the peak position of footprint with the peak footprint position being further from the measurement point when the atmospheric stability condition is closer to stable as denoted by the Obukhov length of -5 and closer to the measurement point for convectively unstable atmospheric conditions as shown by the Obukhov length of -30. Also shown is that a larger fetch is required when the atmosphere is convectively unstable as indicated by the contours plotted on top of the footprint plots.

In general, there seems to be very good agreement in the sensible heat flux values obtained by the two methods, especially since SLS offers areal-averaged sensible heat flux measurements compared to the EC method which basically provides a point measurement. The SLS method therefore offers a better alternative for obtaining sensible heat flux from larger and heterogeneous area - although to a limit of 250 m since beyond 250 m, the method suffers from a saturation problem.

TABLE OF CONTENTS

Chapter 1: Introduction	1
1.1 Introduction	1
1.2 Motivation	13
1.3 Aims and objectives of the study	17
1.4 Thesis structure	18
Chapter 2: Theoretical background	20
2.1 Scintillometer method	20
2.1.1 Structure constant of the refractive index	25
2.1.2 Turbulence spectrum	25
2.1.3 Variance of the logarithmic signal intensity fluctuations	28
2.1.4 Inner scale length, l_o , and SLS measurements of sensible heat flux	29
2.1.5 Monin-Obukhov Similarity Theory (MOST)	30
2.1.6 Estimation of sensible heat and momentum flux	33
2.2 Footprint of measurements	36
2.3 Bowen ratio energy balance method	38
2.3.1 Radiation balance and available energy	40
2.3.2 Soil heat flux	40
2.3.4 Sensible heat and latent energy fluxes	41
2.4 Eddy covariance method	42
2.5 Brief overview of subsequent chapters	44
Chapter 3: Surface layer scintillometer and eddy covariance sensible heat flux comparisons for a mixed grassland community as affected by Bowen ratio and MOST formulations	46
3.1 Introduction	46
3.2 Theoretical background	48
3.2.1 Eddy covariance	48
3.2.2 Bowen ratio energy balance (BREB) method	49
3.2.3 Scintillometer method	49
3.2.4 Derivation of sensible heat flux using different forms of the similarity functions f_T and f_e	51
3.3 Materials and methods	53
3.3.1 Measurements	53
3.3.2 Data collection and analysis	55
3.4 Results and discussion	56
3.4.1 Comparison of C_T^2 measured by SLS and C_T^2 corrected for β	56
3.4.2 Comparison of SLS- and EC-measured sensible heat flux	59
3.4.3 Analysis of sensible heat flux using different forms of the MOST similarity function f_T	68
3.5 Conclusions	74
Chapter 4: Comparison of sensible heat flux by surface layer scintillometer and eddy covariance methods for different atmospheric stability conditions	77
4.1 Introduction	77

4.2 Theory.....	79
4.2.1 Scintillometry	79
4.2.2 Eddy covariance	80
4.2.3 Atmospheric stability and Obukhov length.....	81
4.3 Experimental details	82
4.4 Results and discussion	83
4.5 Conclusions	106
Chapter 5: Influence of wind direction and a slanting beam angle on surface layer scintillometer estimates of sensible heat flux.....	108
5.1 Introduction	108
5.2 Theoretical background	110
5.2.1 Scintillometry	110
5.2.2 Footprint analysis	121
5.3 Experimental.....	114
5.3.1 Study area	114
5.3.2 Wind vector calculations, and analysis.....	116
5.4 Results and discussion	117
5.4.1 Comparison of sensible heat flux using the SLS at a slanting beam angle with EC measurements	117
5.4.2 Comparison of SLS- and EC-measured sensible heat fluxes for different wind directions	112
5.4.3 Footprint analysis	130
5.5 Conclusions	135
Chapter 6: General conclusions and recommendations for further research	137
6.1 Conclusions	137
6.2 Recommendations for future research.....	140
References.....	141

LIST OF TABLES

Table 1.1 Summary of meteorological parameters estimated or required by the various measurement methods	6
Table 1.2 The meteorological parameters determined using different methods.	12
Table 1.3 Studies done using surface layer scintillometer (SLS).....	14
Table 3.1 Statistical analyses results of 2-min F_h obtained using EC and SLS methods for different β values.	61
Table 4.1 Stability categories and stability parameter (Weiss, 2002).	82
Table 4.2 Results of correlation and t -test analysis of the sensible heat flux values obtained by SLS and EC methods for different stability conditions and different data-averaging periods. Also included in the table is the vegetation height h_{canopy}	103
Table 5.1 Summary of the statistical analyses together with canopy height for the comparison of slanting-height SLS sensible heat flux measurements with those obtained using the EC method.....	117

LIST OF PHOTOS

Photo 2.1 The surface layer scintillometer set up showing the transmitter and receiver
as indicated. 23

Photo 2.2 The SLS (a) transmitter, (b) receiver, (c) switch box and (d) signal
processing unit..... 24

LIST OF FIGURES

Fig. 1.1 Structure of the planetary boundary layer and constant flux layer (after Coyle, 2005). The zero-plane displacement height d is approximately 2/3 of the canopy height.	4
Fig. 2.1 Schematic representation of the energy spectrum of turbulence (after Poggio, 1998).	27
Fig. 2.2 The algorithm (Hill, 1997) used for the various estimates obtained using the SLS method based on weak scattering theory and measurements of the variances σ_1^2 and σ_2^2 , for beam 1 and beam 2 respectively, covariance σ_{12}^2 , inputs of beam height above the zero-plane displacement height, beam path length L_{beam} , air temperature T and atmospheric pressure P (based on Weiss (2002)) and modified by Savage et al. (2004) to reflect the role of single-detector variances σ_1^2 and σ_2^2 and that T_* and u_* are required to calculate $f_T(\zeta)$ and $f_\epsilon(\zeta)$	35
Fig. 3.1 A map showing the location of the study area. The scale is for the Pietermaritzburg district (where the study area is located).	54
Fig. 3.2 Comparison of 20-min SLS-measured C_T^2 with that corrected for β for DoY 116 to 138, (April to May) 2004, corresponding to summer season when weather condition is warm.	57
Fig. 3.3 Comparison of 20-min SLS-measured C_T^2 with that corrected for β for DoY 138 to 181 (May to June) 2004, corresponding to end of autumn and winter season.	57
Fig. 3.4 Comparison of 20-min SLS-measured C_T^2 with that corrected for β for DoY 274 to 340 (October to November) 4002, corresponding to summer season when weather condition is warm.	58
Fig. 3.5 Diurnal plot of 2-min measured C_T^2 and C_T^2 corrected for β for DoY 312 to 314 (November) 2004, corresponding to summer when weather condition is warm.	58
Fig. 3.6 Time series plot of the 20-min Bowen ratio values for DoY 274 to 276 (November) 2004, corresponding to summer season when weather condition is warm.	59
Fig. 3.7 (a) Relative error for both EC and SLS measurements (the inset graph shows the relative error values between -1.0 and -0.2) and (b) differences between the corrected (using simulated Bowen ratio values) and uncorrected (measured) sensible heat flux measured by the EC and SLS methods (DoY 279, 14h00). The actual Bowen ratio value for this period was 0.05 and sensible heat flux was 16.1 W m^{-2}	62
Fig. 3.8 Comparison between 2-min sensible heat fluxes derived from EC and SLS when (a) $\beta < 0.6$ and (b) $\beta > 0.6$, for DoY 110 to 117.	63

Fig. 3.9 Comparison between 2-min sensible heat fluxes derived from EC and SLS when (a) $\beta < 0.6$ and (b) $\beta > 0.6$, for DoY 145 to 152.....	64
Fig. 3.10 Comparison between 2-min sensible heat fluxes derived from EC and SLS when (a) $\beta < 0.6$ and (b) $\beta > 0.6$, for DoY 274 to 341.....	65
Fig. 3.11 An example of diurnal plots of 2-min sensible heat flux measured by EC and SLS for (a) DoY 127 and (b) DoY 307.	66
Fig. 3.12 Comparison of the 2-min sensible heat flux obtained using the different forms of the similarity function f_T with that for the EC method for DoY 282.	69
Fig. 3.13 Comparison of the 2-min sensible heat flux obtained using the different forms of the similarity function f_T with that for the EC method for DoY 275.	69
Fig. 3.14 Percentage differences between the 2-min F_h values obtained using the similarity functions suggested by Thiermann (1992) and (a) Wyngaard et al. (1971), and (b) de Bruin et al. (1993), for DoY 275.	71
Fig. 3.15 Percentage differences between the 2-min F_h values obtained using the similarity functions suggested by Thiermann (1992) and (a) Wyngaard et al. (1971), and (b) de Bruin et al. (1993), for DoY 282.	72
Fig. 3.16 Percentage differences of the 2-min F_h values obtained using the similarity function method suggested by Thiermann and Grassl (1992) for DoY 275 compared with F_h obtained using the EC method.	73
Fig. 4.1 SLS beam path-weighted vegetation height. Between DoY 152 to 240, the vegetation height remained low.....	85
Fig. 4.2 Two-min and 20-min averages of the vertical wind speed obtained by EC for (a) DoY 185 and (b) DoY 276.....	87
Fig. 4.3 T-test values for the (a) unstable conditions and (b) near-neutral conditions for the different months spanning different seasons.....	88
Fig. 4.4 Examples of diurnal plot of 2-min sensible heat flux as measured by EC and SLS methods for (a) DoY 275 to 277 and (b) DoY 287.....	89
Fig. 4.5 Correlation of EC and SLS 2-min sensible heat flux for (a) stability parameter $\zeta < -0.05$ (unstable) and (b) stability parameter ζ between -0.05 and 0.05 (near-neutral) for the month of May.	90
Fig. 4.6 Correlation of EC and SLS 20-min averages of sensible heat flux for (a) stability parameter $\zeta < -0.05$ (unstable) and (b) stability parameter ζ between -0.05 and 0.05 (near -neutral) for the month of May.	91

Fig. 4.7 Correlation of EC and SLS 2-min sensible heat flux for (a) stability parameter $\zeta < -0.05$ (unstable) and (b) stability parameter ζ between -0.05 and 0.05 (near-neutral) for the month of June.	92
Fig. 4.8 Correlation of EC and SLS 20-min averages of sensible heat flux for (a) stability parameter $\zeta < -0.05$ (unstable) and (b) stability parameter ζ between -0.05 and 0.05 (near-neutral) for the month of June.	93
Fig. 4.9 Correlation of EC and SLS 2-min sensible heat flux for stability parameter $\zeta < -0.05$ (unstable) for the month of July.	94
Fig. 4.10 Correlation of EC and SLS 2-min averages of sensible heat flux for (a) stability parameter $\zeta < -0.05$ (unstable) and (b) stability parameter ζ between -0.05 and 0.05 (near-neutral) for the month of August.	95
Fig. 4.11 Correlation of EC and SLS 20-min sensible heat flux for (a) stability parameter $\zeta < -0.05$ (unstable) and (b) stability parameter ζ between -0.05 and 0.05 (near-neutral) for the month of August.	96
Fig. 4.12 Correlation of EC and SLS 2-min average sensible heat flux for (a) stability parameter $\zeta < -0.05$ (unstable) and (b) stability parameter ζ between -0.05 and 0.05 (near-neutral) for the month of October.	97
Fig. 4.13 Correlation of EC and SLS 20-min sensible heat flux for (a) stability parameter $\zeta < -0.05$ (unstable) and (b) stability parameter ζ between -0.05 and 0.05 (near-neutral) for the month of October.	98
Fig. 4.14 Correlation of EC and SLS 2-min averages of sensible heat flux for (a) stability parameter $\zeta < -0.05$ (unstable) and (b) stability parameter ζ between -0.05 and 0.05 (near-neutral) for the month of November.	99
Fig. 4.15 Correlation of EC and SLS 20-min sensible heat flux for (a) stability parameter $\zeta < -0.05$ (unstable) and (b) stability parameter ζ between -0.05 and 0.05 (near-neutral) for the month of November.	100
Fig. 4.16 Correlation of EC and SLS 2-min averages of sensible heat flux for (a) stability parameter $\zeta < -0.05$ (unstable) and (b) stability parameter ζ between -0.05 and 0.05 (near-neutral) for the month of December.	101
Fig. 4.17 Correlation of EC and SLS 20-min sensible heat flux for (a) stability parameter $\zeta < -0.05$ (unstable) and (b) stability parameter ζ between -0.05 and 0.05 (near-neutral) for the month of December.	102
Fig. 4.18 (a) Comparison of 2-min EC- and SLS-measured sensible heat flux and (b) diurnal plot of the EC- and SLS-measured sensible heat flux for DoY 110. Also plotted is the diurnal variation of I_o (right-hand y-axis).	105

Fig. 5.1 Schematic of the mixed community grassland research site at Ashburton showing the positioning of the instrumentation used in the study. The SLS beam path distance (from the transmitter to receiver) and wind direction are also indicated. The diagram is not to scale.	115
Fig. 5.2 Scintillometer set up in an inclined beam path with the receiver set at 0.68 m and transmitter at 1.68 m above the ground level. The diagram is not to scale.	116
Fig. 5.3 Comparison of 2-min sensible heat flux measured by EC and SLS methods for DoY 230 to 241, with the SLS beam set at a slanting angle where the transmitter was set at a height of 1.68 m above the ground level and the receiver at a height of 0.68 m. The effective beam height was 1.18 m with the EC method at a height of 2 m.	118
Fig. 5.4 Comparison of 30-min sensible heat flux obtained by EC and SLS methods for DoY 230 to 241, with the SLS beam set at a slanting angle.	119
Fig. 5.5 Diurnal plot of 2-min EC- and SLS- measured sensible heat flux for DoY 234 and 235 for when the SLS beam was set at slanting angle.	120
Fig. 5.6 Comparison of 2-min sensible heat flux measured by EC and SLS methods for DoY 241 to 251, with the SLS beam set at a slanting angle.	120
Fig. 5.7 Comparison of 30-min average sensible heat flux measured by EC and SLS methods for DoY 241 to 251, with the SLS beam set at a slanting angle.	121
Fig. 5.8 Wind vector variation between 06h00 to 18h00 for DoY 275. The arrows point to the wind direction and wind speed is indicated by the length of the arrows. On this particular day wind direction was nearly perpendicular to the SLS beam.	122
Fig. 5.9 Wind vector variation between 06h00 to 18h00 for DoY 287 for which the wind direction was random in the morning hours of the day and nearly perpendicular to the SLS beam path in the afternoon.	122
Fig. 5.10 Wind direction between 06h00 to 18h00 for DoY 131 for which wind direction was nearly perpendicular to the SLS beam path but wind speed low.	123
Fig. 5.11 Wind vector variation between 06h00 to 18h00 for DoY 107 for which the wind direction is random.	123
Fig. 5.12 Comparison of 2-min sensible heat flux measured by EC and SLS methods for DoY 275 for which wind direction is nearly perpendicular to the SLS beam path.	125
Fig. 5.13 Diurnal plot of 2-min SLS- and EC-measured sensible heat fluxes for DoY 275 for which wind direction is nearly perpendicular to the SLS beam path.	125
Fig. 5.14 (a) Diurnal variation of 2-min sensible heat flux measured by EC and SLS methods for DoY 287, (b) SLS sensible heat flux for the different prevailing wind directions - when the wind direction was approximately perpendicular to the SLS beam path or when the wind direction is random, also for DoY 287.	127

Fig. 5.15 Comparison of 2-min sensible heat flux measured by EC and SLS methods for DoY 287 for which the wind direction is random in the morning hours of the day and nearly perpendicular to the SLS beam path in the afternoon.....	127
Fig. 5.16 Diurnal plot of 2-min SLS- and EC-measured sensible heat fluxes for DoY 131 for which wind direction was nearly perpendicular to the SLS beam path but the wind speed low.	127
Fig. 5.17 Comparison of 2-min sensible heat flux measured by EC and SLS methods for DoY 131 for which wind direction was nearly perpendicular to the SLS beam path but the wind speed low.	129
Fig. 5.18 Comparison of 2-min sensible heat flux measured by EC and SLS methods for DoY 107 for random wind directions.	129
Fig. 5.19 Diurnal plot of 2-min SLS- and EC-measured sensible heat flux for DoY 107 for random wind directions.....	130
Fig. 5.20 Footprint calculations for the SLS method for (a) Obukhov length (L) of -30 and (b) Obukhov length of -5. Also shown are the contours of the fetch at the top of the footprint plots.	132
Fig. 5.21 Daytime footprint peak location estimated by the calculations for EC and SLS mid-point position for DoY 131, 11h00.	133
Fig. 5.22 Daytime footprint peak location estimated by the calculations for EC and SLS mid-point beam position for DoY 107, 12h00.....	134
Fig. 5.23 Daytime footprint peak location estimated by the calculations for EC and SLS mid-point beam position for DoY 275, 12h00.....	134

LIST OF ABBREVIATIONS AND SYMBOLS

Abbreviations

ABL	Atmospheric boundary layer
BREB	Bowen ratio energy balance
DoY	Day of year
EC	Eddy covariance
LAS	Large aperture scintillometer
MOST	Monin-Obukhov Similarity Theory
SANCLAH	South African National Chapter of the International Association for Hydrological Sciences
SLS	Surface layer scintillometer
SR	Surface renewal
TKE	Turbulent kinetic energy
XLAS	Extra large aperture scintillometer

Symbols

C_n^2	structure parameter of refractive index	$\text{m}^{-2/3}$
C_T^2	structure parameter of temperature	$\text{K}^2 \text{m}^{-2/3}$
c_p	specific heat capacity of air	$\text{J kg}^{-1} \text{K}^{-1}$
c_{soil}	specific heat capacity of soil	$\text{J kg}^{-1} \text{K}^{-1}$
c_{dsoil}	specific heat capacity of dry soil	$\text{J kg}^{-1} \text{K}^{-1}$
c_w	specific heat capacity of water ($= 4190 \text{ J kg}^{-1} \text{K}^{-1}$)	$\text{J kg}^{-1} \text{K}^{-1}$
d	zero-plane displacement height	m
d_{SLS}	SLS beam displacement distance	mm
D_{SLS}	SLS detector diameter	mm
dt	measurement time interval	s
dT_{soil}	temporal change in soil temperature	$^{\circ}\text{C}$
e	water vapour pressure	Pa
f	footprint at distance x	
f_{ε}	similarity function	
f_{ϕ}	a function that describes the decay of refractive index fluctuations in the dissipation range of turbulence	
f_T	similarity function	
F	Fresnel zone	m
$F(x, z_m - d)$	scalar flux at distance x from the source and a measurement height z_m for a surface with a zero-plane displacement d	W m^{-1}
F_c	carbon dioxide flux	$\text{kg s}^{-1} \text{m}^{-2}$
F_h	sensible heat flux	W m^{-2}
F_{stored}	average soil-stored heat flux density	W m^{-2}
F_s	soil heat flux	W m^{-2}
F_w	water vapour flux	$\text{kg s}^{-1} \text{m}^{-2}$

g	acceleration due to gravity	m s^{-2}
h	height above ground level	m
h_{canopy}	canopy height	m
I	incident radiation at the receiver	
I_{net}	net irradiance	W m^{-2}
I_s	incident shortwave irradiance	W m^{-2}
J_o and J_1	Bessel function of the first kind and order	
k'	Von Karman's constant ($=0.4$)	m^{-1}
k	turbulent wave number	m^{-1}
K	the optical wave number ($2\pi / \lambda$)	m^{-1}
l_o	inner scale length which describes the smallest diameter of occurring eddies	mm
L	Obukhov length	m
L_{beam}	beam distance from transmitter to receiver	m
L_d	downward infrared irradiance	W m^{-2}
L_o	outer scale length of turbulence	mm
L_u	upward infrared irradiance emitted by the surface	W m^{-2}
L_v	latent energy of vaporisation ($L_v \approx 2.43 \text{ MJ kg}^{-1}$)	MJ kg^{-1}
$L_v F_w$	latent heat flux	W m^{-2}
n	refractive index of air	
P	atmospheric pressure	Pa
Pr	Prandtl number ($= 0.72$)	
r, r_1, r_2 and r_{12}	the distance at a particular position along the beam measured from the transmitter	m
$r \cdot I_s$	shortwave irradiance reflected from the surface	W m^{-2}
$S(x)$	source strength per unit area	W m^{-2}
T	air temperature	$^{\circ}\text{C}$
T_*	temperature scale of turbulence	K
T'	air temperature fluctuation	$^{\circ}\text{C}$
\bar{T}	mean air temperature	K or $^{\circ}\text{C}$
u	horizontal component of wind speed in the x direction	m s^{-1}
\bar{u}	mean horizontal wind speed	m s^{-1}
u_*	friction velocity	m s^{-1}
U	horizontal wind speed	m s^{-1}
v	lateral component of wind speed in the y direction	m s^{-1}
w	vertical component of wind speed in the z direction	m s^{-1}
w'	vertical wind speed fluctuation	m s^{-1}
$W(\mu)$	spatial weighting fraction of radiation	
x, x_1 and x_2	positions along the SLS beam path	
x_{max}	peak location of the footprint for sensible heat flux	m
z	measurement height	m
z_m	measurement height	m
z_0	roughness length	m

$\Delta e / \Delta z$	water vapour pressure gradient	Pa m^{-1}
$\Delta T / \Delta z$	vertical air temperature gradient	K m^{-1}
Δt	time difference	s
Δz	depth increment	m
β	Bowen ratio. The ratio of the sensible heat flux to the latent energy flux	
β_1	Obukhov-Corrsin constant (= 0.86)	
∂	partial derivative	
ε	dissipation rate of turbulent kinetic energy	$\text{m}^2 \text{s}^{-3}$
η	Taylor microscale	
σ_{\ln}^2	variance of the logarithm of the fluctuations of a spherical wave front originating from a point source	
σ_{12}^2	covariance of the logarithm of the amplitude of the received SLS beam radiation	
σ_1^2	variance of the logarithm of the amplitude of the SLS beam 1 signal	
σ_2^2	variance of the logarithm of the amplitude of the SLS beam 2 signal	
Φ_h	stability function for sensible heat exchange	
Φ_m	stability function for momentum exchange	
Φ_n	refractive index spectrum which quantifies the optical turbulence in the surface layer	
$\Phi_n(k)$	spectral energy density	kJ nm^{-1}
ρ_{soil}	bulk density of dry soil	kg m^{-3}
θ	gravimetric soil water content	kg kg^{-1}
θ	horizontal wind speed	m s^{-1}
τ	momentum flux	$\text{m}^2 \text{s}^{-2}$
λ	radiation wavelength	m
μ	Kolmogorov microscale	
ν	kinematic viscosity of air	$\text{m}^2 \text{s}^{-1}$
ζ	stability parameter proposed by Monin and Obukhov	
ξ	quantum yield	J kg^{-1}
γ	refractive index coefficient for air ($= 7.89 \times 10^{-7} \text{ K Pa}^{-1}$)	k Pa^{-1}
γ	psychrometric constant (approximately 66 Pa K^{-1})	Pa K^{-1}
ψ_m	integrated stability correction for the adiabatic wind profile	

Chapter 1: Introduction

1.1 Introduction

A key to more improved water management lies in improving our understanding of evapotranspiration, the process that drives water use by plants. Increasing population pressure is placing an unsustainable demand on the world's freshwater resources (Radiff, 1999). In South Africa, as in other water scarce countries, shortage of water resources is a major concern and the need to effectively manage the existing water resources is of paramount importance. As water shortages intensify, the need to improve estimates of evapotranspiration therefore becomes essential for successful water allocations and monitoring.

The land surface is coupled with the atmosphere through the exchange of mass and energy. Understanding the dynamics of vegetation-atmosphere interactions is essential. Micrometeorological research is mainly concerned with the study of the exchange processes and the dynamics of the interactions at the land surface - atmosphere interface (Rosenberg et al., 1983).

The air layer near the ground that is affected by diurnal heat, material or momentum transfer to or from the ground surface is referred to as the atmospheric boundary layer (ABL) (Arya, 2001). The boundary layer is therefore the lowest part of the atmosphere which interacts with, and is directly affected by the heating and cooling of the earth's surface. The thickness of the boundary layer is variable in time and space and ranges from hundreds of meters to a few kilometres (Rosenberg et al., 1983; Arya, 2001). In general the depth of the boundary layer increases during the day, when the ground is heated by the sun, and the depth decreases at night. The boundary layer is important in micrometeorology for two main reasons (Arya, 2001): (i) it is the region in which the energy that drives atmospheric processes originate, as heating from the surface which is warmed by the sun's short wave radiation, and (ii) it is the region in which we live, produce our food and release the bulk of the atmospheric pollution.

The nature of the boundary layer is somewhat different from the 'free' atmosphere, in that its dynamics are dominated by the occurrence of turbulence (Kaimal and Finnigan, 1994; Arya, 2001). The main characteristics of the boundary layer are diurnal variations of its atmospheric parameters such as air temperature and atmospheric water content. Such variations are mainly caused by the underlying surface, which warms and cools in response to solar radiation, which in

turn forces changes in the boundary layer via transport processes. Radiative cooling and heating of the surface is stronger than at higher levels in the atmosphere - the principle sources and sinks of heat are at the surface. Stronger solar heating leads to turbulent convection, and mixing in the boundary layer, whereas strong cooling at night tends to stabilise the boundary layer (Kaimal and Finnigan, 1994).

The nature of the boundary layer is determined by the presence of turbulence involving random motions of air manifested by gustiness (Arya, 2001). These random motions are accompanied by fluctuations in air temperature and humidity for similar timescales. The importance of turbulence is that it acts to cause rapid diffusion, or mixing, of heat, water vapour, chemicals, or momentum (of air). The fact that turbulence also influences wind velocity means that it transfers the friction of the air flowing over the ground into the upper air (Arya, 2001).

The turbulence kinetic energy (TKE) is the mean kinetic energy per unit mass associated with eddies in turbulent flow (Baldocchi, 2005). It is a concept used to assess what contribution to buoyancy is brought about by turbulence. The TKE which characterises the turbulence intensity is a common variable analyzed in studies dealing with roughness change. The production of TKE equals the sum of mechanical/shear/frictional turbulence plus the buoyancy, and must match with the heat dissipated to maintain the energy conservation laws. Balancing the two, we get an equation and thus can make a budget about the TKE. The TKE plays a vital role in determining the atmospheric dynamics and coupling. The TKE depends on TKE dissipation rate or eddy dissipation rate (ε). The parameter ε gives the turbulence in the velocity field and it is one of the fundamental parameters used to determine the turbulence characteristics (Baldocchi, 2005). It represents the rate of energy cascading to smaller eddies until the energy is converted into heat due to the presence of viscous forces.

Under conditions of low wind, radiative transfer at the surface of the earth dominates the production or suppression of turbulence (Kaimal and Finnigan, 1994). The heating of the lower atmosphere depends on the heating of the surface, and the transfer of heat from the surface to the atmosphere. These processes can be quantified by considering the surface energy balance. The surface energy balance is determined by the different flux (flow) of energy at the surface. The system is forced by the radiative balance between net shortwave irradiance and net infrared irradiance. For a flat extensive surface, net irradiance I_{net} is the sum of the net shortwave and net infrared irradiance (Savage et al., 1997):

$$I_{net} = I_s - r \cdot I_s + L_d - L_u \quad 1.1$$

where I_s is the incident shortwave irradiance, $r \cdot I_s$ the shortwave irradiance reflected from the surface, L_d the downward infrared irradiance and L_u the upward infrared irradiance emitted by the surface. The response in terms of energy flux from the surface to the atmosphere has two main components: sensible heat flux F_h and latent energy flux $L_v F_w$ (Arya, 2001). There is also a significant heat flux through exchange with layers below the surface, known as the soil heat flux, F_s . The term energy flux refers to energy flux density, which represents the amount of energy that flows through a horizontal surface per unit time per unit horizontal area with unit $\text{J s}^{-1} \text{m}^{-2}$ (or W m^{-2}).

Energy flux available at the earth's surface is either sensible heat flux F_h , which results in an air temperature change with no phase change of water, or latent energy flux, which results in a phase change of water usually from liquid to vapour with little temperature change (Savage et al., 1997). A major source of energy that drives many processes in the atmospheric boundary layer is solar energy. For an idealised atmospheric boundary layer, which is in equilibrium, the shortened form of the energy balance at the surface is given by the (vertical) one-dimensional energy balance equation (Thom, 1975):

$$I_{net} = L_v F_w + F_h + F_s + \xi F_c \quad 1.2$$

where I_{net} is the net irradiance, ξF_c is the photosynthetic flux, where ξ is the quantum yield (J kg^{-1}) and F_c is the flux of carbon dioxide in $\text{kg s}^{-1} \text{m}^{-2}$. Usually, for the shortened form of the energy balance, ξF_c is assumed to be negligible. Furthermore, advection and heat stored in the canopy is neglected. Advection may include latent and sensible heat forms.

Fluxes vary gradually when the boundary layer extends over homogeneous terrain, being largest at the surface and approximately showing a linear decrease in magnitude towards the top (Wyngaard and Cote, 1971). Many measurement methods are used for obtaining F_h . In this current study, the focus is on the measurement of this sensible heat flux, F_h . From net irradiance, soil heat flux and sensible heat flux measurements, latent energy flux can be estimated as a residual term using the shortened form of the energy balance equation (Eq. 1.2). The lowermost part of the planetary boundary layer is referred to as the constant flux layer, designating its direct contact with the earth's surface (Fig. 1.1).

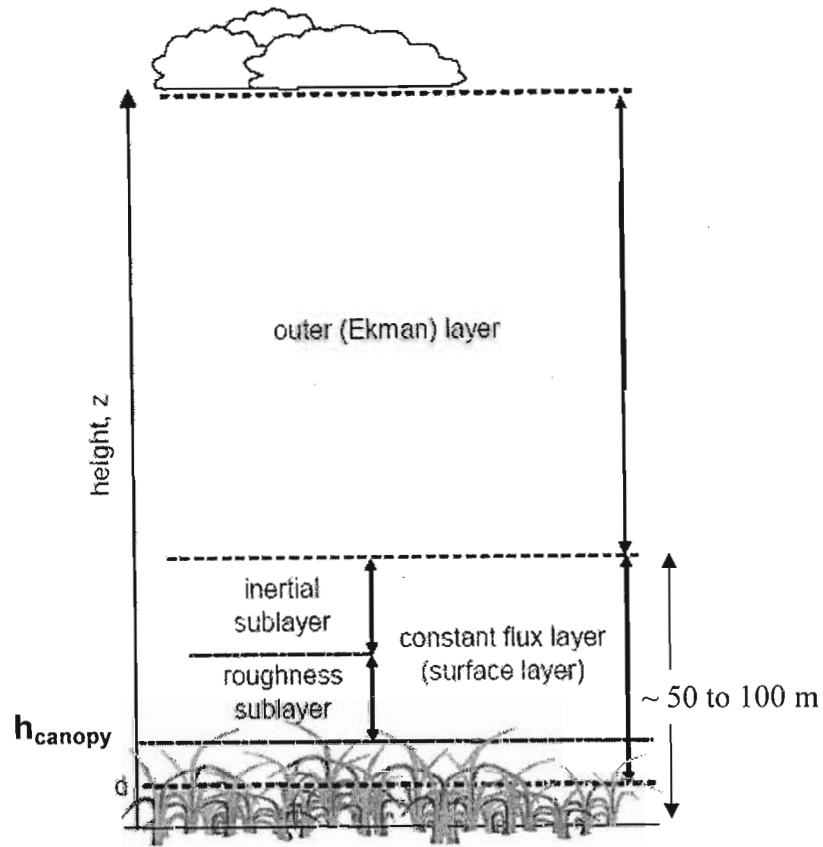


Fig. 1.1 Structure of the planetary boundary layer and constant flux layer (after Coyle, 2005). The zero-plane displacement height d is approximately $2/3$ of the canopy height.

Typically, the surface layer makes up the lowermost 10 % of the planetary boundary layer, which is also the region most accessible for surface flux measurements and the variation of fluxes with height is negligible (Arya, 2001). For this reason this layer is also referred to as the constant flux layer (Fig. 1.1). Flux measured at a certain elevation in the surface layer can be considered as being representative of energy exchanges occurring between the earth's surface and the atmosphere. Most turbulence in the surface layer is generated by wind shear. Buoyant forces tend to become organized higher in the atmosphere and exert their maximum influence in the daytime convective mixed layer (Nakamura and Mahrt, 2001).

The surface layer may be divided into two sub-layers: the roughness sub-layer and inertial sub-layer. The roughness sub-layer extends from the ground to a distance two to three times the canopy height (Fig. 1.1) (Coyle, 2005). The roughness layer begins at the earth's surface and extends vertically into the atmosphere.

The height of the roughness layer is given as $1.5 h_{canopy}$ to $3.5 h_{canopy}$ (where h_{canopy} is a typical height of the surface elements, i.e., vegetation or obstacles) by Prueger and Kustas (2005) and as $5h_{canopy}/3$ by Sellers and Mintz (1986). Shear-induced turbulence in the roughness sub-layer is strongly influenced by canopy features; e.g., the uneven height of plants, the spacing of plants, and the clumping of leaves and branches (Mahrt, 2000). The thickness of the roughness layer is proportional to the degree of 'roughness' and heterogeneity at the canopy surface. Extending 1 to 10 m above the roughness sub-layer is the dynamic or inertial sub-layer (also referred to as the inner region) where under neutral conditions, wind speed profiles can be expected to be generally logarithmic with vertical height (Arya, 2001). Above the roughness sub-layer is the inner region that extends up to 50 to 100 m above the ground surface (Prueger and Kustas, 2005) where the wind profile can also be logarithmic.

Monin-Obukhov Similarity Theory (MOST), the history of which has been reviewed by Foken (2006), and its accompanying empirical stability functions describe the flux of momentum and other quantities in the turbulent surface layer over a homogeneous surface with stationary flow (Monin and Obukhov, 1954). For these conditions, the theory normally works well provided the observations are above the roughness sub-layer.

MOST states that, for a constant flux layer, the structure of turbulence is determined by a few key parameters (Table 1.1) namely: friction velocity u_* (m s^{-1}), temperature scale of turbulence T_* (K), the height above the ground z and the buoyancy parameter g/T (where g is the acceleration due to gravity) and T is the air temperature in K (Monin and Obukhov, 1954).

In contrast to the premises of MOST, the earth's surface is often heterogeneous (Nakamura and Mahrt, 2001). In the surface layer, MOST assumes that the flux-gradient relationship can be formulated in terms of the height above the ground and the Obukhov length L , defined in Chapter 2. So for example, MOST predicts that the ratio of sensible heat flux F_h and the air vertical temperature gradient $\partial T / \partial z$ is a function of $(z - d)$ where the zero-plane displacement height d is depicted in Fig. 1.1. In general, the height above which the MOST is applicable is typically $z - d$ but z varies depending on the type of canopy

Table 1.1 Summary of meteorological parameters estimated or required by the various measurement methods and MOST.

Parameter	Symbol (unit)	Description
Dissipation rate of turbulent kinetic energy	ε ($\text{m}^2 \text{s}^{-3}$)	Refers to the rate of change in turbulent kinetic energy (TKE) per unit mass of fluid, due to viscous effects.
Refractive index structure parameter	C_n^2 ($\text{m}^{-2/3}$)	Spatial statistics used as a measure of the path-averaged strength of refractive turbulence, or simply a measure of the fluctuations in refractive index of air caused mainly by air temperature variations.
Structure function parameter of temperature	C_T^2 ($\text{K}^2 \text{m}^{-2/3}$)	A measure of the structure of air temperature fluctuations (determined from C_n^2).
Inner scale length	l_o (mm)	The smallest diameter of the occurring eddies.
Zero-plane displacement height	d (m)	A height scale in turbulent flow over roughness elements such as vegetation above the ground at which zero wind speed is achieved as a result of the flow obstacles. It is generally approximated as 2/3 of the average height of the obstacles. The displacement height represents the mean height where momentum is absorbed by the canopy (Rosenberg et al., 1983).
Obukhov length	L (m)	The height above the zero-plane displacement height d at which free convection dominates over forced convection (Monin and Obukhov, 1954).
Bowen ratio	β (no unit)	The ratio of sensible heat flux to that of latent energy flux.
Friction velocity	u_* (m s^{-1})	A basic wind speed parameter defined by the square root of τ/ρ where τ is the turbulent horizontal wind stress in the surface boundary layer and ρ is the air density (Thom, 1975).
Temperature scale of turbulence	T_* (K)	A term for the temperature that an air parcel at a height would potentially have if brought adiabatically (i.e. without thermal contact with the surrounding air) to a given height, i.e. the effective temperature of air parcel after removing the heat of the parcel associated solely with compression (Panofsky and Dutton, 1984).
Roughness length	z_o (m)	A parameter that is a measure of terrain roughness. It is the height at which the horizontal wind speed becomes zero for a bare soil surface when the logarithmic wind profile above the roughness sub-layer is extrapolated to zero wind speed (Arya, (2001).

Beyond the inertial sub-layer is the outer region and finally the free atmosphere where the term free refers to that part of the atmosphere that is not influenced directly by surface forcings such as mechanical or buoyancy forces related to turbulence and surface heating generated at the surface (Prueger and Kustas, 2005).

The complex nature of wind flows in the roughness sub-layer makes it difficult to reliably measure or model scalar flux such as momentum flux or sensible heat flux. Measurements or predictions at one point may vary from those a few meters away due to heterogeneity in the surface (Coyle, 2005).

A primary strategy in obtaining surface flux measurements is to elevate the measurement platform above the roughness sub-layer so that statistical characterization of the flow becomes more consistent and reliable. The surface roughness interacts with the wind to cause horizontal wind speed $u = 0 \text{ m s}^{-1}$ at some height away from the surface. The rougher the surface, the higher the level where $u = 0 \text{ m s}^{-1}$ (Pielke, 1998). The distance between the surface and the height at which $u = 0 \text{ m s}^{-1}$ is $z = d + z_o$ (for a canopy surface) where z_o is the aerodynamic roughness length (Table 1.1). The distance between the ground and the displaced surface is known as the zero-plane displacement height d or simply the displacement height. The displacement height represents the mean height where momentum is absorbed by the canopy (Thom, 1975). In the presence of a significant d the most relevant vertical dimension for defining turbulent transport is $z - d$, rather than z alone. This is more important for relatively tall canopies, such as in forest ecosystems or tall crops.

For a soil surface, $u = 0 \text{ m s}^{-1}$ at $z = z_o$. As a general rule for a canopy-covered surface, z_o can be estimated as 0.1 of the canopy height (h_{canopy}) (Thom, 1975). The level that most affects the logarithmic wind profile is not always the ground. Often, the top of a canopy will function as a displaced surface; that is, the characteristic logarithmic profile is displaced upward (Arya, 2001).

Under strongly stable conditions the flux is likely to decrease rapidly with height because turbulent mixing is dampened by negative buoyancy (Arya, 2001). Stability refers to the tendency of the atmosphere to resist or enhance vertical motion and is related both to the change of air temperature with height and the change of wind speed with height. A neutral atmosphere, for instance, neither enhances nor inhibits turbulent mechanical turbulence. An unstable

atmosphere on the other hand enhances turbulence in the vertical whereas a stable atmosphere inhibits mechanical turbulence (Nivolianitou et al., 2004). The internal boundary layer defined by Brutsaert (1982) as the region of the atmosphere affected by a step change in the surface conditions, i.e. the height at which a disturbance has been propagated, is the appropriate layer in which to perform micrometeorological measurements.

Atmospheric transport is mainly an aerodynamic process in both the horizontal and vertical directions. If the surface is horizontally uniform, it implies that horizontal exchanges can be neglected and only vertical transport has to be considered (Wyngaard and Cote, 1971). If in addition to horizontal homogeneity, stationarity can be assumed, in other words, that the statistical properties of the air motions do not change with time, then time averages represent the aerodynamic processes and not the averaging of time itself. An example of non-stationary conditions is during the passage of a warmer or cold air front (Rosenberg et al., 1983). The assumption of horizontal homogeneity and stationarity means that transport can be considered as one-dimensional, which allows spatially representative flux measurements by micrometeorological techniques at one location averaged over a certain time interval (Arya, 2001).

Transport of scalar quantities such as sensible heat in the atmosphere is characterized by chaotic motions referred to as turbulence (Arya, 2001). A characteristic of turbulence is the occurrence of wind whirls or eddies. The eddies vary dynamically in size, space and time especially under strong turbulent conditions. These eddies are responsible for the effectiveness of transport in turbulent flow, when compared to transport through molecular diffusion (Kaimal and Finnigan, 1994). In general, turbulence can be generated by two mechanisms. The first mechanism is mechanical and is caused by retardation of the air flowing over the ground. This frictional drag causes wind shears to develop. The strength of this mechanical turbulence production depends on the wind speed and on the surface roughness, and is associated with the vertical gradient in the wind profile ($\partial w / \partial z$, where w is the vertical wind speed) (Rosenberg et al., 1983). The second driving force is generated by air density variation in the atmosphere and is called buoyancy parcels of relatively warm air rise because they are less dense than the surrounding cooler air (Arya, 2001). The evaporation of water adds to density differences since humid air has a lower density than dry air.

A number of micrometeorology parameters are estimated or required by the various measurement methods and MOST. A brief summary of these parameters is presented in Table 1.1. Measurements of the turbulent flux such as sensible heat, latent energy and momentum flux, are required for various applications in micrometeorological, hydrology, environmental and agricultural studies, and the demand for reliable information of the components of the energy and water balances of land surfaces on a large spatial scale such as watershed or river basin scales is increasing (Meijninger et al., 2002).

Numerous methods for estimating or measuring turbulent flux have been developed and tested. In certain instances these methods are accurate and reliable; in others, they are unsuitable or provide only rough approximations (Drexler et al., 2004; Savage et al., 1997).

The eddy covariance (EC) method is the most direct method for measuring sensible heat and latent energy flux measurements that is possible with micrometeorological methods (Arya, 2001). The EC method for sensible heat flux measurement is based on direct measurements of the temporal mean of the covariance between vertical wind speed and air temperature which by definition corresponds to the mean of the product of vertical wind speed fluctuations (w') and air temperature fluctuations (T'). This yields a direct and point estimate of sensible heat flux F_h at the measurement height (Rosenberg et al., 1983).

For the EC method, no assumptions are made about the land surface properties such as aerodynamic roughness or zero-plane displacement, and no corrections for atmospheric stability are necessary (Savage et al., 2004, 2005). The method is therefore independent of the MOST, and is also quick to set-up (Savage et al., 2004, 2005).

However, the application of the EC method is not without difficulty. The sensors for measurement of wind speed, air temperature and atmospheric humidity must be highly responsive (frequency response of 10 Hz or greater) and at the same time must not show noticeable drift (Wyngaard, 1981; Thiermann and Grassl, 1992). This makes EC sensors delicate, expensive and difficult to calibrate. In addition to these problems, the method also introduces errors in the flux estimations due to reasons such as:

- flow distortions by the sensor, mast, etc., affect the accuracy of the estimations (de Bruin et al., 1993); i.e. act of measurement changes what is to be measured.
- measurements are made at fixed points and require averaging periods of the order of tens of minutes for statistically stable results. Such long averaging periods reduce the temporal

resolution and demand stationarity of the atmosphere throughout the averaging period, which is often not realised in the surface layer. Moreover, sonic anemometers average out turbulent motions over distances less than their path length, typically 0.1 m (Hartogensis et al., 2002), and the sonic temperature is also dependent on humidity through the dependence on the speed of sound in air (Arya, 2001).

Other point-measurement methods commonly used for measurement of turbulent flux include the Bowen ratio energy balance (BREB) method (Bowen, 1926) and the relatively new and simple surface renewal (SR) method. The SR method (Paw U et al., 1995) is a high frequency single-point measurement (2- and 20-min averages) of air temperature above the canopy.

The BREB method, also a point-measurement method for estimating sensible heat flux, is well suited to mixed species communities such as grassland, but is limited by constraints imposed by both fetch distances and measurement height. Thus the technique is not suited to narrow strips (e.g. riparian zones, wetlands, etc), where fetch distances are short, or above tall vegetation where there are small vertical gradients in air temperature and water vapour pressure (caused by increased turbulence above tall canopies) (Savage et al., 1997). These gradients may occasionally be outside the measurement resolution of the instrumentation. The BREB method also does not allow estimation of micrometeorological parameters (Table 1.2) such as the refractive index structure parameter C_n^2 , dissipation rate of turbulent kinetic energy ε , friction velocity u_* , etc (Table 1.1).

The SR method allows for the estimation of sensible heat from measurements of air temperature at a single level using fine-wire thermocouples, at a measurement frequency of 8 Hz. Then, post-measurement methods are used to estimate sensible heat flux (Savage et al., 2004, 2005).

Because of the difficulties experienced by the various measurement techniques, and since all of the methods discussed so far are point-measurement methods, alternative methods have been sought in the recent years for the reliable estimation of turbulent sensible heat and latent energy flux.

The estimation of turbulent flux over large and heterogeneous surfaces cannot therefore be fulfilled without deploying a network of several single point measurements of surface flux (Thiermann and Grassl, 1992). A surface layer scintillometer (SLS) is used to estimate sensible

heat and momentum flux over a path distance. The SLS system consists of two laser beams and either two (SLS20 model) or four (SLS40) detectors (Thiermann and Grassl, 1992). The typical wavelength of the beam is 670 nm with a small displacement of 2.7 mm. The recommended path length of the SLS is between 50 and 250 m. The signal processing unit of the SLS measures C_n^2 and using MOST calculates turbulent kinematic fluxes of heat (k m s^{-1}) and momentum ($\text{m}^2 \text{s}^{-2}$). The beam height is typically 1 m, for a homogenous surface and depending on the atmospheric turbulence, and the typical path length is 100 m. As is the case for large aperture scintillometer (LAS) and extra-large aperture scintillometer (XLAS) systems, an iterative procedure is required for the estimation of F_h and turbulent momentum flux ($\text{m}^2 \text{s}^{-2}$) for each of the stable and unstable atmospheric conditions. This dual-beam scintillometer system allows path-weighted measurements for a beam path length between 50 and 250 m (Table 1.2). Table 1.2 summarises the various meteorological parameters determined using various measurement methods already mentioned.

The SLS method allows for the estimation of spatial evaporation from a surface if data on soil heat flux and net irradiance are also measured alongside the sensible heat flux measurements. Besides some of the technical limitations related to the required horizontal homogeneity of the surface layer, the point measurement methods are also very expensive if used at multiple points or locations for wider area measurements of sensible heat flux since that would require a number of such units (de Bruin et al., 1995).

Optical scintillation of a beam is caused by the refractive index inhomogeneities in the atmosphere that arise from turbulence fluctuations in air temperature and water vapour pressure (Hill, 1992; Thiermann and Grassl, 1992). There are different types of scintillometers, with the difference being mainly in the aperture size of the receiver compared to the Fresnel zone, $F = \sqrt{\lambda \times L_{beam}}$, where λ is the wavelength of the transmitter beam and L_{beam} the beam path length. The SLS has a small receiver aperture, is dual-beam and has a receiver aperture size less than F whereas the large aperture scintillometer (LAS) has a receiver aperture size greater than F (Meijninger et al., 2002).

Table 1.2 The meteorological parameters determined using different methods.

Method used for determination of meteorological parameter	Meteorological Parameters						
	Sensible heat flux (F_h)	Residual latent energy flux ($L_v F_w$)	Friction velocity (u_*)	Dissipation rate of kinetic turbulent energy (ε)	Momentum flux (τ)	CO ₂ flux (F_c)	H ₂ O vapour flux (F_w)
LAS or XLAS	✓	+	-	-	-	-	-
SLS or multi-beam LAS	✓	+	✓	✓	✓	-	-
1-Dimensional EC	✓	+	-	-	-	-	-
3-Dimensional EC	✓	+	✓	-	✓	-	-
Bowen ratio	✓	✓	-	-	-	✓	✓
Surface renewal	✓	+	-	-	-	-	-
CO ₂ sensor and 3-D sonic	✓	-	✓	-	✓	✓	-
H ₂ O sensor and 3-D sonic	✓	+	✓	-	✓	-	✓

✓ Meteorological parameter that can be measured using the method

- Meteorological parameter that cannot be measured or determined using the method

+ Meteorological parameter can be estimated if net irradiance I_{net} and soil heat flux F_s are known.

Extra-large aperture scintillometers (XLAS) have a much larger receiver aperture size, nearly twice that of LAS and are used for surface-layer turbulence measurements over longer distances of up to 10 km (Hartogensis et al., 2002). The LAS and XLAS units are designed for measuring C_n^2 over horizontal path lengths from 250 m to 4.5 km (LAS) and 1 km to 8 km (XLAS). Structure parameter measurements obtained with the LAS or XLAS systems and standard meteorological observations (air temperature, horizontal wind speed and atmospheric pressure) can be used to derive the surface sensible heat flux (Scintec, 2000, 2006), although with multiple-beam LAS, measurements of C_n^2 and cross-wind are also obtained directly by the instrument. Multiple-beam LAS such as the boundary layer scintillometer, unlike single-beam LAS, optically measures atmospheric turbulence, sensible heat flux and crosswind over spatial scales up to 5 km and gives time series output of C_n^2 , C_T^2 , sensible heat flux and crosswind. The scintillometer method allows for the measurement of atmospheric turbulence using the phenomenon of optical scintillation. With the SLS method, the focus of this current study, a transmitter emits two highly parallel and differentially polarised laser beams over a distance of 50

to 250 m (Thiermann and Grassl, 1992; de Bruin and Meijninger et al., 2002; Hartogensis et al., 2002).

The radiation from the laser is scattered by refractive index inhomogeneities in the air which are caused by turbulent fluctuations. At the receiver located 50 to 250 m away from the transmitter, the two beams reach two separate detectors. From the magnitude and the correlation of the intensity modulations, the inner scale length of refractive index fluctuation, l_o (mm), which is the smallest diameter of the occurring eddies (Table 1.1), and the refractive index structure parameter C_n^2 are derived (Thiermann, 1992). The idea behind the use of the SLS method is based upon consideration that the refractive index structure parameter C_n^2 measured directly by the scintillometer can be related to the structure function parameter of temperature C_T^2 ($K^2 m^{-2/3}$), which is then used to derive sensible heat flux F_h if u_* is known. An advantage of the SLS method is the high temporal resolution and the spatial coverage as compared to point-measurement methods like the EC, BREB and SR methods. Furthermore, the SLS method further quantifies the microenvironment through the following parameters obtained by its use: ε , Obukhov length L , and u_* . There is, therefore, an innate attractiveness about using scintillation to obtain turbulence information over target specific scales (Hill, 1992; Hartogensis et al., 2002).

Interest in using optical propagation measurements to infer turbulence information is more recent than the other methods used in measurement of sensible heat flux and latent energy flux, with Wesley (1976) being one of the first to attempt to derive estimates of sensible heat F_h using the method, although the first scintillometry measurements of C_n^2 were made earlier by Tatarskii (1961). Much of the appeal of optical techniques is derived from the opportunity for spatial averaging and the requirement of only very short averaging periods to give statistically reliable measurements (Wyngaard and Clifford, 1978).

1.2 Motivation

Most of the studies carried out using the scintillometer method for measurement of sensible heat flux have used the LAS method with only few of these studies involving use of the SLS method.

Table 1.3 Studies done using surface layer scintillometer (SLS).

Reference	Measurement distance (m)	Surface on which study was done	Duration of study	Measurement height (m)	Comments / main findings
Thiermann (1992)	100	Not mentioned	One day	1.90 m above ground level	<ul style="list-style-type: none"> With the SLS one can obtain path averaged turbulent flux with much higher temporal resolution than obtained using the EC method. Comparison of F_h values measured by SLS show good agreement with EC F_h measured values.
Thiermann and Grassl (1992)	120	Stubble field surrounded by flat and agriculturally-used terrain	One week	2 m above ground level	<ul style="list-style-type: none"> Results of one- and 10-min averages between 10h00 to 18h00 show more scatter (one-min data) due to short-term variations of turbulence along beam path.
Green et al. (1994)	100	<ul style="list-style-type: none"> Horizontally homogenous pasture sward well supplied with water Sparse thyme canopy in a semi-arid environment 	First experiment done for one month and second one for another one month	1.2 and 1.5 m above ground level	<ul style="list-style-type: none"> Excellent agreement obtained between the flux measured by SLS with those measured by EC system. Friction velocities obtained using EC and SLS methods agreed within 2 % over the range 0 to 0.9 m s⁻¹.
Anandakumar (1999)	70	Wheat canopy (average wheat crop height = 0.9 m)	One month	1.4 m above surface (0.5 m above wheat crop)	<ul style="list-style-type: none"> Estimated sensible heat flux measured by SLS were found to be in good correspondence with the surface renewal measured ones, with the SLS ones showing smoother variations.
de Bruin et al. (2002)	117	Old dead grass	Ten days	2.15 m above ground level	<ul style="list-style-type: none"> Random errors in the SLS measurements of F_h are small compared to scatter found with two eddy-covariance systems. Assuming that the hot-film system yields the 'true' flux measurements, the SLS appears to overestimate u_* when u_* is less than 0.2 m s⁻¹ and underestimate u_* at high wind speeds. The derived F_h appears to be less sensitive to errors in l_o and C_T^2 because errors in these quantities tend to cancel out.
Hartogensis et al. (2002)	112	Grassland	One month	2.45 m above ground level	<ul style="list-style-type: none"> There is good agreement between dissipation rate of kinetic energy measured by SLS and those measured by EC method. Proposed revision of beam displacement to improve results for friction velocity measured by SLS.

Kanda et al. (2002)	250	Densely built-up neighbourhood in Tokyo	Two days	3.5 m above building heights (16 and 32 m above ground level)	<ul style="list-style-type: none"> Scintillometer-derived sensible heat flux obtained at height 3.5 times the building height agree well with those obtained using EC technique. Source areas for the scintillometer flux are larger than for the EC sensors, so that at low heights over inhomogeneous terrain scintillometry offers advantages.
Weiss (2002)	Varied with various measurement days between 76 to 77	Varied from homogeneous and flat terrain to flat non-homogenous terrain in an alpine valley	Three months and 12 days	1.1 m above the ground level	<ul style="list-style-type: none"> The SLS method is applicable to deriving line-averaged refraction correction values over various types of terrain and for different atmospheric conditions with a good temporal resolution.
Salmond et al. (2003)	116 171	Urban roughness sub-layer	Seventeen days	15.1 m and 19.3 m above street level	<ul style="list-style-type: none"> Good correlation between sensible heat flux measured by EC and SLS methods, although the increased spatial averaging of turbulent eddies in the SLS flux results in a smoother diurnal cycle compared to EC flux. SLS is shown to be an appropriate tool for the measurement of turbulent heat flux in the urban roughness sub-layer with careful determination of d and the use of urban forms of MOST.
Savage et al. (2004, 2005) and Savage (2007)	50 and 101	Mixed grassland with canopy height varying between 0.2 m to 1.3 m	More than two years	1.5 and 1.68 m above ground level	<ul style="list-style-type: none"> 20-min measurements of F_h by BREB, EC, SLS and SR methods were in good agreement most of the times, especially for cloudless days. SLS- and EC-measured F_h compares closely/agree well. There was no evidence of consistent underestimation of F_h by EC method compared to SLS method. Beam height above $d + z_0$ needs to be known accurately as the error in beam height contributes the most to the overall error in SLS measurements of F_h.
Nakaya et al. (2006)	86	Deciduous forest canopy	Four months	10 m above forest canopy (28 m above the ground level)	<ul style="list-style-type: none"> The greater value of dissipation rates by SLS is remarkable under the atmospheric unstable conditions with weak wind or under strong wind conditions. The dissipation rates by EC indicated greater values than by SLS under atmospheric neutral and weak wind conditions. The displaced-beam SLS tended to overestimate the sensible heat flux against the EC method, and did not indicate a clear relationship to the wind direction.

These studies indicate that scintillometer measurements, mostly using the SLS method, can be adopted for reliable routine momentum and sensible heat flux measurements (Kohsiek, 1985; Hill, 1992; Hill et al., 1992; de Bruin et al., 1995). Once the sensible heat flux measurements are obtained using the SLS method, latent energy (evapotranspiration) can be obtained from the shortened form of the energy balance equation (Eq. 1.2) as a residual, as long as net irradiance and soil heat flux are also known. Measurement of sensible heat flux is therefore very important and SLS being an instrument that can allow spatial measurement of sensible heat as opposed to the EC (and other methods) that can only obtain point measurements of sensible heat is very useful in this regard.

In spite of this, this idea of routine and long-term measurements using the scintillometer method and in particular the SLS method has not been achieved. This work attempts to address this lack. In Table 1.3, the few studies involving use of the SLS are shown. Apart from the work of Savage et al. (2004, 2005) and Savage (2007), only short-term studies have been undertaken using the SLS method. Also, out of the few studies using the SLS method, it is only that by Savage et al. (2004, 2005) and Savage (2007) that involved measurements of sensible heat flux over a mixed grassland community.

Scintillometry offers several advantages over the EC and other conventional methods for measuring sensible heat flux. The advantages include (Wyngaard, 1981; Anandakumar, 1999; Nakaya et al., 2006): flow distortion effects are minimised due to intensity fluctuations being path-weighted in a parabolic manner with a maximum at midway and tapering to zero at either end of the optical path; averaging over the propagation path, reducing the averaging period which boosts spatial representivity of the method; depending on source characteristics and measurement height, path-averaging is possible up to several hundred metres, a range which offers possibilities for validating remote sensing estimates of sensible heat; no absolute instrument calibration is required. This arises because the quantity measured is the variance of the logarithmic signal intensity so that any multiplicative calibration factors cancel and constant terms are removed by band-pass filtering at scintillation frequencies.

However, scintillometry has the following disadvantages: it uses numerous assumptions, including MOST, to derive fluxes (Hill, 1992) and the zero-plane displacement height d needs to be known. Necessary assumptions are that the turbulent field through which the beam passes is isotropic and that the scintillations are weak (Tatarskii, 1963). The SLS method used in this study

suffers from the problem of saturation when scintillations are not weak and hence measurements are limited to a maximum of 250 m between the transmitter and receiver units. Moreover, the direction of the sensible heat flux cannot be determined by the SLS method and so air temperature measurements at two vertical heights may be used to obtain this direction. The method is also comparatively expensive.

There is also a need to know whether the SLS beam is in the roughness sub-layer (in which case the effective height of the sensor height above the ground level z) or in the overlying inertial layer (in which case the effective height is determined as $z - d$) (Sellers and Mintz, 1986). The separating height between the roughness sub-layer and the inertial layer is typically $5h_{canopy}/3$ (Sellers and Mintz, 1986).

The most optically-active eddies have sizes of the order of the first Fresnel zone ($=\sqrt{\lambda L_{beam}}$, where λ is the optical wavelength and L_{beam} the path length) (Thiermann and Grassl, 1992).

Since the small-scale eddies are likely to be in equilibrium with the local terrain, it might appear that scintillation techniques allow some relief from general fetch restrictions on micrometeorological measurements by, for example, the BREB method, and thus provide averaging over horizontally inhomogeneous terrain.

Also the scintillometer method depends on MOST (details of MOST are in Chapter 2) to link measurements in the dissipation or inertial sub-range of frequencies to the entire range of eddy sizes contributing to turbulent transport (Thiermann and Grassl, 1992; de Bruin and Meijninger, 2002; Hartogensis et al., 2002). Unfortunately, large eddies adjust only slowly to changing surface conditions and therefore reflect terrain and surface features well upstream of the measurement position (Højstrup, 1981; Panofsky and Dutton., 1984).

1.3 Aims and objectives of the study

In view of the relatively few studies and the paucity of data involving use of the SLS method (Table 1.3), the main aim of this study was to investigate the long-term use and performance of the SLS method for estimating areally-averaged F_h for a mixed grassland community surface and to compare SLS measurements with those obtained using the EC method. Factors affecting the

SLS method or the accuracy of the SLS data collected were also investigated. The factors include the influence of the Bowen ratio, the influence of atmospheric stability and the influence of wind direction.

The approach was to measure areally-averaged F_h at an existing grassland research site and compare it with the estimates of F_h measured using the EC method.

The following are the specific objectives of this study:

- to investigate the performance of the SLS method for different Bowen ratio values and hence determine the reliability of the SLS method for various atmospheric humidity conditions as other researchers have suggested correcting the SLS-measured sensible heat for the Bowen ratio as required by the theory. The different methods for deriving the MOST similarity functions used for both stable and unstable atmospheric conditions were evaluated by comparing the sensible heat flux obtained through an iterative determination of Monin-Obukhov parameters used in sensible heat flux calculations to confirm their accuracy and/or reliability;
- to compare the sensible heat flux obtained by the EC and SLS methods for different atmospheric stability conditions and seasons to find out if there is any significant difference in the EC and SLS measurements of sensible heat flux due to differences in the footprint of the measurements obtained using the two methods, as atmospheric stability influences the footprint. The footprint of a turbulent flux measurement defines the spatial context of the measurement, something akin to the field of view of the measurement of the surface-atmosphere exchange (Schmid, 2002) and indicates the relative weight of the contribution of a source or sink at a defined position to the measurements at the sensor location;
- to compare the sensible heat flux obtained by the EC and SLS methods for different scintillometer beam heights and orientation and also for cases when the prevailing wind flow direction is approximately parallel, or approximately perpendicular to the beam path to check if there is impairment in the SLS sensible heat flux for a slanting SLS beam path.

1.4 Thesis structure

This thesis consists of six chapters with **Chapters 1** and **2** as the introductory part of the entire work. In Chapter 2 the focus is mainly on the literature review, especially on the theoretical

background of the methods used in this study including a review of previous work done using the SLS method.

In **Chapter 3**, an analysis of the performance of the SLS method for different Bowen ratio values is presented. The concern here is to find out if there is a need for correcting sensible heat flux obtained by the SLS method for the Bowen ratio as required by the theory. In this chapter, sensible heat flux obtained by the EC and SLS methods are compared and evaluated. A sensitivity analysis of the SLS sensible heat flux is also done to further confirm the influence of the Bowen ratio on the SLS sensible heat flux and also the influence of Bowen ratio on the EC sensible heat flux. Also presented in this chapter is an analysis of the different forms of the MOST similarity functions suggested by various authors, done by comparing the resulting SLS sensible heat flux with that calculated through an iterative determination of the Monin-Obukhov parameters.

In **Chapter 4**, the sensible heat flux obtained by the two methods (EC and SLS) is compared for different atmospheric stability conditions. The main idea is to investigate differences in the sensible heat flux obtained by the EC and SLS methods due to the influence of atmospheric stability which determines the footprint for the two methods.

Chapter 5 deals mainly with the comparison of sensible heat flux from EC and SLS methods, for different prevailing wind directions relative to the SLS beam path, and evaluation of the agreement between sensible heat flux by EC and SLS methods when the transmitter and receiver units of the SLS are set up in sloping orientation (mimicking a sloped surface and invalidating MOST), with the transmitter being at a higher elevation than the receiver. This is done in order to find out if the beam orientation impairs the sensible heat flux measurements by the SLS method.

Chapter 6 gives the overall summary and conclusions as well as some recommendations for further studies.

Chapter 2: Theoretical background

In this chapter, a brief review of the literature focusing on some of the methods used for estimating sensible heat flux in the study is presented. Specifically, the principles of operation for the surface layer scintillometer (SLS), the eddy covariance (EC) and the Bowen ratio energy balance (BREB) methods are reviewed. These methods are atmospheric methods relying on the turbulent exchange between the surface and the atmosphere above. Turbulence in the atmosphere is the most effective transport mechanism for many scalar quantities, including sensible heat and latent energy flux.

2.1 Scintillometer method

When electromagnetic radiation propagates through the atmosphere it is distorted by a number of processes that can influence its characteristics e.g. its intensity (or amplitude), polarization and phase. Two of these processes are scattering and absorption, by constituent gases and particles in the atmosphere, which remove energy from the beam and thus lead to attenuation.

Atmospheric turbulence produces small fluctuations in the refractive index of air through the influence of associated changes in air temperature. Although the magnitude of the individual fluctuations is very small, the cumulative effect in propagation along an atmospheric path may be very significant (Andreas, 1989). The turbulence-induced fluctuations in the refractive index produce a phase distortion of the wave front (Böckem et al., 2000). The movement of small eddies through the path of a beam therefore causes random deflections and interference between different portions of the beam wave front (Hill, 1992). This causes the beam spot to constantly change pattern like the boiling effect of water. A small detector would measure intensity fluctuations or scintillations.

Scintillation in science is usually treated as a disturbance especially in optical communications and astronomical observations (Tatarskii, 1961; cited by Tatarskii, 1993; Böckem et al., 2000). But it has also been recognised that scintillation can be used to characterise atmospheric turbulence and to measure crosswind speed (Daoo et al., 2004).

An important mechanism that influences the propagation of electromagnetic radiation, as mentioned above, is due to the small fluctuations in the refractive index of air stemming from air temperature-induced fluctuations. These turbulent refractive index fluctuations in the atmosphere

lead, for example, to intensity fluctuations and are known as scintillations (Hill, 1992). Some examples that clearly show the distortion of wave propagation by the turbulent atmosphere, which can be seen regularly, are the twinkling of stars, image dancing and image blurring above hot surfaces as seen in a mirage.

The refractive index of air is a function of air temperature and to a lesser degree the humidity of air. As eddies transport both sensible heat and water vapour, their refractive index fluctuates and this results in scintillations (Hill, 1992).

Since the 1950s many scientists have conducted theoretical studies to explain the scintillation phenomenon (Tatarskii, 1961; Jenkins and White, 1976). Several different theoretical approaches have been proposed to describe the propagation of electromagnetic radiation in a turbulent medium. In some approaches the turbulent eddies are visualised as a collection of concave and convex lenses which focus and defocus the beam resulting in scintillations (Hill, 1992). In others, diffractive effects are taken into account. In the 1960s with the invention of the laser, experimental studies were conducted to validate the proposed propagation models (Tatarskii, 1961; cited by Tatarskii, 1993).

Due to the success of the models that are able to relate the propagation statistics of electromagnetic radiation with the turbulent patterns of the atmosphere, it is now possible to measure and quantify the turbulent characteristics of the atmosphere using a remote sensing method, also known as the scintillation method using a scintillometer (Andreas, 1989).

The energy spectrum of turbulence, representing the scale of turbulence from the so-called energy-containing range through to the inertial sub-range of turbulence to the dissipation range (Meijninger, 2003), may be defined through the use of a wave number for turbulence. The range of the turbulent wave number k is defined by the range in the eddy size values experienced in the atmosphere at that time with the wave number defined as $k = 2\pi/l$, where l is the size of the eddy (Meijninger, 2003). These eddy sizes reflect the turbulence regime of the atmosphere and may impact on the transmission of electromagnetic radiation.

A scintillometer is an optical instrument that consists of a radiation source (transmitter) and a receiver which consists of a highly sensitive detector and a data acquisition system that can register the intensity of fluctuations of the radiation after propagation through a turbulent medium, to deduce the different meteorological parameters (Hill, 1992; Thiermann and Grassl, 1992). A beam of radiation is transmitted over a path and the fluctuations in the radiation

intensity at the receiver are analysed to give the variations in the refractive index along the path. Specifically, the variance of the natural logarithm of the intensity incident at the receiver is related to a property called the refractive index structure parameter (C_n^2 , $\text{m}^{-2/3}$) defined as (Hill, 1992):

$$C_n^2 = \frac{n(r_1)^2 - n(r_2)^2}{r_{12}^{2/3}} \quad 2.1$$

where $n(r)$ is the refractive index at location r and r_{12} (m) is a distance lying between two length scales r_1 and r_2 characteristic of the turbulence (Tennekes and Lumley, 1972).

The distance between the transmitter and the receiver can range from tens to thousands of metres depending on the type of instrument (Thiermann and Grassl, 1992). There are different types of scintillometers and the difference is mainly based on the size of the transmitter and receiver aperture size compared to the Freznel zone (defined in Chapter 1). If the aperture size is less than the Freznel zone, the scintillometer is classified as a small aperture scintillometer and the ones with aperture sizes greater than the Freznel zone are referred to as large aperture scintillometers. Different types of radiation sources can be used. The beam wavelength for the different scintillometer types is also different, with the large and extra-large aperture scintillometer types having beam wavelength of $930 \text{ nm} \pm 5 \text{ nm}$. In this study, a displaced-beam surface layer scintillometer (SLS), that emits two parallel and differently polarised laser beams with the separating distance, d_{SLS} , was used. The SLS40-A used in this study uses a class 3a type laser at a wavelength λ of 670 nm , a beam displacement distance, d_{SLS} of 2.7 mm and a detector diameter, D_{SLS} of 2.5 mm . With this instrument the beam of one source is split into two parallel, displaced beams with orthogonal polarizations. By determining both the variances of the logarithm of the amplitude of the two beams, σ_1^2 and σ_2^2 and the covariance of the two beams, σ_{12}^2 , inner scale length, l_o (mm) (smallest diameter of the occurring eddies) and C_n^2 can be obtained (Hartogensis et al., 2002). At the receiver located 50 to 250 metres away from the transmitter, the two beams reach two separate detectors. The SLS set up is shown (Photo 2.1) with a close-up of the transmitter, receiver, junction box and signal processing unit of the SLS (Photo 2.2).

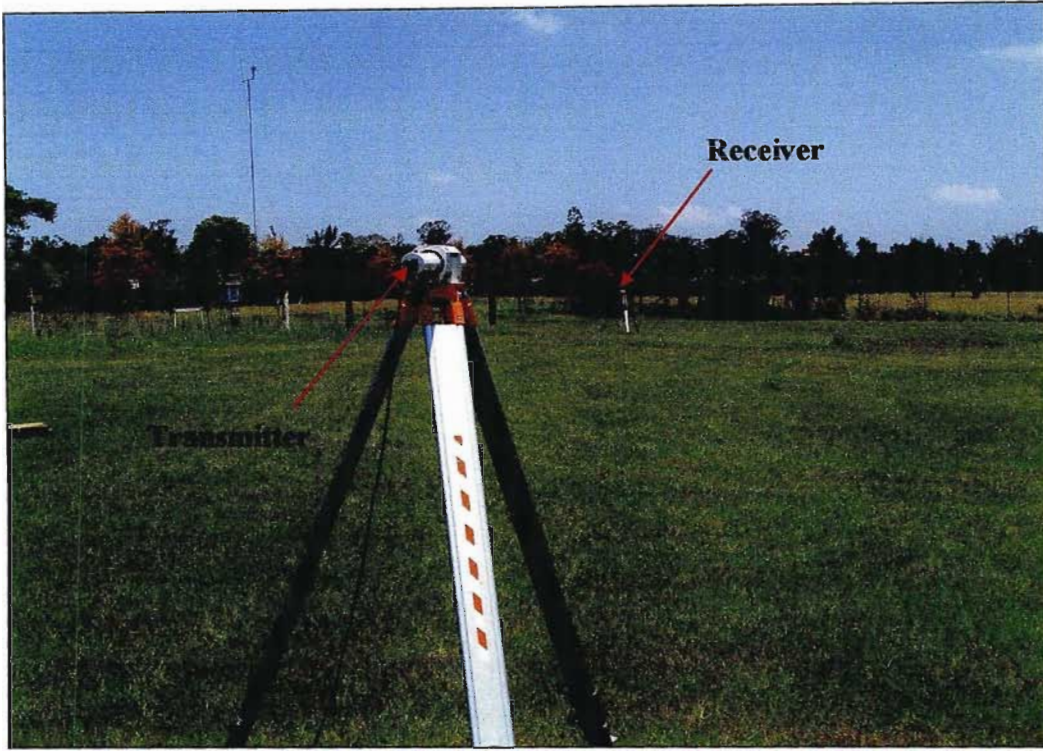


Photo 2.1 The surface layer scintillometer set up showing the transmitter and receiver as indicated.

By determining both the variances of the respective intensities σ_1^2 and σ_2^2 , and the covariance of the logarithmic signal intensity σ_{12}^2 (from the variances and covariances of the intensity modulations of the received signals), I_o and C_n^2 can be related to σ_{12}^2 following Hill and Lataitis (1989) via a function dependent on k , and $\Phi_n(k, I_o, C_n^2)$, where:

$$\sigma_{12}^2(k, I_o, C_n^2) = 4\pi^2 K^2 \int_{r=0}^{L_{beam}} \int_{k=0}^{\infty} k \Phi_n(k, I_o, C_n^2) \cdot \sin^2 \left[\frac{k^2 \cdot r \cdot (L_{beam} - r)}{2K L_{beam}} \right] dk \cdot dr \quad 2.2$$

$$\sigma_{12}^2(k, I_o, C_n^2, d_{SLS}) = 4\pi^2 K^2 \int_{r=0}^{L_{beam}} \int_{k=0}^{\infty} k \Phi_n(k, I_o, C_n^2) J_o(k d_{SLS}) \cdot \sin^2 \left[\frac{k^2 \cdot r \cdot (L_{beam} - r)}{2K L_{beam}} \right] \cdot \left[\frac{4J_1^2(k D_{SLS} r / 2L_{beam})}{(k D_{SLS} r / 2L_{beam})^2} \right] dk \cdot dr \quad 2.3$$

where k is the turbulent wave number, $\Phi_n(k, I_o, C_n^2)$ the spectrum of the refractive index fluctuations given as $\Phi_n(k, I_o, C_n^2) = 0.033 \cdot C_n^2 \cdot k^{-11/3} f_\Phi(k I_o)$, d_{SLS} is the beam displacement

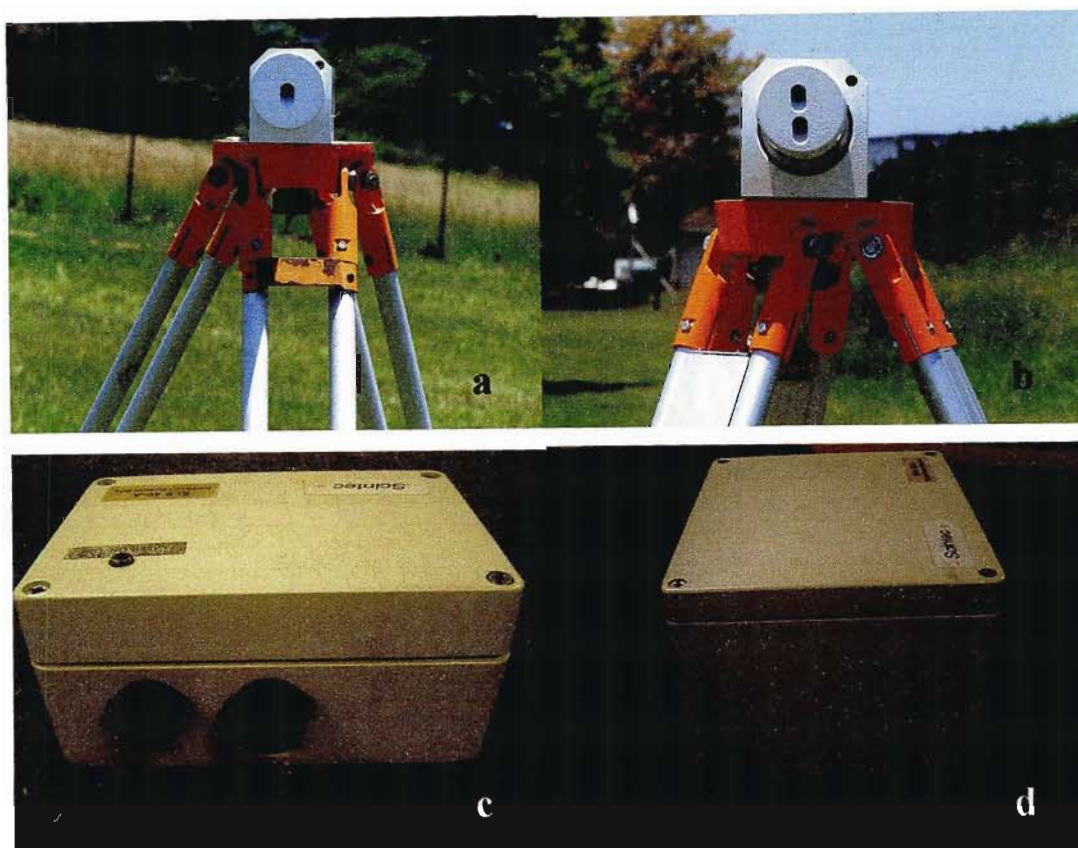


Photo 2.2 The SLS (a) transmitter, (b) receiver, (c) switch box and (d) signal processing unit.

distance ($= 2.7$ mm for SLS), r is the distance at a particular position along the beam measured from the transmitter, L_{beam} is the SLS beam path length, $K = 2\pi / \lambda$ is the optical wave number, where λ is the beam wavelength, J_0 and J_1 are Bessel functions of the first kind of order one, and D_{SLS} the aperture diameter of the scintillometer detectors. Equation 2.3 is only valid as long as scattering is weak, i.e. $\sigma_{12}^2 < 0.3$ (Thiermann and Grassl, 1992).

Saturation occurs if the beam scattering is not weak, in which case the measured σ_{12}^2 is less than that predicted by Eq. 2.3 (Wang et al., 1978; Thiermann, 1992). Due to this fact, the maximum path length for the SLS used in this study is limited to 250 m. The minimum path length should be 50 m since at path lengths less than this, the measured inner scale length would often be less than the recommended value of 3.5 mm for this path length making the instrument susceptible to measurement errors (Scintec, 2006).

To overcome the saturation problem, which limits the SLS measurements to a beam path distance of 250 m, the beam path length should be decreased or beam height position increased (Savage et al., 2004, 2005). Otherwise a LAS would be the option for obtaining sensible heat flux over longer path lengths, e.g. of up to 5 to 10 km (McAneney et al., 1995).

At optical wavelengths the contribution of temperature fluctuations dominates the scintillometer signal at the receiver, that is, compared to water vapour pressure fluctuations. The structure parameter of temperature C_T^2 ($K^2 m^{-2/3}$) can be deduced from the C_n^2 measurement (Andreas, 1989; Hill, 1992). Dissipation rate of the turbulent kinetic energy ε ($m^2 s^{-3}$) can be deduced from l_o and the definition of Kolmogorov scale η :

$$\eta = l_o \cdot \left(\frac{3 \beta_1}{Pr} \right)^{-\frac{3}{4}} = \left(\frac{\nu^3}{\varepsilon} \right)^{\frac{1}{4}} \quad 2.4$$

where β_1 is the Obukhov-Corrsin constant ($= 0.86$), Pr the Prandtl number ($= 0.72$) and ν the kinematic viscosity of air ($m^2 s^{-1}$) (Andreas, 1989):

The structure parameter of temperature, C_T^2 , and l_o follow Monin-Obukhov Similarity Theory (MOST) (Monin and Obukhov, 1954), discussed later, to give the flux of sensible heat and momentum (Andreas, 1989).

2.1.1 Structure parameter of the refractive index

The changes in the refractive index of air caused by air temperature fluctuations are usually random functions in both time and space. Thus, turbulence intensity of the refractive index of air $n(r, t)$ can only be determined by the average of certain quantities, such as the structure parameter of the refractive index fluctuations, C_n^2 (Eq. 2.1). Assuming the random process generating the changes in refractive index is isotropic, then $C_n^2(r) = C_n^2 \cdot |r|$ (Hill and Clifford, 1978; Tatarskii, 1993).

2.1.2 Turbulence spectrum

The refractive index spectrum Φ_n quantifies the optical turbulence in the boundary layer of the atmosphere. The refractive index (n) in a turbulent medium is a random function of time (t) and position (x). The spectrum is modelled by the inner scale length l_o and the structure parameter

C_n^2 of the refractive index fluctuations (Andreas, 1989; Hill, 1992), where the fraction of the refractive index spectrum $\Phi_n(k)$ is given by:

$$\Phi_n(k) = 0.033 C_n^2 k^{-1/3} f_\phi(k, l_o) \quad 2.5$$

where k is the turbulent wave number (m^{-1}), l_o is the smallest diameter of eddies, the function f_ϕ is the decay of the refractive index fluctuation in the dissipation range and equals unity in the inertial range, and $l_o \cong h/2$ where h is the height above the ground.

Turbulent flow in the atmosphere is neither homogeneous nor isotropic, because of the presence of the rigid boundary of the earth's surface (Poggio, 1998). However, the flow can be considered locally homogeneous and isotropic in small sub-regions of the atmosphere far from the earth's surface. Kolmogorov (1941) (cited by Poggio, 1998) introduced two hypotheses stating that during the cascade process, in which any large-scale flow in the atmosphere breaks down into motions of smaller scales, the direct influence of larger eddies is lost and smaller eddies tend to have independent properties, universal for all types of turbulent flows. Consequently, these smaller eddies should be isotropic.

Kolmogorov's first hypothesis (Kolmogorov, 1941, cited by Poggio, 1998) applies in the range determined by the inequality $l_o \ll 1 \text{ m} < \mu$ (called the equilibrium range), where μ is called the Kolmogorov microscale. The Kolmogorov microscale defines the size of eddies dissipating the kinetic energy. The second hypothesis is for sufficiently large Reynolds numbers. The sub-range defined by $\eta < 1 \text{ m} \ll L_o$, is called the inertial sub-range, where L_o is the outer scale length and is approximately equal to the scintillometer measurement height and η is the Taylor microscale (which marks where the viscous effect becomes significant) and is dominated by inertial forces whose actions redistribute the energy across the turbulent spectrum.

The graph of the refractive index spectrum is shown in Fig. 2.1. According to Kolmogorov (1941) (cited by Poggio, 1998), in the inertial sub-range, energy neither enters the system nor is dissipated. It is merely transferred at rate ε from smaller wave numbers to larger wave numbers, where it is dissipated. As a result, the three-dimensional spectral density function $\Phi_n(k)$ would depend on the viscous dissipation rate ε and the turbulent spatial wave number k only.

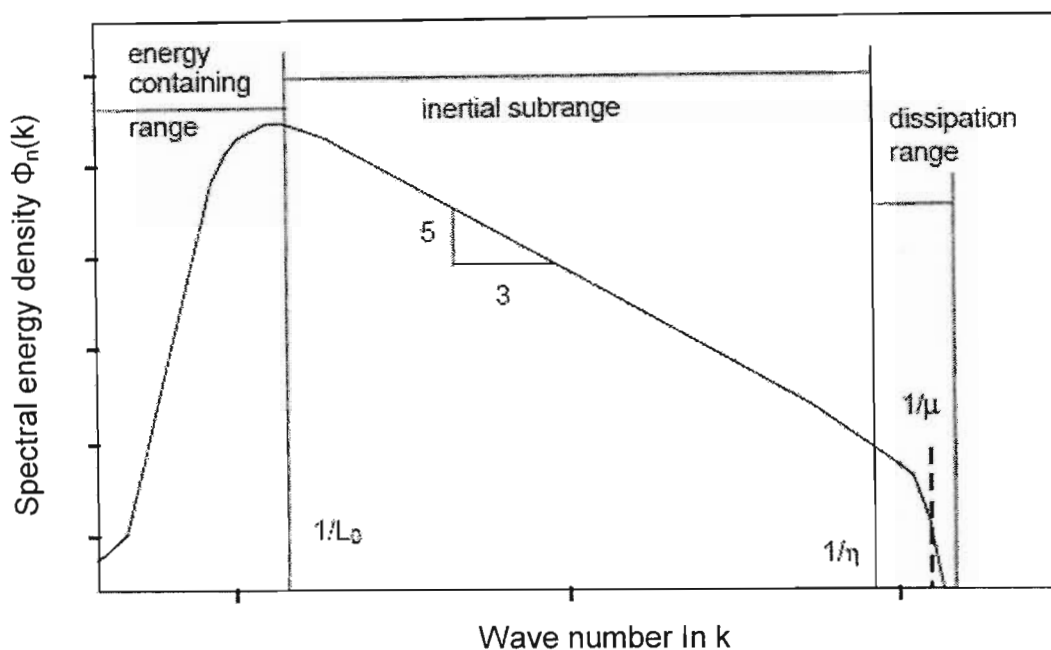


Fig. 2.1 Schematic representation of the energy spectrum of turbulence (after Poggio, 1998).

If the parameters C_n^2 and l_0 of the spectrum of refractive index are measured and the level of the line of sight above ground is approximately known, the turbulent energy flux can be determined using MOST. Based on Tatarskii's (1961) theory, Clifford et al. (1974) showed that the variance of natural logarithm of the radiation I incident at the receiver is:

$$\sigma_{\ln}^2 = \sum \frac{[\ln(I) - \overline{\ln(I)}]^2}{n} = \int_0^1 C_n^2(\mu) W(\mu) d\mu \quad 2.6$$

where the sum is over time, typically a 2-min interval, n is the number of measurements in the 2-min interval, I is transmitted radiation at time t and the over bar represents a spatial weighting average, where $W(\mu)$ is a spatial weighting function determined by the Kolmogorov microscale μ which is given by:

$$W(\mu) = 4\pi^2 K^2 L_{beam} \int_0^\infty (\Phi_n(k) / C_n^2(r)) \sin^2(k^2 L_{beam} (1-r) / 2K) \times \quad 2.7$$

$$[4J_1(x_1)J_1(x_2) / x_1 x_2]^2 dk$$

where $r (= x / L_{beam})$ is the normalized path distance from the transmitter at position x along the beam path, L_{beam} is the path length; $K = 2\pi / \lambda$ is the optical wave number; J_1 is Bessel function of the first kind of order one, $x_1 = \frac{KD_{SLS}r}{2}$, $x_2 = \frac{KD_{SLS}(1-r)}{2}$ where D_{SLS} is the receiver/transmitter aperture diameter; k is the turbulent wave number; and Φ_n , the three-dimensional Kolmogorov spectrum of the refractive index describes the turbulent medium in terms of its Fourier components k :

$$\Phi_n(k) = 0.033 C_n^2 k^{-11/3} f_\Phi(k, l_o). \quad 2.8$$

Refractive index structure parameter C_n^2 can be obtained as a linear function of σ_{ln}^2 (Andreas, 1989), measured by the scintillometer as $C_n^2 = C \sigma_{ln}^2 \cdot D_{SLS}^{7/3} L_{beam}^{-3}$ where $C = 1.12$ for C_n^2 ranging from 10^{-17} to $10^{-12} \text{ m}^{-2/3}$. In the optical domain, C_n^2 depends mainly on air temperature fluctuations in the atmosphere and only slightly on humidity fluctuations (Green et al., 1994).

Assuming no error in the measurement of atmospheric pressure P (Pa) and air temperature T (K), the spatially averaged structure parameter of temperature C_T^2 is related to C_n^2 (Green et al., 1994):

$$C_T^2 = C_n^2 \cdot \left(\frac{T^2}{\gamma P} \right)^2 \cdot \left(1 + \frac{0.03}{\beta} \right)^{-2} \quad 2.9$$

where $\gamma = 7.89 \times 10^{-7} \text{ K Pa}^{-1}$ and β is the Bowen ratio which is incorporated as a humidity correction such that C_T^2 decreases with increasing evaporation rate, provided air temperature and atmospheric humidity fluctuations are strongly correlated (Thiermann, 1992) and consistent with MOST.

2.1.3 Variance of the logarithmic signal intensity fluctuations

For optical propagation, the variance of the logarithm of the fluctuations (σ_{ln}^2) of a spherical wave front originating from a point source (e.g. a laser) as measured at the receiver, is related to

the refractive index structure parameter C_n^2 by the following relationship, according to Hill and Clifford (1978):

$$\sigma_{12}^2 = 0.496 K^{7/6} L_{beam}^{11/6} C_n^2 \Phi_n \left(l_o / \sqrt{\lambda L_{beam}} \right) \quad 2.10$$

where λ is the beam wavelength. Equation 2.10 is valid provided that the integrated amount of scintillation over the optical path is small ($\sigma_{12}^2 < 0.3$) to avoid saturation (Wang et al., 1978).

For a given optical wave number $K = 2\pi / \lambda$, the variance depends upon fluctuations in refractive index changes described by C_n^2 and the inner scale length l_o via the function $\Phi_n \left(l_o / \sqrt{\lambda L_{beam}} \right)$ (Andreas, 1989). The inner scale marks the transition from the inertial-convective to the viscous-convective range and is a measure of the approximate dimensions of the small-scale viscous motions in which turbulent energy is converted into sensible heat (Tennekes and Lumley, 1972). Hill and Clifford (1978) gives l_o as $l_o = 7.4 \cdot (\nu^3 / \varepsilon)^{1/4}$, based on Eq. 2.4, where ν is the viscosity of air and ε the dissipation rate of turbulent kinetic energy.

2.1.4 Inner scale length and SLS measurements of sensible heat flux

The small aperture scintillometer responds to eddies with diameters close to the Fresnel zone size. Such eddies may belong either to the inertial sub-range (large eddies) or to the dissipation sub-range (small eddies) of turbulence (Scintec, 2000). The two ranges are separated by the inner scale length l_o . Scintillometers evaluate the measured intensity variances at the receiver to derive C_n^2 . However, for eddies in and close to the dissipation range, the measured variances do not only depend on C_n^2 but also depend on l_o , and since l_o is a function of the dissipation rate of turbulent kinetic energy ε and varies with it, it is impossible to derive C_n^2 from small aperture scintillometer measurements as long as l_o is unknown (Hill, 1992).

A property of interest to describe the main difference between LAS and the SLS systems is the Fresnel zone ($F = \sqrt{\lambda L_{beam}}$, with λ as the beam wavelength, and L_{beam} the SLS path length), as already described in Chapter 1. The aperture diameter, D_{SLS} , of the SLS is small since $D_{SLS} < F \approx l_o$ applies. The LAS aperture is considered large because $l_o < F \ll D_{LAS}$. The inner

scale length, l_o , marks the transition between the inertial and viscous energy dissipating range of eddy sizes and is of the order 2 to 20 mm near the surface (Fig. 2.1). For the SLS, F is a measure of the optically most effective eddies (~ 10 mm), which lies in the energy dissipation range of eddy scales.

The SLS method used in this study uses a scintillometer with two displaced and differentially polarised laser beams which are independently observed by two detectors having the same displacement. The inner scale length l_o of the refractive index fluctuations is calculated from the correlation of the two intensities at the two detectors. The variance of the intensities and covariances of the logarithm of the intensities are evaluated to derive both C_n^2 and l_o . The SLS therefore measures C_n^2 and l_o and from these C_T^2 and ε are derived (Thiermann, 1992; Scintec, 2006). This makes the SLS method superior to the single-beam LAS method which can only measure C_n^2 , or derived from that, C_T^2 using β , T , P and C_n^2 measurements (Thiermann, 1992).

Moreover, for the SLS method, the sensible heat flux is calculated from C_T^2 and ε for all stability conditions and virtually any measurement height (Thiermann, 1992). Also, XLAS and LAS systems require measurements of friction velocity (u_* , m s^{-1}) for sensible heat flux to be determined while SLS and multi-beam LAS do not require u_* since l_o is obtained.

The specific design of Scintec's SLS with its dual-beam (Scintec, 2006) makes the spatial weighting function (the relative contribution at different positions along the beam path) very similar for measurement intensity variances and covariances. This minimises effects of varying turbulence statistics along the propagation path. Also, the weighting function has a maximum value in the centre of the propagation path and decreases to zero at the transmitter and receiver sides. Hence disturbances of the wind flow in the vicinity of the instruments and mountings/towers, as may be experienced with the EC and other point measurements/methods, only have little or negligible effects on the sensible heat flux measurements.

2.1.5 Monin-Obukhov Similarity Theory (MOST)

The atmospheric surface layer is also known as the constant flux layer because under the assumption of steady-state and horizontal homogeneous conditions, the vertical turbulent flux is nearly constant with height, with variations of less than 10 % (Panofsky and Dutton, 1984). Flux

profile relationships relate the turbulent flux of momentum and sensible heat to their respective profiles of mean vertical wind speed and air temperature. The MOST, on which most commonly-used flux profile relationships are based, predicts that the dimensionless gradient of the mean horizontal wind speed \bar{u} and of the mean potential temperature $\bar{\theta}$ are universal functions of atmospheric stability (Hartogensis et al., 2002). The potential temperature θ of a parcel of air at pressure P is the temperature that the parcel would acquire if the parcel is adiabatically brought to a standard reference pressure, usually 100 kPa. The profile relationships for momentum and sensible heat are:

$$\frac{k(z-d)}{u_*} \frac{d\bar{u}}{dz} = \Phi_m(\zeta) \quad 2.11$$

$$\frac{k(z-d)}{T_*} \frac{d\bar{\theta}}{dz} = \Phi_h(\zeta) \quad 2.12$$

where the subscripts m and h refer to momentum and sensible heat respectively, and the over bars denote a mean quantity, k is von Karman's constant, h the height above the ground, d the displacement height, Φ the stability function for the exchange of u , the friction velocity and T_* (K) is the temperature scale of turbulence (Thiermann and Grassl, 1992). The stability variable is defined as $\zeta = (z-d)/L$, where L is the Obukhov length.

Empirical MOST relations are used to convert the scintillometer measurements of the inner length scale of turbulence, l_o , and the structure parameter of the refractive index, C_n^2 , into flux of momentum and sensible heat (Hartogensis et al., 2002). Validity of MOST and the determination of the effective measurement height therefore dominate the applicability of flux calculation from optically-determined C_n^2 and l_o .

In this study, the approach adopted by Thiermann and Grassl (1992) is followed in which a simultaneous optically-measured inner scale length l_o is related to the dissipation rate of turbulent kinetic energy ε and one assumes that ε obeys MOST. A fixed C_T^2 and l_o then corresponds to a set of values for sensible heat flux and momentum flux (τ , Pa) which is an expression of the drag force per unit area of level ground caused by horizontal air motion. According to MOST, for a constant flux, the structure of turbulence is determined by the following parameters (Monin and Obukhov, 1954):

$$u_* = \sqrt{\tau / \rho} \quad 2.13$$

$$T_* = \frac{F_h}{\rho c_p u_*} \quad 2.14$$

where c_p the specific heat capacity of dry air at constant pressure ($\text{J kg}^{-1} \text{K}^{-1}$), ρ the air density and F_h is the sensible heat flux (W m^{-2}).

According to MOST, C_n^2 and ε , are made dimensionless by respectively scaling them with the temperature scale T_* and friction velocity u_* , are universal functions of the stability parameter $\zeta = (z-d)/L$ with the Obukhov length L defined by:

$$L = \frac{T}{k g} \cdot \frac{\rho c_p}{F_h} \cdot u_*^3 \quad 2.15$$

where g is the acceleration due to gravity (9.81 m s^{-2}) (Monin and Obukhov, 1954),

$$f_T(\zeta) = \frac{C_T^2 z^{2/3}}{T_*^2} \quad 2.16$$

and

$$f_\varepsilon(\zeta) = \frac{\varepsilon k z}{u_*^3} \quad 2.17$$

A number of similarity functions have been proposed: Wyngaard (1973), Hill et al. (1992), Thiermann and Grassl (1992) and de Bruin et al. (1993). In this study the functions used for stable and unstable conditions as proposed by Thiermann and Grassl (1992) and which are used to derive F_h by the Scintec SLSRUN software developed for the SLS used, are adopted. An analysis of other proposed functions is however also carried out for comparison (Chapter 3).

Thiermann and Grassl (1992) give the following semi-empirical expressions:

for $\zeta > 0$ (stable condition)

$$C_T^2 \cdot z^{2/3} T_*^{-2} = 4\beta_1 \cdot (1 - 7\zeta + 20\zeta^2)^{-1/3} \quad \text{and} \quad 2.18$$

$$\varepsilon k z u_*^{-3} = (1 - 4\zeta + 16\zeta^2)^{-1/2}; \quad 2.19$$

and for $\zeta < 0$ (unstable condition)

$$C_T^2 \cdot z^{2/3} T_*^{-2} = 4\beta_1 \cdot (1 - 7\zeta + 75\zeta^2)^{-1/3} \quad 2.20$$

$$\varepsilon k z u_*^{-3} = (1 - 3 \zeta)^{-1} - \zeta, \quad 2.21$$

where $\beta_1 = 0.86$ is the Obukhov-Corrsin constant.

Hill et al. (1992), on the other hand, proposed that for unstable atmospheric conditions for which $\zeta < 0$:

$$f_T(\zeta) = C_T^2 z^{2/3} T_*^{-2} = 8.1 \cdot (1 + 15 \zeta)^{-1/3}. \quad 2.22$$

Equations 2.18 to 2.21 can be solved for F_h and τ using a numerical iterative scheme to obtain u_* and T_* for both the stable and unstable cases. Sensible heat flux F_h and momentum flux τ are finally obtained from (Thiermann and Grassl, 1992):

$$F_h = \rho c_p u_* T_* \quad 2.23$$

and

$$\tau = \rho u_*^2. \quad 2.24$$

2.1.6 Estimation of sensible heat and momentum flux

Equation 2.10 indicates that the measured signal from a low-power laser contains information not only on sensible heat flux but also on mechanical turbulence indicated by l_o . Hill et al. (1992), Thiermann (1992) and Thiermann and Grassl (1992) adopt various optical methods for determining l_o . For the scintillometer method, since atmospheric stability determines the sensible heat and momentum flux, which also influences turbulent transport.

An iterative procedure is necessary to obtain sensible heat flux from measurements of σ_{12}^2 (Eq. 2.10). This procedure involves using Eq. 2.22. Then, the structure parameter of temperature C_T^2 , and ε are written in dimensionless form, which are assumed to be universal functions of $\zeta = (z - d)/L$ where L is the Obukhov length (Wyngaard et al., 1973):

$$C_T^2 z^{2/3} T_*^{-2} = f(\zeta) = 4.9 (1 + 7 |\zeta|)^{-2/3}$$

and

$$\frac{\varepsilon k z}{u_*^{-3}} = h(\zeta) = \left(1 + 0.5 |\zeta|^{2/3}\right)^3 \quad 2.25$$

for $-2 \leq \zeta \leq 0$.

The approach adopted by Green et al. (1994) is to solve for ζ iteratively using values of ζ estimated from measurements of mean wind horizontal speed (\bar{u}) and an assumed initial value of ζ . For unstable conditions, the vertical profile of mean horizontal wind speed is given by:

$$\bar{u} = u_* \left[\ln \left((z-d)/z_o \right) - \psi_m(\zeta) \right] / k \quad 2.26$$

where d is the zero-plane displacement, z_o is a measure of the surface roughness, and ψ_m is the commonly-used integrated stability correction for the adiabatic wind profile (Panofsky and Dutton, 1984). For vegetative surfaces, z_o and d can be taken as fractions of the vegetation height (h_{canopy}) ($d \approx 0.66 h_{canopy}$ and $z_o \approx 0.1 h_{canopy}$) after Stanhill (1969) and Tanner and Pelton (1960), respectively. Equation 2.26 allows u_* to be determined, as long as $\psi_m(\zeta)$ is known and given a measurement of \bar{u} and calculation of ε and l_o , which allow C_T^2 to be calculated from the measured optical signal σ_{12}^2 . Sensible heat flux F_h is then determined iteratively from L . Of particular note is the fact that the algorithm used by SLS for obtaining F_h and τ (Fig. 2.2) applies to both the unstable and stable cases but that the algorithm does not allow for the determination of the sign of the flux.

The scintillometer method has been applied and tested by several authors (Kohsiek, 1985; Hill, 1992; Hill et al., 1992; de Bruin et al., 1995) and studies carried out in the past have revealed that the scintillometer method is an attractive alternative to the commonly-used point measurement methods such as EC, for estimation of sensible heat flux. In most of these studies, the method showed good agreement with EC sensible heat flux estimates.

Anandakumar (1999), for example, carried out a study which was designed to compare the estimates of turbulent sensible heat flux over a wheat canopy with the widely-used EC method to obtain an understanding of the performance of the SLS method and confirmed good agreement between the sensible heat flux obtained by the EC and SLS methods.

A similar study carried out by Green et al. (1994) over grassland for a period of two months confirmed a better correlation between EC and SLS estimates of sensible heat flux observed for wind directions parallel to the scintillometer beam path compared to when the prevailing wind direction is traverse to the beam path.

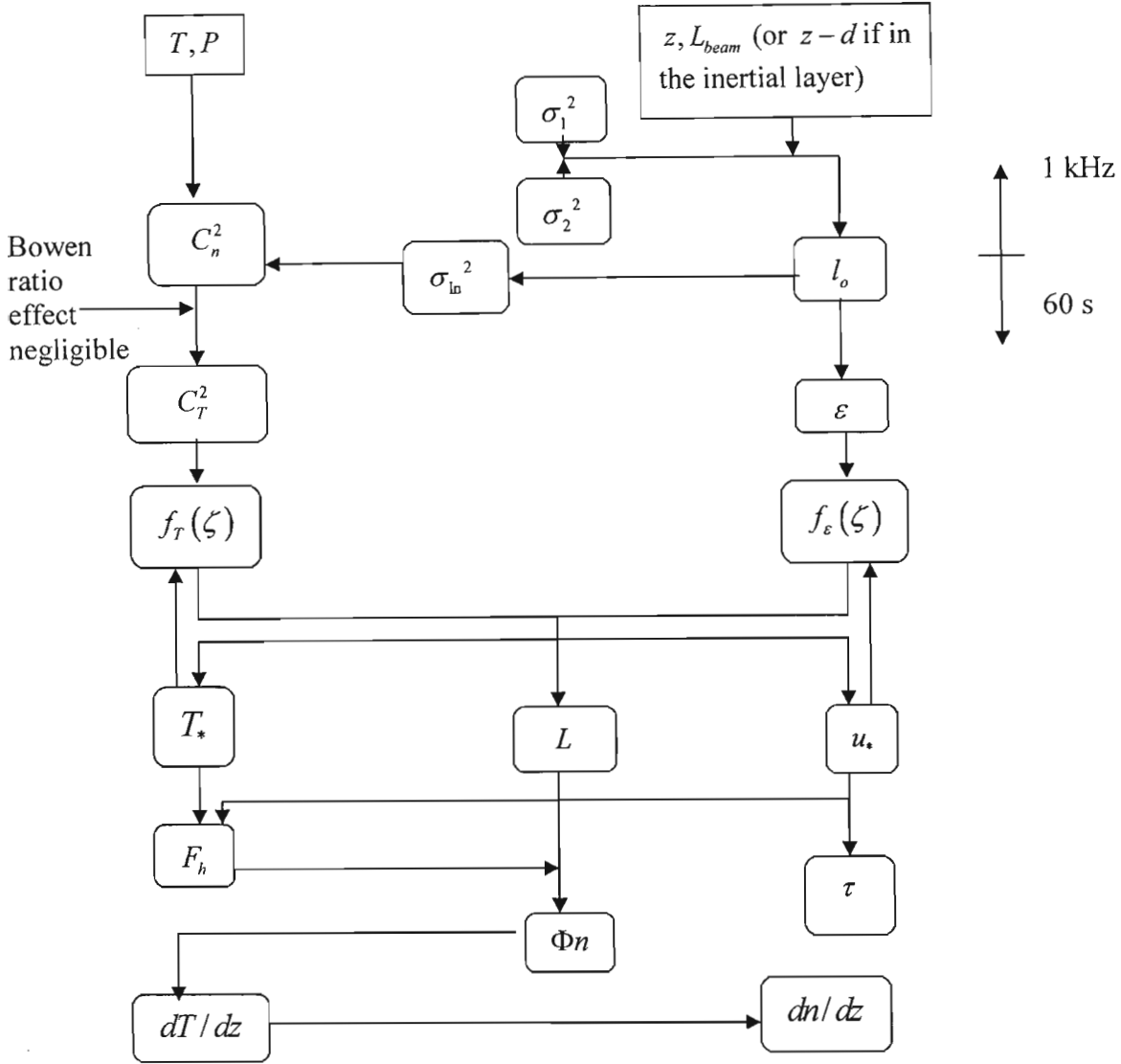


Fig. 2.2 The algorithm (Hill, 1997) used for the various estimates obtained using the SLS method based on weak scattering theory and measurements of the variances σ_1^2 and σ_2^2 , for beam 1 and beam 2 respectively, covariance σ_{12}^2 , inputs of beam height above the zero-plane displacement height, beam path length L_{beam} , air temperature T and atmospheric pressure P (based on Weiss (2002)) and modified by Savage et al. (2004) to reflect the role of single-detector variances σ_1^2 and σ_2^2 and that T_* and u_* are required to calculate $f_T(\zeta)$ and $f_\epsilon(\zeta)$.

Thiermann and Grassl (1992) show that 10-min averages between 10h00 to 18h00 appear more scattered due to short-term variations of turbulence along the beam path (Table 1.3).

Work by Weiss (2002) showed that the SLS method is applicable to derive line-averaged sensible heat flux over various types of terrain and for different atmospheric conditions giving good temporal resolution. The findings from the same study carried out over different surfaces, ranging from flat terrain to alpine valley, also show that an inclined SLS propagation path does not impair the accuracy of turbulence sensible heat flux derived by SLS for all fetch and stability conditions.

Thiermann (1992) carried out a study to compare SLS-determined inner scale length (l_o) and his model calculations based on wind speed and solar radiation measurements using 5- and 10-min averages of sensible heat flux for a 100-m beam path length at a height of 1.9 m. His findings confirm an agreement between the model calculations and those measured by the SLS.

Findings by de Bruin et al. (2002) using the SLS method indicated u_* is overestimated when u_* is less than $\sim 0.2 \text{ m s}^{-1}$ (for very stable or unstable cases) and underestimated at high wind speed (or under near neutral conditions). This could imply that the SLS measurements of l_o , a direct measure for the dissipation rate of turbulent kinetic energy, are biased, resulting in biased F_h . The SLS method has also been used for studying the turbulence flux above rough urban surfaces. In a study conducted by Kanda et al. (2002) in a densely built-up residential neighbourhood in Tokyo, Japan, the EC and SLS methods were employed for the estimation of sensible heat flux.

SLS measurements of sensible heat flux obtained at a height 3.5 times the average building height agreed well with those obtained using the EC method. Source areas for the scintillometer flux are larger than those for the EC method, so that at low heights over inhomogeneous terrain, the SLS method offers advantages.

2.2 Footprint of measurements

Micrometeorological measurements are not only influenced by the terrain directly underneath the sensor location: the field of view of the instruments stretches upwind of their position (Gash, 1986) and may include very large areas composed of many different types of sources or sinks. This spatial context is commonly referred to as the footprint of a measurement, a term that would

also mean the same thing as the effective fetch (Pasquill, 1972, cited by Göckede, 2004) or source area of a sensor. Flux footprint functions allow estimation of the location and relative importance of passive scalar sources influencing flux measurements at a given sensor height. These footprint estimates vary in size, depending on sensor height, atmospheric stability, and surface roughness (Göckede, 2004).

The footprint of a turbulent flux measurement defines the spatial context of the measurement, something akin to the field of view of the measurement of the surface-atmosphere exchange (Schmid, 2002) and indicates the relative weight of the contribution of a source or sink at position (x, z) to the measurements at the sensor location (x, z_m) (Leclerc et al., 2003) where $z_m > d + z_0$ is the measurement height. The cross-wind integrated footprint function $F(x, z_m - d)$ for the ground source is then formally defined as (Horst and Weil, 1992):

$$F(x, z_m - d) = \int_{-\infty}^x S(x) \cdot f(x, z_m - d) dx \quad 2.27$$

where $F(x, z_m - d)$ is the flux measured at height z_m at point $(x, z_m - d)$, $S(x)$ the source strength per unit area, f the footprint at distance x (with distance x taken as the downwind fetch) and z_m the measurement height.

The vertical scalar flux measured at a point is therefore the integrated contribution from all upwind surface contributions weighted by the footprint function. Footprint models allow determination of the spatial context of a measurement by defining a transfer function between sources or sinks of the signal and the sensor position (Göckede, 2004). When turbulent flux sensors are deployed, the objective is usually to measure signals that reflect the influence of the underlying surface on the turbulent exchange.

Over a homogenous surface, the exact location of a sensor is not much of an issue, because the flux from all parts of the surface are by definition equal, although this depends on the size of the homogeneous area (Schmid, 2002). However, if the surface is inhomogeneous, the measured signal depends on which part of the surface has the greatest influence on the sensor, and thus on the size of its footprint as well as the prevailing wind direction.

2.3 Bowen ratio energy balance method

The energy balance method is one of the many methods currently available for investigating surface energy exchanges (Baldocchi, 1997). These exchanges using the shortened energy balance equation, describe how the available flux at the surface, defined as net irradiance less the soil heat flux is partitioned into sensible heat flux and latent energy flux.

Energy terms related to biological processes, such as photosynthesis and the heat storage in plant biomass are considered negligible, and are not included in the shortened form of the energy balance equation (Blad and Rosenberg, 1974). Energy terms related to the horizontal transfer of energy (convective heat and latent energy), referred to as advection, are also not included because they are assumed to be small compared to the vertical transfer of heat.

The Bowen ratio is defined as the ratio of the sensible energy flux to the latent energy flux. The BREB method is used to estimate latent energy flux to quantify crop water use, evaluate water use models, or investigate aspects of soil-plant-atmosphere water relations. This method has been used to quantify water use (Malek et al., 1992; Fritschen, 1996), calculate crop coefficients (Malek and Bingham, 1993), investigate plant-water relations (Grant and Meinzer, 1992) and evaluate crop water use models (Farahani and Bausch, 1995; Todd, 1996). The BREB method is considered to be fairly robust, and has been compared favourably with other methods such as the weighing lysimeter (Grant, 1975; Askarab et al., 1989; Bausch and Benard, 1992; Pruger et al., 1997), EC (Cellier and Olioso, 1993) or water balance (Malek et al., 1992) methods. Most of the studies that showed agreement were conducted mostly when Bowen ratios were positive and advection absent. Others showed less certain agreement (Blad and Rosenberg, 1974; Dugas et al., 1991; Xiangun, 1996).

From the energy point of view, evapotranspiration can be considered as the energy employed for transporting water from the intercellular spaces of leaves and plant organs (through transpiration), and soil or water surfaces (through evaporation) to the atmosphere as water vapour (Xiangun, 1996). The energy used in the evapotranspiration process is the latent energy of vapourisation ($L_v \approx 2.43 \text{ MJ kg}^{-1}$). The BREB method estimates latent energy flux from a surface using measurements of vertical air temperature and water vapour pressure gradients ($\Delta T / \Delta z$ and $\Delta e / \Delta z$, respectively), net irradiance and soil heat flux (Fritschen and Simpson, 1989). The

BREB method is an indirect method, compared to others such as the EC method, which directly measures turbulent flux, or a weighing lysimeter, which measures the change in mass of an isolated soil volume containing plants. The BREB method is relatively straight forward and simple (Rosenberg et al., 1983; Xiangun, 1996). The method:

- requires no information about the aerodynamic characteristics of the surface of interest;
- allows the integration of latent energy flux over large areas;
- allows estimation of latent energy flux on fine time scale (less than an hour) and provides continuous, unattended measurements.

Disadvantages of the method include (Rosenberg et al., 1983):

- sensitivity to the biases of the instruments which measure gradients and the other energy balance terms;
- the possibility of discontinuous data when the Bowen ratio approaches -1,
- and the requirement, common to micrometeorological methods, of adequate fetch to ensure adherence to the assumptions of the method. Furthermore there are
- greater maintenance requirements compared to the EC method, the requirements of long-term measurements of a water vapour pressure gradient are not trivial (Savage et al., 1997).

The BREB method relies on several assumptions listed by Fritschen and Simpson (1989):

- turbulent flux transport is assumed to be one-dimensional, with no horizontal gradients of air temperature and water vapour pressure;
- sensors which measure the vertical gradients are assumed to be located within the equilibrium sub-layer where flux are assumed to be constant with height;
- the surface is assumed to be homogeneous with respect to sources and sinks of heat, water vapour and momentum;
- the eddy diffusivity of sensible heat and latent energy are assumed to be equal.

The first two assumptions are usually met if adequate upwind fetch is available. A fetch to height-above-surface ratio of 100:1 is often considered a rule of thumb (Rosenberg et al., 1983), although a ratio as low as 20:1 was considered adequate when Bowen ratios were small and positive (Heilman et al., 1989). Sensors at different heights respond to different upwind source areas (Schmid, 1997), so that all measurements must have adequate fetch.

Generally, the error in measuring evapotranspiration using the BREB method is thought to be 10 to 15 % of the actual value (Fuchs and Tanner, 1970; Sinclair et al., 1975). The method

is most accurate when the Bowen ratio is small ($-0.5 < \beta < 0.5$), and the vertical gradients of air temperature and water vapour pressure are large (Gash and Stewart, 1977; Spittlehouse and Black, 1980). One of the main sources of error in the method arises from inaccuracies in measuring the vertical gradients of air temperature and water vapour pressure. Current sensor resolution for Bowen ratio air temperature gradient measurements is around 0.006°C and that for water vapour pressure is 0.01 kPa (Beringer et al., 2003). The resolution of the sensors becomes important when the observed vertical air temperature gradients over various surfaces are considered.

2.3.1 Radiation balance and available energy

Net irradiance, which is the sum of all incoming and outgoing irradiances at the surface of the earth is the major energy source that drives the evapotranspiration process (Arya, 2001). It is considered positive when the sum of incoming irradiances exceeds the sum of the outgoing irradiances.

For a flat extensive surface, the net irradiance (I_{net}) is the sum of the incoming short and infrared irradiance, less the short wave reflected irradiance and infrared emittance from the surface:

$$I_{net} = I_s - r \cdot I_s + L_d - L_u \quad 2.28$$

(commonly referred to as the radiation balance equation). The available energy flux, in $\text{J s}^{-1} \text{m}^{-2}$ or in W m^{-2} , is the difference between the net irradiance and the soil heat flux (Savage et al., 1997):

$$\text{available energy flux} = I_{net} - F_s = L_v F_w + F_h. \quad 2.29$$

2.3.2 Soil heat flux

The subsurface heat flux, F_s , is the flux stored in the soil and is a function of the change in soil temperature with time and the thermal and physical properties of the soil. The soil heat flux F_s is estimated from the flux measured by the heat flux plate sensor, G , plus the energy flux that is stored in the layer above it, F_{stored} :

$$F_s = G + F_{stored}. \quad 2.30$$

The storage flux is calculated using the definition of specific heat capacity the volumetric (or gravimetric) heat capacity of the volume of soil above the soil heat plate sensor and the temporal change in soil temperature. The storage flux, F_{stored} is calculated as (Savage et al., 1997):

$$F_{stored} = \rho_{soil} c_{soil} \Delta z_{soil} dT_{soil} / dt \quad 2.31$$

where ρ_{soil} is the bulk density of dry soil, c_{soil} the specific heat capacity of the soil ($\text{J kg}^{-1} \text{K}^{-1}$), Δz_{soil} the soil depth, dT_{soil} the change in soil temperature ($^{\circ}\text{C}$) during a measurement interval dt (typically 1200 s), and $c_{soil} = c_{dsoil} + \theta c_w$ where c_{dsoil} is the dry soil specific heat capacity, θ the soil water content (kg kg^{-1}) and c_w the specific heat capacity of water ($= 4190 \text{ J kg}^{-1} \text{K}^{-1}$).

2.3.3 Sensible heat and latent energy fluxes

Sensible heat flux (F_h) results from the temperature difference between the soil and plant canopy and the overlapping atmosphere. Sensible heat flux is temperature driven and directly relates to the turbulent transfer of heat. Methods for estimating the sensible heat flux include: BREB, EC and scintillometer methods, including SLS.

Energy flux that is consumed by evapotranspiration is the latent energy flux, and is related to the vertical water vapour pressure gradient and the turbulent transfer of water vapour. At the earth's surface the difference between net irradiance and the soil heat flux is the available energy flux which is partitioned into sensible heat and latent energy flux (often referred to as turbulent fluxes).

Net irradiance and soil heat flux can be measured directly in the field. Sensible heat flux can also be determined using BREB, EC or scintillometer methods. However, Bowen (1926) determined that if the transfer coefficients are assumed to be equal, the ratio of sensible heat flux to latent energy flux is proportional to the ratio of the vertical gradient of air temperature to that for water vapour pressure. Using the assumption that the eddy diffusivity for sensible heat flux K_h and latent energy flux K_w are equal, and measuring the air temperature and water vapour pressure gradients between two heights, β is obtained as (Rosenberg et al., 1983):

$$\beta = \gamma \frac{K_h}{K_w} \frac{\Delta T / \Delta z}{\Delta e / \Delta z} = \gamma \frac{\Delta T}{\Delta e} \quad 2.32$$

where ΔT and Δe are the air temperature and water vapour pressure differences between the two measurement heights z_1 and z_2 , where $\Delta z = z_2 - z_1$ and γ is the psychrometric constant (approximately 66 Pa K^{-1}). The sign convention used for the energy flux is I_{net} , F_h and $L_v F_w$ being positive upwards and F_s being positive when heat is stored in the soil. Under certain conditions, the Bowen ratio approaches -1 and application of the method is invalidated. When this happens, the calculated value of latent energy flux loses numerical meaning.

The Bowen ratio compares the relative magnitudes of the sensible heat and latent energy flux. This is based on the shortened surface energy balance:

$$I_{net} = F_s + F_h + L_v F_w \quad 2.33$$

where I_{net} is net irradiance, F_s the soil heat flux, F_h the sensible heat flux and $L_v F_w$ is latent energy flux, all in W m^{-2} .

If I_{net} and F_s are measured directly, then the partitioning of F_h and $L_v F_w$ can be calculated (Bowen, 1926).

The Bowen ratio is combined with the shortened energy balance equation yielding the following expressions for F_h and $L_v F_w$:

$$F_h = \frac{\beta}{1 + \beta} \cdot (I_{net} - F_s) \quad 2.34$$

where $\beta \neq -1$.

The energy balance equation can then be written in terms of the Bowen ratio to solve directly for the latent energy flux, as:

$$L_v F_w = \frac{I_{net} - F_s}{1 + \beta} \quad 2.35$$

where I_{net} , F_s , F_h , and $L_v F_w$ are as previously stated and β , is the Bowen ratio (Bowen, 1926) and where $\beta \neq -1$.

2.4 Eddy covariance method

Eddies are turbulent, highly rotational air flows that move across the surface of the earth transporting water vapour and heat between the surface and the atmosphere (Rosenberg et al.,

1983). In turbulent air flow, sensible heat and latent energy flux vary irregularly in time and space; for this reason, statistical analyses are used to represent turbulent flow. For example, the covariance between vertical wind speed (w) and air temperature (T) is directly related to turbulent flux (Arya, 2001).

The theory behind the EC method relies on the observation that turbulent flux in the atmosphere are driven by the covariance between vertical wind speed and the wind vector or turbulence (Garratt, 1992). In other words, the transport of scalar (water vapour, heat, CO₂ etc) and vectorial amounts (i.e. momentum) in the low atmosphere in contact with the canopies is mostly governed by air turbulence. In turbulent flow, wind velocity components and a scalar quantity transported by this wind vary irregularly in space and time (Arya, 2001). Due to the turbulent motion, each air parcel in the atmosphere contains scalars like heat, water vapour, other gases and possibly dry aerosols and liquid droplets. These scalars closely follow the turbulent motion if they are sufficiently small. When measured as two time series of wind vector \vec{v} and a corresponding scalar c , a certain level of statistical covariance between the two is observed in case there is a transport of c .

With regard to atmospheric studies, it is generally the vertical exchange between the atmosphere and the underlying surface that is of interest. Therefore, the wind vector \vec{v} is expressed by its three components u , v and w that correspond to the horizontal wind speed along the mean wind direction, the wind speed perpendicular to the mean wind direction, and the vertical wind speed w , respectively. The w component is the most relevant for vertical exchange (Swinbank, 1951). Instantaneous values of w and T can be decomposed into a mean and a fluctuating part: $w = \bar{w} + w'$; $T = \bar{T} + T'$, where the over bar indicates temporal mean and the primes indicate instantaneous deviations from the mean, e.g. $w' = w - \bar{w}$ (Rosenberg et al., 1983).

The EC method calculates a flux from high frequency measurements of w and T (or any other scalar quantity as the case may be). Over a given time interval, deviations of w and T from the time-averaged means are calculated and sensible heat flux is calculated from the covariance of w and T over the time interval. The flux of sensible heat is given as (Arya, 2001):

$$F_h = \rho c_p \overline{\text{covariance}(w, T)}$$

$$= \rho c_p \overline{(\bar{w} + w') \cdot (\bar{T} + T')}.$$

As already mentioned, the primary transport mechanism by which heat and water vapour are transported from the canopy to the atmosphere is by the turbulent motion of the air near the surface (Garratt, 1992; Arya, 2001). For heat to move from the surface vertically into the atmosphere, the upward motions of the turbulence consist of air parcels that are warmer than those moving downwards (Kaimal and Finnigan, 1994). Similarly, for water vapour to undergo turbulent transport from the land surface to the atmosphere, upward air motions must be more humid than the downward motions.

For the EC method, just like the BREB method, an adequate fetch is required. A fetch to height ratio of 100 is usually considered adequate but greater fetch is desirable (Wieringa, 1993). The distribution of eddy size contributing to vertical transport creates a range of frequencies important for EC measurements (Kaimal and Finnigan, 1994). The sensors must therefore respond adequately to measure the frequencies at the high end of the range, while the covariance averaging time must be long enough to include frequencies at the low end (Kaimal et al., 1972).

The turbulent flux in the vertical direction can be expressed by the covariance between w and a scalar where the scalar is represented by T the air temperature in case of sensible heat flux measurements (Kaimal and Finnigan, 1994). The EC method is therefore based on measurements of the instantaneous fluctuations of vertical wind speed w' and of air temperature T' at adequate frequency to obtain the contribution from all the significant eddy sizes and averaging their product over a given time scale (say 20 min).

$$F_h = \rho c_p \overline{w'T'}. \quad 2.37$$

The air temperature for most EC systems is actually the sonic temperature (Kaimal and Finnigan, 1994) but alternatively a fine wire-thermocouple may be used. Ham and Heilman. (2003) used both methods and found that very similar estimates of sensible heat resulted.

2.5 Brief overview of subsequent chapters

Discussions on comparison between measurements of F_h obtained by the EC and SLS methods are presented in the following chapters. The SLS method assumes that C_T^2 can be estimated from C_n^2 , air temperature T and atmospheric pressure P . Furthermore, the SLS method is dependent on MOST, the formulation of which is not unique. Chapter 3 is mainly concerned with

the comparison of F_h measurements by the two methods (EC and SLS) but for different Bowen ratio values. Since the EC method is independent of MOST and the zero-plane displacement height compared to the SLS method, it is important to check the validity of the SLS method for a range of stability conditions. Chapter 4 mainly deals with the comparison of F_h obtained by the SLS method with the measurements by the EC method under a range of atmospheric stability conditions. Chapter 5 on the other hand concentrates on the comparison of F_h obtained by the SLS method with those obtained by the EC method for a range of wind directions; limited to when wind direction is either approximately perpendicular or parallel to the SLS beam path, as well a comparison of the F_h values obtained by the two methods for slanting SLS beam orientation. The aim is to confirm the performance of the SLS method for different atmospheric conditions and wind directions. The performance of the SLS method for non-homogeneous surfaces is also tested by way of setting up the SLS transmitter and receiver in a slanting position.

Chapter 3: Surface layer scintillometer and eddy covariance sensible heat flux comparisons for a mixed grassland community as affected by Bowen ratio and MOST formulations

3.1 Introduction

The 1998 Republic of South Africa National Water Act (National Amendment Water Act, 1998) suggests a possible prescription for water allocation and charges for different land uses and this makes it even more crucial to consider how evaporation, which is one of the main components of the water balance, is to be measured or estimated routinely with reliable accuracy and precision (Savage et al., 2004, 2005).

Reliable estimation of energy fluxes from a surface is also important for understanding atmospheric boundary layer stability, regional water balance, irrigation needs, and weather forecasting (Smarakoon et al., 2000), as well as to generally address a growing list of environmental issues that range from definition of local water balance to accounting for land-atmosphere interactions in support of climate modelling. Several methods can be used to measure or estimate surface fluxes such as sensible heat and latent energy (Savage et al., 1997). Development and testing of methods for estimating energy fluxes that are reliable and simple to apply are important aspects of micrometeorological research. Methods such as the Bowen ratio energy balance (BREB) method and the eddy covariance (EC) method (Tanner, 1960), have been widely used in micrometeorological research before (Ashktorab et al., 1989; Cellier and Brunet, 1992; Bland et al., 1996; Steduto and Hsiao, 1998). Some methods, for example the scintillometer method, involve measurement of the sensible heat flux from which evaporation would be estimated from measurement of the net irradiance and soil heat flux and application of shortened energy balance equation.

In the recent past, methods such as scintillometry which appear to offer greater spatial coverage are gaining popularity in surface energy balance studies especially given that this method can be used for evapotranspiration studies covering large heterogeneous areas

(Meijninger et al., 2002). Apart from the operational simplicity, the main appeal of the large aperture scintillation method in boundary-layer physics is their promise of providing spatially-averaged fluxes at scales of the order of several metres to even kilometres depending on the aperture size and type of beam used (Green et al., 1997). Measurements of sensible heat flux using large aperture scintillometry can be used to validate and/or calibrate satellite measurements of sensible heat and latent energy fluxes over large areas (Bastiaanssen, 2000; Watts et al., 2002; Hemakumara et al., 2003). The surface layer scintillometer (SLS) used in the current study has a limitation of saturation which means that the signal variance no longer increases linearly with C_n^2 as the refractive turbulence increases above a certain threshold. The SLS method therefore suffers from the problem of saturation and hence measurements are limited to a maximum of 250 m between the transmitter and receiver units. The minimum path length should be 50 m since at path lengths less than this, the inner scale length is less than the recommended minimum of 2 mm making the instrument susceptible to measurement errors (Scintec, 2006).

In this chapter, the performance of the SLS method for measuring sensible heat flux for different Bowen ratio values is evaluated against the widely-used EC method at a grassland site. It is assumed that the SLS-derived sensible heat fluxes require correction when the Bowen ratio β is within the range $0 < \beta < 0.6$ (de Wekker, 1996). Furthermore the estimates of SLS-derived sensible heat flux are dependent on the Monin-Obukhov Similarity Theory MOST (Monin and Obukhov, 1954) and on the Bowen ratio (Eq. 2.9). The influence of the assumption that $0.03/\beta \ll 0$ on the estimates of the SLS-derived sensible heat is investigated. Through an iterative procedure, this chapter investigates the sensitivity of the SLS sensible heat flux estimations to the Bowen ratio. Some studies have found that the sensible heat flux measured by the SLS method needs to be corrected for the Bowen ratio (Green and Hayashi, 1998; Meijninger and de Bruin, 2000). Green and Hayashi (1998), for example, used a large aperture scintillometer above a paddy field, with its large evaporation. They suggest the need for some water vapour correction for scintillometer sensible heat flux estimates under small Bowen ratio conditions. However, even in their case, the difference between corrected and uncorrected values of sensible heat flux was about 5 % at most.

3.2 Theoretical background

Only a brief review of the theory on which the methods used in the study (BREB, EC and SLS) are based is presented in this section as a more elaborate theoretical review is already given in Chapter 2.

3.2.1 Eddy covariance

The EC method is a direct method based on the measurement of the temporal mean of the covariance between vertical wind speed and air temperature which by definition corresponds to the product of vertical wind speed fluctuations (w') and air temperature fluctuations (T') yielding a direct estimate of sensible heat flux F_h (W m^{-2}) at the measurement height (Rosenberg et al., 1983). Sensible heat flux F_h is calculated by multiplying the density of air (ρ) and the specific heat capacity for air at constant pressure (c_p) with the time-averaged covariance between w and T :

$$F_h = \rho c_p \overline{w'T'} \quad 3.1$$

where the over bar indicates a time average of the instantaneous deviations and the primes indicate instantaneous deviations from the mean e.g. $w' = w - \bar{w}$.

The primary transport mechanism by which sensible heat and water vapour move from the canopy to atmosphere is by the turbulent motion of the air near the surface (Garratt, 1992). For sensible heat directed to the surface to the atmosphere, the upward motions of the turbulence must be warmer than the downward motions. Similarly, for water vapour to undergo turbulent transport from the land surface to the atmosphere, upward air motions must be more humid than the downward motions (Arya, 2001). The covariance between vertical wind speed and humidity is positive during evaporation (upwards), and negative during dew or frost formation (downwards).

As is the case for the BREB method, the EC method requires an adequate fetch. A fetch to height ratio of 100:1 is usually considered adequate but a greater fetch is desirable (Kaimal and Finnigan, 1994). The distribution of eddy size contributing to vertical transport creates a range of frequencies important to EC measurements. The EC sensors must therefore be sufficiently responsive to respond to the frequencies at the high end of the range such as 10 Hz, while the

covariance averaging time must be long enough to include frequencies at the low end such as 1 Hz (Kaimal and Finnigan, 1994).

The main advantage of the EC method is that it offers the most direct means of measurement of sensible heat and latent energy fluxes that is possible with micrometeorological methods without invoking MOST. No assumptions are made about the land surface properties such as aerodynamic roughness or zero-plane displacement, and no corrections for atmospheric stability are necessary. Furthermore, unlike the SLS method, the sign of the fluxes are automatically assigned through the covariances. The method is however a point-based method.

3.2.2 Bowen ratio energy balance (BREB) method

The BREB method is an indirect method for estimating sensible and latent energy fluxes at a point. The Bowen ratio (β) is estimated from the vertical gradients of air temperature ($\Delta T / \Delta z$) and water vapour pressure ($\Delta e / \Delta z$) between two heights, where ΔT and Δe are the differences in measurements of air temperature and water vapour pressure, respectively. The Bowen ratio is therefore calculated as (Bowen, 1926):

$$\beta = \gamma \frac{\Delta T / \Delta z}{\Delta e / \Delta z} = \frac{F_h}{L_v F_w} \quad 3.2$$

where L_v is the specific latent energy of vaporisation (J kg^{-1}) of water and F_w is the mass flux of water vapour ($\text{kg s}^{-1} \text{ m}^{-2}$). The method assumes that the eddy diffusivities for heat and water vapour respectively are equal (Rosenberg et al., 1983). The vertical gradients in air temperature and water vapour pressure are measured by air temperature sensors (fine-wire thermocouples) and humidity sensors mounted at two different heights above ground level or a single humidity sensor that alternately measures the air stream between the two heights.

3.2.3 Scintillometer method

A surface-layer scintillometer (SLS) consists of a dual-beam laser transmitter and a receiver separated by a distance of between 50 and 250 m. The SLS measures intensity fluctuations from a beam, or ‘amount’ of scintillations, expressed as the structure parameter of the refractive index of air (C_n^2 , $\text{m}^{-2/3}$) which is a representation of the turbulent strength of the atmosphere, after propagation through a turbulent medium (Chehbouni et al., 1999). The turbulent strength of the

atmosphere describes its ability to transport scalars, such as sensible heat, latent energy and other species (gases etc.). It is assumed that these intensity fluctuations are caused by inhomogeneities in the refractive index resulting from the turbulent eddy motions along the beam path. These eddy motions (turbulence) are generated by fluctuations in air temperature and atmospheric humidity (Thiermann, 1992). Since fluctuations in air temperature and humidity cause changes in the refractive index of air, the measured C_n^2 is directly related to the turbulent structure parameter of temperature, C_T^2 (Thiermann, 1992). For visible to near-infrared wavelengths used for the wavelength of the scintillometer beam, it is fluctuations in air temperature that are primarily responsible for atmospheric scintillation, with humidity fluctuations playing only a minor role (Green et al., 1994). In this wavelength region (visible and infrared) the spatially-averaged C_n^2 measured directly by the SLS is related to C_T^2 ($\text{K}^2 \text{m}^{-2/3}$) as follows, provided air temperature and atmospheric humidity fluctuations are strongly correlated (Thiermann, 1992) and consistent with MOST:

$$C_T^2 = C_n^2 \cdot \left(\frac{T^2}{\gamma P} \right)^2 \cdot \left(1 + \frac{0.03}{\beta} \right)^{-2} \quad 3.3$$

where T is the absolute air temperature (K), P is the atmospheric pressure (Pa), assuming no errors in measurements of T and P , γ is $7.89 \times 10^{-7} \text{ K Pa}^{-1}$ at 670 nm and β is the Bowen ratio and when there is no correlation between the fluctuations in air temperature and water vapour pressure:

$$C_T^2 = C_n^2 \cdot \left(\frac{T^2}{\gamma P} \right)^2 \cdot \left(1 + \left(\frac{0.03}{\beta} \right)^2 \right)^{-1} \quad 3.4$$

The last bracketed term in Eq. 3.3, $\left(1 + \frac{0.03}{\beta} \right)^{-2}$, is a correction factor for the effect of humidity on the SLS measurement of F_h . The influence of β on C_T^2 via Eq. 3.4 is much reduced compared to Eq. 3.3, Eq. 3.4 accounts for a relatively minor influence of humidity. Neglecting the Bowen ratio term is assumed to result in errors in the SLS-measured F_h , especially when $0 < \beta < 0.6$ (de Wekker, 1996). de Wekker (1996), who used a large aperture scintillometer for areally-averaged measurements of sensible heat over complex terrain, has shown that the Bowen

ratio correction can be neglected or ignored when $\beta > 0.6$. This would also mean that the F_h values determined by the SLS method should be corrected for $\beta < 0.6$, especially for humid areas since neglecting the Bowen ratio (or humidity) influence would impair the accuracy of the SLS-derived F_h values (Weiss, 2002). However the contribution of humidity-related scintillations is much smaller than temperature-related scintillations, i.e. the laser (used in SLS) is primarily sensitive to temperature-related scintillations (Thiermann, 1992). When the surface conditions are dry F_h is larger than $L_v F_w$, resulting in large β values (> 3) (Rosenberg et al., 1983). This means that the correction term in Eq. 3.3 approaches 1. Over wet surfaces, β is small (< 0.6). Hence a significant amount of scintillation may be caused by humidity fluctuations, resulting in a larger correction.

One of the ways in assessing the accuracy of the measurement of surface fluxes to increase the confidence in the measurements or values obtained (Twine et al., 2000) is through comparison of the agreement in measurements or values obtained by two micrometeorological methods used at the same time period and same site. Agreement between two independent methods for measuring surface fluxes would therefore increase confidence in both approaches so a comparison of sensible heat fluxes measured by EC and SLS is of paramount importance. The SLS yields an areally-averaged value of F_h because it is derived from line-averaged values of C_T^2 and MOST parameters.

3.2.4 Derivation of sensible heat flux using different forms of similarity functions f_T and f_ϵ

Monin-Obukhov Similarity Theory (MOST) states that (Thiermann and Grassl, 1992; Cain et al., 2001), where $\zeta = \frac{z-d}{L}$:

$$f_T(\zeta) = \frac{C_T^2 \cdot (z-d)}{T_*^2} \quad 3.5$$

$$f_\epsilon(\zeta) = \frac{\epsilon k z}{u_*^3} \quad 3.6$$

where z is the height above ground (m), d the zero-plane displacement height (m), T_* a temperature-scaling parameter (K) defined as $F_h / \rho c_p u_*$, where ϵ is the dissipation rate of

turbulent kinetic energy ($\text{m}^2 \text{s}^{-3}$) and u_* the friction velocity (m s^{-1}). The Obukhov length L is as defined in Eq. 2.15.

As already pointed out in Section 2.1.5, based on different datasets different researchers have used various semi-empirical forms of the similarity functions f_T and f_ε , which are different for unstable and stable atmospheric conditions, to derive turbulent fluxes (Cain et al., 2001). The empirical functional dependence of the similarity function f_T on ζ , suggested by Wyngaard et al. (1971) and de Bruin et al. (1993), for unstable conditions is:

$$f_T\left(\frac{z-d}{L}\right) = C_{T1} \cdot (1 - C_{T2} \zeta)^{-2/3} \quad 3.7$$

where constant $C_{T1} = 4.9$ and C_{T2} is given as 7 by Wyngaard et al. (1971) and 9 by de Bruin et al. (1993). Thiermann (1992) (cited by Thiermann and Grassl (1992)) on the other hand proposed f_T as:

$$f_T(\zeta) = 6.23 \cdot (1 - 7\zeta + 75\zeta^2)^{-1/3}. \quad 3.8$$

Hill et al. (1992), on the other hand, used for unstable atmospheric conditions:

$$f_T(\zeta) = C_T^2 z^{2/3} T_*^{-2} = 8.1 \cdot (1 + 15\zeta)^{-1/3}. \quad 3.9$$

For stable atmospheric conditions, de Bruin et al. (1993) suggested that f_T is independent of ζ :

$$f_T(\zeta) = 5. \quad 3.10$$

The form of f_T suggested by Wyngaard et al. (1971) for stable conditions is:

$$f_T(\zeta) = 4.9 \cdot (1 + 2.75\zeta) \quad 3.11$$

and that suggested by Thiermann and Grassl (1992) is:

$$f_T(\zeta) = 6.23 \cdot (1 + 7\zeta + 20\zeta^2)^{1/3}. \quad 3.12$$

An iterative scheme can be used to solve Eq. 3.5 for L where $\zeta = (z-d)/L$ using each of the given forms of the empirical similarity functions f_T for unstable and stable atmospheric cases to obtain T_* , which can then be used to compute F_h , if measurements of u_* are available. Friction velocity u_* is calculated from Eq. 3.6, measurements of ε and an iterative procedure, from which the sensible heat is calculated using:

$$F_h = \rho c_p u_* T_*. \quad 3.13$$

3.3 Materials and methods

3.3.1 Measurements

Field measurements were carried out from January to December 2004 over an open, mixed community grassland site in Ashburton ($30^{\circ}27' \text{ E}$, $29^{\circ}40' \text{ S}$) close to Pietemaritzburg in KwaZulu-Natal, South Africa, (Fig. 3.1), at an altitude of 671.3 m. The surface above which the SLS was installed was nearly flat over a distance of 135 m along the prevailing S-E wind direction, with a downward slope of $1^{\circ}15'$ to the S-E (Savage et al., 2004, 2005). To the north of the study site is a residential area with tall trees. KwaZulu-Natal, on the eastern seaboard of South Africa (Fig. 3.1), is bordered by the warm Indian Ocean to the east and the high escarpment of the Drakensberg Mountains to the west. The climate is sub-tropical and humid with summer rainfall. Occasional frosts occur in winter.

A dual-beam surface layer scintillometer (SLS40-A, Scintec Atmosphärenmesstechnik, Tübingen, Germany) was set up at a height of about 1.68 metres (m) above the ground surface and the path length between the transmitter and receiver units was 101 metres.

Beam alignment, which is crucial to the SLS use, was done to ensure that the laser beam from the transmitter pointed directly to the receiver. Initial alignment was done by ensuring that the beam was located through the alignment hole on the SLS receiver. The use of two-way radios by two people, one person at the SLS receiver and the other at the transmitter, was necessary to reduce time taken alignment. After the initial alignment, final alignment was done using the SLSRUN software.

Input values of air temperature ($^{\circ}\text{C}$), atmospheric pressure (hPa), beam path length (m) and effective height (which is the beam height above the ground level minus $d + z_o$) were entered into the SLSRUN program before commencement of measurements. For each site visit, the following were checked: Error Free Data (EFD) should be greater than 25 %; the inner scale length l_o should be greater than 2 mm for the beam path distance used in this study since if l_o falls out of this range, the instrument is susceptible to measurement errors; beam distance, which should be greater than 80 % and the signal strength, which should range between 700 and 1400 digits for both beams and both channel detectors.

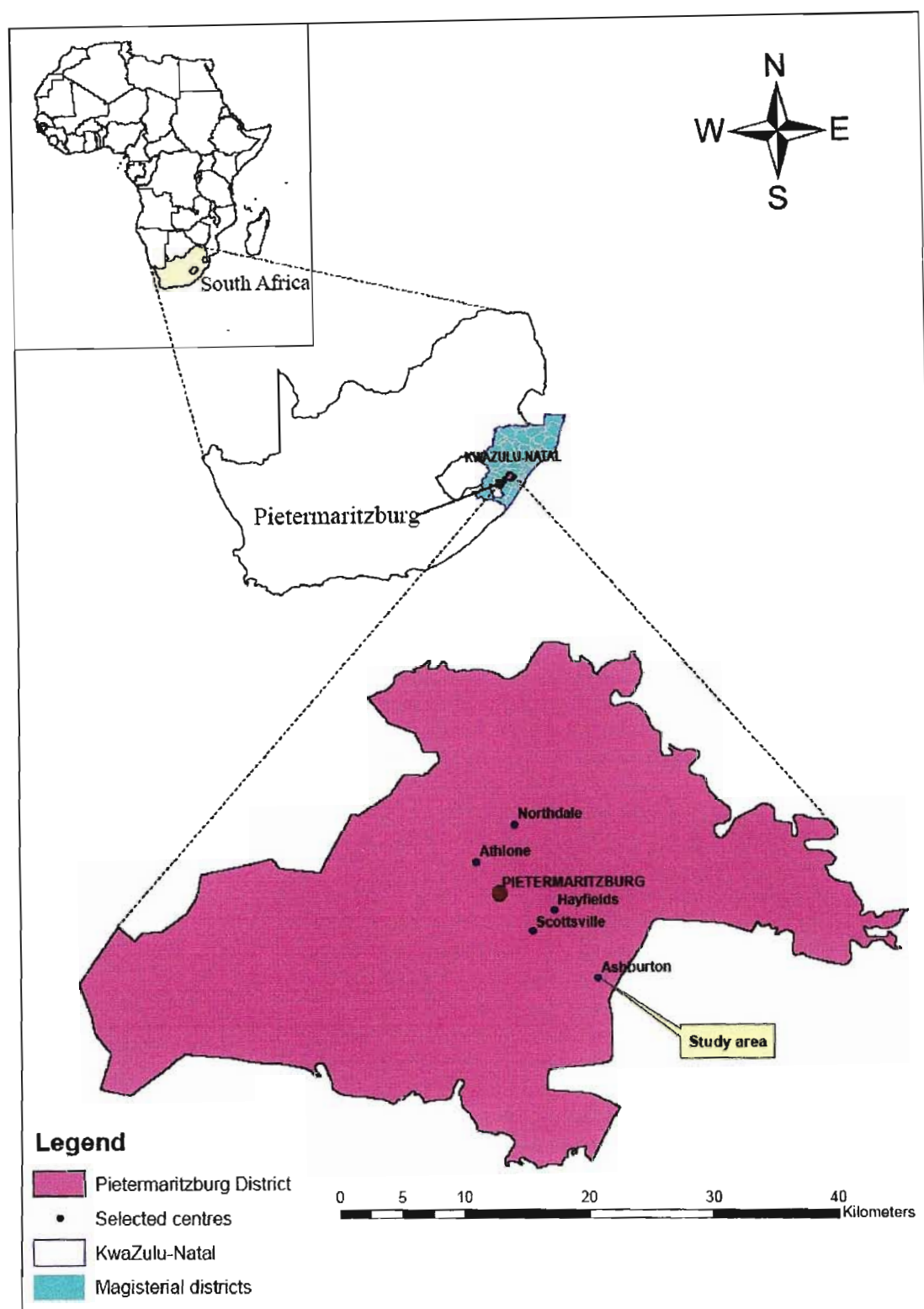


Fig. 3.1 A map showing the location of the study area. The scale is for the Pietermaritzburg district (where the study area is located).

The beam distance refers to the distance of the beam from the central position and is given in percent of the possible scan range. Zero percent means that the beam is in the centre while values close to 100 % mean that the beam reached the outer area of the scan cone. To account for future drifts a manual re-alignment should be performed if the beam distance approaches values of 80 % or greater (Scintec, 2006). The SLSRUN program automatically rejects the data if $EFD < 25\%$, $l_o < 2\text{ mm}$, the beam is cut by raindrops, insects, or the beam is misaligned.

The canopy height along the beam path length was measured using a tape measure. An EC system and BREB instruments were mounted at a height of 2 m about midway along the scintillometer beam path. The EC setup which provided sensible heat flux and friction velocity (u_*) consisted of a 3-dimensional sonic anemometer (SWS-211/3V, Applied Technologies, Boulder, Colorado, USA). Sensible heat flux was then obtained using Eq. 3.1. Sonic temperature, corrected for measured relative humidity, was used for air temperature.

Data collected using the BREB method include air temperature, measured at two heights using 75- μm type-E thermocouples; water vapour pressure, measured using a cooled dew point mirror; net irradiance, measured using four net radiometers (model Q*7 REBS, Seattle, Washington, USA); soil heat flux, measured using HFT-3 (REBS), at a depth of 0.08 m below the soil surface and a system of parallel thermocouples at depths of 0.02 and 0.06 m below the soil surface used to calculate soil heat flux stored above the soil plate; volumetric soil water content was measured using a frequency domain reflectometer (ThetaProbe model ML2x, Delta-T Devices, Cambridge, UK) with the sensor inserted from the surface to a depth of 0.06 m.

3.3.2 Data collection and analysis

Online measurements of sensible heat flux, and dissipation rate of turbulent kinetic energy, were obtained from the SLS from which 2-min averages were calculated for comparison with sensible heat flux measured using the EC method. The measurement frequency of the SLS method is 1 kHz compared to 10 Hz for the EC method and 1 Hz for the BREB method. The EC and BREB data were downloaded from the two 23X data loggers used and transferred to a computer spreadsheet for further manipulation and analysis. The SLS data that did not meet certain specifications were rejected using a filtering procedure so that only data that falls within the defined limits were used for analysis. For instance, SLS data were rejected if the percentage of

error free data (EFD) was less than or equal to 25 % and inner scale length was less than or equal to 2 mm.

3.4 Results and discussion

3.4.1 Comparison of C_T^2 measured by SLS and C_T^2 corrected for β

Assuming that there is no error in air temperature T and atmospheric pressure P , and that air temperature and humidity fluctuations are strongly correlated, C_T^2 is a function of C_n^2 , T , P and Bowen ratio β (Eq. 3.3). Calculated C_T^2 values (Eq. 3.3) were compared with the C_T^2 values measured by SLS. This was done to check for any significant differences between the C_T^2 corrected for β and the uncorrected C_T^2 values measured directly by SLS. The assumption that $\beta \gg 0$ is made (Eq. 3.3).

The C_T^2 values, calculations from measurements of C_n^2 were corrected for β . The β value was obtained by dividing the 20-min sensible heat flux and latent energy flux obtained using the BREB method. In Figs 3.2, 3.3 and 3.4 linear regression of the corrected and measured C_T^2 , including the error mean squared (EMS) of the measurements, are shown for each figure. The agreement between the C_T^2 values is nearly perfect, with $R^2 = 0.998$ ($n = 15\ 836$), with a slope of 0.901, for DoY 116 to 138 (2004), (Fig. 3.2) and $R^2 = 0.997$ ($n = 19\ 897$) with a slope of 0.891, for DoY 138 to 180 (2004) (Fig. 3.3). The same is the case with Fig. 3.4 which shows the corrected C_T^2 plotted against the measured values for DoY 274 to 340 (2004), with R^2 being 0.996 ($n = 32\ 662$) with a slope of 0.895. From the slope values (less than 1) there appears to be a very slight bias in the measured C_T^2 , but this is very small. The bias from the 1:1 line, which is consistent for all the days for which comparisons were done, indicates that the corrected C_T^2 values are slightly greater than the measured ones. The diurnal plot of C_T^2 for DoY 312 to 314 is shown in Fig. 3.5. The mean value for β during the study period was 1.0, with a range of -10 to 10. For most of the time β was between 0 and 3 (Fig. 3.6). The good agreement between the corrected C_T^2 and measured C_T^2 by SLS with no correction for β was also consistent throughout the different seasons, both warm summer and cold winter seasons.

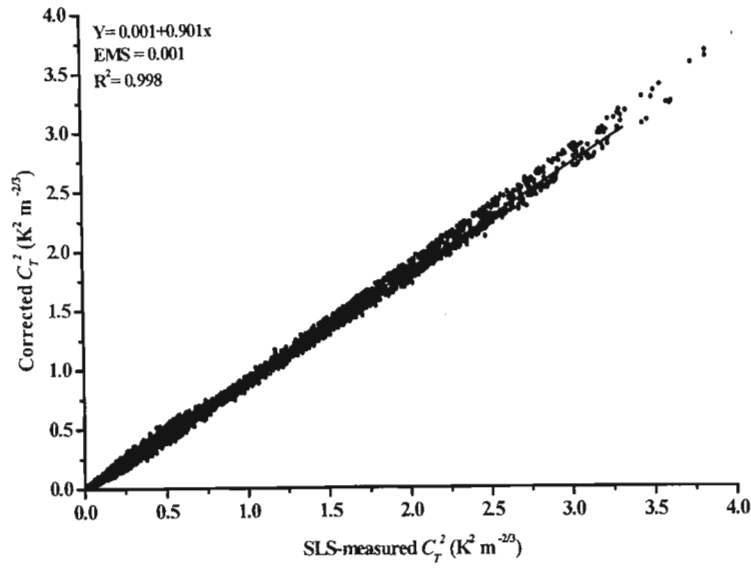


Fig. 3.2 Comparison of 20-min SLS-measured C_T^2 with that corrected for β for DoY 116 to 138, (April to May) 2004, corresponding to summer season when weather condition is warm.

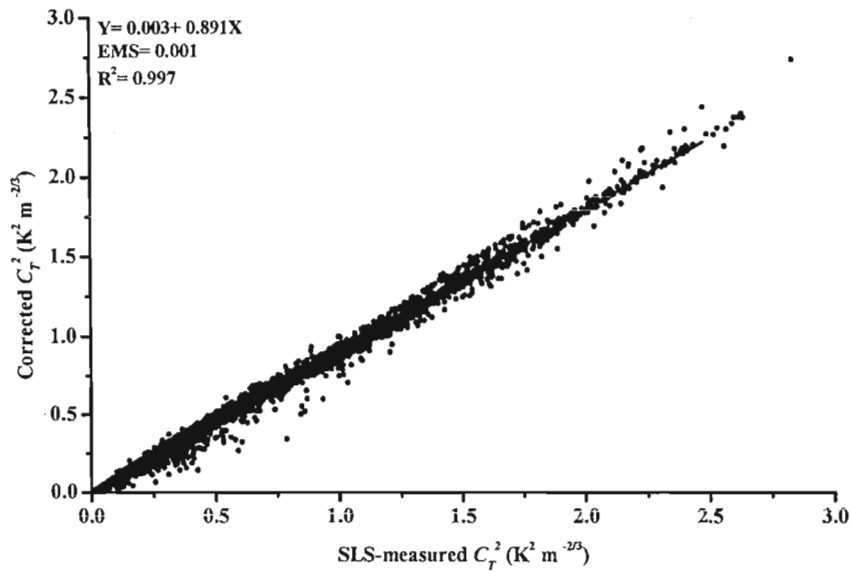


Fig. 3.3 Comparison of 20-min SLS-measured C_T^2 with that corrected for β for DoY 138 to 181 (May to June) 2004, corresponding to end of autumn and winter seasons.

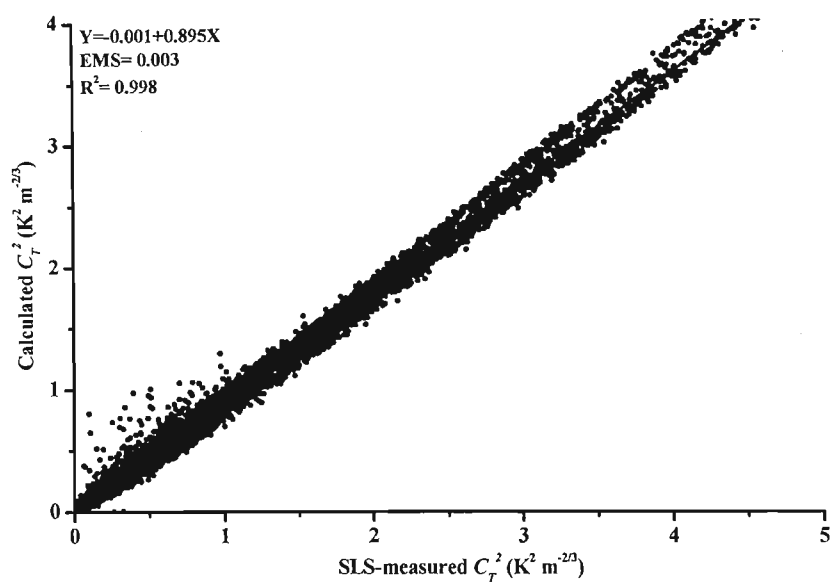


Fig. 3.4 Comparison of 20-min SLS-measured C_T^2 with that corrected for β for DoY 274 to 340 (October to November) 2004, corresponding to summer season when weather condition is warm.

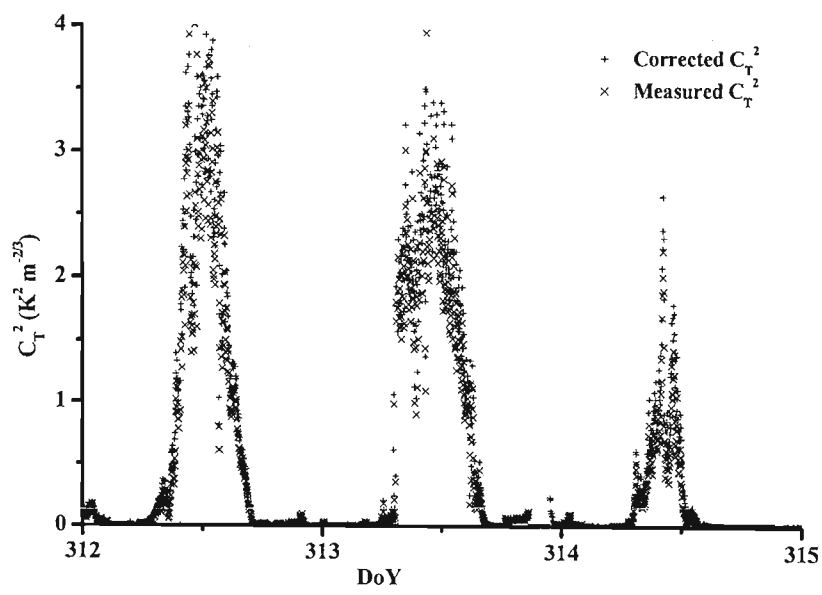


Fig. 3.5 Diurnal plot of 2-min measured C_T^2 and C_T^2 corrected for β for DoY DoY 312 to 314 (November) 2004, corresponding to summer season when weather condition is warm.

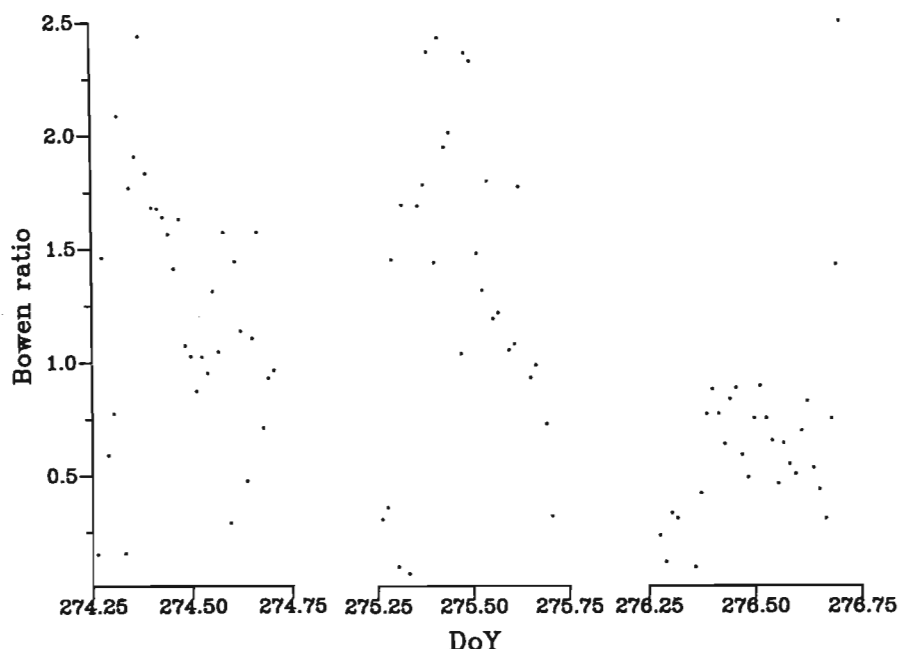


Fig. 3.6 Time series plot of the 20-min Bowen ratio values for DoY 274 to 276 (November) 2004, corresponding to summer season when weather condition is warm.

As can be seen from the diurnal plots of the same variables (β -corrected and measured C_T^2) (Fig. 3.5) the two sets of data show similar trend without much variation from each other, confirming the good agreement observed by the high coefficient of determination values as already shown in the linear regression plots. Scatter around midday when the C_T^2 values are highest is noted. At this time the two data sets appear not to very agree well but still display a similar diurnal trend. Around the same time, the measured C_T^2 appears to be slightly greater than the corrected values resulting in the stated slope bias of about 10 % overestimation in the measured C_T^2 .

A time series plot of the Bowen ratio values over the period 06:00-18:00 for DoY 274 to 276 is shown in Fig. 3.6.

3.4.2 Comparison of SLS- and EC-measured sensible heat flux

In this section, the F_h values obtained by the EC and SLS methods for different Bowen ratio values covering different seasons of the year are compared. This was done to capture periods of

rainfall and high humidity and also dry seasons when Bowen ratio values are expected to be different. Statistical analysis of F_h measured by both EC and SLS methods are compared for small ($\beta < 0.6$) and large ($\beta > 0.6$) Bowen ratio values.

Both the EC and SLS methods are humidity dependent through the Bowen ratio. For the SLS method, the dependence is determined using Eq. 3.3. For the EC method, the dependence is via the relationship:

$$F_{h\text{corrected}} = F_{h\text{ EC measured}} / (1 + 0.07 / \beta). \quad 3.14$$

(Lumley and Panofsky, 1964). The correction is due to the humidity dependence of the speed of sound and its effects on the sonic temperature (Lumley and Panofsky, 1964).

A sensitivity analysis of the influence of the Bowen ratio on F_h measurements by the SLS method also indicates that for Bowen ratio values less than 1.0, there is an increased influence of the Bowen ratio on F_h measurements.

In Fig. 3.7 (a), the relative error resulting from not correcting F_h measured by the EC and SLS methods is shown. The correction to the EC measurements of sensible heat flux for the humidity dependence of the speed of sound dependent sonic temperature (Eq. 3.14) is similar to the correction for the SLS measurements (Fig. 3.7 a). For $\beta > 0.74$, the relative error is greater for the EC measurements than for the SLS measurements. The differences between the corrected and non-corrected F_h measurements are also shown in Fig. 3.7 b. The differences in SLS F_h values (Fig. 3.7 b) range from 4 to 33 W m⁻². In Table 3.1 the statistical analysis results obtained by the EC and SLS methods for different β values are presented. The correction for β for both EC and SLS methods is shown (Fig. 3.7). The EC method shows greater dependence on β than the SLS method for $\beta < 0.74$. The comparison between the sensible heat flux measurements obtained by the SLS against the ones obtained by EC for $\beta < 0.6$ and $\beta > 0.6$ are presented in Figs 3.8 to 3.10. In Fig. 3.11 the diurnal plots for the sensible heat flux measurements are presented.

The EC method shows less dependence on β for $\beta > 0.6$ than the SLS method but appears to be more dependent on β for $\beta < 0.6$ (Fig. 3.7 a). But generally, the measurement of F_h by the two methods correspond well for β values of 0.3 to 0.6. This is as also reflected in the diurnal plots of F_h measured by the EC and SLS methods as shown in Fig. 3.10 (a) and (b).

Table 3.1 Statistical analyses results of 2-min F_h obtained using EC¹ and SLS² methods for different β values.

Fig.	DoY (2004)	h_{canopy} (m)	β	n	R^2	t -value	t -table	Slope
3.8a	110 to 117	0.71	< 0.6	682	0.757	52.90	1.9635	0.755
3.8b	110 to 117	0.71	> 0.6	623	0.751	49.94	1.9638	0.778
3.9a	145 to 152	0.20	< 0.6	847	0.709	53.89	1.9628	0.843
3.9b	145 to 152	0.20	> 0.6	861	0.681	51.89	1.9627	0.758
3.10a	274 to 341	0.19	< 0.6	835	0.910	96.21	1.9628	0.967
3.10b	274 to 341	0.19	> 0.6	829	0.939	116.44	1.9628	1.055

1. The measurement height from ground level for the EC system was 2 m.
2. The measurement height from ground level for the SLS system was 1.68 m.

Some studies have found that sensible heat flux measured by the SLS method needs to be corrected for the Bowen ratio (Green and Hayashi, 1998; Meijninger and de Bruin, 2000). Green and Hayashi (1998), for example, used a large aperture scintillometer above a paddy field, with its great evaporation. They suggest the need for some correction for the water vapour pressure to scintillometer estimates of F_h under low Bowen ratio. However, even in their case, the difference between corrected and uncorrected sensible heat flux was about 5 % at most. Both EC and SLS estimates of F_h are almost equally affected by the Bowen ratio correction and this therefore tends to mask the need for correction for β for the SLS method.

Noticeable in the linear regression plots is also the fact that there is some departure of the values obtained by the EC and SLS methods from the 1:1 line especially when the sensible heat flux is greater than 100 W m^{-2} . This is more clearly visible in Figs 3.8 a and 3.9 a, and diurnal plots (Fig. 3.11), where the two methods result in more scattered values around midday when the F_h values are larger. Also, the agreement between the F_h measurements by the two methods is much improved on days when the measured F_h values are large e.g. greater than 300 W m^{-2} (for DoY 274 to 341 (Fig. 3.10) i.e. warm summer months of October through to December.

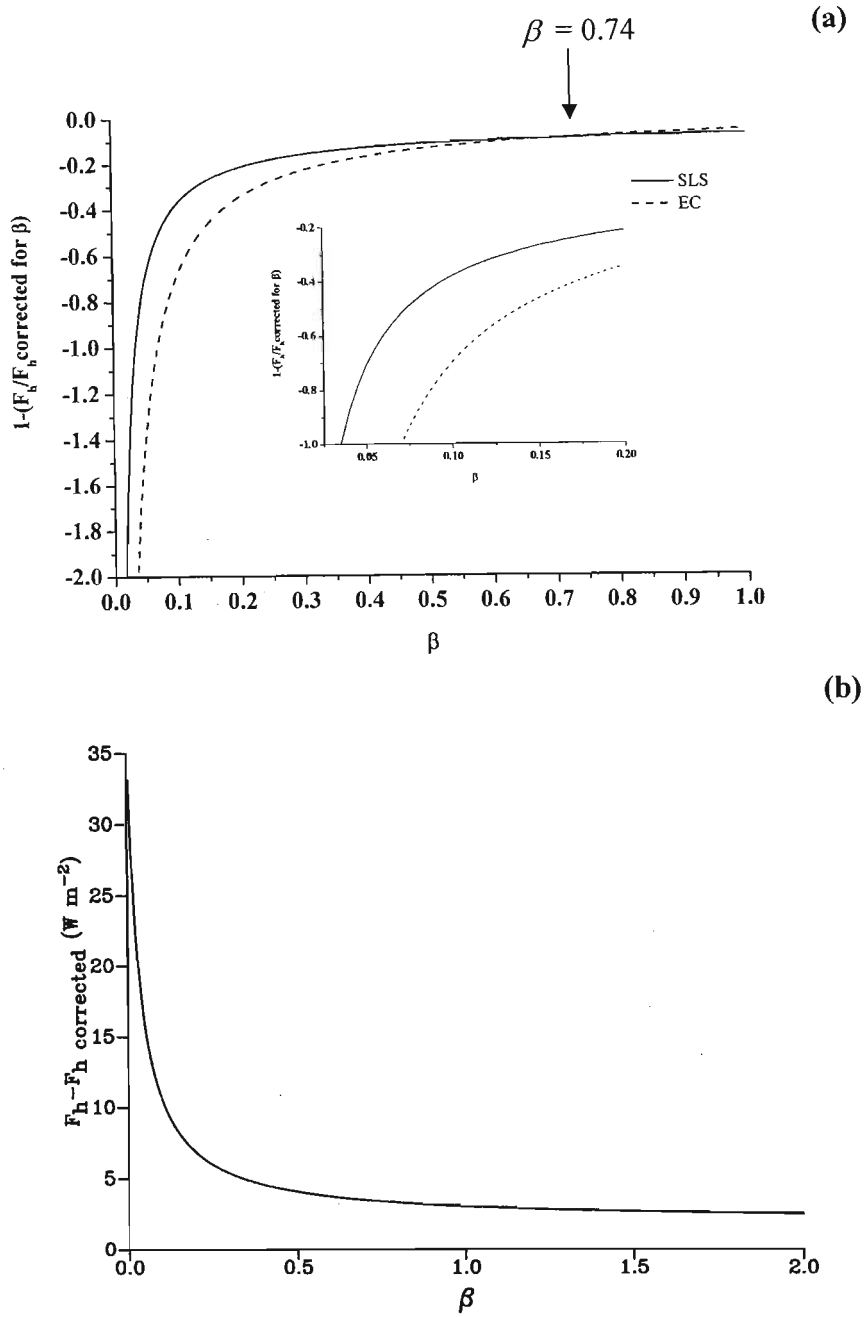


Fig. 3.7 (a) Relative error for both EC and SLS measurements (the inset graph shows the relative error values confined between -1.0 and -0.2) and (b) differences between the corrected (using simulated Bowen ratio values) and uncorrected (measured) sensible heat values measured by the EC and SLS methods (DoY 279, 14h00). The actual Bowen ratio value for this time period was 0.05 and sensible heat flux was 16.1 W m^{-2} .

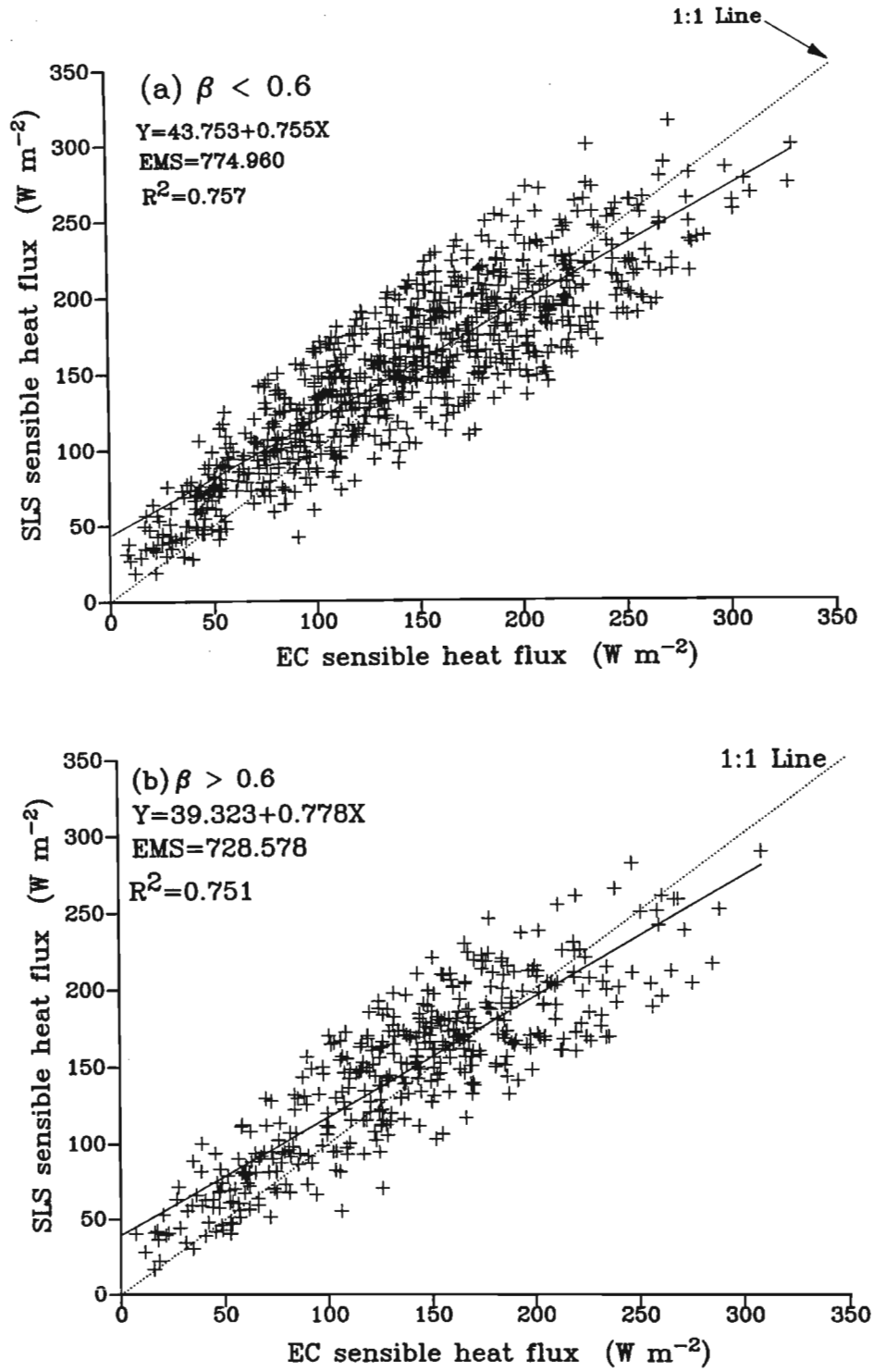


Fig. 3.8 Comparison between 2-min sensible heat fluxes derived from EC and SLS when (a) $\beta < 0.6$ and (b) $\beta > 0.6$, for DoY 110 to 117.

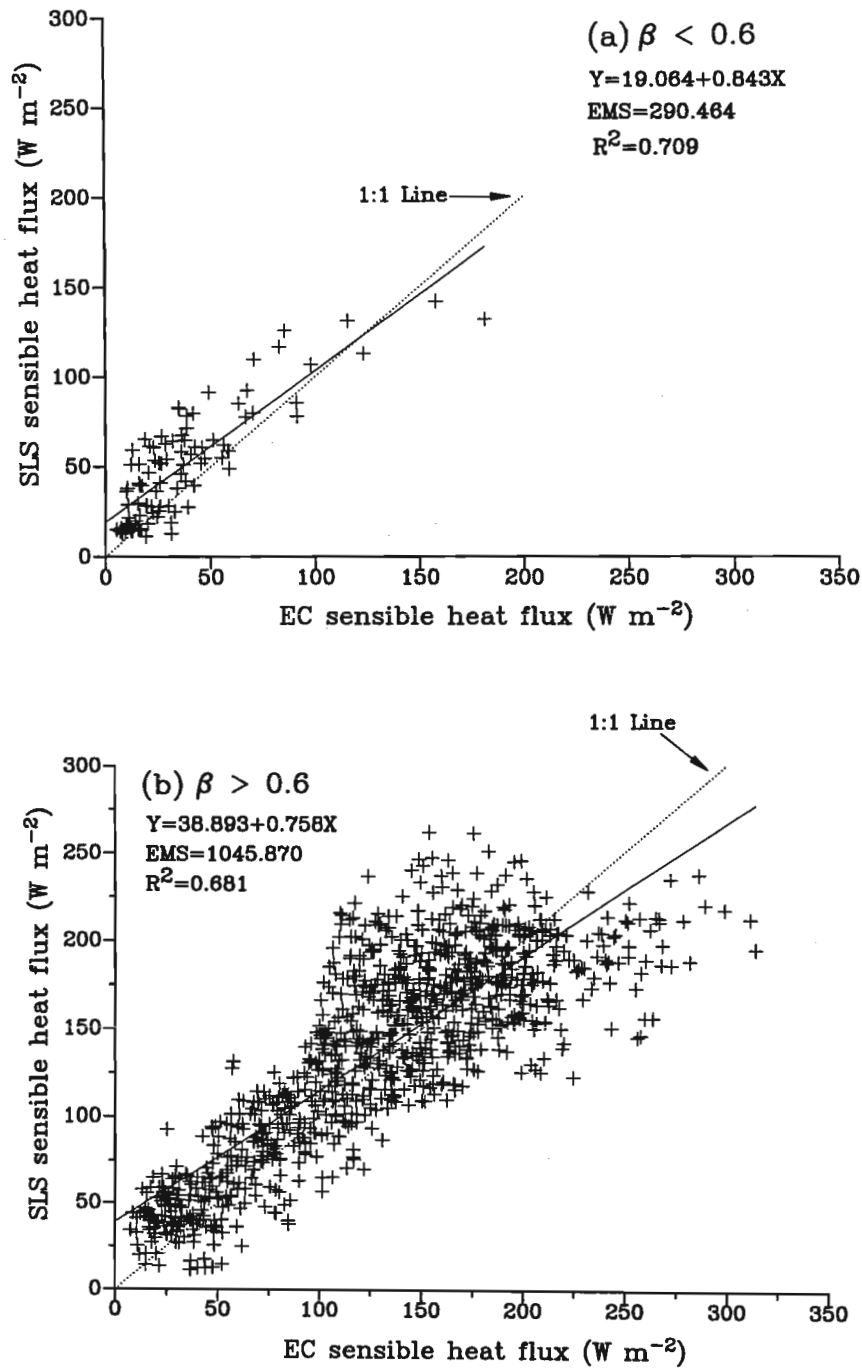


Fig. 3.9 Comparison between 2-min sensible heat fluxes derived from EC and SLS when (a) $\beta < 0.6$ and (b) $\beta > 0.6$, for DoY 145 to 152.

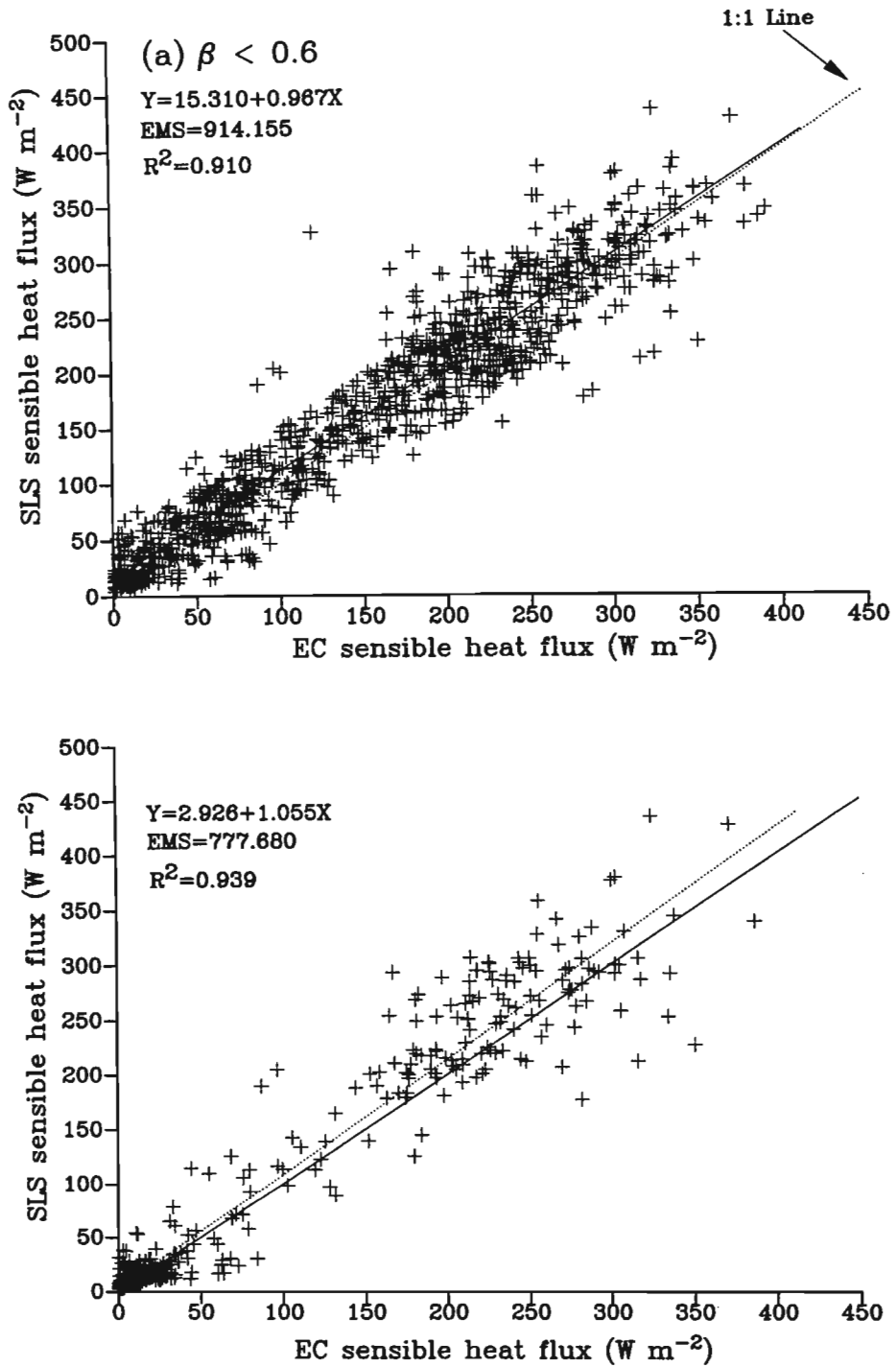
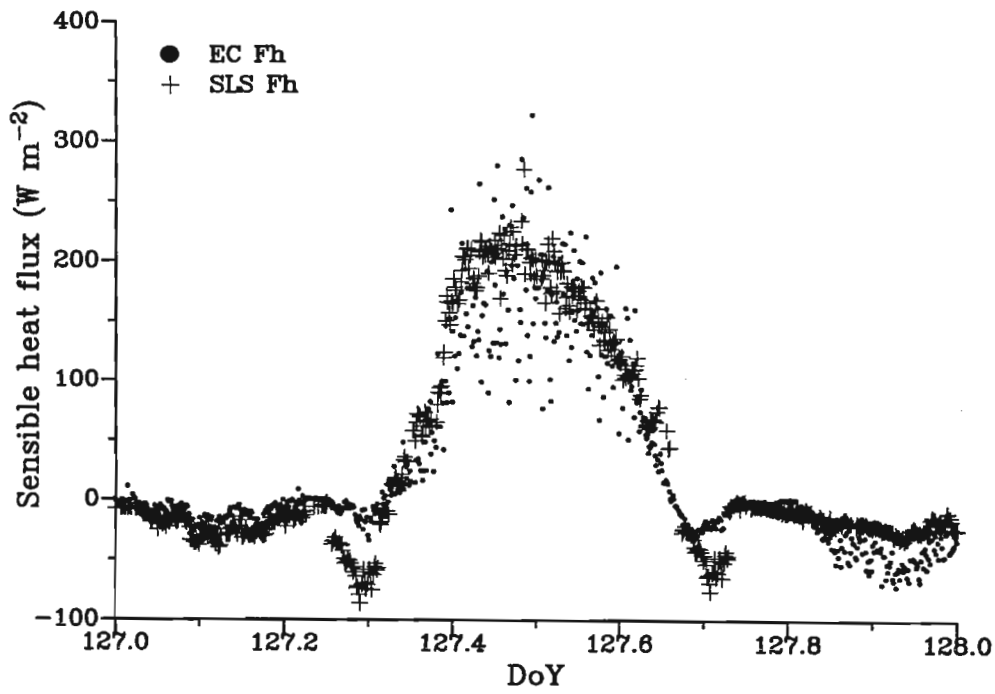


Fig. 3.10 Comparison between 2-min sensible heat fluxes derived from EC and SLS when (a) $\beta < 0.6$ and (b) $\beta > 0.6$, for DoY 274 to 341.

(a)



(b)

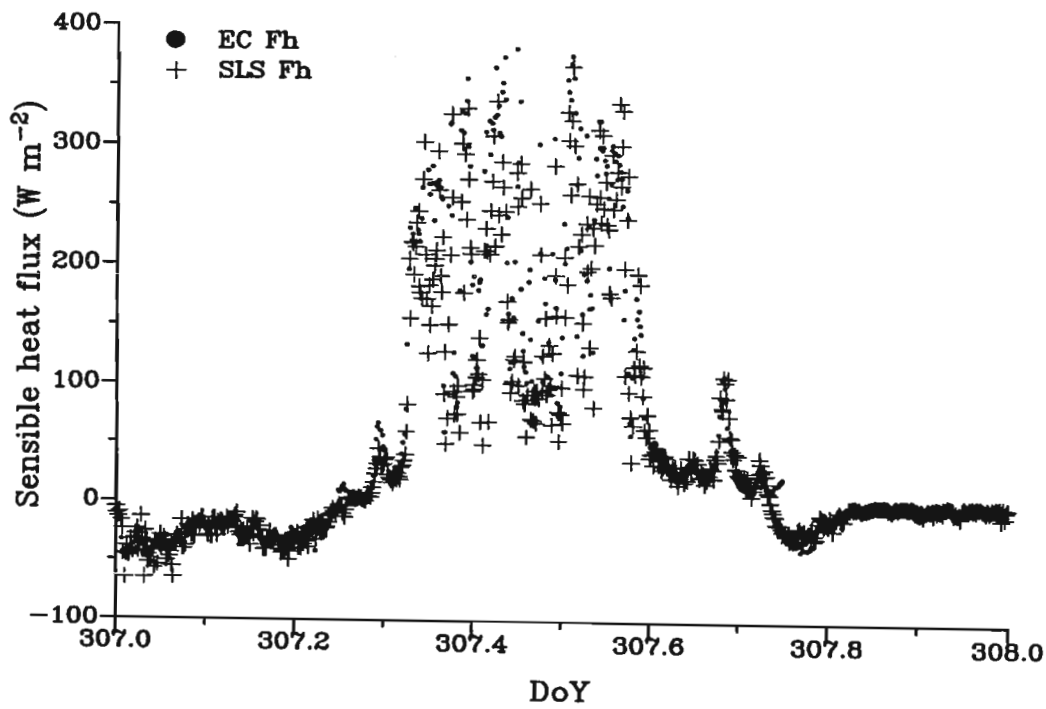


Fig. 3.11 An example of diurnal plots of 2-min sensible heat flux measured by EC and SLS for (a) DoY 127 and (b) DoY 307.

Although the agreement between the sensible heat flux values obtained by the two methods is improved for Bowen ratio values greater than 0.6, the difference in the regression values (obtained from comparisons of EC and SLS measurements when $\beta > 0.6$ and when $\beta < 0.6$) is not significantly large (Figs 3.8 to 3.10) so as to warrant correction for humidity in the case of SLS measurements of sensible heat flux in this study, as suggested by de Wekker (1996) (Eq. 3.3) as they are both affected similarly by β . This is also supported by the closer agreement between the measured and corrected C_T^2 . Meijninger and de Bruin (2000), however, reported that the scintillometer sensible heat flux depends on the Bowen ratio and that a variation of the Bowen ratio from 0.3 to 1 causes a variation in the sensible heat flux by about 15 %, although their argument is based on expected or roughly-approximated Bowen ratio values and not what was actually measured at the same site where the sensible heat flux measurements were obtained. In their study, they used a large aperture scintillometer for measurements of sensible heat flux over irrigated areas. Considering that the two methods are independent flux-measuring methods, relying on such different physical principles, with the SLS method providing an integrated value of the sensible heat flux over the beam path, which in the present study was 101 m, and the EC method on the other hand is essentially a point measurement, the agreement in the F_h obtained by the two methods can be considered very good.

Other studies carried out before (for example Thiermann 1992, Thiermann and Grassl, 1992; Green et al., 1994; Savage et al., 2004, 2005) have found close agreement between the EC and SLS F_h measurements, the latter considered as the standard method for surface energy flux measurements.

The study by Thiermann and Grassl (1992) was carried out in a stubble field surrounded by flat and agriculturally-used terrain. In the case of the study by Green et al. (1994), over a thyme canopy in a semi-arid environment and pasture sward well supplied with water (Table 1.3), there was near-perfect agreement between the F_h values measured by EC and SLS and no correction of SLS data for Bowen ratio was applied. The small disagreement in measurements of F_h by the two methods would most likely be due to the fact that the SLS senses the sensible heat flux from a larger footprint than for the EC measurement method. However, there may also be differences due to the SLS method being dependent on MOST and the EC method not.

It therefore appears that not correcting F_h measurements for the Bowen ratio is a lesser issue in applying the SLS method as suggested by Savage et al. (2004) but should nonetheless be considered as a possible cause of slight variation in F_h measurements by the SLS method. Overriding influences such as MOST being applied for the SLS method but not for the EC method, differences in areal SLS measurements and point EC measurements and that sonic temperature is used for EC measurements instead of the actual air temperature may be masking the influence of the Bowen ratio on the SLS measurements. Also, the error correction of the EC F_h measurements for β is similar to that for the correction for the F_h measurements by the SLS method, as demonstrated in Fig. 3.7 a. These findings show that the SLS method can be used even over very humid surfaces although correcting the F_h values for Bowen ratio may be necessary. The correction for the SLS measurements use Eq. 3.3 for which the percentage difference between SLS-measured and actual sensible heat flux is greater in magnitude than if Eq. 3.4 were applied. In general therefore, the correction magnitude would be less. Further studies over different kinds of vegetation cover as well as surfaces of different soil water content would be necessary for a complete and more conclusive understanding, in this regard.

3.4.3 Analysis of sensible heat flux using different forms of the MOST similarity function f_T

In this section, results of the analysis of the F_h values calculated using the various MOST similarity functions are presented.

In Figs 3.12 and 3.13, diurnal plots of the computed F_h values together with the ones measured by the EC system are shown. It can be noticed from the plots that there is a clear difference in F_h , in some cases by a wide margin, with the method suggested by de Bruin et al. (1993) resulting in lower F_h values than the other two. This is also noticed for DoY 275 (Fig. 3.13) as well as in other days whose results are not presented here.

Sensible heat flux computed using the method suggested by Wyngaard et al. (1971) for the unstable condition results in values nearly comparable to the ones obtained by Thiermann (1992) (cited by Thiermann and Grassl, 1992).

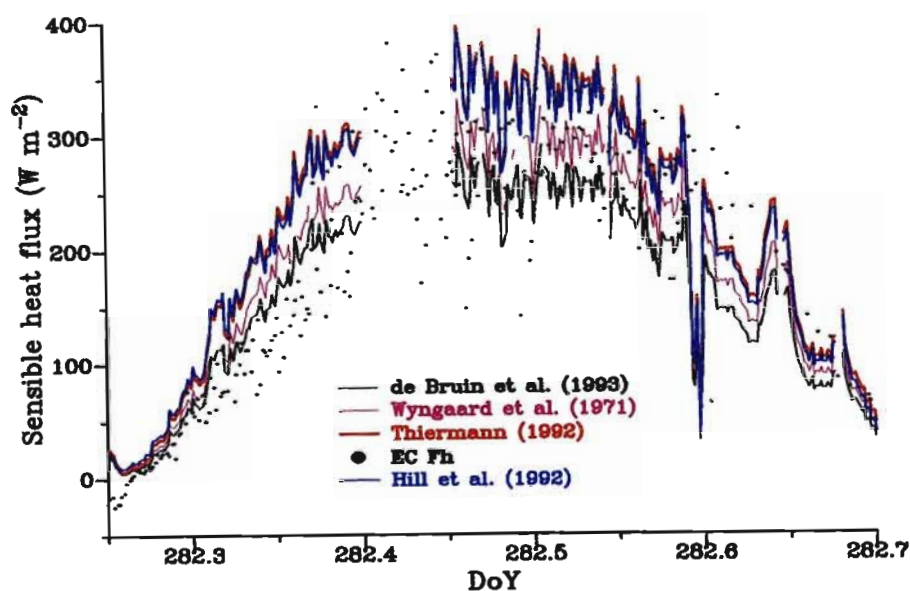


Fig. 3.12 Comparison of the 2-min sensible heat flux obtained using the different forms of the similarity function f_T with that for the EC method for DoY 282.

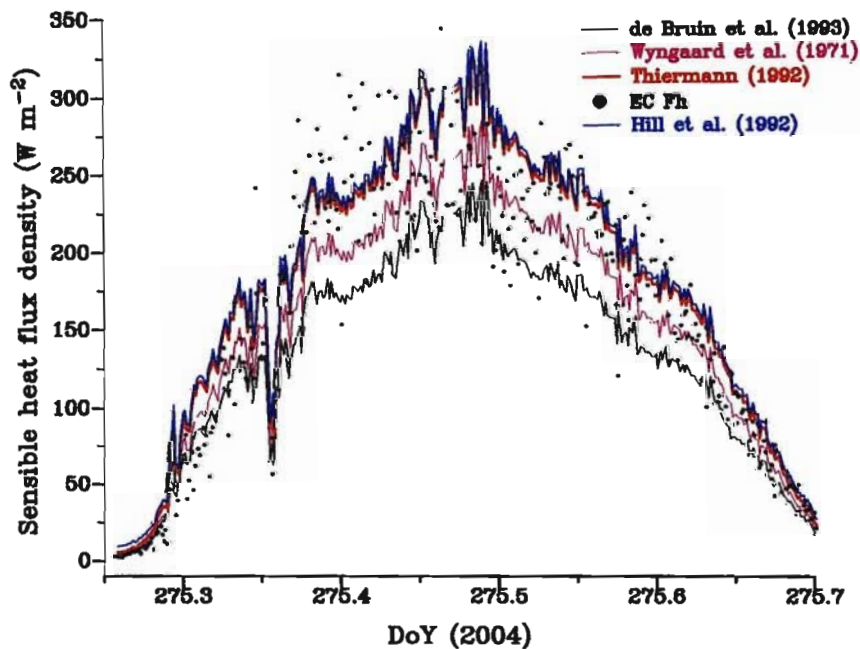


Fig. 3.13 Comparison of the 2-min sensible heat flux obtained using the different forms of the similarity function f_T with that for the EC method for DoY 275.

The sensible heat flux obtained using the method suggested by Hill et al. (1992) corresponds even more closely with that obtained using the method by Thiermann (1992) (Fig. 3.13). The EC values of F_h also compare well with those obtained by the Thiermann (1992) and Wyngaard et al. (1971) methods but not so well for the method of de Bruin et al. (1993). The differences are confirmed by calculating the percentage differences relative to F_h estimates using the method of Thiermann (1992). In Figs 3.14 to 3.15, the percentage difference obtained by comparing the F_h values obtained using either the de Bruin et al. (1993) ($\pm 25\%$) or Wyngaard et al. (1971) (up to $\pm 18\%$) methods are plotted against those obtained using Thiermann's method.

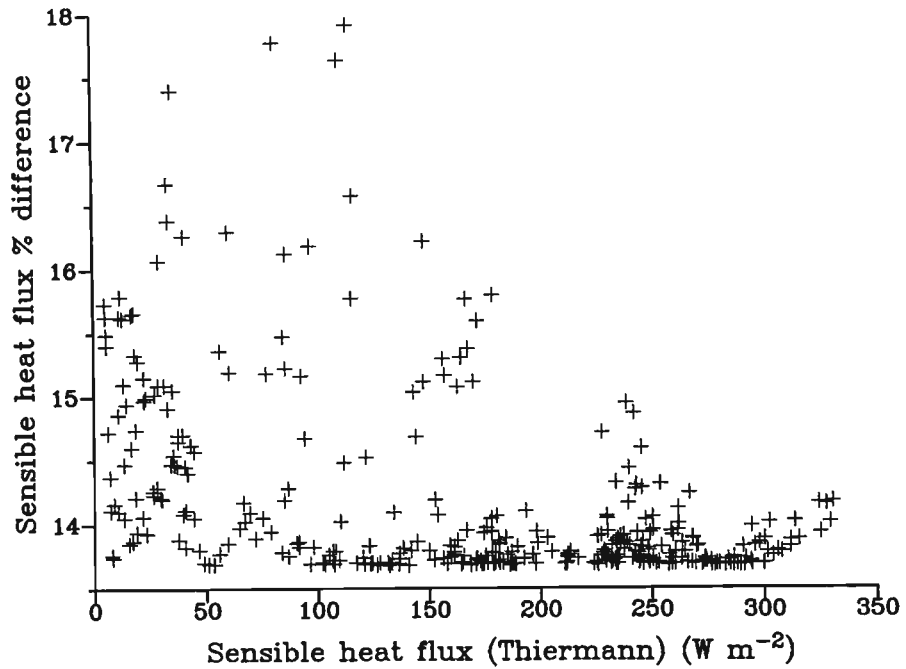
From the plots, F_h values computed following the similarity functions suggested by de Bruin et al. (1993) lead to larger percentage differences compared to the ones calculated using the method suggested by Wyngaard et al. (1971). The percentage difference obtained for DoY 275 using the method suggested by Wyngaard et al. (1971) ranges from 13.5 to 18.0 % (Fig. 3.14 a). For the same DoY (275), the percentage difference values obtained using de Bruin's method as compared to Thiermann's method ranges from 25.6 to 25.8 % (Fig. 3.14 b).

In Fig. 3.16, the percentage difference obtained by comparing the F_h values obtained using Thiermann's method with the F_h measured by the EC method are presented. From Fig. 3.16 it can be observed that F_h as measured by EC methods compares closely with SLS estimates of F_h when Thiermann's similarity function is employed in preference to alternative similarity functions, with the percentage difference ranging from 0.4 to 8.5 %.

Also noted is the fact that the F_h percentage differences seem to decrease as F_h increases, for both Thiermann's and de Bruin's methods (Fig. 3.14).

The same pattern is observed for DoY 282 when the percentage difference obtained from the analysis using the method suggested by Wyngaard et al. (1971) is from 13.5 to 18.0 % (Fig. 3.15 a) whereas the range of percentage difference obtained from the analysis of sensible heat flux computations using method suggested by de Bruin et al. (1993) compared to that of Thiermann's ranges from 25.6 to 25.7 % (Fig. 3.15 b). Also noticed from the analysis is that the percentage difference obtained from the de Bruin et al. (1993) method varies more for low sensible heat flux values ($F_h < 50 \text{ W m}^{-2}$) but becomes nearly constant as F_h increases (Figs 3.13 and 3.15).

(a)



(b)

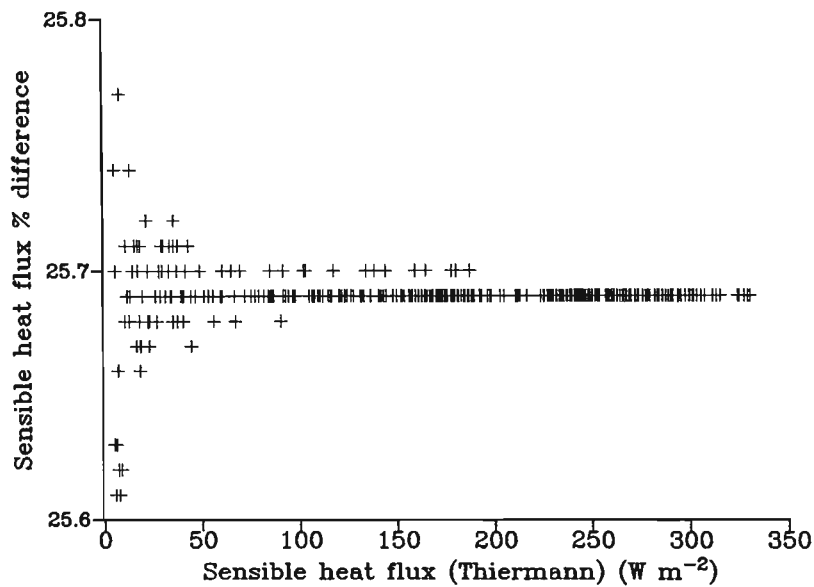


Fig. 3.14 Percentage differences between the 2-min F_h values obtained using the similarity functions suggested by Thiermann (1992) and (a) Wyngaard et al. (1971), and (b) de Bruin et al. (1993), for DoY 275.

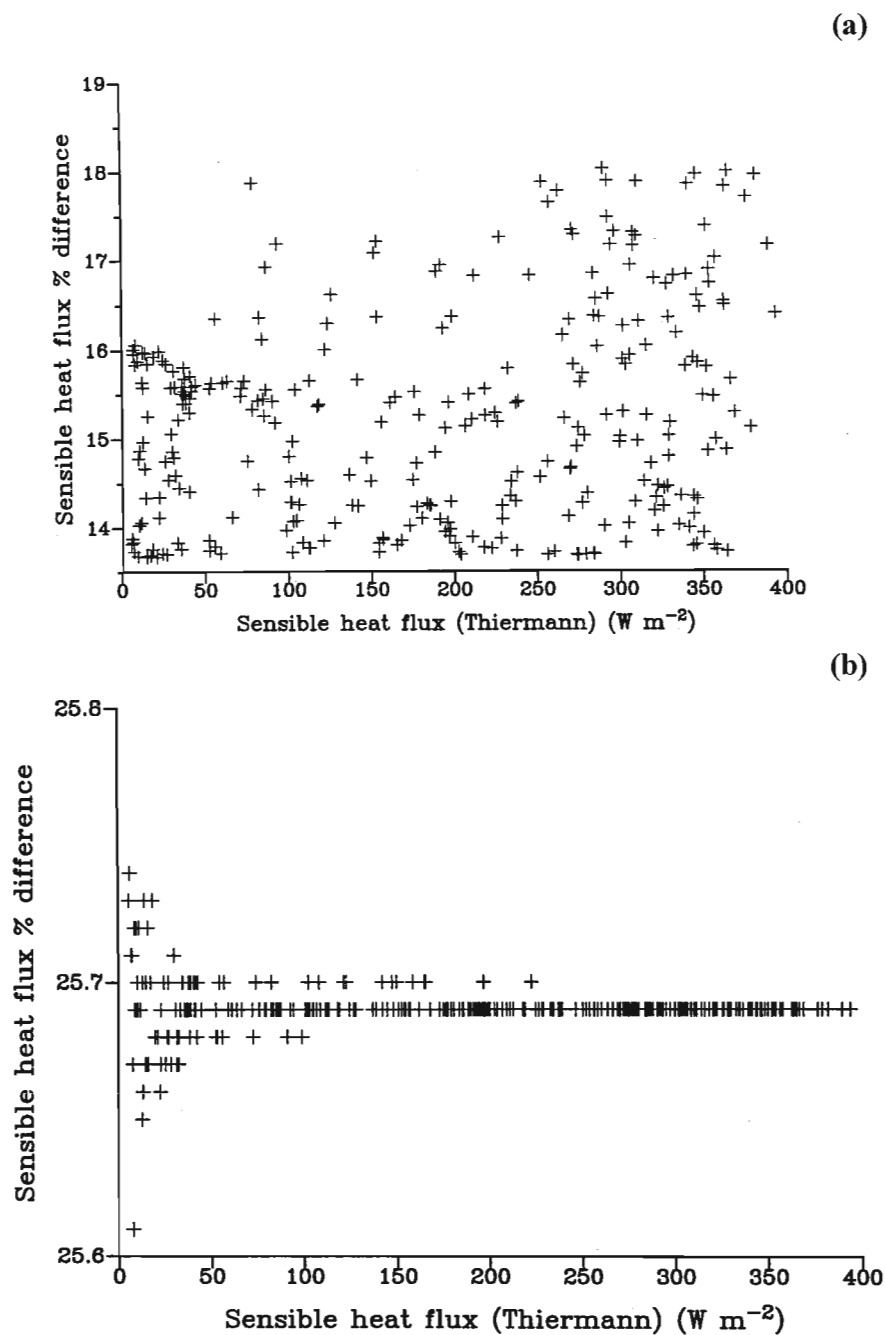


Fig. 3.15 Percentage differences between the 2-min F_h values obtained using the similarity functions suggested by Thiermann (1992) and (a) Wyngaard et al. (1971), and (b) de Bruin et al. (1993), for DoY 282.

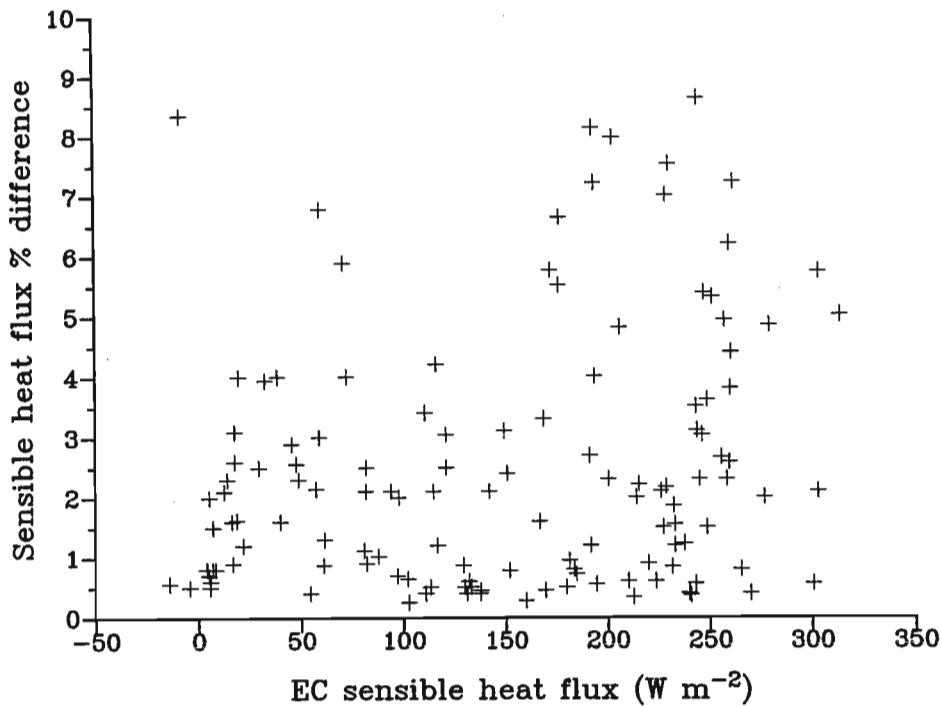


Fig. 3.16 Percentage differences of the 2-min F_h values obtained using the similarity function method suggested by Thiermann and Grassl (1992) for DoY 275 compared with F_h obtained using the EC method.

On the other hand, the percentage differences obtained from a comparison between the sensible heat flux obtained using the EC method and that computed using the method suggested by Thiermann and Grassl (1992) are within the range of 0 to 9 % (Fig. 3.16), which is less than that obtained by the methods of de Bruin et al. (1993) and Wyngaard et al. (1971) (data not shown). Since the EC method is used as the standard method for measuring turbulent fluxes, it can be concluded from these findings that the method proposed by Thiermann and Grassl (1992) results in more correct F_h values and those by de Bruin et al. (1993) and Wyngaard et al. (1971) underestimate F_h . On this particular day however, the percentage difference between the F_h values obtained by the method by Wyngaard et al. (1971) and those obtained by Thiermann and Grassl (1992) remain large even when F_h values get larger.

These findings seem to be in agreement with those by Savage (2007) who carried out an analysis of the variation of the relative difference in F_h calculated using the MOST similarity functions suggested by Wyngaard et al. (1971), Hill et al. (1992) and de Bruin et al. (1993), with stability (given as $-z/L$). In his study, Savage (2007) noted that the relative percentage difference in F_h obtained using the MOST similarity function suggested by Hill et al. (1992) with those obtained by the MOST similarity functions suggested by Thiermann (1992) are less than the ones obtained using the Wyngaard and the de Bruin methods. The relative difference in F_h calculated using the MOST similarity functions suggested by Wyngaard et al. (1971) and de Bruin et al. (1993) follow a similar trend although the F_h obtained using the MOST similarity functions suggested by de Bruin et al. (1993) differ more with those calculated using the MOST similarity functions suggested by Thiermann (1992).

From these results it is observed that the different methods for computing the MOST similarity functions suggested by different authors result in slightly different F_h values and therefore caution should be exercised in the choice of method used in computing the similarity function. The methods suggested by Thiermann (1992) and Hill et al. (1992) result in F_h values which compare very well with the corresponding EC values, currently used as the standard method for the measurement of turbulent fluxes.

3.5 Conclusions

The study was carried out from January to December, 2004 at a mixed community grassland site to compare the sensible heat flux measurements by the EC and SLS methods, the SLS method depends on the Bowen ratio and various MOST similarity functions.

First, a comparison of the calculated and SLS-measured C_T^2 (calculated from C_n^2) was carried out, with the results showing very good agreement between the two, indicating that even without correcting the F_h for Bowen ratio does not result in statistically significant variations in the resulting C_T^2 values, and hence sensible heat flux measurements.

Comparison of the sensible heat flux measured using EC and SLS methods for $\beta < 0.6$ and $\beta > 0.6$ show good correspondence between the values obtained using the EC and SLS methods, although the agreement is slightly improved for cases when $\beta > 0.6$. A sensitivity

analysis further confirms that the influence of β on SLS sensible heat flux measurements results in a change of SLS measurements to within 20 W m^{-2} . A sensitivity analysis on the influence of β on F_h measurements by both the EC and SLS methods further indicate that the influence of β on F_h measurements is not large enough to warrant correcting the F_h measurements for β . The F_h measurements by the EC method appears to be influenced more by the β especially for β values greater than 0.7. Hence, the SLS-measured sensible heat values require no correction for β and allows for long-term and continuous sensible heat flux measurements using the SLS method since the values obtained compare very well with that using the EC method which is considered the standard method for surface flux measurement.

In spite of the fact that the EC method is used as the standard for F_h measurement, this estimate is also dependent on humidity through the speed of sound estimate used for the sonic temperature calculation. The correction of the EC measurements of F_h for the humidity dependence of the speed of sound dependent sonic temperature is similar to the correction for the SLS measurements. However, sensitivity analysis of the influence of β on the F_h measurements by the EC method shows that the relative error for uncorrected EC measurements of F_h is greater than for those measured by the SLS method for $\beta < 0.74$.

The SLS method offers the advantage of a larger measurement footprint than the EC method does. It would therefore be a preferred method for a wide area (within the limit of 50 to 250 m) measurements of sensible heat and latent energy flux measurements which are crucial in hydrological modelling, microclimate and micrometeorological studies, and environmental studies. In view of the fact that the MOST similarity functions are used to obtain SLS-derived sensible heat flux, the role of stability on these estimates needs to be investigated further. This role is investigated in Chapter 4.

A comparison of the various methods for computing the empirical similarity functions used by MOST was also carried out and the results show a significant difference in the F_h computed following the various MOST methods suggested by different researchers when compared to the EC measurements. The results show that the empirical functions suggested by de Bruin et al. (1993), especially, results in F_h values which differ more from the F_h values obtained using the other methods. Larger percentage differences were obtained from the analysis

using the empirical functions suggested by de Bruin et al. (1993) compared to those used by Thiermann and Grassl (1992). The proposed functions used by Thiermann and Grassl (1992) results in F_h estimates which correspond more closely to EC measurements, which is a standard method for measuring turbulent fluxes. The other functions used by de Bruin et al. (1993) and Wyngaard et al. (1971) result in lower F_h estimates compared to the EC measurements, with the one by de Bruin et al. (1993) resulting in the largest difference i.e. far lower values of F_h than the EC measurements. The method used in computing the similarity functions should therefore be carefully chosen since the different functions used lead to F_h percentage differences that are as high as 25.6 %.

Chapter 4: Comparison of sensible heat flux as measured by surface layer scintillometer and eddy covariance methods under different atmospheric stability conditions

4.1 Introduction

Surface fluxes of sensible heat and latent energy are important in many atmospheric processes and can be measured with reasonable accuracy over homogeneous surfaces. Direct measurements of turbulent fluxes such as sensible heat and latent energy, which are components of the shortened energy balance, are usually achieved by the eddy covariance (EC) method, which is considered the standard method for sensible heat and latent energy flux measurement and basically involves the use of single-point measurements from EC instruments mounted on a mast. However, the application of the EC method is often problematic. The necessary sensors for wind speed, air temperature and humidity must respond very quickly and at the same time must not show noticeable drift. This makes them delicate, expensive and in many cases difficult to calibrate. However more serious is the fact that flow distortions by the sensor, mast, etc., as well as horizontal misalignments often cause significant errors (Wyngaard, 1981).

In addition, there are statistical problems due to the fact that temporal co-spectra, measured at a fixed local sensor extend to very low frequencies. To achieve acceptable significance often demands averaging periods of tens of minutes (Thiermann and Grassl, 1992; Anandakumar, 1999). Such long averaging periods reduce the temporal resolution and conflict with the requirement of atmospheric stationarity within the averaging periods. The EC method for sensible heat flux measurement is also dependent on humidity through the speed of sound effect on the sonic-measured air temperature (Lumley and Panofsky, 1964).

Turbulent fluxes play important roles in governing the transfer processes in the lower layers of the atmosphere and in fact are the basic parameters, which are directly related to thermal and mechanical turbulence in the atmosphere and characterise the turbulence condition of the atmosphere in terms of ‘atmospheric stability’ (Dao et al., 2004). Atmospheric stability, via $\zeta = (z - d) / L$, is one of the crucial parameters used as an input parameter in atmospheric dispersion or air quality models.

Scintillometry is a relatively new technique used for measuring turbulence fluxes such as sensible heat and momentum flux measurements within the surface and/or boundary layer of the atmosphere. The scintillometer method offers the ability to make path-averaged measurements of turbulent fluxes of sensible heat and momentum. It provides a different approach from the point measurement methods, such as Bowen ratio energy balance (BREB) and EC methods, to obtaining more spatially-representative sensible heat flux measurements over a given land surface. Because F_h is derived from the line integral of the structure parameter of the refractive index, an average of F_h is obtained over an area formed by the path-length of the beam of the scintillometer and an area in the upwind direction (de Bruin et al., 1995).

Atmospheric stability characterises atmospheric turbulence quantitatively. Turbulence is an inherent property of the atmosphere which causes diffusion of such scalar quantities as sensible heat flux (Daou et al., 2004). The extent of the diffusion depends on the intensity of atmospheric turbulence and hence it is related to atmospheric stability. The atmospheric stability condition also partly influences the footprint for turbulence flux measurements. Sensible heat flux F_h is related to the atmospheric stability and the scintillometer method provides direct measurement of F_h , is ideal for evaluating atmospheric stability through the measurement of the Obukhov length L .

In this study, results of the EC and surface layer scintillometer (SLS) estimations of sensible heat flux for different atmospheric stability conditions, namely, unstable, and near-neutral atmospheric stability conditions are presented. The aim of the study is to assess sensible heat flux measurements obtained by SLS, which relies on Monin-Obukhov Similarity Theory (MOST) and therefore assumes stationarity and homogeneity of the surface where measurements are taken (as already discussed in Chapter 2) with those obtained using the EC method for different stability conditions and different times (seasons) of the year. No published work (known to the author) has been carried out comparing EC measurements of sensible heat with measurements with the SLS ones, in terms of atmospheric stability. This work therefore attempts to fill this gap.

4.2 Theory

4.2.1 Scintillometry

A scintillometer is an optical instrument that consists of a light/radiation source (transmitter) and a receiver. The receiver consists of a highly sensitive detector and a data acquisition system that can register the reduction in the intensity of fluctuations of a beam after propagation through a turbulent medium from which the different meteorological parameters are deduced. Scintillometers have been widely used for measuring turbulent flux of sensible heat and momentum (e.g. Thiermann and Grassl, 1992; de Bruin et al., 2002; Hartogensis et al., 2002). The use of the scintillometer method for the measurement of turbulent flux is based on the fact that the refractive index structure parameter C_n^2 ($\text{m}^{-2/3}$) measured directly by the scintillometer can be related to the structure function parameter of temperature C_T^2 ($\text{K}^2 \text{m}^{-2/3}$) from which sensible heat flux F_h (W m^{-2}) is derived. A beam is transmitted over a path and the fluctuations in the beam intensity at the receiver are analysed to give the variations in the refractive index along the path. Specifically, the turbulent intensity of the refractive index of air can be expressed by C_n^2 defined by Thiermann and Grassl (1992) as:

$$C_n^2 = \frac{\overline{n(r_1)^2 - n(r_2)^2}}{r_{12}^{2/3}} \quad 4.1$$

where $n(r)$ is the refractive index of air at location r and the distance r_{12} is between r_1 and r_2 , the so called inner scale of turbulence (marks the transition between the inertial and viscous dissipation range of eddy sizes and is of the order of 5 to 10 mm) and the outer scale (dominant inhomogeneities which are of the order of the height of the beam above the surface).

The intensity fluctuations are caused by inhomogeneities in the refractive index of air, which are due to turbulent eddy motions along the scintillometer path. The transmitter emits a beam with a known wavelength. At a known horizontal distance from the beam source, the intensity fluctuations (expressed as C_n^2) at the receiver that are caused by the turbulent eddies are analysed. These eddy motions are generated by air temperature and atmospheric humidity fluctuations, and can be regarded as a collection of converging and diverging lenses focusing and defocusing the scintillometer beam. Because the measured variance of the logarithm of the signal

intensity fluctuations is a measure of the turbulent behaviour of the atmosphere, it can indirectly be related to the transport of certain quantities such as sensible heat, latent energy and gases.

By emitting a beam with a specific wavelength through the atmosphere over a horizontal path, the intensity fluctuation can be observed at the receiver end. The intensity fluctuations are caused by turbulent temperature and humidity fluctuations and are expressed through C_T^2 and hence F_h . In the optical domain, C_n^2 mainly depends on temperature fluctuations in the atmosphere and only slightly on humidity fluctuations as was demonstrated in Chapter 3.

The distance between the transmitter and the receiver can range from tens of meters to tens of kilometers depending on the type of instrument. There are different types of scintillometers and the difference is mainly based on the size of the receiver aperture size compared to the Freznel zone (defined as, $F = \sqrt{\lambda L_{beam}}$ where λ is the optical wavelength and L_{beam} the path length), so that if the aperture size is less than the Freznel zone, the scintillometer is classified as a small aperture scintillometer and the ones with larger aperture sizes greater than the Freznel zone are referred to as large aperture scintillometers. In this study, a surface layer (small aperture) scintillometer (SLS) (Scintec SLS40-A) which emits two parallel and differently polarised laser beams was used. This unit uses a class 3a type laser at a wavelength of 670 nm, a beam displacement distance of 2.7 mm and a detector diameter of 2.5 mm, which is a small aperture scintillometer.

4.2.2 Eddy covariance

Swinbank (1951) proposed an 'eddy correlation', otherwise properly referred to as eddy covariance (EC) method to estimate vertical flux of heat and water vapour from a fully turbulent mean flow. The upward flux density of an entity is given by the covariance between the vertical wind speed and entity θ over a time interval:

$$F = \rho c_p \overline{\text{covariance}(w, \theta)} \quad 4.2$$

where F is the flux of the entity θ (in this case heat), c_p , specific heat capacity of dry air, ρ the air density and w the vertical wind speed.

By definition the mean of a fluctuation should be zero (i.e. the positive and negative deviations from a mean should sum to 0), and so $\overline{w'} = 0$ (Arya, 2001). Hence $w' = w - \overline{w}$ and

$F = \rho c_p \overline{w' \theta'}$, where over bars represent component means and primes denote the instantaneous deviation from the mean (i.e. the effects from individual eddies).

The influence of sensor tilt or terrain irregularity can contaminate the computation of the flux by causing an apparent mean velocity (Finnigan et al., 2003). Often it is difficult to orient the vertical wind velocity sensors so that the mean vertical wind speed is zero, or at least nearly so; or find a perfectly flat experimental site. Rotation of the coordinate system of the three wind velocity components making the vertical and lateral velocity components equal zero is therefore necessary before proceeding with computation of turbulent fluxes (Turnipseed et al., 2003). Sensible heat flux is expressed as:

$$F_h = \rho c_p \overline{w' T'}. \quad 4.3$$

4.2.3 Atmospheric stability and Obukhov length

The Obukhov length, L , (m) is the height above the zero-plane displacement height d at which free convection dominates over forced convection. Therefore the Obukhov length is a measure of the dynamic atmospheric stratification, with $L > 0$ for stable conditions and $L < 0$ for unstable conditions. Unstable conditions occur when part of the turbulence energy is generated by convection. Neutral conditions occur when the turbulence is generated by wind shear near the ground with convection providing no energy. Stable conditions occur when part of the turbulence energy is consumed by vertical motions. The turbulence persists in so far as the mechanical production equals the sum of consumptions (Weiss, 2002).

The Obukhov length is calculated using:

$$L = \frac{T}{k g} \cdot \frac{\rho c_p}{F_h} \cdot u_*^3 \quad 4.4$$

(Monin and Obukhov, 1954) where T is the air temperature (K), $k = 0.4$ is von Karman's constant, g the acceleration due to gravity, F_h the sensible heat flux and u_* is the friction velocity. The non-dimensional stability parameter ζ is calculated by dividing the measurement height relative to d by L : $\zeta = (z - d) / L$. The calculated stability parameter is then used to divide data into the three atmospheric stability categories as shown in Table 4.1. In this study, data for two stability categories, namely unstable and near-neutral (mainly daytime data), were used in the

Table 4.1 Stability categories and stability parameter (Weiss, 2002).

Stratification	$\zeta = (z - d) / L$
Stable	$\zeta > +0.05$
Near-neutral	$-0.05 \leq \zeta \leq 0.05$
Unstable	$\zeta < -0.05$

analysis since the night-time (stable atmospheric condition) results are not always reliable for either methods (EC and SLS) due to mist and/or condensation of water on the sensors.

Statistical analysis of the sensible heat flux data obtained by the EC and SLS methods was then carried out for each of the stability categories to compare the performance and agreement in measurement for the two methods. Most of the published work involving use of the SLS is only for short periods and does not focus on the estimation of sensible heat by the EC and SLS under different atmospheric stability conditions (Table 1.3).

4.3 Experimental details

Measurements of energy flux and weather variables were at a mixed grassland community site in Ashburton, Pietermaritzburg, South Africa (Fig. 3.1). This was part of a research study using EC and SLS methods to estimate sensible heat and latent energy flux. The data analysed here resulted from measurements carried out from March to December 2004, spanning all the seasons in a year. Different methods were used for the determination of sensible heat flux namely: EC, SLS and an energy balance system for the determination of net irradiance and soil heat flux.

A dual-beam scintillometer (SLS40-A, Scintec Atmosphärenmesstechnik, Tübingen, Germany), operating at a frequency of 1 kHz, was set up at a height of about 1.68 m above the ground surface and the path length between the transmitter and receiver units was 101 m. The sensor height was referenced to the zero-plane displacement height $d \approx 2/3 \times h$ where h is the vegetation height. Vegetation height along the beam-path was measured using a tape measure in metres.

The Scintec SLSRUN software together with the instrument makes online measurements of the refractive index structure parameter (C_n^2), the structure function constant of temperature

(C_T^2) the inner scale length (l_o , mm), the kinetic energy dissipation rate (ε , $\text{m}^2 \text{s}^{-3}$), the sensible heat flux (F_h), and the Obukhov length (L , m). Two-minute averages of all the above parameters were stored on a computer for further analysis. Scintillometer data were rejected if l_o was less than 2 mm and the percentage error free data less than 25 %.

An EC system together with the energy balance system was installed approximately midway of the SLS path length and at a height of 2 m above the soil surface. A three-dimensional sonic anemometer (SWS-211/3V, Applied Technologies, Boulder, Colorado, USA), was used as an EC system to measure the sensible heat flux. Measurements of the three wind speed components and sonic temperature were performed every 0.1 s (frequency of 10 Hz) and 2-min turbulent fluxes were calculated from the covariance between vertical wind speed and sonic temperature using a 23X datalogger (Campbell Scientific, Logan, USA).

Net irradiance was measured at the site using a net radiometer (model Q*7.1, Radiation and Energy Balance Systems, (REBS), Seattle, Washington, USA). Soil heat flux was determined using soil heat flux plates (model HFT-3, REBS) buried at a depth of 0.08 m and a system of parallel thermocouples at 0.02 and 0.06 m used to calculate the soil heat flux stored above plates. The volumetric soil water content for the 0- to 0.06-m soil layer was measured using a frequency domain reflectometer (ThetaProbe, model ML2x, Delta-T Devices, Cambridge, UK).

Two-minute sensible heat flux data obtained using EC and SLS methods were then compared for the various stability categories as outlined in Table 4.1. Correlation analyses and t-tests were carried out to assess how the sensible heat flux values obtained by the EC and SLS methods compare for the different periods/seasons.

4.4 Results and discussion

In this section, a comparison of the sensible heat flux measured by the EC and SLS methods for the unstable and near-neutral atmospheric stability conditions are presented and discussed. Brief discussions on the diurnal variations of l_o as well as the influence of vegetation height on sensible heat flux measurements are also presented.

Only daytime sensible heat flux data were used in the analysis since the sensible heat flux measurements were mainly being used to estimate evaporation and this happens mainly during the day. The comparison of the EC and SLS methods, mainly performed to get an understanding about the performance of the SLS system with respect to the widely-used EC method, was

therefore restricted to two atmospheric stability conditions, namely unstable and near-neutral as is already explained in Section 4.3. Real-time coordinate rotations for the EC measurements of the three wind velocity components namely u , v and w was not done due to resource limitations.

The 23X datalogger used for storing the EC data at the research site could not store the raw data needed to do coordinate rotation and we also did not have a laptop permanently connected to the datalogger which could have been used for storing the raw data, and performing the necessary rotations.

Results for both 2-min and 20-min averages of sensible heat flux measurements are presented. In some cases there were only a few data points for the time periods chosen. In most of these cases the problem was due to the missing friction velocity data from the EC method and hence the Obukhov length could not be calculated. The lack of u_* data from the SLS measurements due to error in measurements for the coinciding periods also restricted the data that could be compared to the EC ones as well.

In Fig. 4.1, the path-weighted vegetation height is shown. The vegetation height varied with season and maintenance activities at the site such as mowing which takes place in the months of May and August each year and burning which is carried out in mid-August. The weighted vegetation height at the site for the research period varied from 1.02 to 0.02 m. The effective measurement height of the SLS was 1.68 m.

The 20-min average data results in loss of a lot of data points and therefore only few data are available for analysis. A comparison of the 2-min and 20-min averages of the vertical wind speed was therefore carried out to check if using 2-min data would be good enough for comparison with the SLS data. Example of plots of 2-min and 20-min averages of the vertical wind speed (\bar{w}) measured by the EC method are shown in Fig. 4.2.

As is shown in Fig. 4.2, \bar{w} deviates around 0 m s^{-1} , with the data points falling between -0.17 and 0.45 m s^{-1} (Fig. 4.2 a) (DoY 185, 2004) and for DoY 276, 2004, the \bar{w} data range is between -0.12 and 0.26 m s^{-1} (Fig. 4.2 b). As can be seen from Fig. 4.2, both 2-min and 20-min \bar{w} averages deviate from 0 m s^{-1} with the same trend. Considering that some of the EC data are averaged out for 20-min averages, 2-min averages of EC data were used in the analysis.

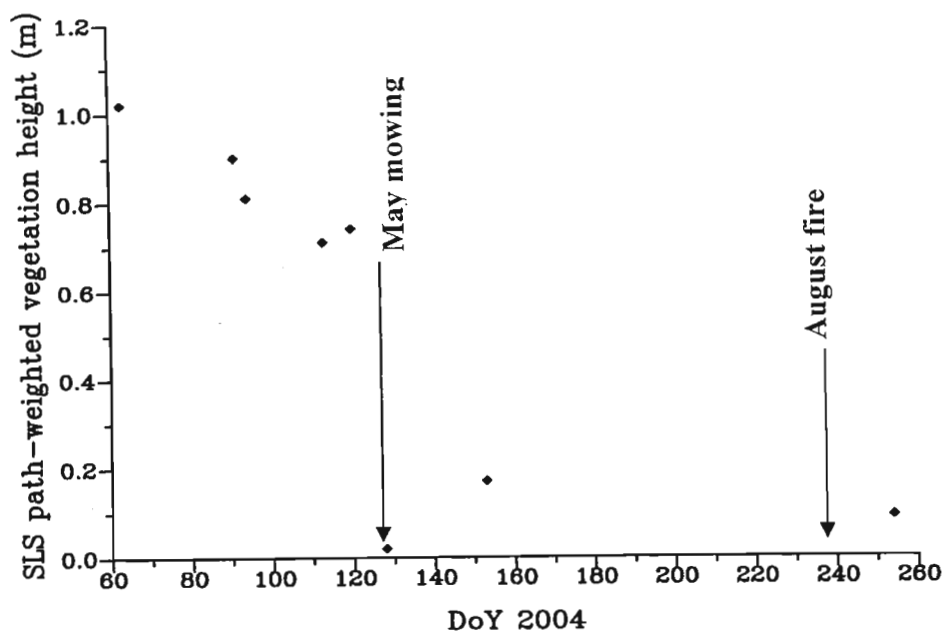


Fig. 4.1 SLS beam path-weighted vegetation height. Between DoY 152 to 240, the vegetation height remained low.

In Fig. 4.3, the t -test values relating to differences between corresponding F_h values as measured by EC and SLS methods under unstable conditions and near-neutral conditions spanning different seasons, are shown. Greater t -values were obtained for the unstable conditions, with the largest t -value being 110.97 obtained in the month of June.

Sensible heat flux measurement by the SLS was done within the inertial sub-layer (beyond the transition layer) where MOST is valid. Linear regression analysis of the EC and SLS sensible heat flux data for the various atmospheric stability conditions as well as a t -test were used to evaluate how well corresponding values obtained by the two methods agree with each other are shown in Figs 4.4 to 4.17.

In this study, 2-min averages of EC data were used in the analysis. The use of 2-min averages of sensible heat flux was based mainly on the fact that smoothening (or averaging out) of data occurs for 20-min averages of EC data whereas with 2-min average EC data, some data may be averaged out but there is still enough left from which 20-min averages are obtained. The 2-min averages of sensible heat from the SLS were then compared with the corresponding EC measurements.

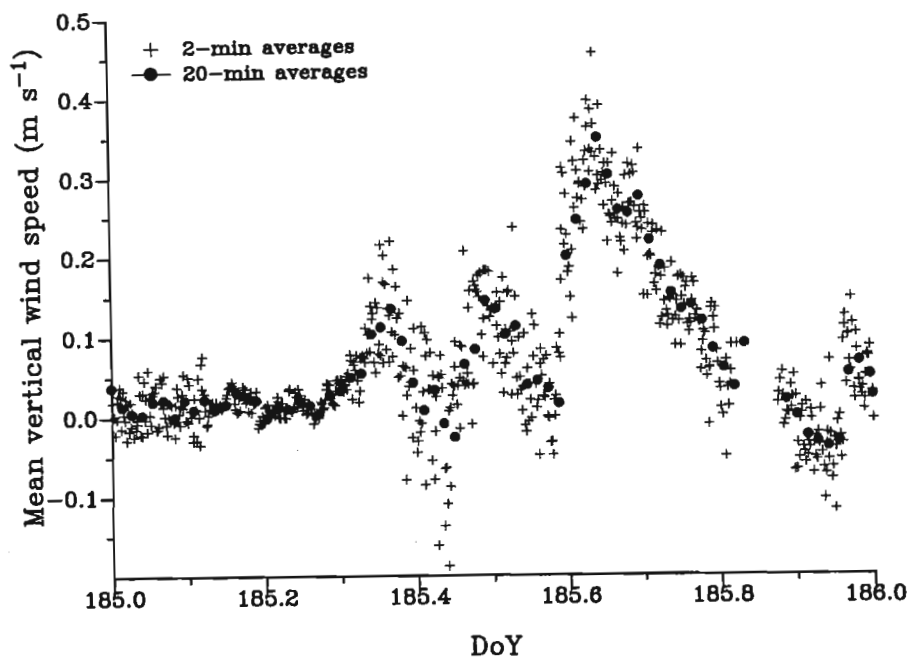
A general comparison of the sensible heat flux measurements from the two methods (EC and SLS) show reasonably good agreement as shown both in the diurnal plots of sensible heat flux (Fig. 4.4) and the statistical analyses (Figs 4.5 to 4.17). The EC values appear more scattered especially around midday when peak sensible heat values are recorded compared to the smoother variations of the sensible heat flux measured by the SLS.

The sensible heat flux values measured by the EC and SLS methods therefore appear more in agreement when the values are low as is the case from early morning hours until late morning and again after the midday peak as observed from the diurnal plots as well as the regression curves where the data points appear more widely scattered around the line of best fit. Greater t -values were obtained for the unstable conditions with the highest t -value (110.97) recorded in June. There is a bias in the EC measurements as indicated by the slope values and deviation of the line of best fit from the 1:1 line (Table 4.2 and Fig. 4.3). The reason for the bias in EC measurements when the atmospheric stability condition is unstable is not known. For the unstable condition, there is a better agreement in F_h values measured by EC and SLS, as denoted by greater t -values, in cold winter months of June and August while smaller t -values are obtained in warmer months of October, November and December.

However the comparison of the F_h measurements by the two methods for the near-neutral atmospheric condition show better agreement in the warm months of the year (September to December). In July and September there were very few data points since the missing friction velocity data from the EC system meant that Obukhov length could not be calculated. The lack of u_* data from the SLS measurements due to error in measurements for the coinciding periods also restricted the data that could be compared to the EC ones as well. This problem resulted in the reporting of only unstable condition data, for July and no comparison results for September.

There is a noticeable bias in the F_h values with the SLS F_h measurements greater than those measured by the EC method especially when the atmospheric condition is unstable while the EC method records slightly greater F_h values when the atmosphere is near-neutral (Table 4.2 and Figs 4.5 to 4.17). The bias can be observed from the regression slope as well as from the deviation of the line of best fit from 1:1 line (Figs 4.5 to 4.17), although the reason for the bias is not known.

(a)



(b)

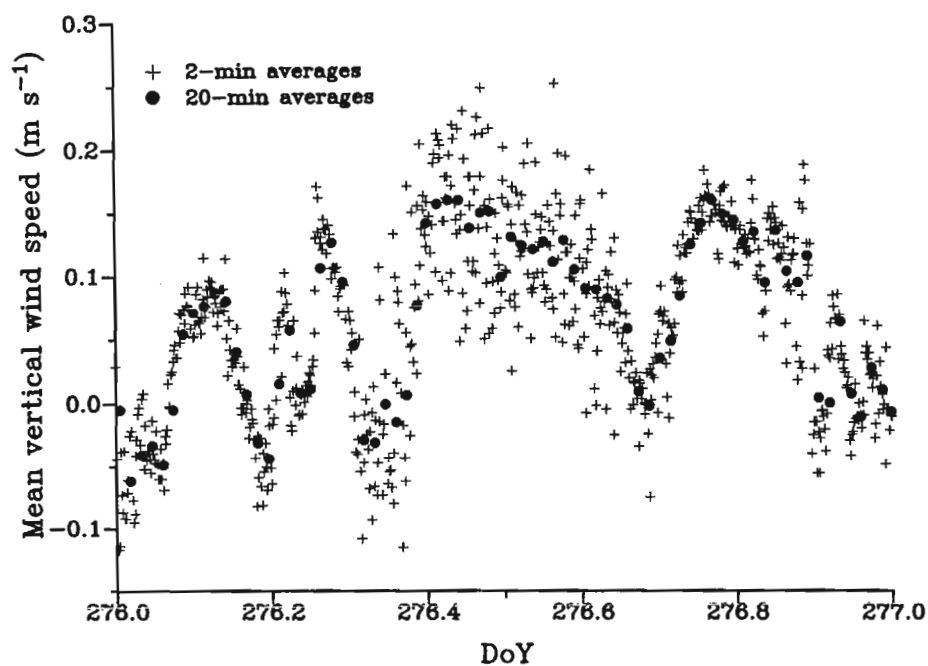
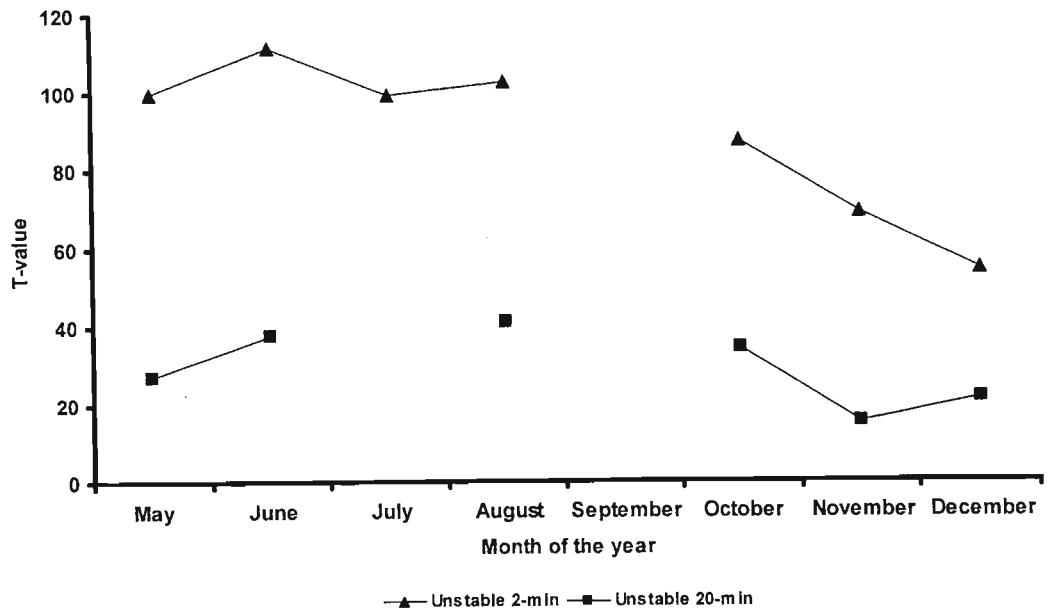


Fig. 4.2 Two-min and 20-min vertical wind speed obtained by EC for (a) DoY 185 and (b) DoY 276.

(a)



(b)

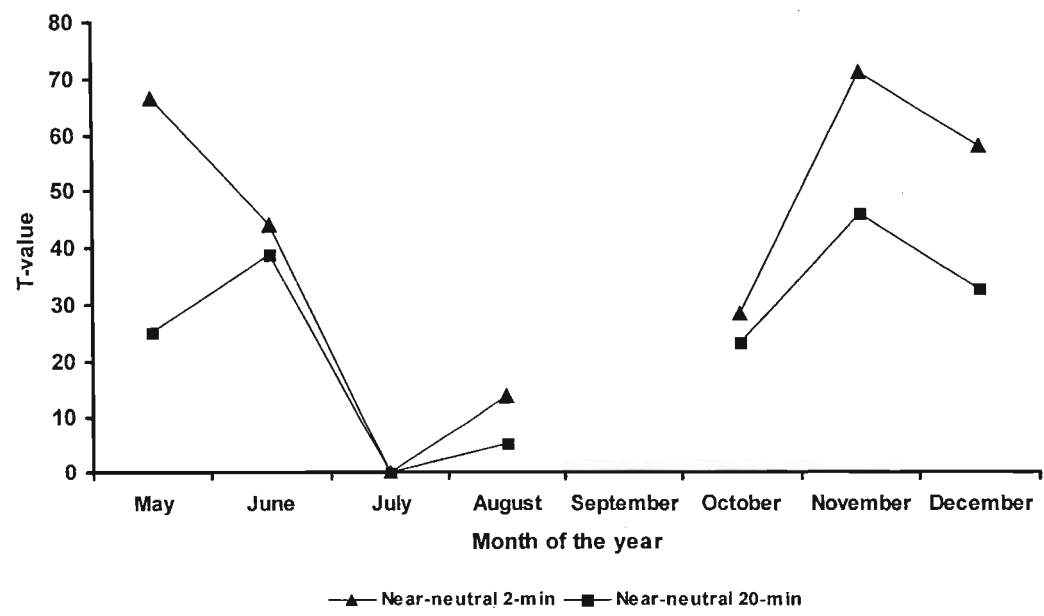


Fig. 4.3 T-test values obtained from an analysis of F_h measurements by the EC and SLS methods for the (a) unstable conditions and (b) near-neutral conditions for the different months spanning different seasons.

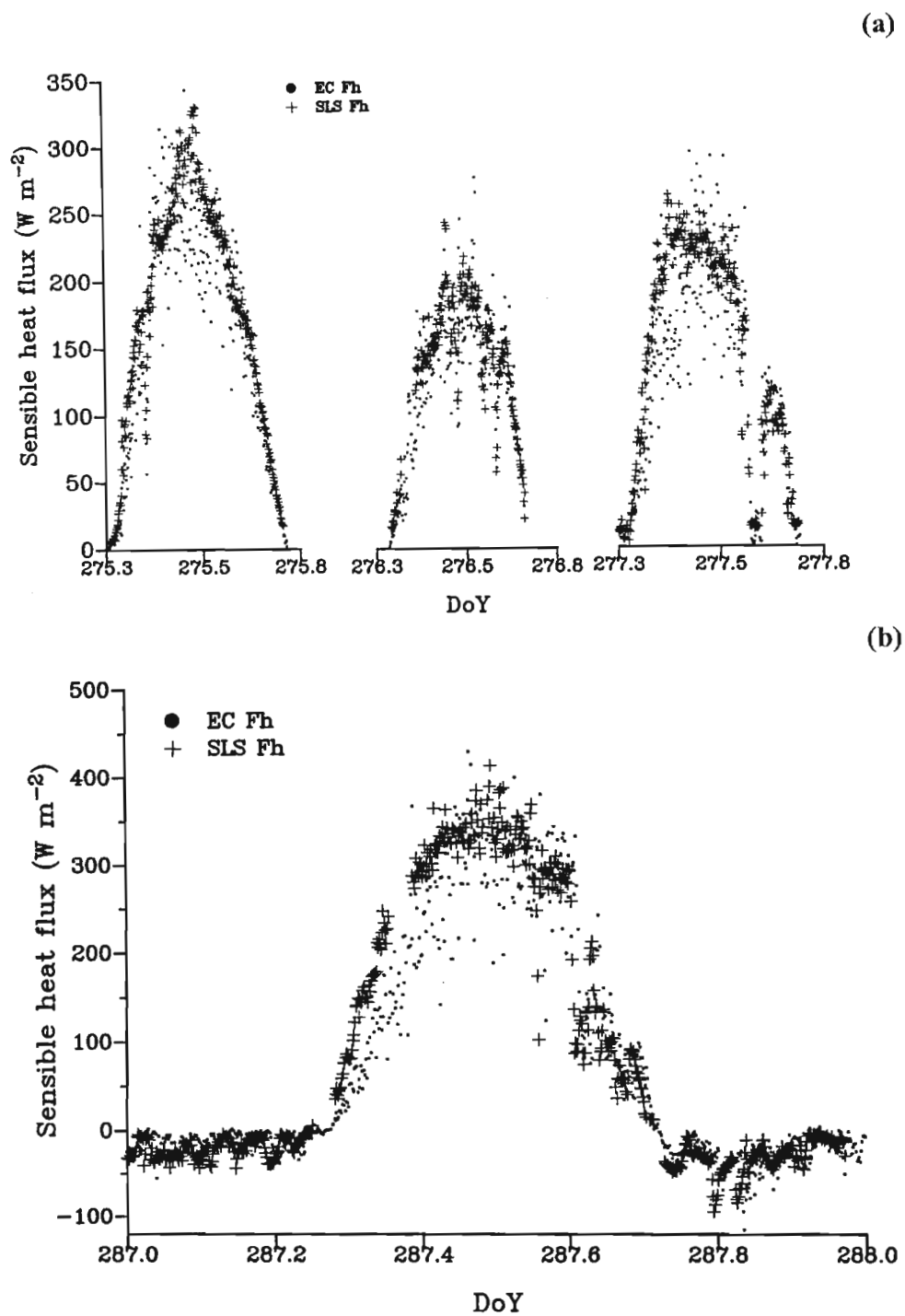


Fig. 4.4 Examples of diurnal plot of 2-min sensible heat flux as measured by EC and SLS methods for (a) DoY 275 to 277 and (b) DoY 287.

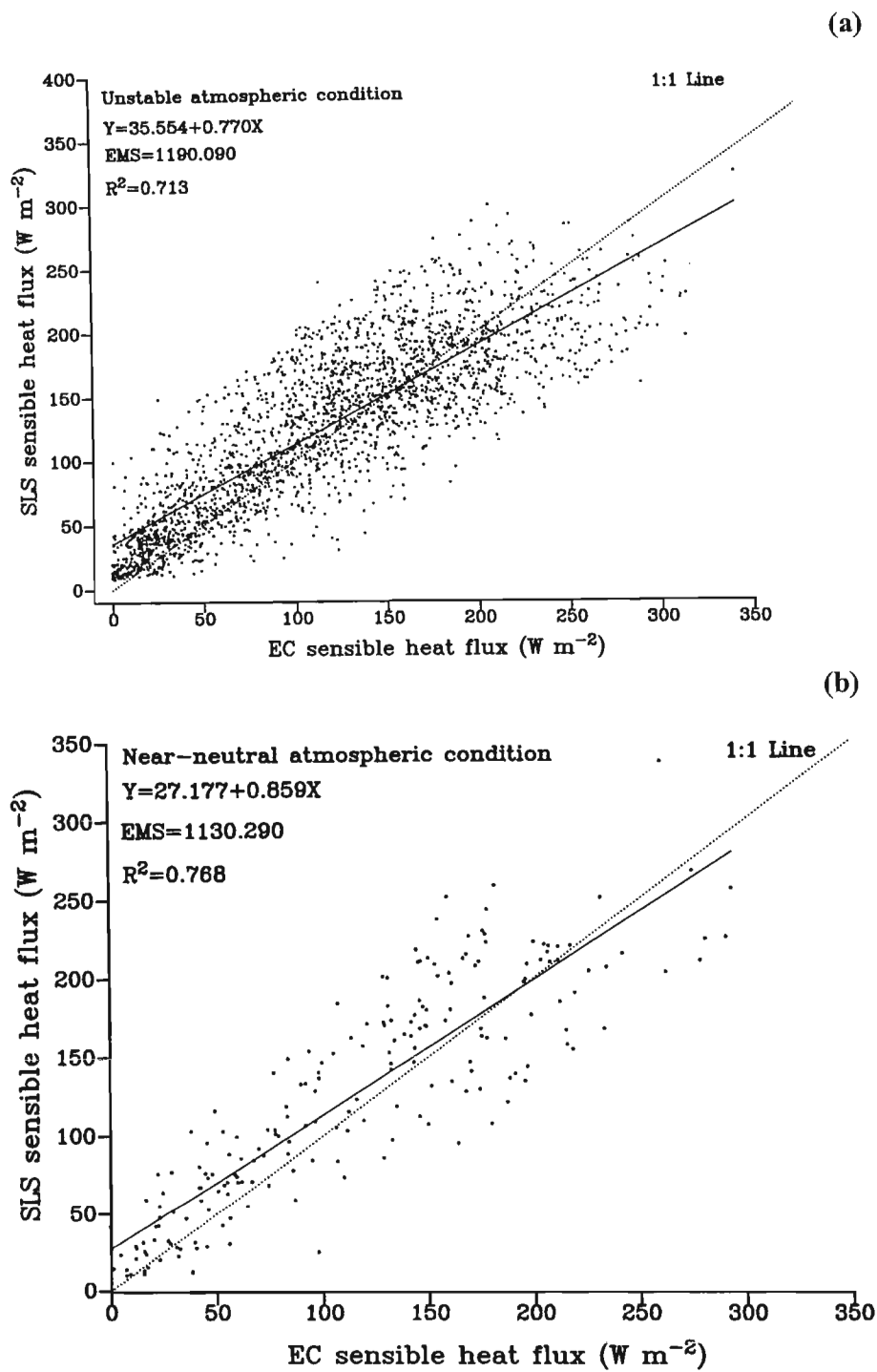
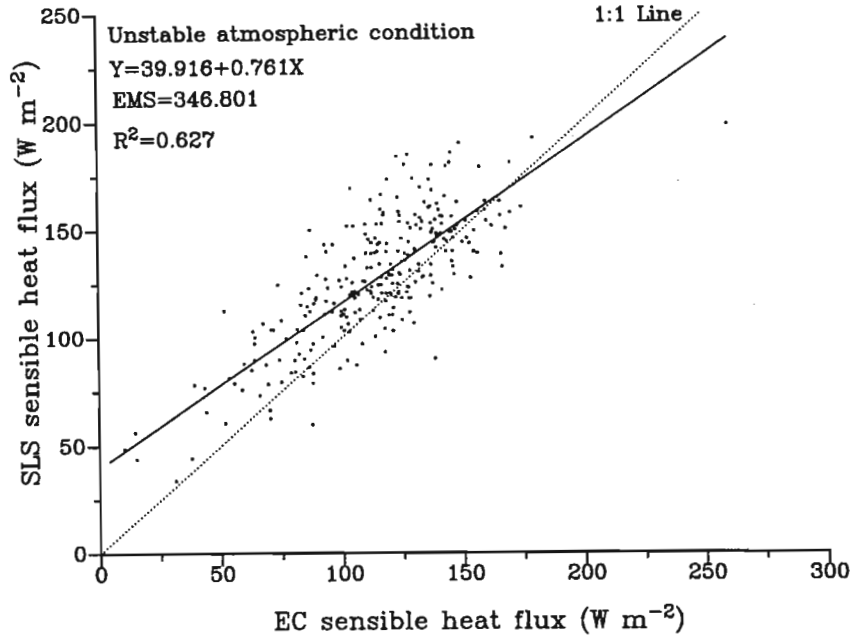
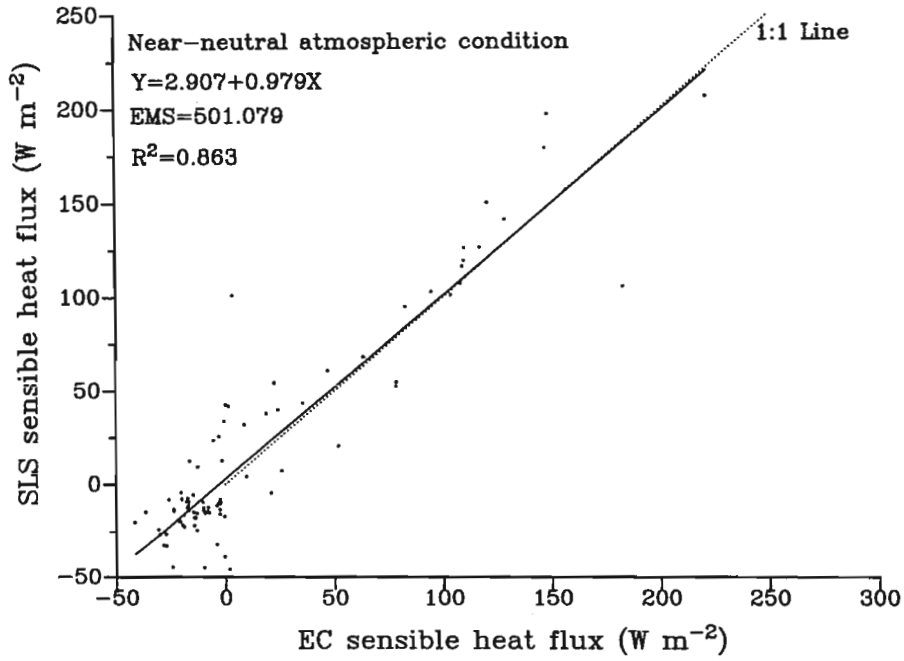


Fig. 4.5 Correlation of EC and SLS 2-min sensible heat flux for (a) stability parameter $\zeta < -0.05$ (unstable) and (b) stability parameter ζ between -0.05 and 0.05 (near-neutral) for the month of May.

(a)



(b)



(a)

Fig. 4.6 Correlation of EC and SLS 20-min sensible heat flux for (a) stability parameter $\zeta < -0.05$ (unstable) and (b) stability parameter ζ between -0.05 and 0.05 (near-neutral) for the month of May.

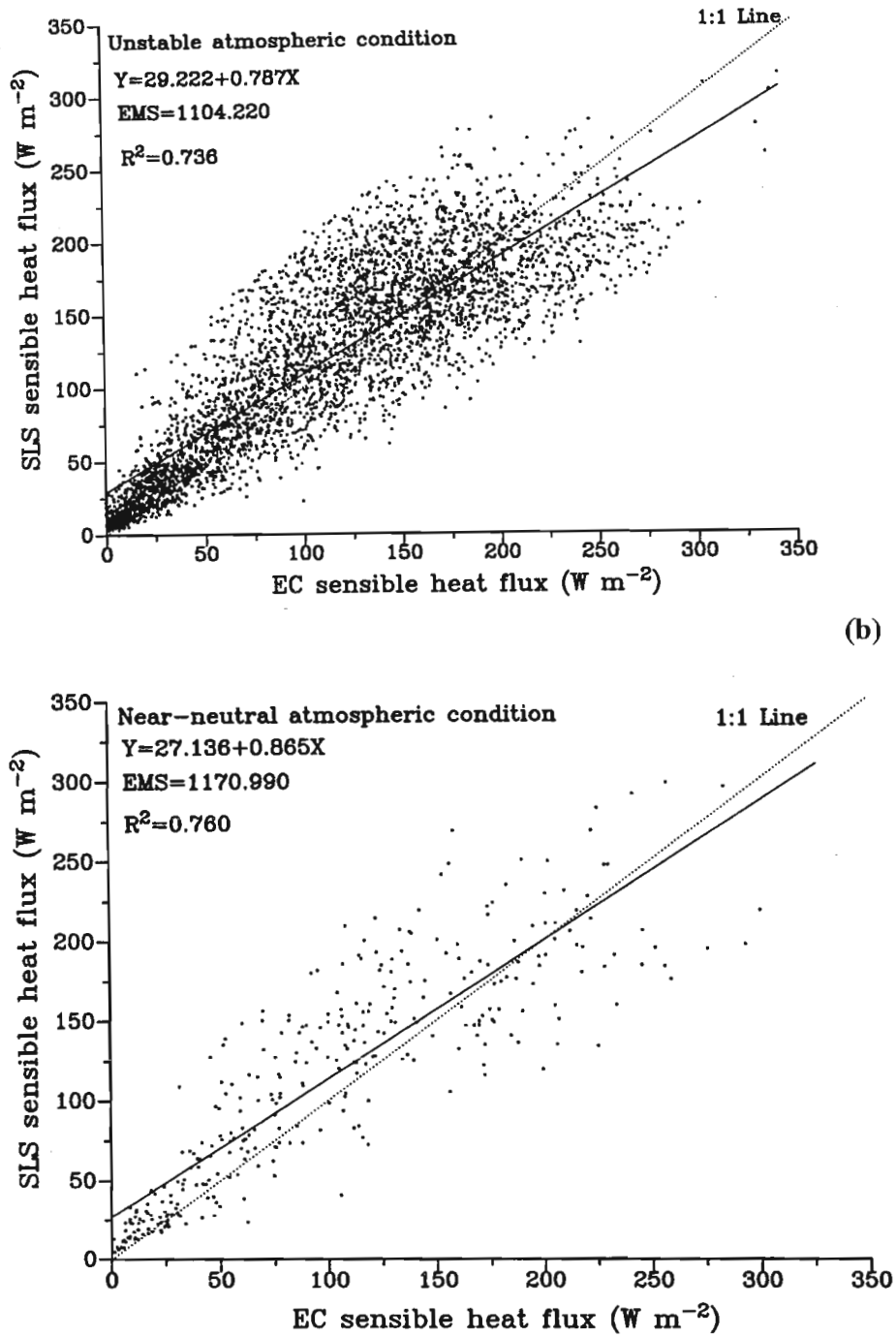


Fig. 4.7 Correlation of EC and SLS 2-min sensible heat flux for (a) stability parameter $\zeta < -0.05$ (unstable) and (b) stability parameter ζ between -0.05 and 0.05 (near-neutral) for the month of June.

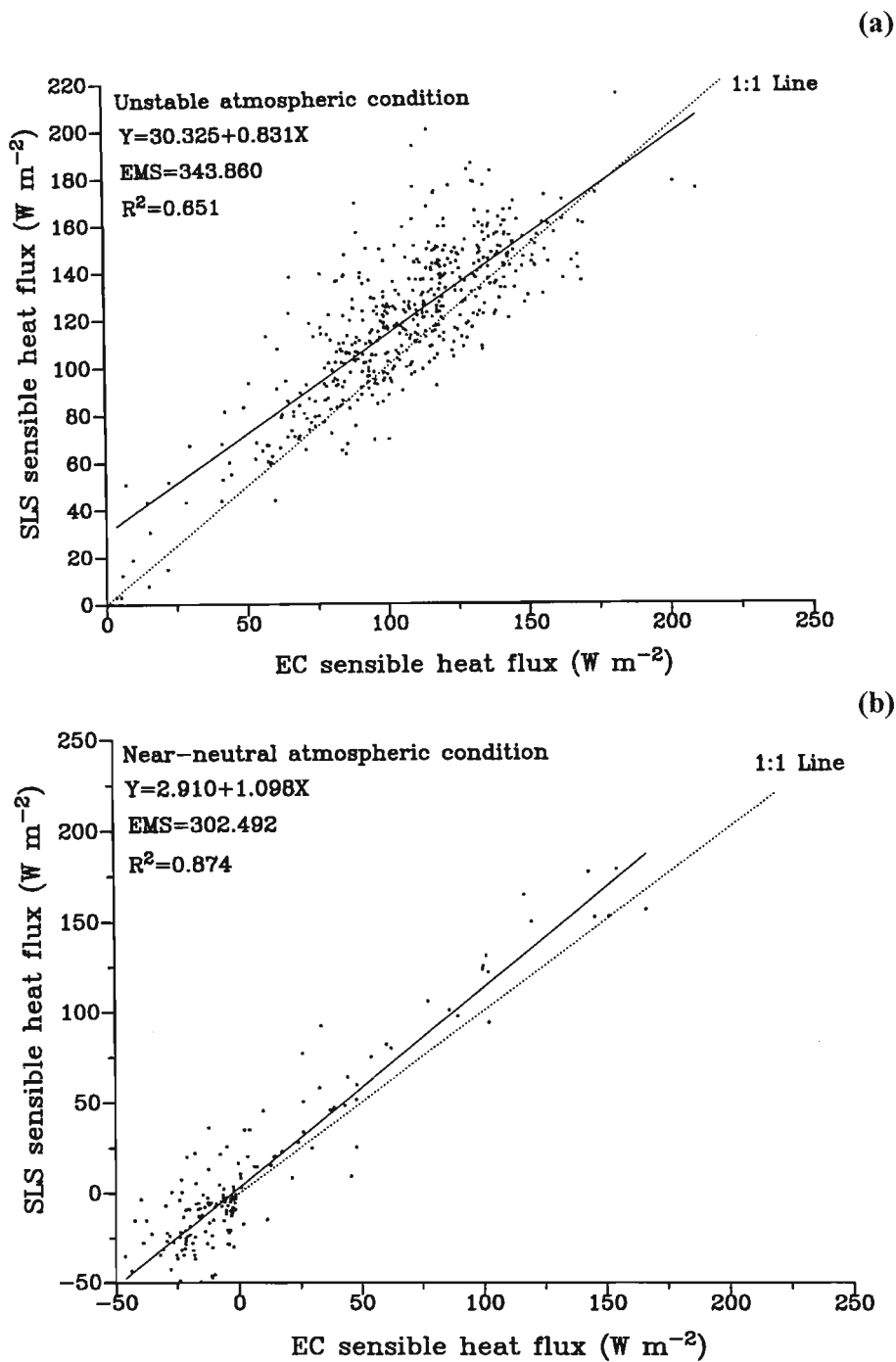


Fig. 4.8 Correlation of EC and SLS 20-min sensible heat flux for (a) stability parameter $\zeta < -0.05$ (unstable) and (b) stability parameter ζ between -0.05 and 0.05 (near-neutral) for the month of June.

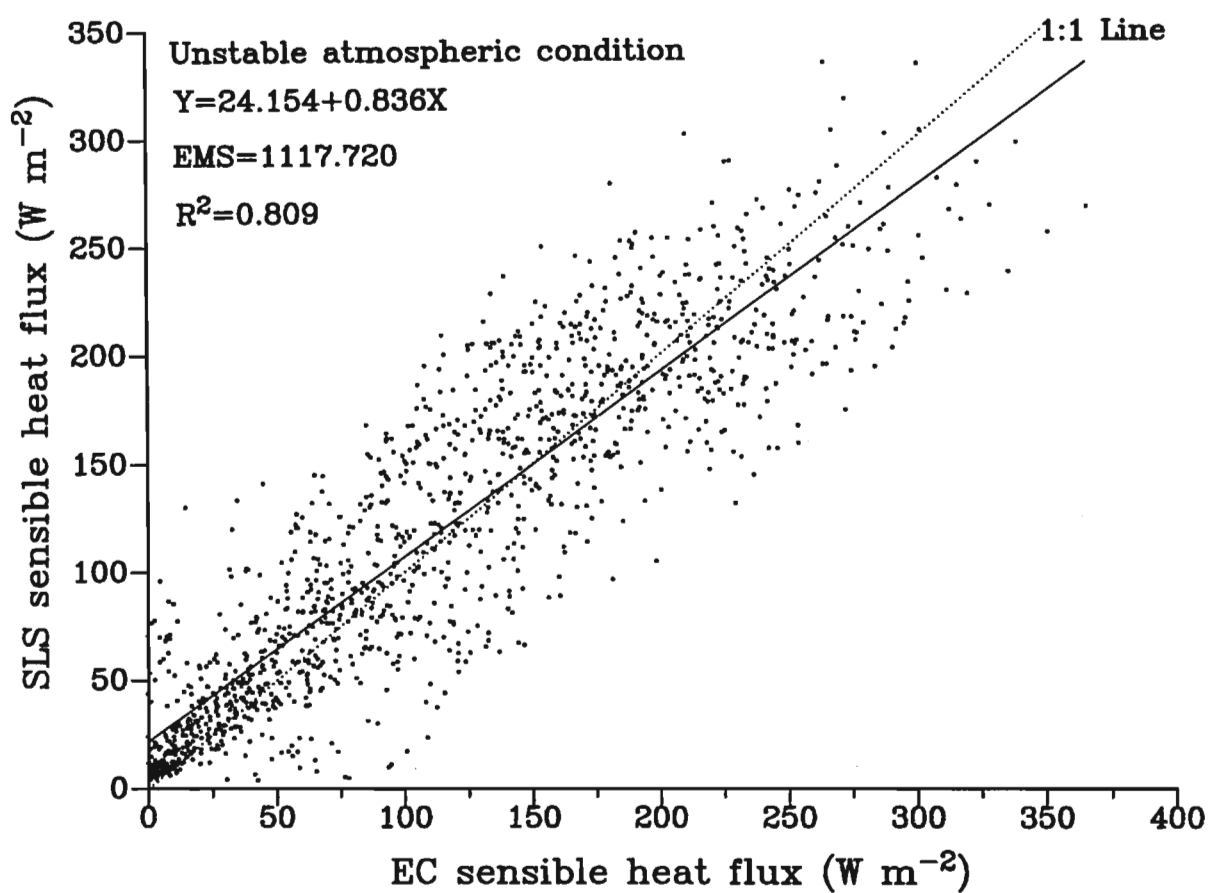


Fig. 4.9 Correlation of EC and SLS 2-min sensible heat flux for stability parameter $\zeta < -0.05$ (unstable) for the month of July.

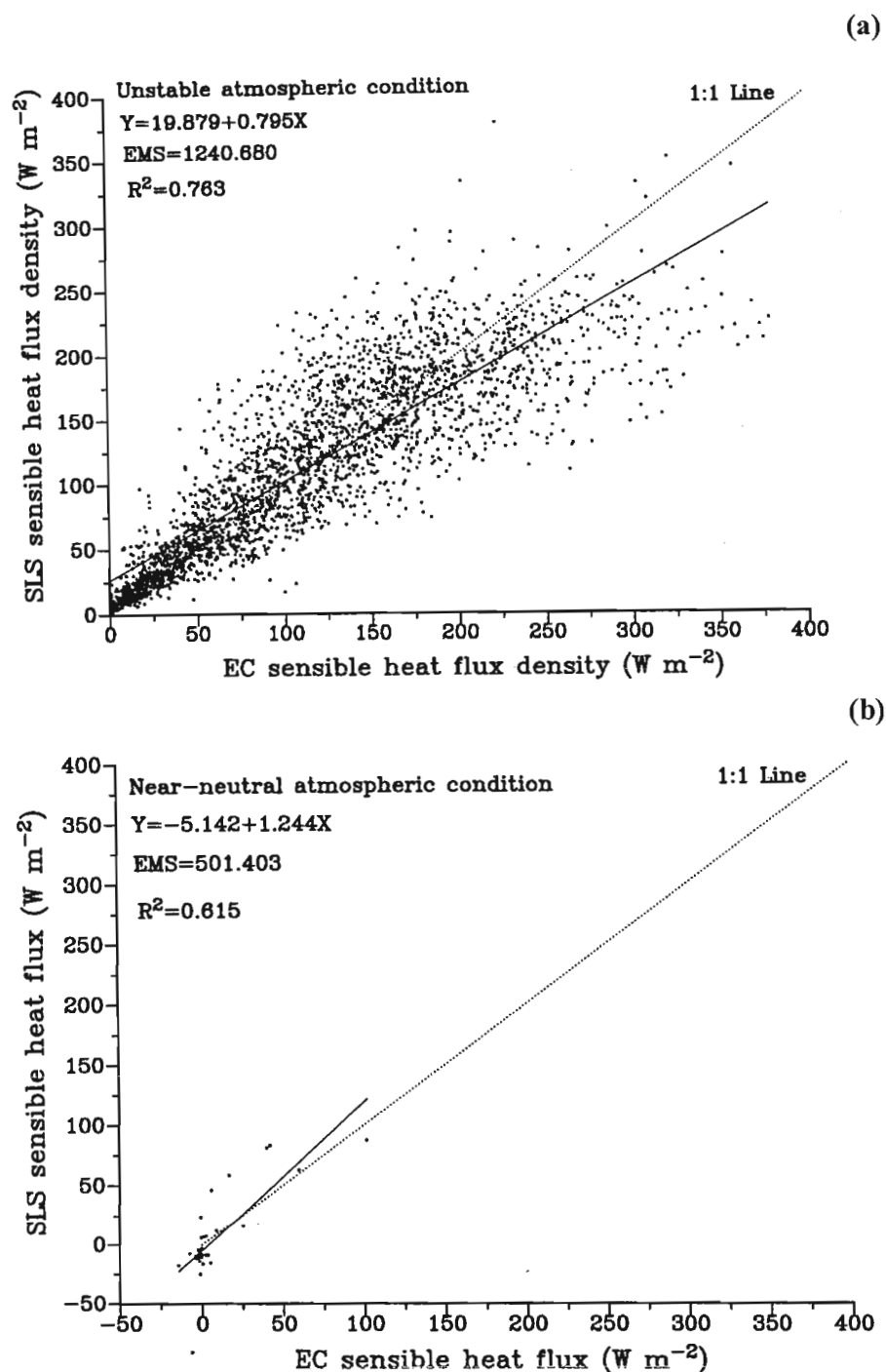


Fig. 4.10 Correlation of EC and SLS 2-min sensible heat flux for (a) stability parameter $\zeta < -0.05$ (unstable) and (b) stability parameter ζ between -0.05 and 0.05 (near-neutral) for the month of August.

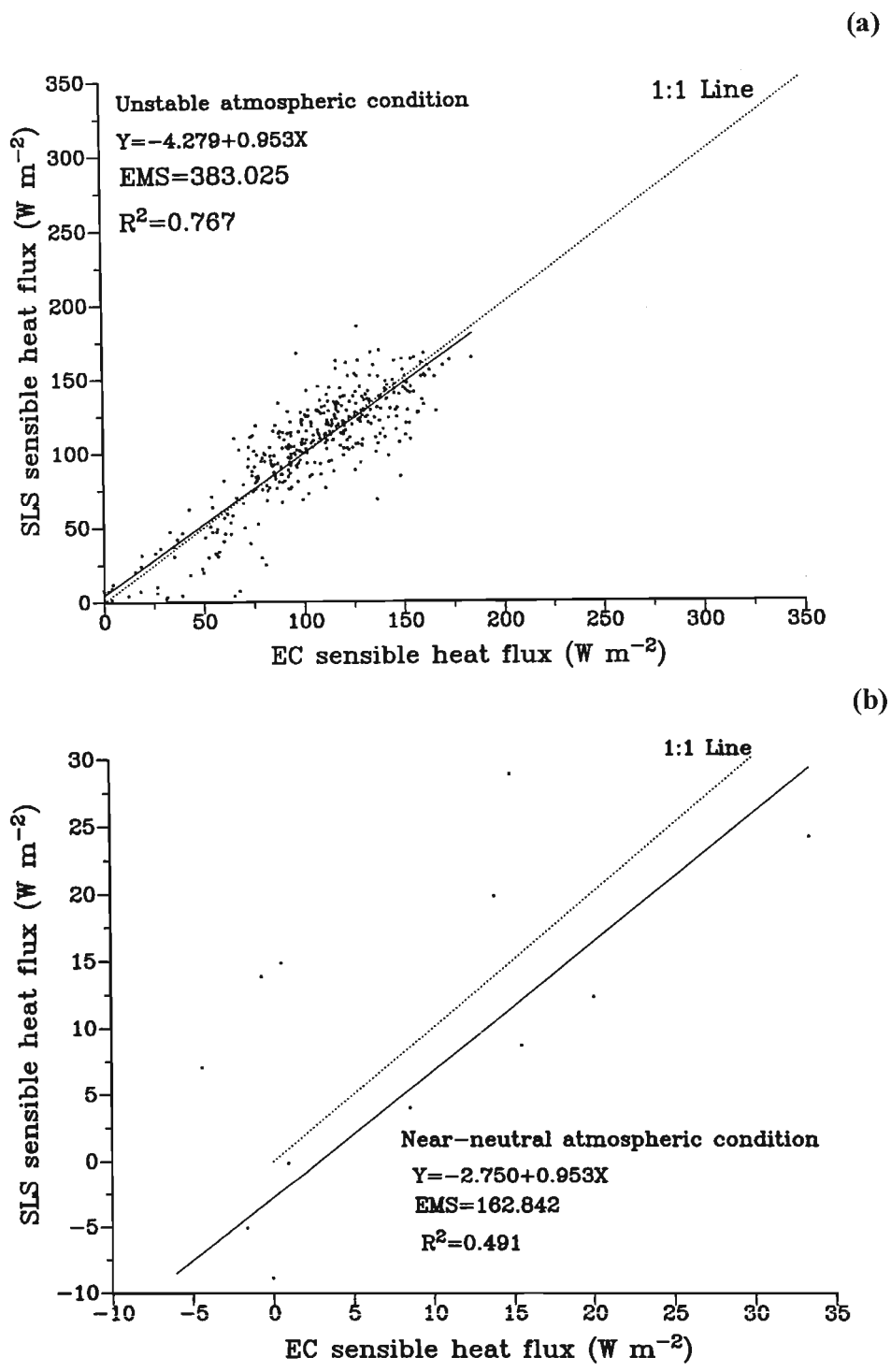


Fig. 4.11 Correlation of EC and SLS 20-min sensible heat flux for (a) stability parameter $\zeta < -0.05$ (unstable) and (b) stability parameter ζ between -0.05 and 0.05 (near-neutral) for the month of August.

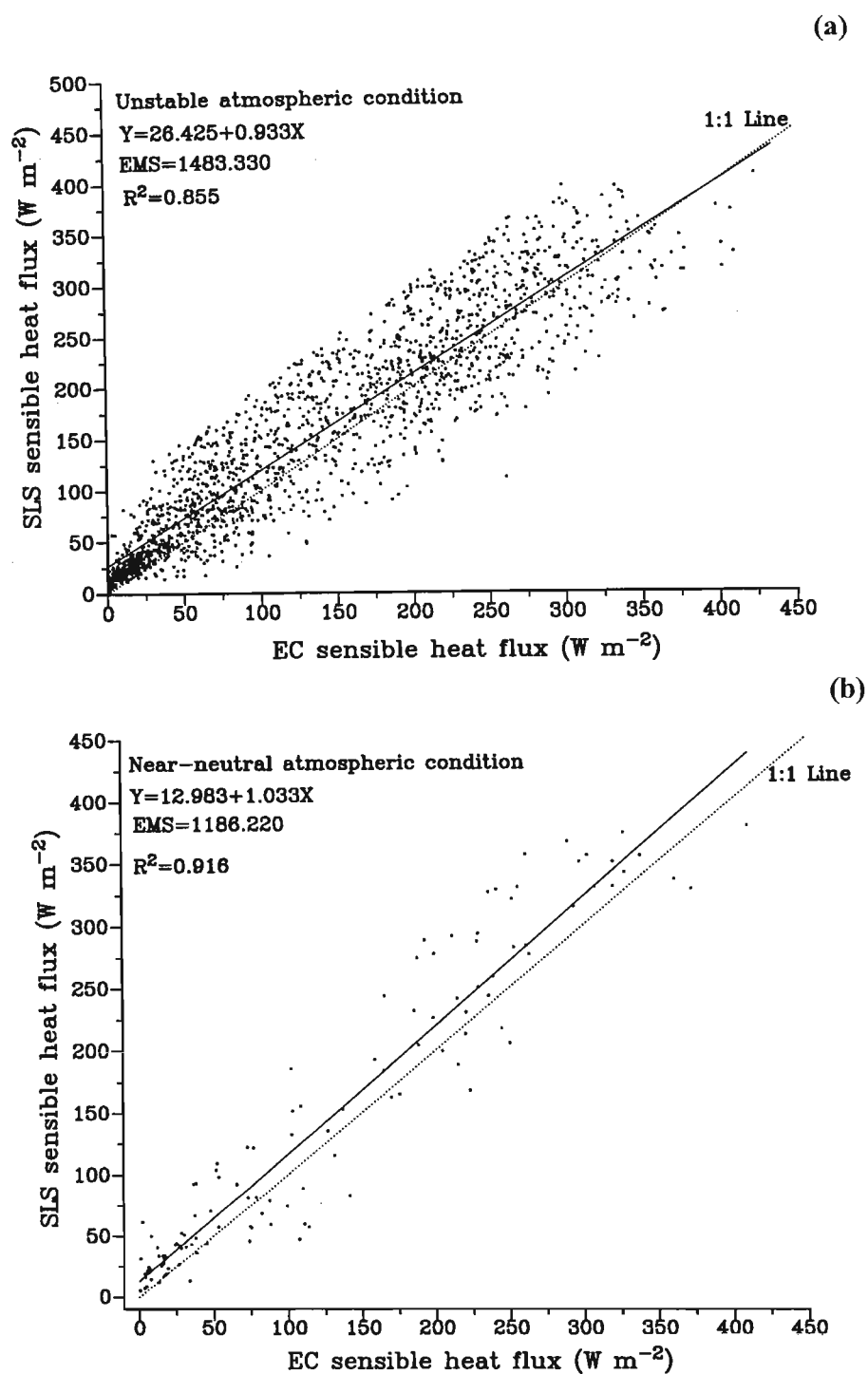


Fig. 4.12 Correlation of EC and SLS 2-min sensible heat flux for (a) stability parameter $\zeta < -0.05$ (unstable) and (b) stability parameter ζ between -0.05 and 0.05 (near-neutral) for the month of October.

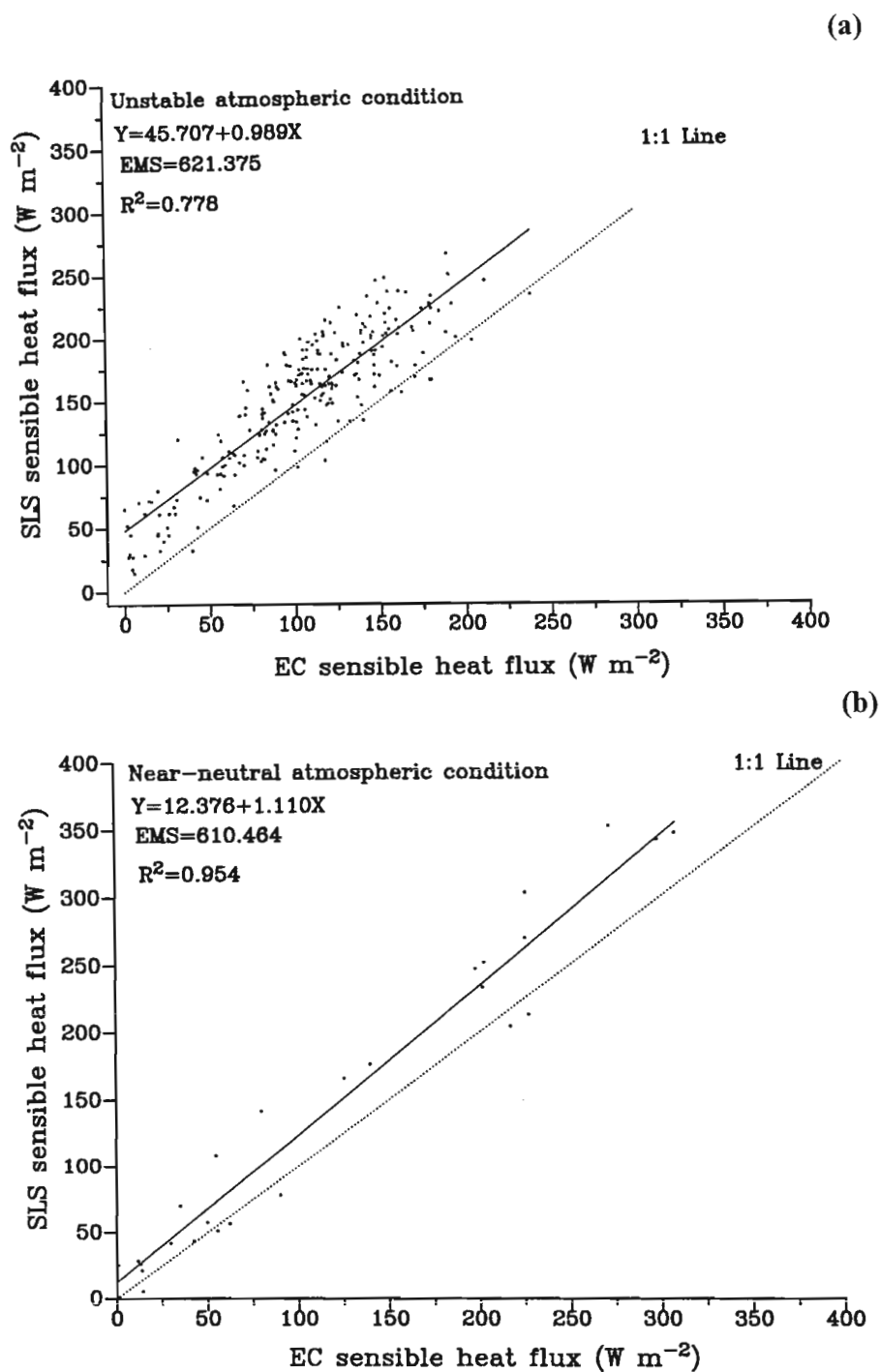


Fig. 4.13 Correlation of EC and SLS 20-min sensible heat flux for (a) stability parameter $\zeta < -0.05$ (unstable) and (b) stability parameter ζ between -0.05 and 0.05 (near-neutral) for the month of October.

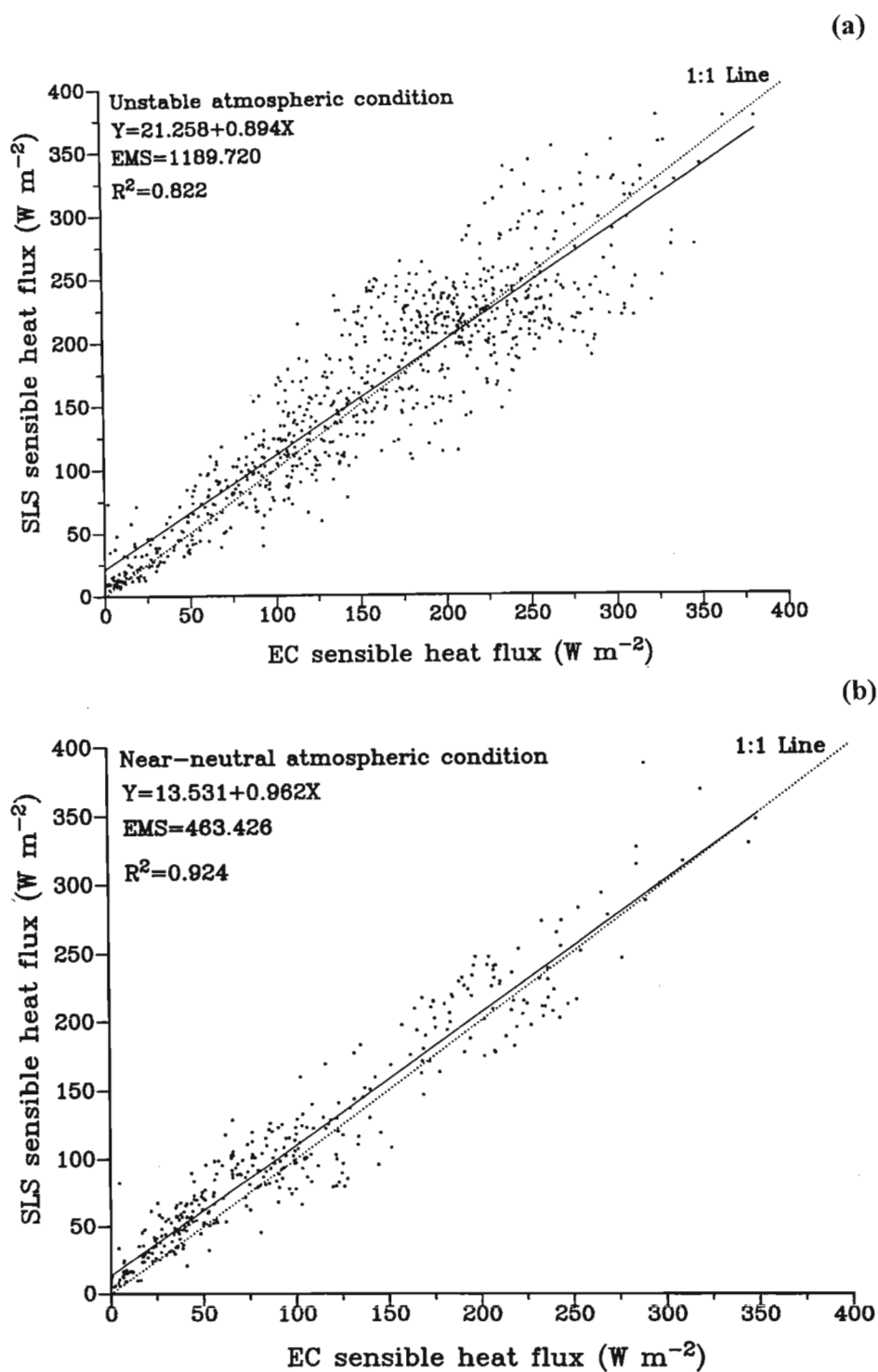


Fig. 4.14 Correlation of EC and SLS 2-min sensible heat flux for (a) stability parameter $\zeta < -0.05$ (unstable) and (b) stability parameter ζ between -0.05 and 0.05 (near-neutral) for the month of November.

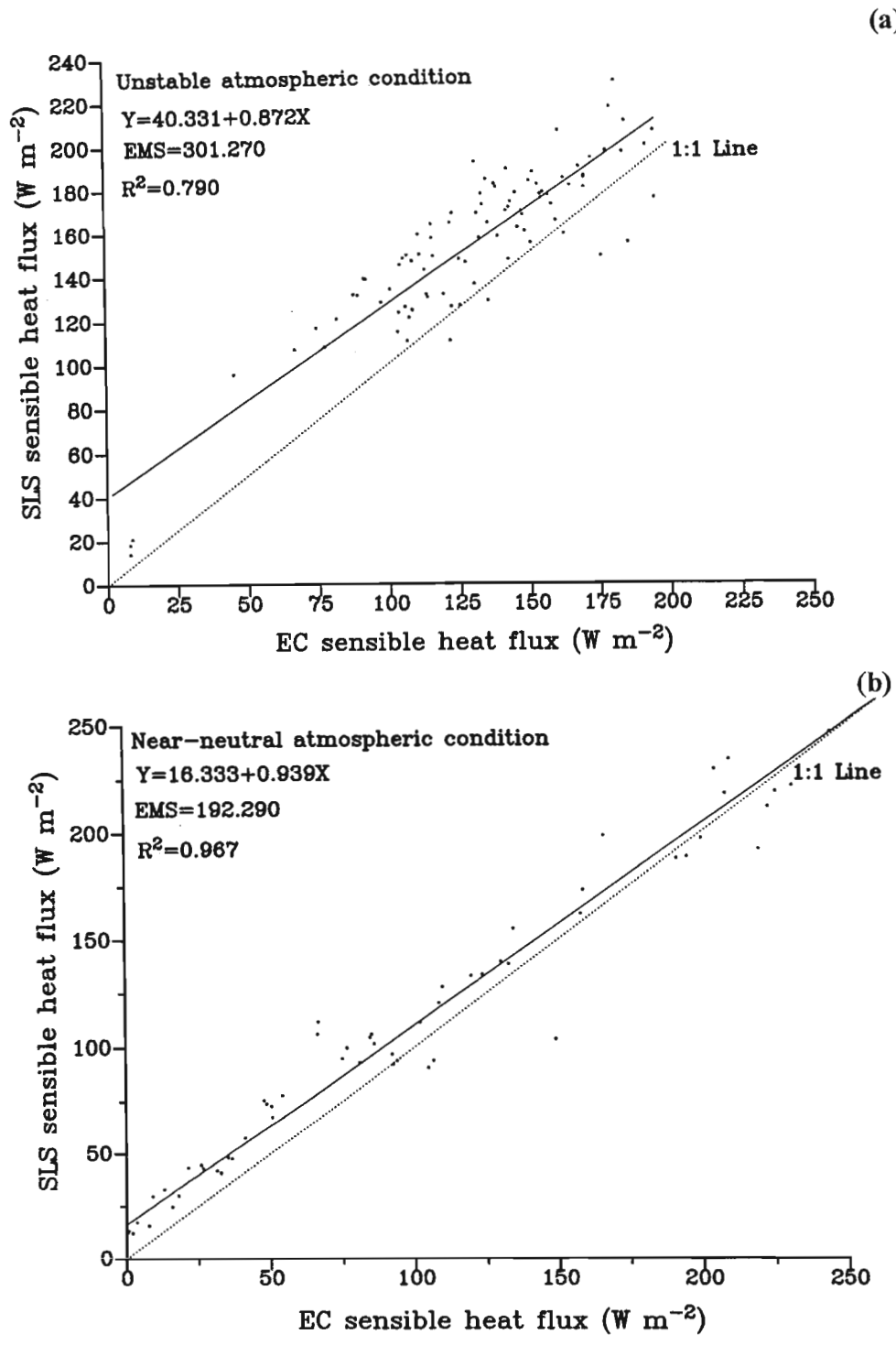


Fig. 4.15 Correlation of EC and SLS 20-min sensible heat flux for (a) stability parameter $\zeta < -0.05$ (unstable) and (b) stability parameter ζ between -0.05 and 0.05 (near-neutral) for the month of November.

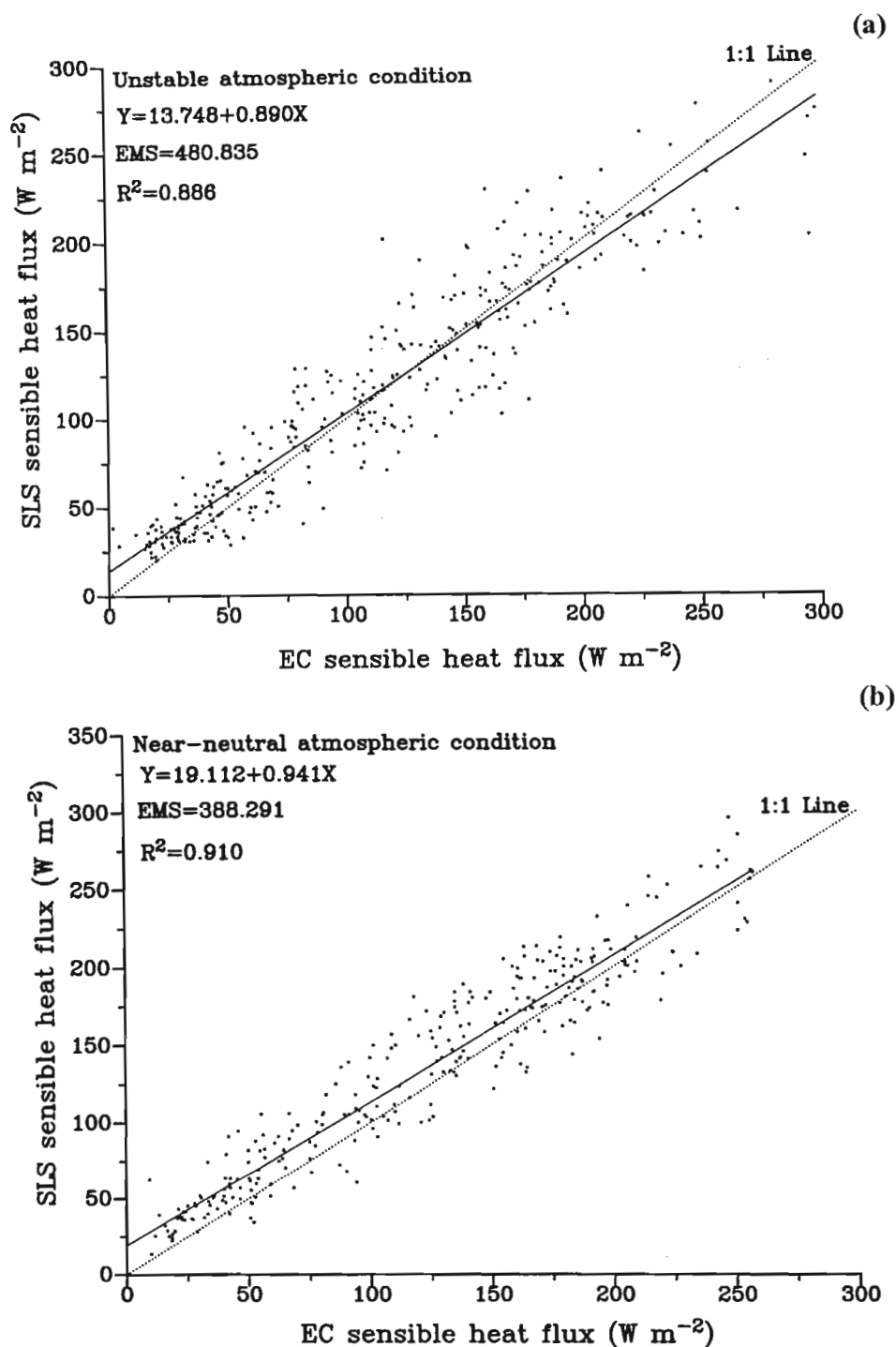
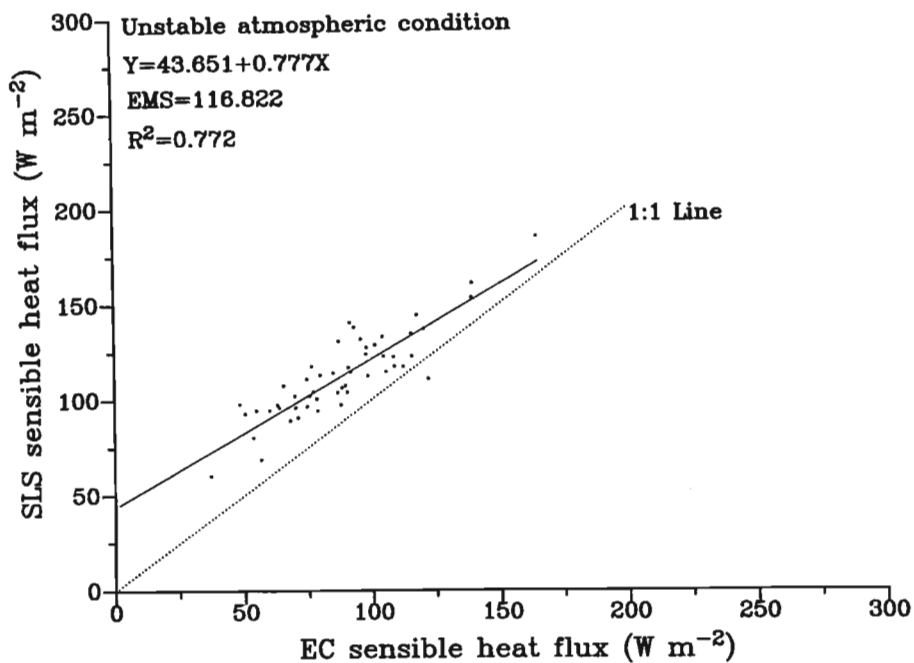


Fig. 4.16 Correlation of EC and SLS 2-min sensible heat flux for (a) stability parameter $\zeta < -0.05$ (unstable) and (b) stability parameter ζ between -0.05 and 0.05 (near-neutral) for the month of December.

(a)



(b)

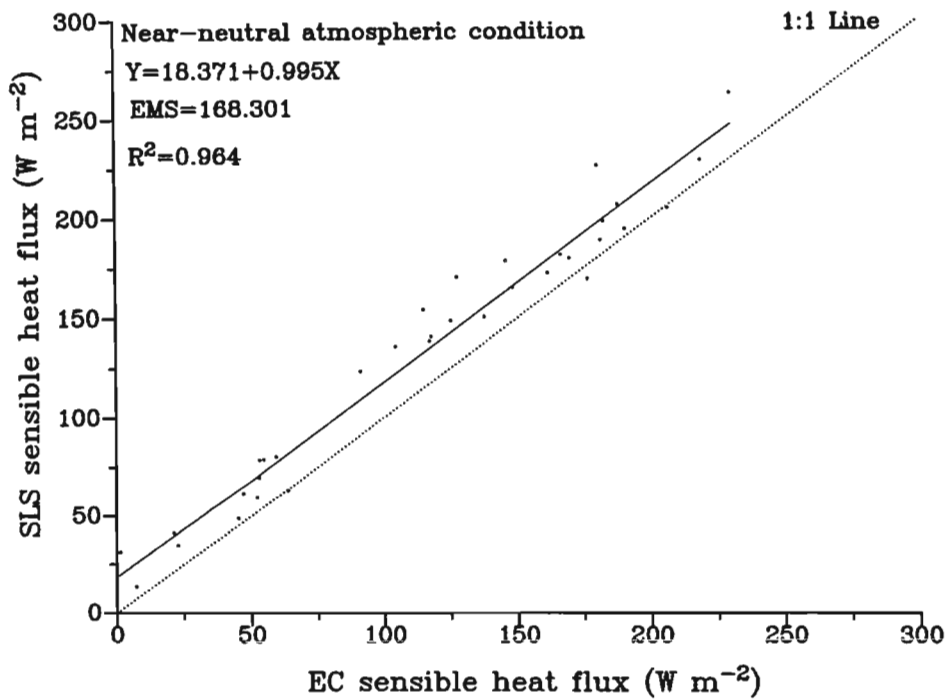


Fig. 4.17 Correlation of EC and SLS 20-min sensible heat flux for (a) stability parameter $\zeta < -0.05$ (unstable) and (b) stability parameter ζ between -0.05 and 0.05 (near-neutral) for the month of December.

Table 4.2 Results of correlation and t-test analysis of the sensible heat flux values obtained by SLS and EC methods for different stability conditions and different data-averaging periods. Also included in the table is the vegetation height h_{canopy}

Month	h_{canopy} ¹ (m)	Stability condition	<i>n</i>	R^2	<i>t</i> -value	<i>t</i> -table	Slope
May	0.02	Unstable 20-min	278	0.627	27.202	1.969	0.761
June	0.17	Unstable 20-min	495	0.651	37.585	1.965	0.831
July	-	Unstable 20-min	-	-	-	-	-
August	0.10	Unstable 20-min	390	0.767	40.807	1.966	0.953
October	0.19	Unstable 20-min	258	0.778	33.958	1.969	0.989
November	0.43	Unstable 20-min	54	0.772	15.102	2.007	0.777
December	0.46	Unstable 20-min	93	0.790	20.817	1.986	0.872
May	0.02	Unstable 2-min	2852	0.711	99.306	1.961	0.769
June	0.17	Unstable 2-min	3290	0.733	110.971	1.961	0.789
July	0.19	Unstable 2-min	1856	0.809	98.523	1.961	0.836
August	0.10	Unstable 2-min	2462	0.763	101.881	1.961	0.795
October	0.19	Unstable 2-min	1086	0.855	86.463	1.962	0.933
November	0.43	Unstable 2-min	829	0.822	68.162	1.963	0.894
December	0.46	Unstable 2-min	330	0.886	53.639	1.967	0.890
May	0.02	Near-neutral 20-min	88	0.863	25.055	1.988	0.979
June	0.17	Near-neutral 20-min	190	0.874	38.627	1.973	1.098
July	-	Near-neutral 20-min	-	-	-	-	-
August	0.10	Near-neutral 20-min	15	0.491	5.054	2.160	0.952
October	0.19	Near-neutral 20-min	26	0.954	22.842	2.064	1.110
November	0.43	Near-neutral 20-min	70	0.967	45.394	1.995	0.939
December	0.46	Near-neutral 20-min	40	0.964	32.489	2.024	0.995
May	0.02	Near-neutral 2-min	1027	0.768	66.469	1.962	0.859
June	0.17	Near-neutral 2-min	463	0.760	43.827	1.965	0.865
July	-	Near-neutral 2-min	-	-	-	-	-
August	0.10	Near-neutral 2-min	76	0.615	13.864	1.993	1.243
October	0.19	Near-neutral 2-min	68	0.916	28.031	1.997	1.033
November	0.43	Near-neutral 2-min	380	0.924	70.524	1.966	0.962
December	0.46	Near-neutral 2-min	300	0.910	57.542	1.968	0.941

¹ SLS measurement height for the SLS was 1.68 m. The EC method measurement height was 2 m.

The better agreement between EC and SLS F_h measurements during unstable atmospheric conditions could be explained by the fact that the increased turbulence during these periods causes greater mixing of the air and so the sensible heat flux is almost uniform within the surface layer over a wider area so the SLS (giving a spatially-averaged sensible heat flux measurement) and EC (a point measurement method) measurements seem to agree well.

However, in spite of the slight bias sometimes noticed in the measurements and hence reduced correspondence in F_h obtained by the two methods, the agreement in the F_h obtained is generally good to excellent considering that the EC method represents a point-estimate of sensible heat flux and SLS a path-weighted estimate. The general agreement is also an indication of the correct choice of $z-d$ used for the SLS MOST calculations and that the MOST coefficients used resulted in accurate determination of sensible heat flux.

The comparison of EC- and SLS-measured sensible heat flux for a day when l_o values (for part of the day) was around 2 mm (Fig. 4.18 a) is also presented. On this particular day the correspondence between the EC- and SLS-measured sensible heat values was poorer as indicated by $R^2 = 0.741$, slope = 0.896. It can also be noted from the diurnal plot of the EC and SLS sensible heat flux values for the same day (Fig. 4.18 b) that for the period when l_o is around 2 mm, the correspondence in the sensible heat values is less than for the period when l_o values are greater than 2 mm. Around midday when l_o approaches 2 mm, the sensible heat flux values measured by the EC and SLS methods appear more scattered. This can be attributed to high turbulent mixing during the unstable atmospheric condition compared to low turbulent mixing when the atmosphere is mainly stable.

Vegetation height also seems to slightly influence the agreement in the F_h measurements obtained by the two methods (EC and SLS) as is noticed from the slope values (Table 4.2 and Figs 4.5 to 4.17). However, this influence is not very consistent. For instance, for the 20-min F_h values during the unstable atmospheric conditions, the slopes corresponding to 0.10 m and 0.19 m vegetation height (short vegetation cover) are 0.953 and 0.989 respectively, which are greater than the slope values of 0.777 and 0.872 for vegetation heights of 0.43 m and 0.46 m (tall vegetation cover) respectively. On the other hand, for the 2-min averages under unstable atmospheric conditions, greater slope values are obtained for tall vegetation cover.

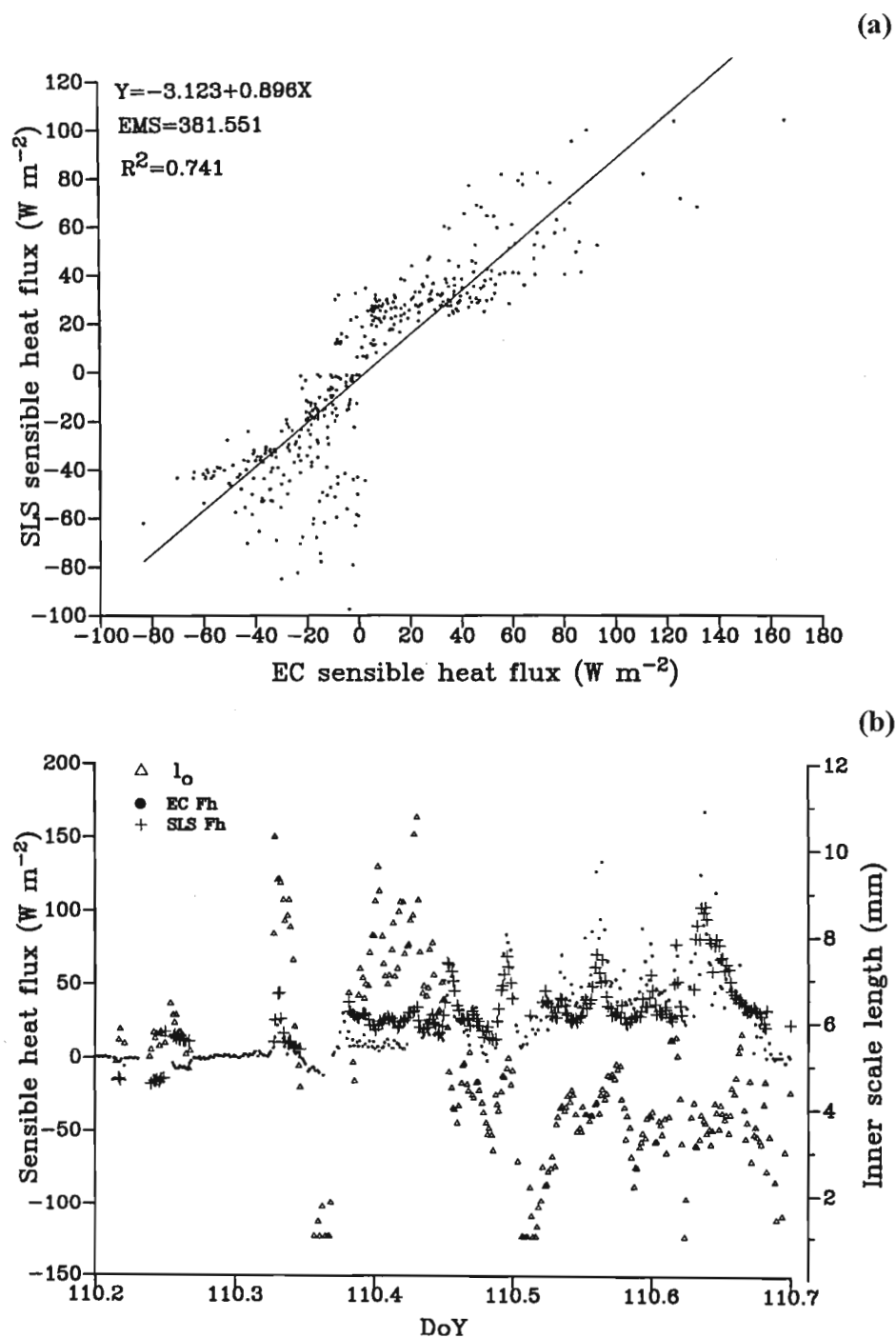


Fig. 4.18 (a) Comparison of 2-min EC- and SLS-measured sensible heat flux and (b) diurnal plot of the EC- and SLS-measured sensible heat flux for DoY 110. Also plotted is the diurnal variation of l_0 (right-hand y-axis).

For vegetation heights of 0.43 and 0.46 m, slope values of 0.894 and 0.890 corresponding to tall vegetation height are obtained, whereas the slopes corresponding to shorter vegetation heights of 0.10 m and 0.19 m are 0.836 and 0.795 respectively.

4.5 Conclusions

In this chapter an analysis of the F_h values measured by the two methods (EC and SLS) for different atmospheric stability conditions, unstable and near-neutral, was carried out. Also presented are the mean vertical wind speed plots as well as the path-weighted vegetation height. The mean vertical wind speed values measured by the EC method vary about 0 m s^{-1} for most of the days, both for the 2-min and 20-min averages. The 20-min averaging period results in data loss and therefore only few data were available for analysis. The 2-min average data used in the statistical analysis were good enough for comparison with the SLS data, resulting in reasonable results. The statistical analysis of the data reveals a seasonal trend in the F_h comparisons between the two measurement methods. There seems to be a better agreement in the F_h measurements the two methods as noted by higher correlation coefficients and t -values obtained during unstable atmospheric conditions in the cold months of June and August while lower agreement in the values are recorded in warm summer period from November to December. Also noted is a slight bias in the SLS measurement of F_h compared to the EC measurements. The bias in SLS F_h measurements is noticed for unstable atmospheric conditions whereas the EC method seems to record slightly greater values when the atmospheric condition is near-neutral. However the agreement between the F_h values measured by the two measurement methods is still good. The agreement is even more remarkable considering that the EC method is a point measurement method depending on the covariance between w and sonic temperature T whereas the SLS method is an areal-averaging method that depends on MOST and therefore also on $z - d$.

The inner scale length l_o values measured by the SLS method are larger in the evening and night-time when the atmospheric condition is stable than during the daytime when the atmosphere is mainly unstable. This can be attributed to greater turbulent mixing during the unstable atmospheric condition compared to low turbulent mixing when the atmosphere is mainly stable. As for the agreement in the sensible heat flux values measured by the EC and SLS methods, there is no distinct or consistent pattern. Vegetation height also seems to slightly

influence the agreement in the F_h measurements obtained by the two methods (EC and SLS) as is noticed from the slope values (Table 4.2 and Figs 4.5 to 4.17). In general, the slope values approach 1 with increasing vegetation height for both unstable and near-neutral atmospheric conditions, although there are exceptions especially for the month of November.

In this chapter, the main focus was on comparison of sensible heat flux measured by the EC and SLS methods for different atmospheric stability conditions with the aim of assessing the influence of atmospheric stability on the sensible heat flux measurements by the two methods. The influence of wind direction to the SLS beam path as well as the beam orientation was also carried out, the results of which are presented in Chapter 5.

Chapter 5: Influence of wind direction and a slanting beam angle on surface layer scintillometer estimates of sensible heat flux

5.1 Introduction

Understanding the partitioning of net irradiance into its component energy balance fluxes including sensible heat and latent energy flux measurements can provide valuable information about the local weather patterns. Such information is useful for water resource management, agriculture and environmental studies.

Estimation of areally-averaged turbulent surface flux measurements over large and heterogeneous surfaces has been addressed in the framework of different field experiments such as EuroFlux and Ameriflux (Baldocchi et al., 2001; Wilson et al., 2002) although these experiments have concentrated on carbon dioxide fluxes. It is well accepted that to obtain such areal estimates of turbulent heat flux including sensible heat and latent energy flux measurements, a deployment of a network of several point measurements would be required (Wyngaard, 1981; Thiermann and Grassl, 1992).

Due to their ability to integrate atmospheric processes along a path length, that may range from a few hundred metres to a few kilometres, optical methods based on the analysis of scintillation are considered as alternatives and a useful supplement to classical micrometeorological methods such as eddy covariance (EC) (Lagouarde, 2000). The use of scintillometry for surface flux measurement is therefore gaining in popularity, especially for studies done at a larger spatial scale and for validation of remotely sensed radiation and energy balance estimates (Tunick et al., 1994).

Scintillometry assumes that the Monin-Obukhov Similarity Theory (MOST) (Monin and Obukhov, 1954), which should only be valid for homogeneous surfaces, applies. In order to derive fluxes for the scintillometer method, therefore, one has to rely on MOST. Since MOST requires horizontal homogeneity of the surface, and given that environmental conditions that strictly meet this requirement of horizontal homogeneity are very rare, the question arises

whether scintillometer-derived sensible heat flux would be valid for heterogeneous surfaces. A number of authors (Beljaars, 1982; Meijninger et al., 2002; Weiss, 2002) have paid attention to the applicability of MOST over heterogeneous terrain.

A surface layer scintillometer (SLS) with its dual-beam has a path length of between 50 and 250 m and calculates a path-weighted sensible heat flux estimation with inputs of atmospheric pressure, air temperature, beam path length, beam height and measurements of the refractive index structure parameter (C_n^2) and through invocation of MOST (Hill, 1992). The work by Weiss (2002) carried out using a SLS (Thiermann and Grassl, 1992) in a slanting position was aimed at testing the applicability of the scintillometer method for estimation of sensible heat flux over a heterogeneous surface. Weiss (2002) indicates that the SLS measurements are not impaired by the slanting beam path which could mean that the scintillometer could be used to obtain sensible heat flux measurements over non-homogeneous land surfaces.

Apart from the beam angle orientation, the performance of the SLS method for the estimation of surface energy flux measurements in comparison to EC, which is always assumed to be the standard method for measuring the surface energy fluxes, has also been considered by some authors. The comparisons of sensible heat flux measurements obtained by the EC and SLS methods can be done in terms of a number of factors, or considering several factors, such as atmospheric stability, wind direction, etc. In a study carried out by Green et al. (1997), the SLS method appears to lose some of its advantage of line-averaging over the EC point-measurement method when the wind direction is parallel to the beam. In other words, the shape of the footprint of the scintillometer approaches more closely that for EC measurements. According to findings by Green et al. (1997), this results in closer agreement between the sensible heat flux measured by the two methods during the times when the wind direction is parallel to the beam compared to when the wind direction is nearly perpendicular to the beam. With the wind perpendicular to the beam, a wide source area is computed and the peak of the source is much more pronounced (Meijninger, 2003; Göckede et al., 2005). Green et al. (1997) suggested that studies in this area should be conducted with closer attention devoted to the performance of the scintillometer *vis á vis* wind direction relative to the optical path. On the other hand, recent findings by Nakaya et al. (2006), in a study carried out above a deciduous forest under unstable atmospheric conditions

using a SLS, found no clear relationship between sensible heat flux and wind direction for their site.

The accuracy of the measurements obtained by one method is judged by comparison of the measurements obtained by those of another method, considered or assumed to be the standard. As is already mentioned, the EC method is taken as the standard method for the determination of sensible heat flux. The EC method does not involve MOST and the flux estimates do not involve any height parameters such as the measurement height or vegetation height.

The main objective of this chapter is therefore to compare sensible heat flux estimated by the SLS method with that obtained by the EC method for wind direction approximately or nearly perpendicular to the SLS beam path, with measurements obtained when the wind direction is approximately parallel to the beam path. Also investigated in this chapter is the comparison of sensible heat flux measured by the SLS at slanting beam angles with that obtained by the EC method, as well as determination of the SLS footprint and comparison with the EC footprint.

The main assumption is that the agreement between the sensible heat flux measured by the two methods will be better when the wind direction is nearly parallel to the beam compared to when the wind is at an angle or nearly perpendicular to the SLS beam and when the SLS beam is horizontal. This is assumed given that the source area for the SLS is greater than that of the EC system when the wind is nearly mainly perpendicular to the beam path.

5.2 Theoretical background

5.2.1 Scintillometry

Full details of the theoretical background information on scintillometry and the reviews on optical scintillometry method are available in the papers by Andreas (1990) and Hill (1992), and other literature on the use of scintillometers for surface energy flux measurements. In this chapter, only a brief discussion of the theory behind the scintillometer is presented.

The use of the scintillometer method for the measurement of turbulent fluxes is based on the fact that the refractive index structure parameter measured directly by the scintillometer (C_n^2 , $\text{m}^{-2/3}$) can be related to the structure function parameter of temperature C_T^2 ($\text{K}^2 \text{m}^{-2/3}$) from which sensible heat flux (F_h , W m^{-2}) is derived using MOST. A beam is transmitted over a path and the

fluctuations in the beam intensity at the receiver are analysed to give the variations in the refractive index along the path. The variance of the logarithm of amplitude fluctuations measured by SLS is related to the path-averaged refractive index structure parameter C_n^2 , when $l_o \ll F \ll L_o$, where l_o is the inner scale length, $F = \sqrt{\lambda \times L_{beam}}$ the Fresnel zone and L_o is the outer scale length, and is approximately equal to the measurement height, as follows:

$$\sigma_{12}^2 = 0.496 K^{7/6} L_{beam}^{1/6} C_n^2 \cdot \Phi_n \left(l_o / \sqrt{\lambda L_{beam}} \right) \quad 5.1$$

where $K = 2\pi / \lambda$ is the optical wave beam number, λ is the beam wavelength, Φ_n is the three-dimensional spectral function and L_{beam} is the SLS beam path length (Wang et al., 1978). Equation 5.1, which is based on the first-order scattering theory, is only valid in the weak scattering regime and is therefore only applicable when $\sigma_{12}^2 < 0.3$ (Clifford et al., 1974).

The intensity fluctuations are caused by inhomogeneities in the refractive index, which are due to turbulent eddy motions along the scintillometer path. The transmitter emits a beam with a certain wavelength for a known horizontal beam path length, the intensity fluctuations (expressed as C_T^2) that are caused by the turbulent eddies are analysed to give sensible heat flux measurements. These eddy motions are generated by air temperature and humidity fluctuations, and can be regarded as a collection of converging and diverging lenses. Because the measured variance of the logarithm of the signal intensity fluctuations is a measure of the turbulent behaviour of the atmosphere, it can be indirectly related to the transport of certain quantities such as sensible heat, latent energy and flux measurements of other matter (Thiermann and Grassl, 1992).

In this study, a displaced-beam small aperture scintillometer (Scintec Atmosphärenmesstechnik, Tübingen, Germany), referred to as surface layer scintillometer (SLS) that emits two parallel differently polarised laser beams with a small separating distance was used. The Scintec SLS40-A uses a class 3a type laser at a wavelength of 670 nm, a beam displacement distance, d_{SLS} , of 2.7 mm and a receiver detector diameter, D_{SLS} of 2.5 mm. With this instrument a laser beam of one source is split into two parallel, displaced beams with orthogonal polarization. By determining both the variances of the logarithm of the amplitude of

the two beams, σ_1^2 and σ_2^2 and the covariances of the logarithm of the amplitude fluctuations between the two beams, σ_{12}^2 , one can derive l_o and C_n^2 as follows (Hartogensis et al., 1994):

$$\sigma_{12}^2(k, l_o, C_n^2) = 4\pi^2 K^2 \int_{r=0}^{L_{beam}} \int_{k=0}^{\infty} k \Phi_n(k, l_o, C_n^2) \cdot \sin^2 \left[\frac{k^2 \cdot r \cdot (L_{beam} - r)}{2K L_{beam}} \right] dk \cdot dr \quad 5.2$$

$$\sigma_{12}^2(k, l_o, C_n^2, d_{SLS}) = 4\pi^2 K^2 \int_{r=0}^{L_{beam}} \int_{k=0}^{\infty} k \Phi_n(k, l_o, C_n^2) J_0(k d_{SLS}) \cdot \sin^2 \left[\frac{k^2 \cdot r \cdot (L_{beam} - r)}{2K L_{beam}} \right] \cdot \left[\frac{4J_1^2(k D_{SLS} r / 2L_{beam})}{(k D_{SLS} r / 2L_{beam})^2} \right] dk \cdot dr \quad 5.3$$

where k is the turbulent wave number of the radiation, $\Phi_n(k, l_o, C_n^2)$ the spectrum of the refractive index fluctuations given as $\Phi_n(k, l_o, C_n^2) = 0.033 \cdot C_n^2 \cdot k^{-11/3} f_\phi(k l_o)$, J_0 and J_1 are Bessel functions of the first kind of order one, D_{SLS} the aperture diameter of the scintillometer detectors, d_{SLS} is the beam displacement distance ($= 2.7$ mm for SLS), r is the distance at a particular position along the beam measured from the transmitter, and $K = 2\pi / \lambda$ is the optical wave number. Equation 5.3 is only valid as long as scattering is weak, i.e. $\sigma_{12}^2 < 0.3$ (Thiermann and Grassl, 1992). From the variances and covariances of the intensity modulations of the received signals, C_n^2 and l_o can be derived.

5.2.2 Footprint analysis

Knowledge of the spatial extent and relative importance of upwind source areas to downwind turbulent fluxes can be obtained through a footprint analysis. Such an analysis is commonly used to describe the relative contribution of each upwind surface source to the measured flux - in this case, sensible heat flux and depends mainly on the measurement height, surface roughness and the atmospheric stability (Gash, 1986; Leclerc and Thurtell, 1989; Savage et al., 1995, 1996, 1997; Hsieh et al., 2000).

The relative contribution from upwind areas to the flux (f) is estimated from a footprint function which relates the measured flux at measurement height z_m to the spatial distribution of surface flux (Gash 1986; Horst and Weil, 1992):

$$F(x, z_m - d) = \int_{-\infty}^x S(x) \cdot f(x, z_m - d) dx \quad 5.4$$

where $F(x, z_m - d)$ is the flux measured at height z_m at point $(x, z_m - d)$, $S(x)$ the source strength per unit area, f the footprint at distance x (with distance x taken as the downwind fetch) and z_m the measurement height.

Following the footprint model used by Hsieh et al. (2000), which is analytically-based and combines the results from a Lagrangian stochastic model and uses dimensional analysis, footprint function f in this study is defined as a function of the downwind fetch distance x , the Obukhov length L , a length scale z_u , and similarity constants D and P :

$$f(x, z_m - d) = \frac{1}{k^2 x^2} D z_u^P |L|^{1-P} \exp\left(\frac{-1}{k^2 x} D z_u^P |L|^{1-P}\right) \quad 5.5$$

where k ($= 0.4$) is the von Karman's constant. Values for the similarity constants for different atmospheric stability conditions are, as obtained by Hsieh et al. (2000), as specified below:

$D = 0.28$ and $P = 0.59$, for unstable conditions;

$D = 0.97$ and $P = 1$ for near neutral and neutral conditions;

$D = 2.44$ and $P = 1.33$, for stable conditions.

The expression by Hsieh et al. (2000) for the length scale z_u was corrected by Savage et al. (2004) who then also included the z_o and d terms:

$$z_u = (z_m - d) \cdot \frac{z_m - d}{z_m - (z_o + d)} \cdot \left[\ln \frac{z_m - d}{z_o} - 1 + \frac{z_o}{z_m - d} \right], \quad 5.6$$

where d is the displacement height (which is estimated as 2/3 times the canopy height) and z_o roughness height (which is estimated as 0.1 times the canopy height). Equation 5.6 is only valid for $z_m > d + z_o$.

The explicit estimation of the peak location (x_{\max}) of the footprint model as a function of the atmospheric stability (based on L) and z_u (Brutsaert, 1982), is determined by differentiating Eq. 5.5 with respect to x and setting the resultant equation to zero. Hence the peak location (x_{\max}) is given as:

$$x_{\max} = \frac{D z_u^p |L|^{1-p}}{2k^2} \quad 5.7$$

5.3 Experimental details

5.3.1 Study area

Field measurements were carried out from January to December 2004 over an open mixed grassland site in Ashburton (30°27' E, 29°40' S) close to Pietemaritzburg in KwaZulu-Natal, South Africa, Fig. 3.1, with an altitude of 671.3 m. The climate is humid and sub-tropical with summer rainfall and long dry periods in winter. Air temperature ranges between -4 and 42 °C (Weather SA, 2006). The surface within 135 m in the prevailing south east wind direction was nearly level with a slope of 1° 15' to the south east (Savage et al., 2004, 2005). KwaZulu-Natal, on the eastern seaboard of South Africa (Fig. 3.1), is bordered by the warm Indian Ocean to the east and the high escarpment of the Drakensberg Mountains to the west. The climate is sub-tropical and humid with summer rainfall. Occasional frosts occur in winter.

Surface flux measurements were carried out using three different measurement methods, namely a SLS and an EC system together with Bowen ratio energy balance (BREB) measurements. The EC and BREB systems were positioned at the midpoint of the SLS beam path (Fig. 5.1). The SLS was installed over a path-length of 101 m at an effective height of 0.68 m (although this changed for the sloping beam path orientation). The EC set up consisted of a 3-dimensional sonic anemometer (SWS-211/3V, Applied Technologies, Boulder, Colorado, USA). The EC instruments were positioned at a height of 1.45 m above the ground surface, although this was later changed to a height of 2.12 m above the ground. The input of sonic temperature and the three wind velocity components namely u , v , w in the x , y and z directions respectively, were recorded using a Campbell Scientific 23X (Logan, Utah, USA) datalogger every 0.1 s (at a frequency of 10 Hz), after which the covariance between w and sonic temperature (T) for an averaging period of 2 min was used to calculate the sensible heat flux (F_h).

So as to test the scintillometry method for non-ideal (heterogeneous) surfaces, the SLS was set up in an inclined position (Fig. 5.2) from DoY 230 to 241. The receiver was placed at 0.68 m above the ground level and transmitter at 1.68 m, resulting in an effective height of 1.18 m, calculated as the average height of the two heights less the vegetation height at the midpoint of the scintillometer beam path where the weighting of sensible heat flux is greatest since the site

where the measurements were done was relatively flat and vegetation height nearly uniform across the field. The vegetation height at the mid point was ~ 0.1 m.

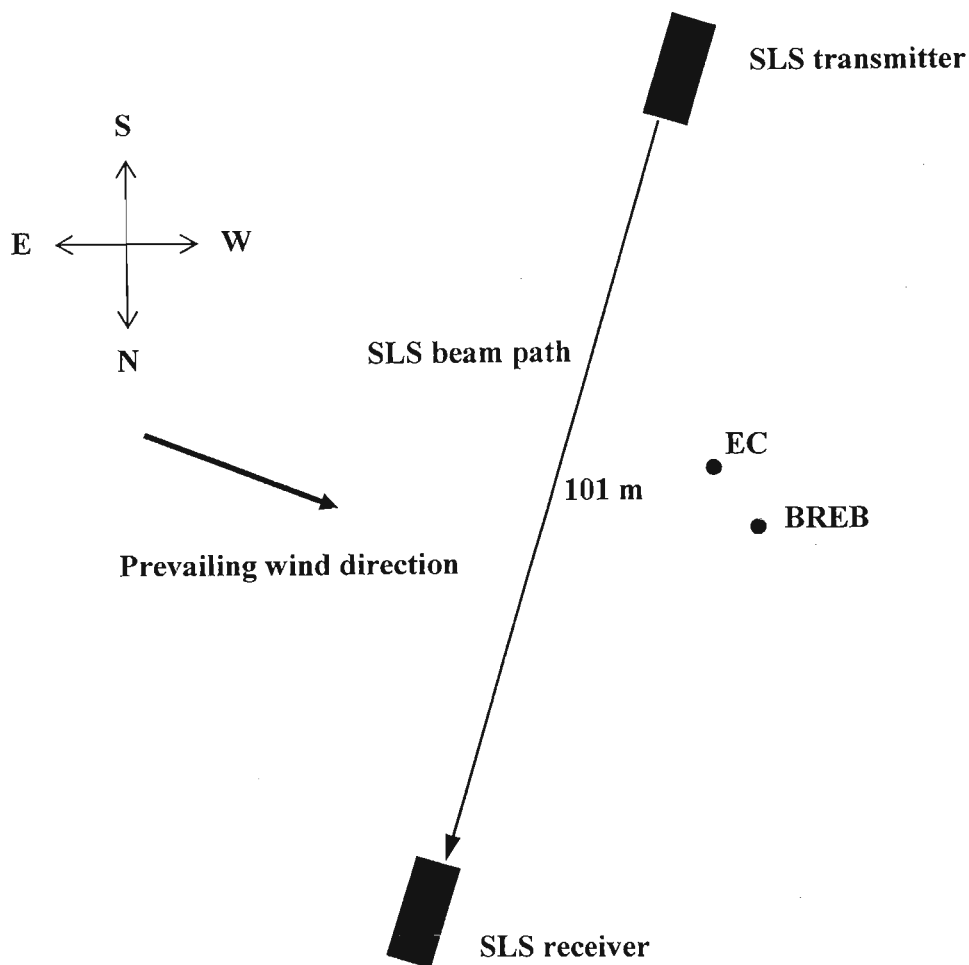


Fig. 5.1 Schematic of the mixed community grassland research site at Ashburton showing the positioning of the instrumentation used in the study. The SLS beam path distance (from the transmitter to receiver) and wind direction are also indicated. The diagram is not to scale.

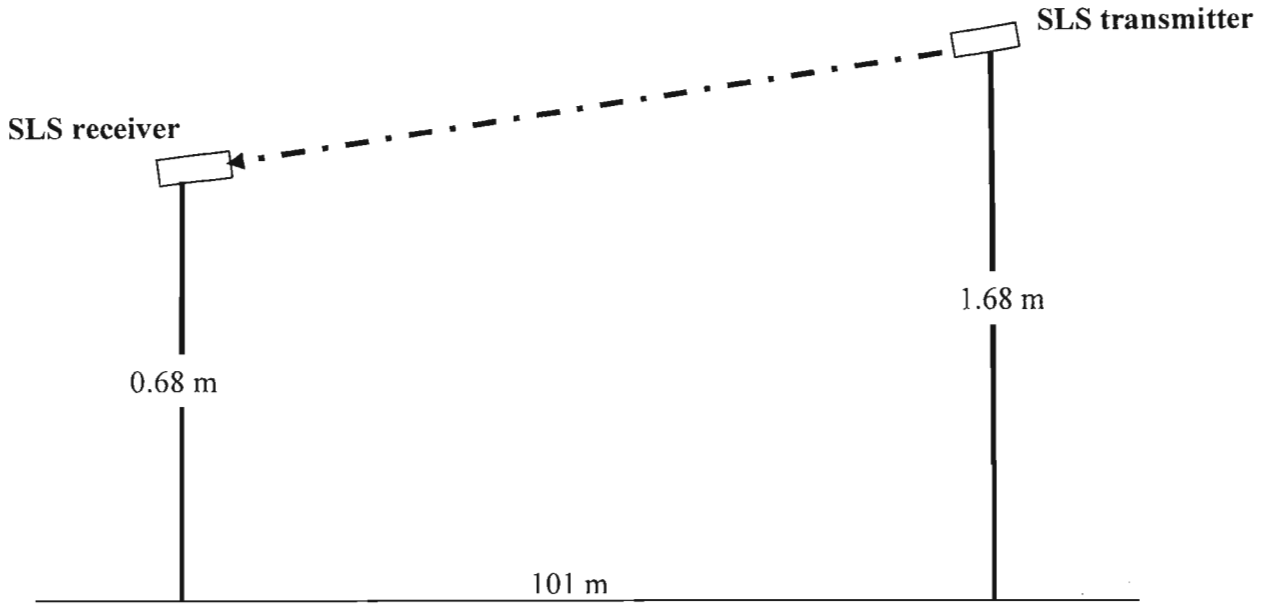


Fig. 5.2 Scintillometer set up in an inclined beam path with the receiver set at 0.68 m and transmitter at 1.68 m above the ground level. The diagram is not to scale.

Sensible heat flux data obtained using the SLS method for an inclined beam angle were subsequently analysed and compared with data obtained using the EC method. The data were treated in the same way as the rest (those measured with the SLS transmitter and receiver set at the same height above ground) before comparison with EC measurement. Both 2-min and half-hourly averages of sensible heat flux obtained using the EC and SLS methods were compared.

5.3.2 Wind vector calculations, and analysis

Daytime (06h00 to 18h00) wind speed values were calculated from 2-min values of the horizontal wind speed (U) and wind direction (θ) referenced to North and anticlockwise from North using vector algebra for which the number of data points n in the 2-min period is 1200:

$$\bar{u}_x = u = (\sum U \cos \theta) / n$$

$$\bar{u}_y = v = (\sum U \sin \theta) / n$$

5.8

$$U = \sqrt{u^2 + v^2}$$

$$\theta = \arctan (\bar{u}_y / \bar{u}_x).$$

5.4 Results and discussion

5.4.1 Comparison of sensible heat flux using the SLS at a slanting beam angle with EC measurements

A summary of the statistical analyses results are shown in Table 5.1. Both the 2-min and half-hourly averages of sensible heat flux show good agreement for the two methods. An improved correspondence (due to the averaging) is noticed for the half-hourly averages of sensible heat flux measured by the EC and SLS methods.

Corresponding sensible heat flux comparisons are presented in Figs 5.3 to 5.7, with Figs 5.3 and 5.6 showing correlation analysis results for 2-min averages of sensible heat flux for the two methods, and Figs 5.4 and 5.7 for the half-hourly averages. An example of the diurnal variation of sensible heat flux measured by the two methods (EC and SLS) is presented in Fig. 5.5. For the half-hourly averages comparison, t -value = 73.89, with a slope of 0.940 (Fig. 5.4); and $t = 59.94$, with a slope of 0.977 (Fig. 5.7), for DoY 230 to 241 and DoY 241 to 251, 2004, respectively were obtained. For the 2-min EC and SLS F_h comparisons, $t = 166.94$, with a slope of 0.887 (Fig. 5.3); and $t = 104.63$ with a slope of 0.980 (Fig. 5.6) for DoY 230 to 241 and 241 to 251, 2004, respectively.

Table 5.1 Summary of the statistical analyses together with canopy height for the comparison of SLS sensible heat flux measurements with those obtained using the EC method.

Fig.	DoY and averaging period	Slanting beam path	h (m)	n	R^2	t -value	t -table	Slope
5.3	230 to 241 (2-min)	Yes	0.10	2371	0.915	166.94	1.961	0.887
5.4	230 to 241 (30-min)	Yes	0.10	204	0.963	73.89	1.972	0.940
5.6	241 to 251 (2-min)	Yes	0.12	1228	0.888	104.63	1.962	0.980
5.7	241 to 251 (30-min)	Yes	0.12	196	0.946	59.94	1.972	0.977
5.9	275 (2-min)	No	0.19	718	0.945	114.10	1.963	1.046
5.16	131 (2-min)	No	0.02	632	0.885	74.02	1.964	0.931
5.13	287 (2-min)	No	0.20	631	0.888	74.94	1.964	1.028
5.18	107 (2-min)	No	0.73	622	0.932	95.49	1.964	0.992

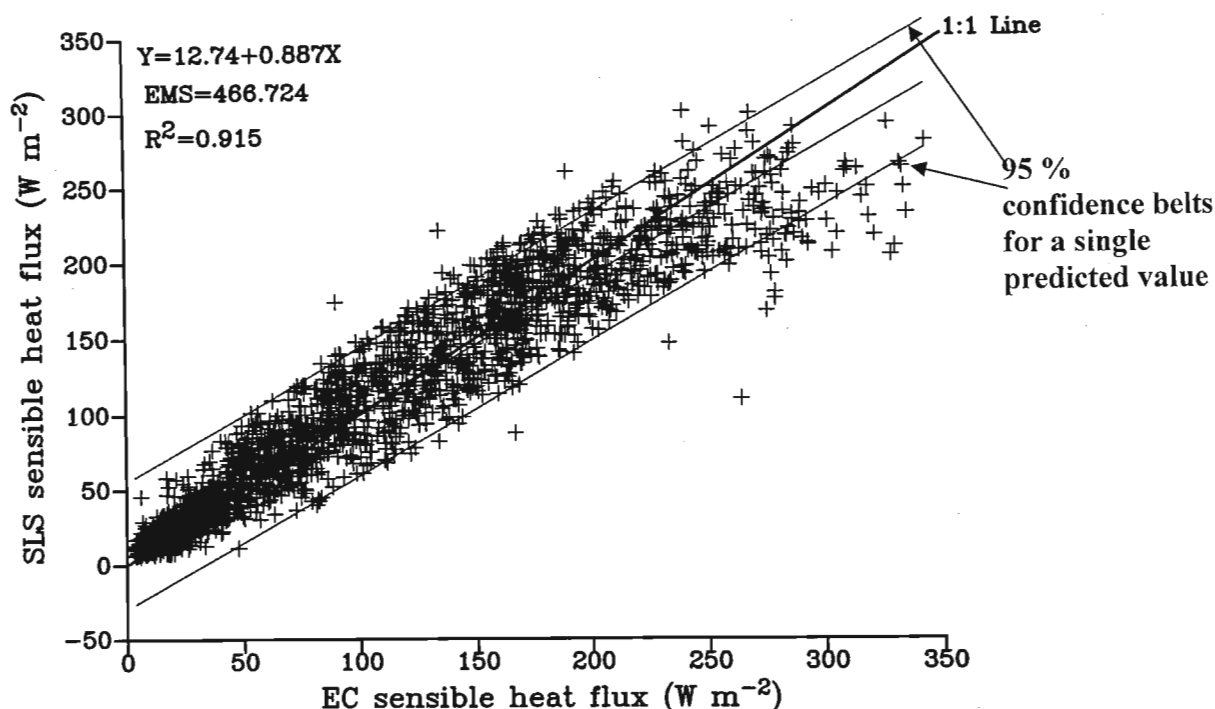


Fig. 5.3 Comparison of 2-min sensible heat flux measured by EC and SLS methods for DoY 230 to 241, with the SLS beam set at a slanting angle where the transmitter was set at a height of 1.68 m above the ground level and the receiver at a height of 0.68 m. The effective beam height was 1.18 m with the EC method at a height of 2 m.

The comparison is better for $F_h > 300 \text{ W m}^{-2}$ as is shown by most data points within the 95 % confidence belts for a single predicted value (Fig. 5.3).

There is also a greater bias of the regression line from the 1:1 line for large sensible heat flux values indicating bias in the comparisons when the sensible heat flux values are large (Fig. 5.3). The finding is in good agreement with that of Weiss (2002) who carried out a study in Switzerland using SLS (model SLS20) set up at a slanting position, and obtaining sensible heat flux measurements which agreed well with those obtained by the EC method. Whereas Weiss's research was conducted for only few days (Table 1.3), this current study was carried out over a year spanning different seasons in a year with different meteorological conditions such as various stability conditions. The consistent close agreement of the sensible heat flux measurements by the EC and SLS methods confirms the suitability of the method (SLS) for turbulence flux measurements even for heterogeneous surfaces and when the beam is not

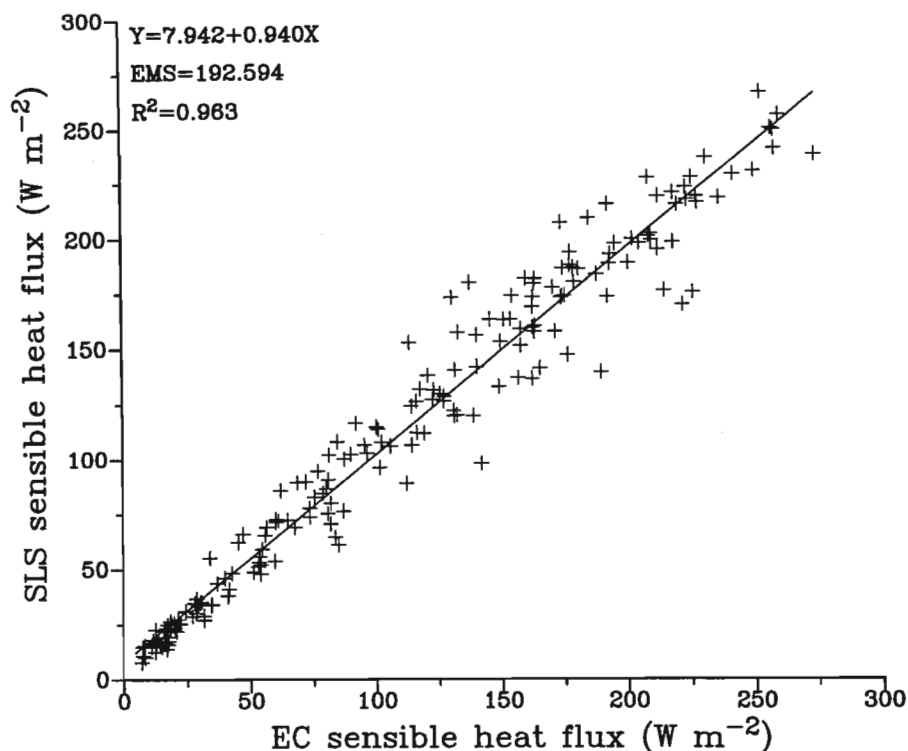


Fig. 5.4 Comparison of 30-min sensible heat flux obtained by EC and SLS methods for DoY 230 to 241, with the SLS beam set at a slanting angle.

horizontal as is required by MOST.

An example of the diurnal trend (Fig. 5.5) of sensible heat for the two methods further confirms the good agreement between them. From the plots, the EC sensible heat flux shows more scatter compared to the SLS-measured F_h , especially around midday when the measured F_h values are at their peak value, but generally the two plots coincide well. This is mainly because the SLS method gives line-averaged measurements of sensible heat with smoother (less varying) data points compared to the EC-measured sensible heat flux.

The findings confirm that the SLS setup does not impair its performance in measuring sensible heat flux. This also shows that the SLS would work well in non-ideal (heterogeneous) conditions which the inclined optical beam path mimics. In most cases real field measurements take place under such conditions and hence the importance of testing the SLS for such.

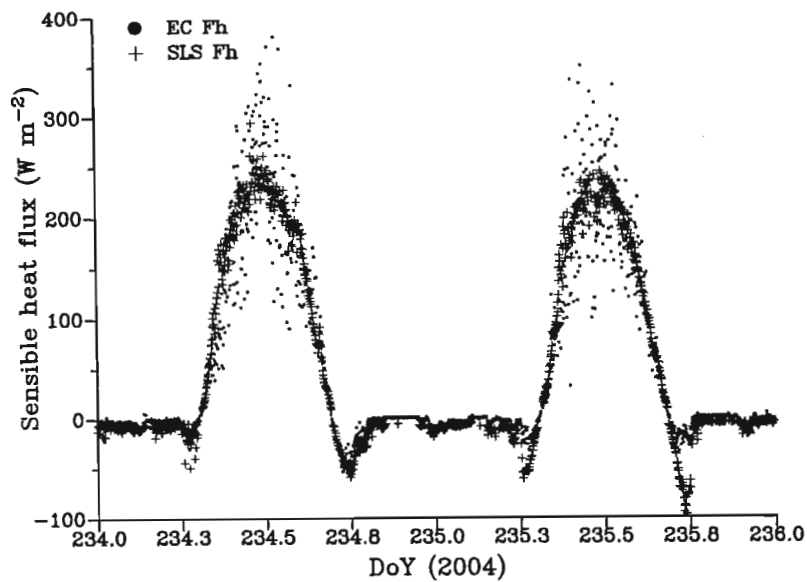


Fig. 5.5 Diurnal plot of 2-min EC- and SLS- measured sensible heat flux for DoY 234 and 235 for when the SLS beam was set at slanting angle.

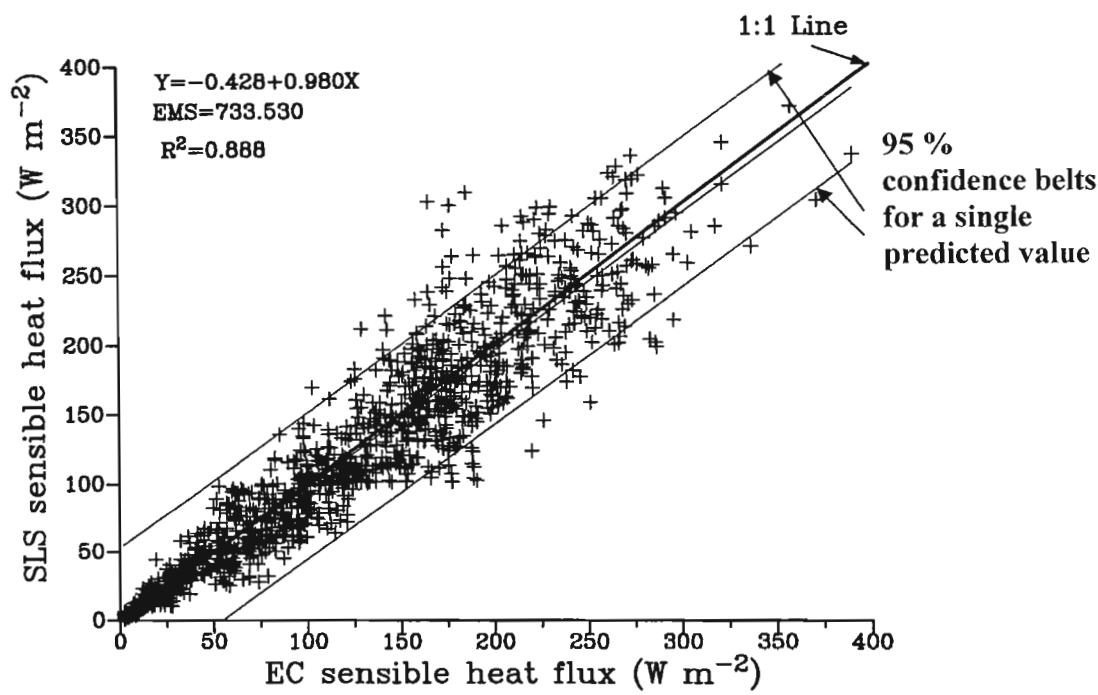


Fig. 5.6 Comparison of 2-min sensible heat flux measured by EC and SLS methods for DoY 241 to 251, with the SLS beam set at a slanting angle.

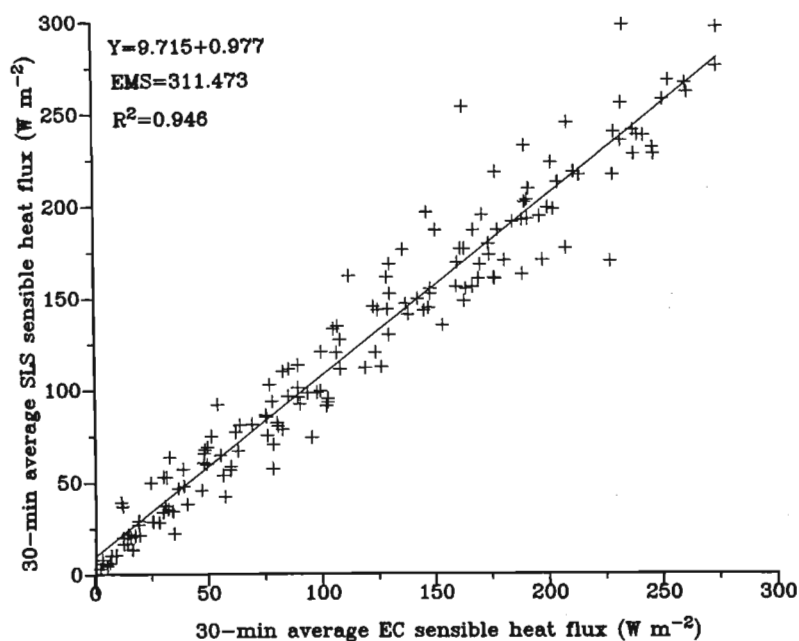


Fig. 5.7 Comparison of 30-min sensible heat flux measured by EC and SLS methods for DoY 241 to 251, with the SLS beam set at a slanting angle.

5.4.2 Comparison of EC- and SLS-measured sensible heat flux measurements for different wind directions

Two-min wind direction and horizontal wind speed data obtained by the EC method were analysed and results for selected days when the prevailing wind direction was either approximately perpendicular, parallel to the SLS beam path, or irregular, are presented in Figs 5.8 to 5.11. In these diagrams, for example, 12h30 wind vector occurs at $y=12h$ and $x=30\text{ min}$. The wind direction data obtained from the EC system were converted to radians and plotted using Origin software (OriginLab, 2000). Only daytime data (from 06h00 to 18h00) were plotted. Wind direction is shown by the direction of the arrows whereas horizontal wind speed is indicated by arrow length so that a longer arrow indicates greater wind speed than a shorter one. The orientation of the SLS beam path is also shown on the plots as well as the compass direction.

For most days, the prevailing wind direction was more or less perpendicular to the beam path, although there were days when the wind direction was irregular. Even for the days when the wind direction was mainly perpendicular to the SLS beam path, for some hours during the day there was irregularity in the direction (e.g. DoY 287, 2004).

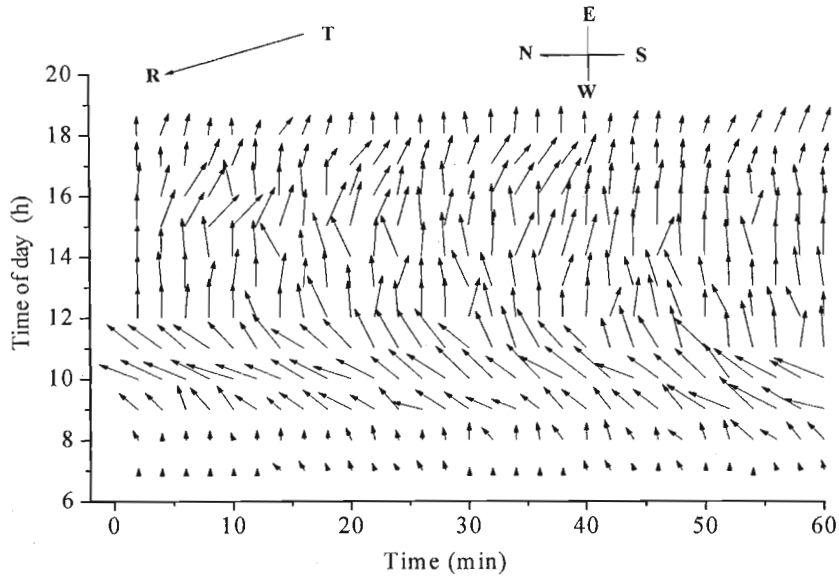


Fig. 5.8 Wind vector variation between 06h00 to 18h00 for DoY 275. The arrows point to the wind direction and wind speed is indicated by the length of the arrows. On this particular day wind direction was nearly perpendicular to the SLS beam.

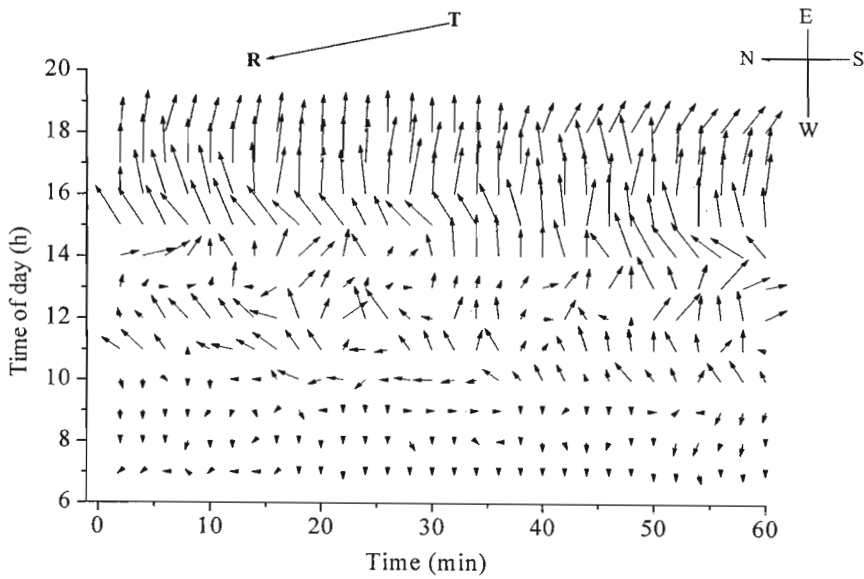


Fig. 5.9 Wind vector variation between 06h00 to 18h00 for DoY 287 for which the wind direction was random in the morning hours of the day and nearly perpendicular to the SLS beam path in the afternoon.

Fig. 5.11 Wind vector variation between 06h00 to 18h00 for DoY 107 for which the wind direction was random.

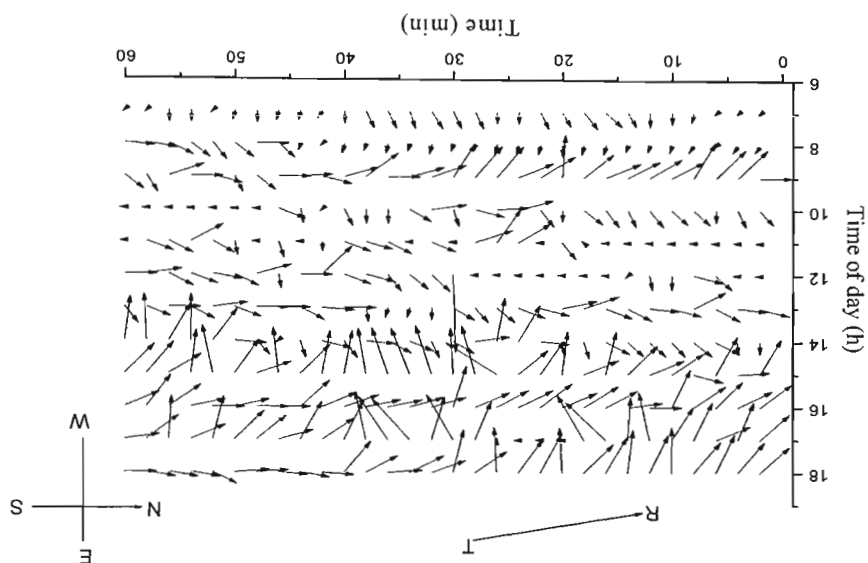
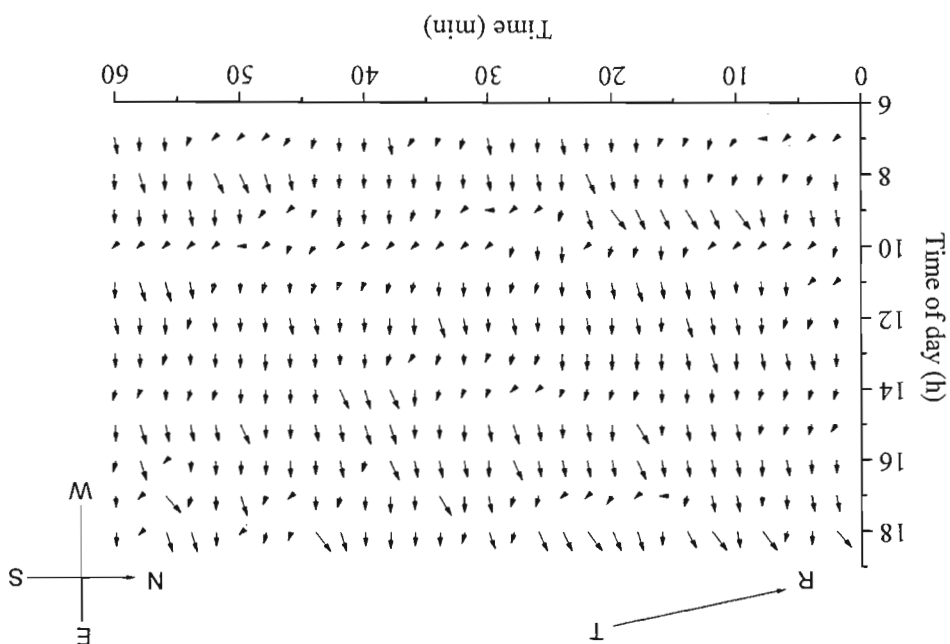


Fig. 5.10 Wind direction between 06h00 to 18h00 for DoY 131 for which wind direction was nearly perpendicular to the SLS beam path but with low wind speed.



In Figs 5.8 and 5.10 (DoY 275, and 131, respectively) the wind direction is mainly perpendicular to the SLS beam path nearly throughout the day whereas in Fig. 5.9 (DoY 287), the wind direction is perpendicular to the beam except between 11h00 and 14h00, when the wind direction is irregular. Figure 5.11 (DoY 107) on the other hand is an example of when the wind pattern was irregular throughout the daytime period considered in the analysis.

For those days when the wind direction was approximately perpendicular to the SLS beam path, the sensible heat flux (F_h) values obtained by the EC and SLS methods seem to be in better agreement than for those days when the wind direction is irregular. For instance, for DoY 275, $t = 114.10$, and slope = 1.046 (Fig. 5.12). The diurnal plots for the respective days also show good agreement in the F_h values obtained by the two methods for the days when the wind direction is mainly perpendicular to the SLS beam path. This is well demonstrated in Fig. 5.13.

An example of one of the days when the wind direction was random for part of the day and perpendicular to the beam for the rest of the day is DoY 287 when the wind direction was irregular between 11h00 and 14h00 but perpendicular for the rest of the day (Fig. 5.14 b). On this particular day, the diurnal plot of F_h (Fig 5.14 a and for emphasis b) shows the effect the wind direction or pattern has on the agreement in F_h values estimated by the EC and SLS methods. It can be seen from this plot that in the interval when the wind pattern was highly irregular, there seem to be a disagreement in the F_h values. This is also reflected by the t -value obtained by correlating the F_h estimates for the two methods, with $t = 74.94$ and slope = 1.028 (Table 5.1, Fig. 5.15). In Fig. 5.14 b, the distinction between SLS estimates of sensible heat flux for times when the wind direction was approximately perpendicular to the beam and when the wind direction was random makes this more clear as can be seen from the diurnal plot. In the early hours of the day (mainly before midday) the sensible heat flux measurements obtained by the two methods do not agree well - this coincides with times when the wind direction was irregular - as compared to the time after midday when the agreement in sensible heat flux measurement by the two methods, as indicated by the coincidence in the plots, is improved.

In Fig. 5.16, the diurnal plot of 2-min SLS- and EC-measured sensible heat flux for DoY 131 with wind direction was nearly perpendicular to the SLS beam path is shown but when the wind speed was low.

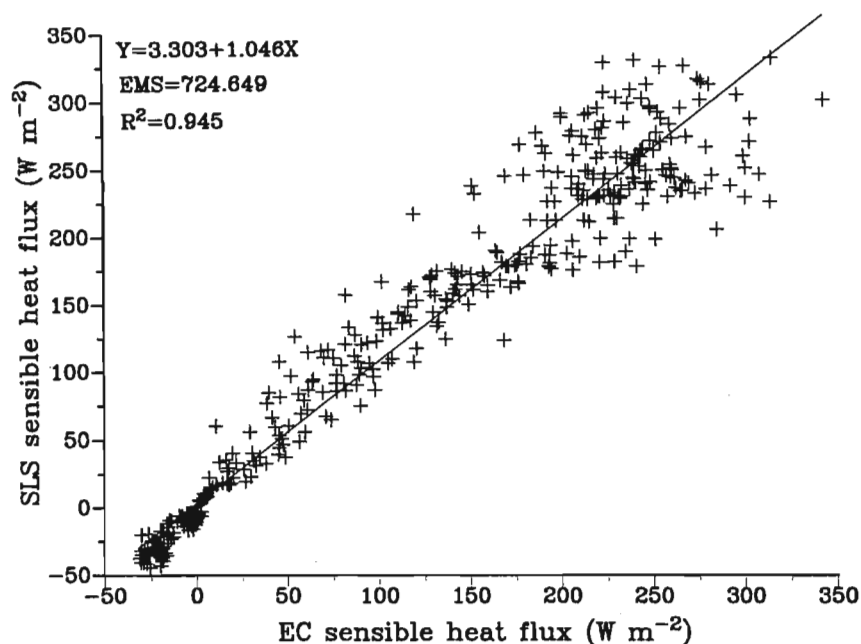


Fig. 5.12 Comparison of 2-min sensible heat flux measured by EC and SLS methods for DoY 275 for which wind direction is nearly perpendicular to the SLS beam path.

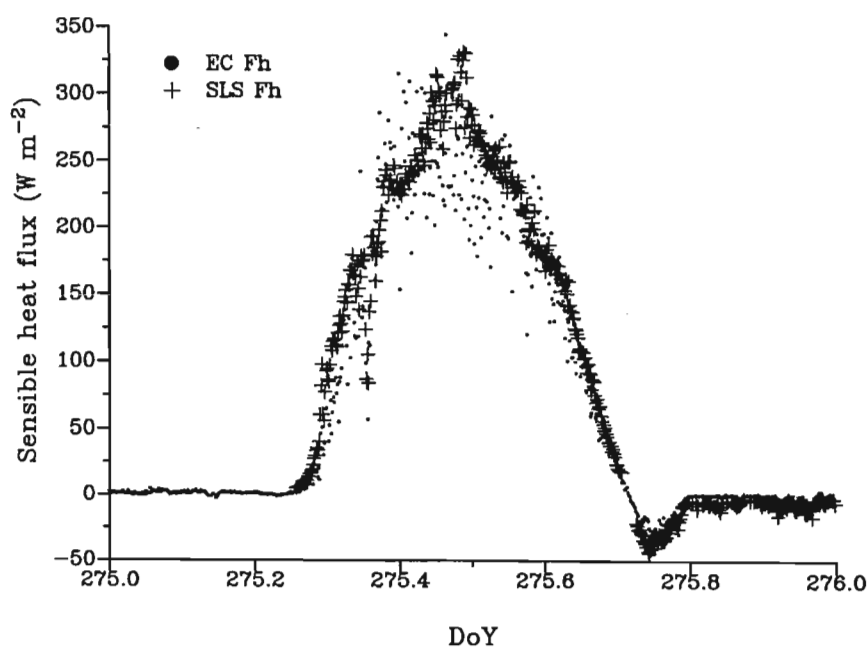
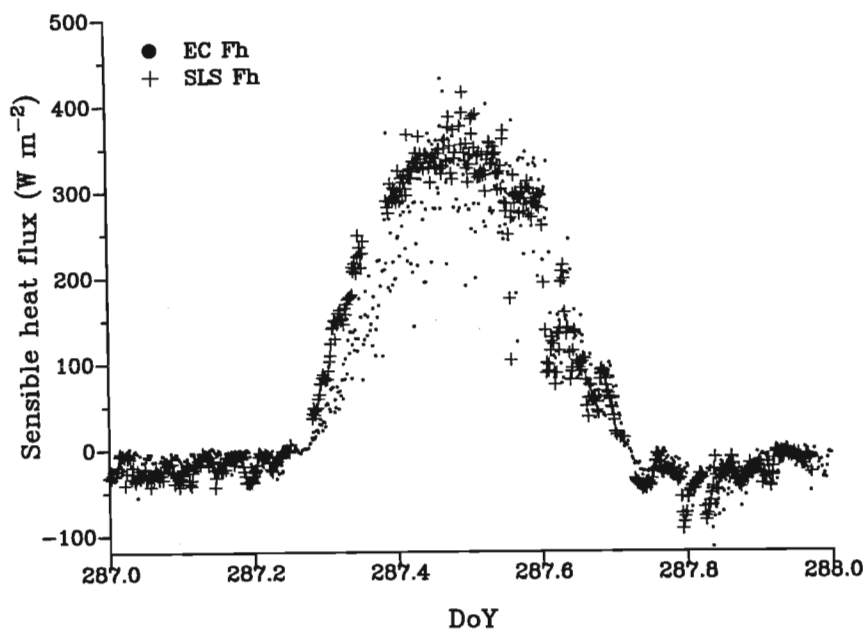


Fig. 5.13 Diurnal plot of 2-min SLS- and EC-measured sensible heat flux for DoY 275 for which wind direction is nearly perpendicular to the SLS beam path.

(a)



(b)

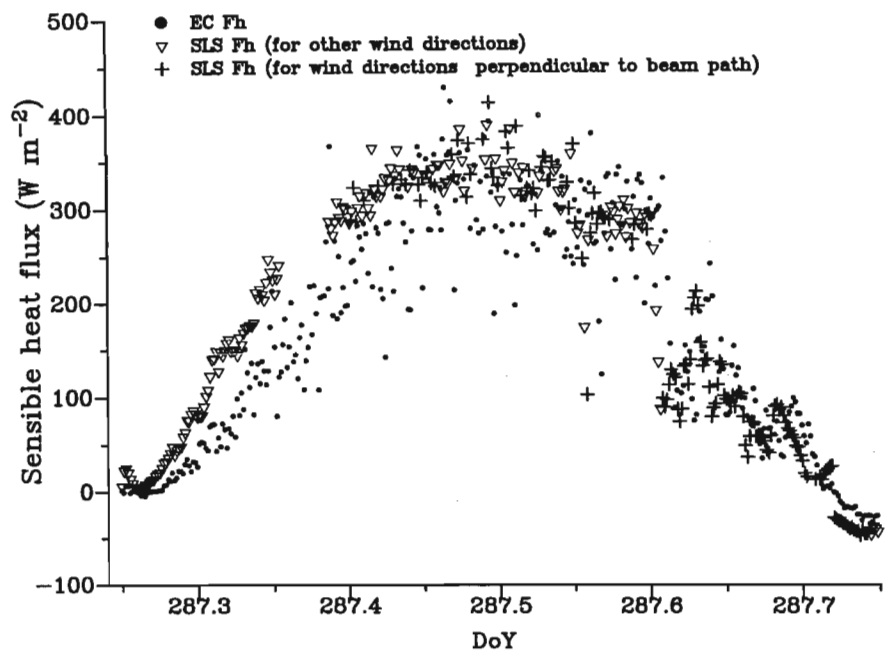


Fig. 5.14 (a) Diurnal variation of 2-min sensible heat flux measured by EC and SLS methods for DoY 287, (b) SLS sensible heat flux for the different prevailing wind directions – for wind directions nearly perpendicular to the SLS beam path or random wind directions, also for DoY 287.

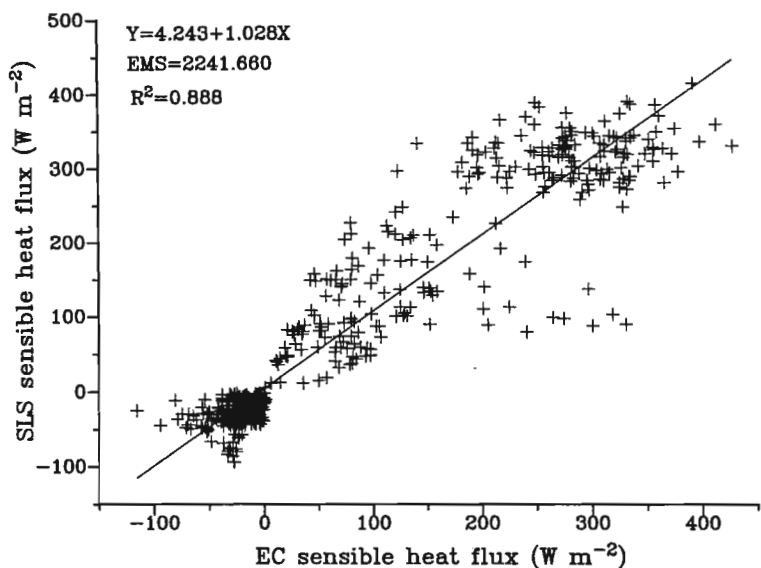


Fig. 5.15 Comparison of 2-min sensible heat flux measured by EC and SLS methods for DoY 287 for which the wind direction is random in the morning and nearly perpendicular to the SLS beam path in the afternoon.

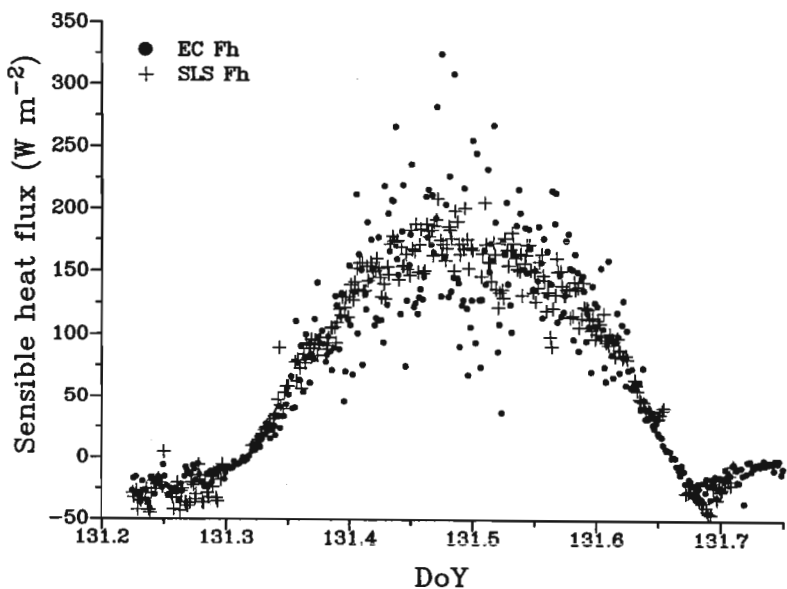


Fig. 5.16 Diurnal plot of 2-min SLS- and EC-measured sensible heat flux for DoY 131 for which wind direction was nearly perpendicular to the SLS beam path but the wind speed low.

Wind speed appears to influence the F_h measurements by the EC and SLS methods. The influence of wind speed is noticeable, for example, on DoY 107 (Fig. 5.18) ($t = 95.49$) when even though the wind direction appears random, the agreement between the EC and SLS measurements of F_h is better compared to the agreement for DoY 131 ($t = 74.02$) (Fig. 5.17) when wind is more or less perpendicular to the beam path.

One of the days (DoY = 107) for which the wind direction was random is shown (Fig. 5.11). The statistical analysis of the F_h estimates by EC and SLS results in a t -value of 95.49 and a slope of 0.992 (Table 5.1 and Fig. 5.18), which is less than for days when the wind direction is nearly perpendicular to the beam. The diurnal plot of F_h values (Fig. 5.19) for this day (DoY 107) exhibits more scatter for most of the day especially from around 10h00 to 14h00 when the F_h values are large. On this day the atmospheric condition was stable and as is already shown in Chapter 4, the EC- and SLS-measured F_h appear to agree well when the atmospheric condition is unstable and there is more turbulence.

In Fig. 5.10 (DoY 131), the wind direction is similar to that of Fig. 5.8 - nearly perpendicular to the SLS beam path, but the wind speed is less on DoY 131 compared to that for 275 DoY. It can be assumed that the lower wind speeds on DoY 131 resulted in the poorer agreement ($t = 74.02$ with a slope of 0.931, Table 5.1) as shown in Fig. 5.17, since the wind direction is similar for both days. The influence of wind speed is also noticeable on DoY 107 ($t = 95.49$) when even though the wind direction appears random, the agreement between the EC and SLS measurements of F_h is better compared to the relationship on DoY 131 (Figs 5.10 and 5.17) when wind is more or less perpendicular to the beam path. Wind speed plays a role in atmospheric stability and on DoY 131 the atmospheric condition was near-neutral while on DoY 107 the atmospheric condition was unstable.

The findings of this study, however, do not seem to agree with those of Green et al. (1997) who showed that the agreement between the estimates of F_h obtained by EC and SLS methods tend to have improved correspondence when the wind is parallel to the beam path as compared to when the wind is perpendicular to the SLS beam path. Their explanation is that when the wind direction is parallel to the beam path, the scintillometer loses its advantage of larger fetch as a result of the smaller footprint area.

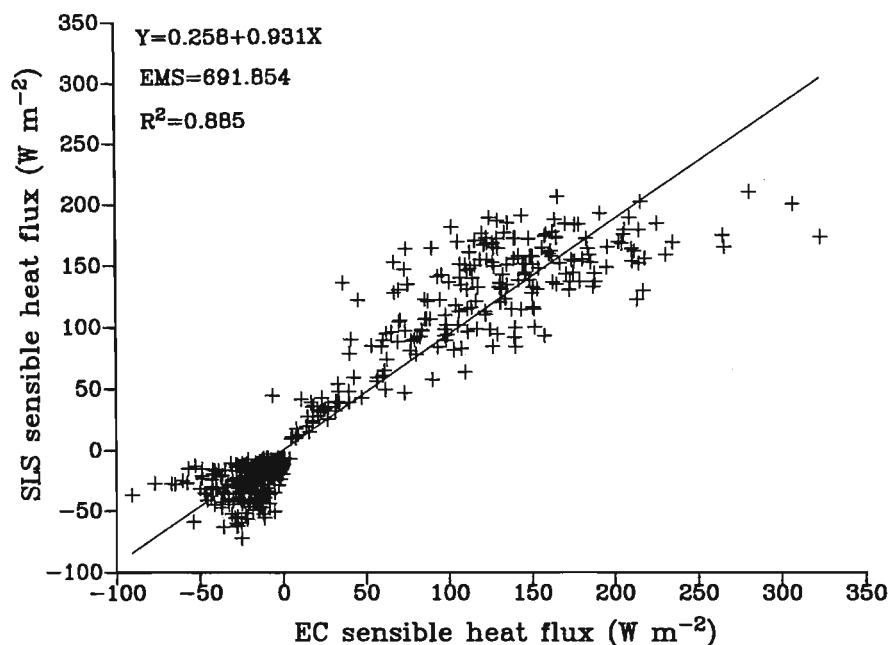


Fig. 5.17 Comparison of 2-min sensible heat flux measured by EC and SLS methods for DoY 131 for wind directions nearly perpendicular to the SLS beam path but with low wind speed.

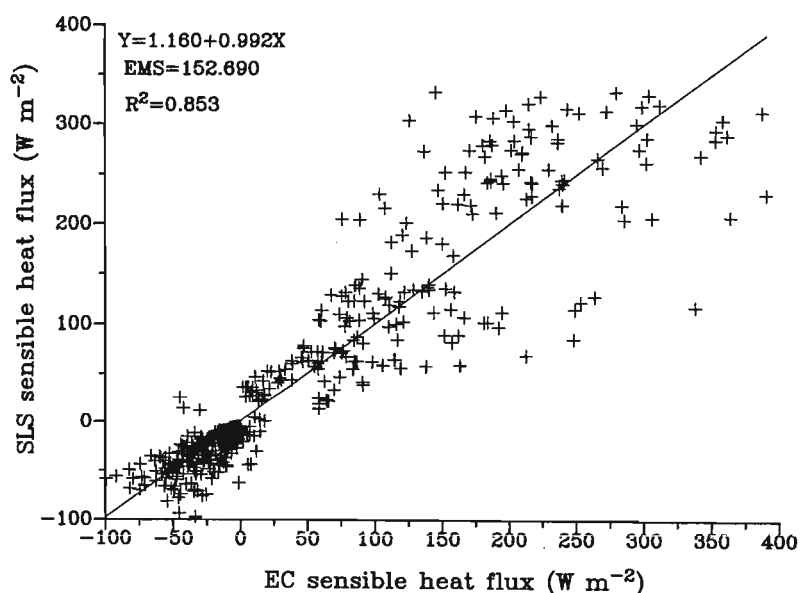


Fig. 5.18 Comparison of 2-min sensible heat flux measured by EC and SLS methods for DoY 107 for random wind directions.

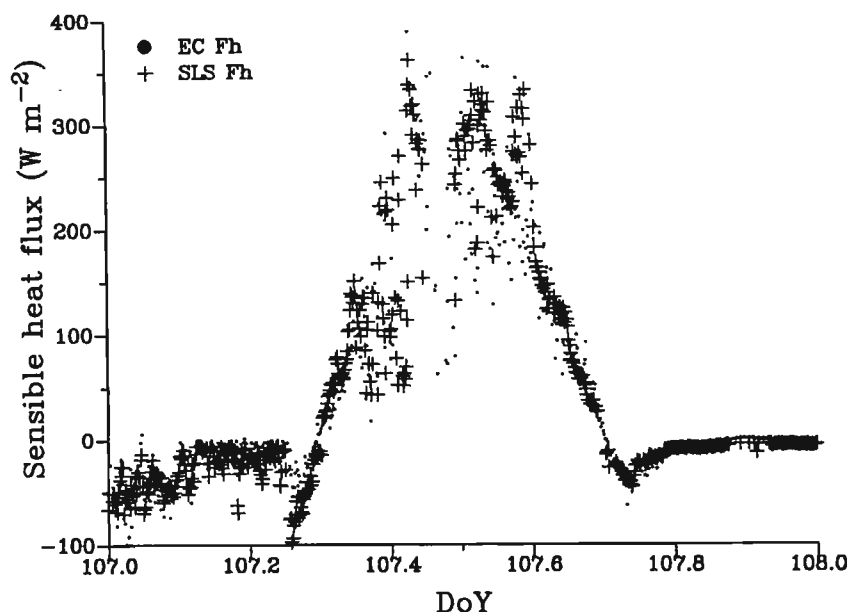


Fig. 5.19 Diurnal plot of 2-min SLS- and EC-measured sensible heat flux for DoY 107 for random wind directions.

5.4.3 Footprint analysis

To aid in the interpretation of the surface area responsible for the flux estimations by the two methods (EC and SLS), a footprint analysis was carried out. The model developed by Hsieh et al. (2000), and corrected and modified by Savage et al. (2004), was used to estimate relative contributions from areas at various upwind distances x . Wang et al. (1978) used a bell-shaped spatial weighting function applied to C_n^2 to account for the fact that scintillations near the centre of the beam contribute more greatly than those nearer the receiver and those nearer the transmitter. Three-dimensional surface colour maps of the footprint function for the surface layer scintillometer beam were created using the Origin (version 7.5) software. The contour was defined as:

$$C(f, x, y) = f(x) \times W(y) \quad 5.9$$

where $f(x)$ is the footprint function as a function of distance x perpendicular to the scintillometer beam and $W(y)$ is the beam path weighting function based as a function of distance along the beam measured from the transmitter. The function $W(y)$ is based on Eq. 2.8.

The footprint function, $f(x)$ (m^{-1}), used was based on the Hsieh et al. (2000) and modified by Savage et al. (2004).

$$f(x) = (2 x_{\max} / x^2) \cdot \exp(-2 x_{\max} / x) \quad 5.10$$

where x_{\max} is the peak of the footprint given by $x_{\max} = \frac{D z_u^P |L|^{1-P}}{2k^2}$ and the beam path weighting function $W(y)$ given approximately by (Meijninger, 2003):

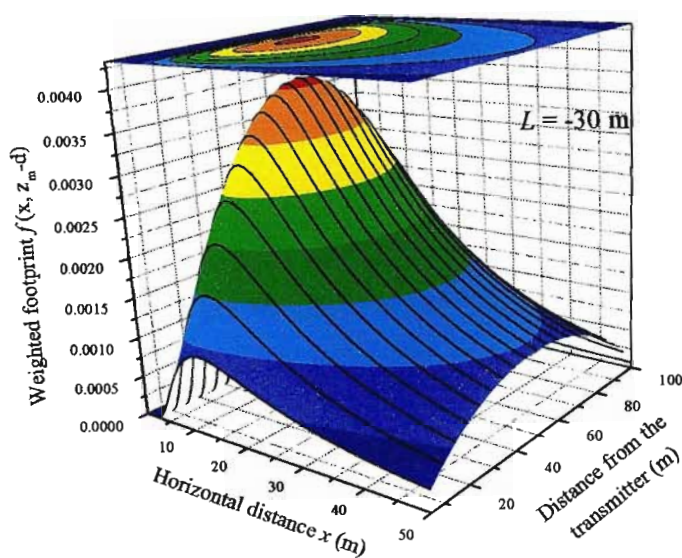
$$W(y) = \left((y / L_{\text{beam}}) \cdot (1 - y / L_{\text{beam}}) \right)^{5/6} \quad 5.11$$

. In Figs 5.20 a and b, the weighted footprint plots for the SLS method against horizontal distance for two different stability conditions are shown. A clear picture that emerges from the plots is that atmospheric stability influences the peak position of footprint with the peak footprint position being further from the measurement position when the atmospheric stability condition is closer to stable as denoted by the Obukhov length of -5 and closer to the measurement position for convectively unstable atmospheric conditions as shown by the Obukhov length of -30. Figures 5.20 a and b, show that a larger fetch is required when the atmosphere is convectively unstable as indicated by the contours plotted on top of the footprint plots.

These findings agree well with those of Kljun et al. (2004) who also show that the footprint peak location (x_{\max}) varies with atmospheric stability conditions, with the location being further from the measurement point when the atmospheric stability condition is neutral and nearer the measurement position when the atmospheric condition is strongly convective. This therefore means that when the atmosphere is stable, the source area associated with the SLS method is greater than when the atmospheric stability condition is convectively unstable. This may influence how well the measurements obtained by the two methods (EC and SLS) agree.

In Figs 5.21 to 5.23 the different locations for the peak of footprint as well as the footprint magnitude estimated by the footprint plots for EC and SLS are shown, with Figs 5.21 and 5.22 showing the footprint plots for DoY 131 and 107 when the agreement in sensible heat flux measurements by the two methods seem to deviate more than for DoY 275 for which the measurements by the two methods appear to be very good ($R^2 = 0.945$, and slope = 1.046, cf. Table 5.1 and Fig. 5.12). The footprint magnitude for SLS measurement is also larger than for the EC. For these two days (DoY 107 and 131) therefore, the two methods appears to have differing associated sensible heat flux source areas.

(a)



(b)

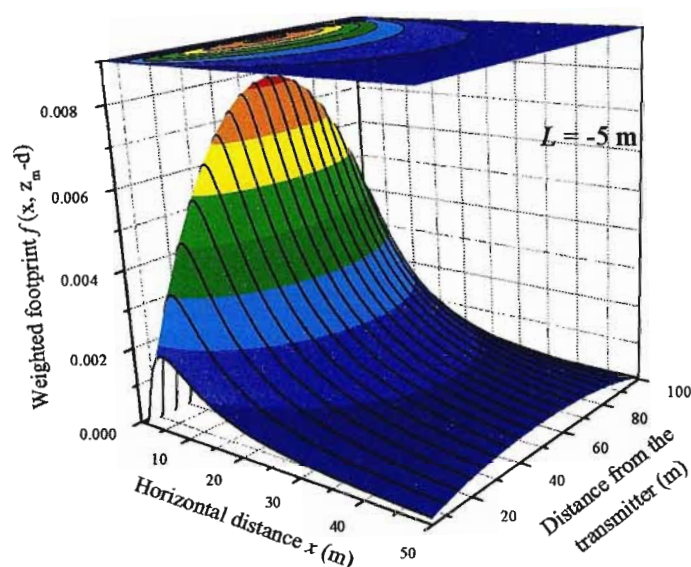


Fig. 5.20 Depiction of the SLS beam-weighted footprint function for (a) Obukhov length (L) of -30 m and (b) Obukhov length of -5 m. Also shown is the contour for a view of the footprint function, in the horizontal plane, at the top of the footprint plot.

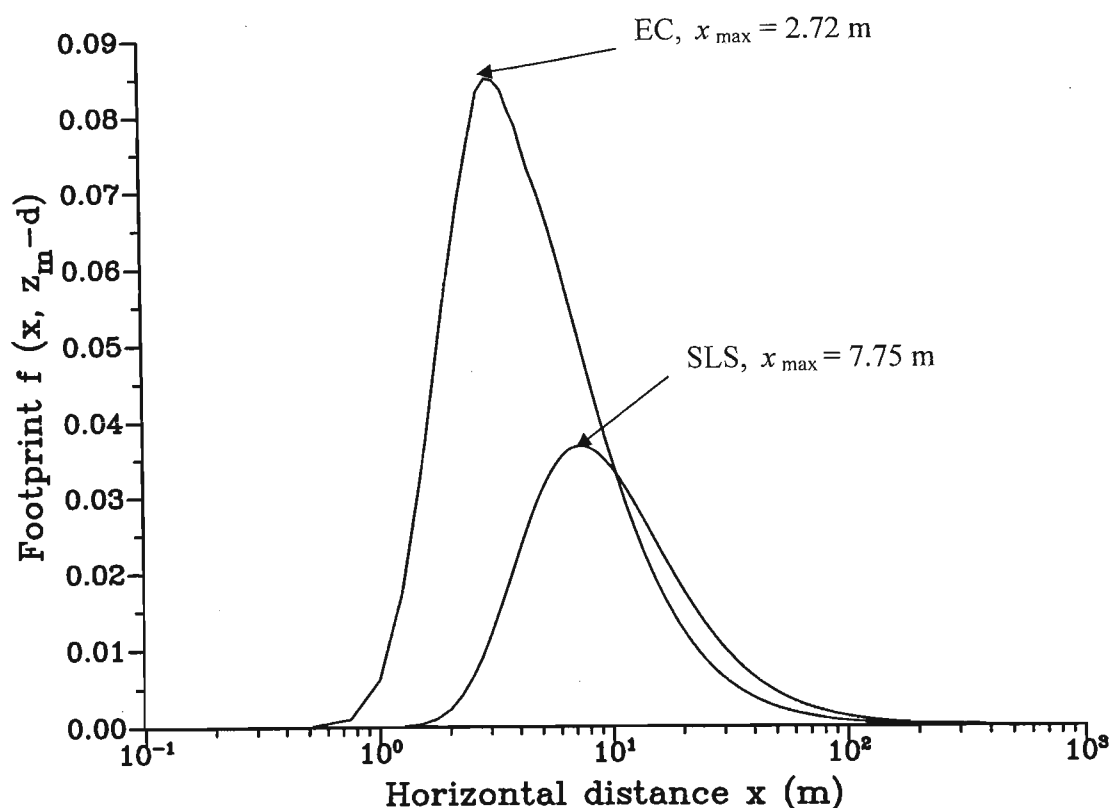


Fig. 5.21 Daytime footprint peak location estimated by the calculations for EC and SLS mid-point position for DoY 131, 11h00. On this day wind direction was nearly perpendicular to the SLS beam path and wind speed low.

For DoY 275, the peak location of the footprint for the two methods appear closer, with EC footprint peak being 4.64 m and that of SLS 6.74 m. As noted earlier, the wind direction on this day (DoY 275) was predominantly perpendicular to the SLS beam path compared to DoY 107 when the prevailing wind direction was more random. Wind direction and atmospheric stability condition seem to have a similar effect on the agreement between the sensible heat flux measurements by the EC and SLS methods. On DoY 131, wind speed was lower as is indicated by the short length of the wind direction and wind velocity plots in Fig. 5.14. The footprint plot for DoY 131 (Fig. 5.21) indicates that the source area and peak location of the two methods are different confirming further the effect of wind speed on the measurements from both EC and SLS methods.

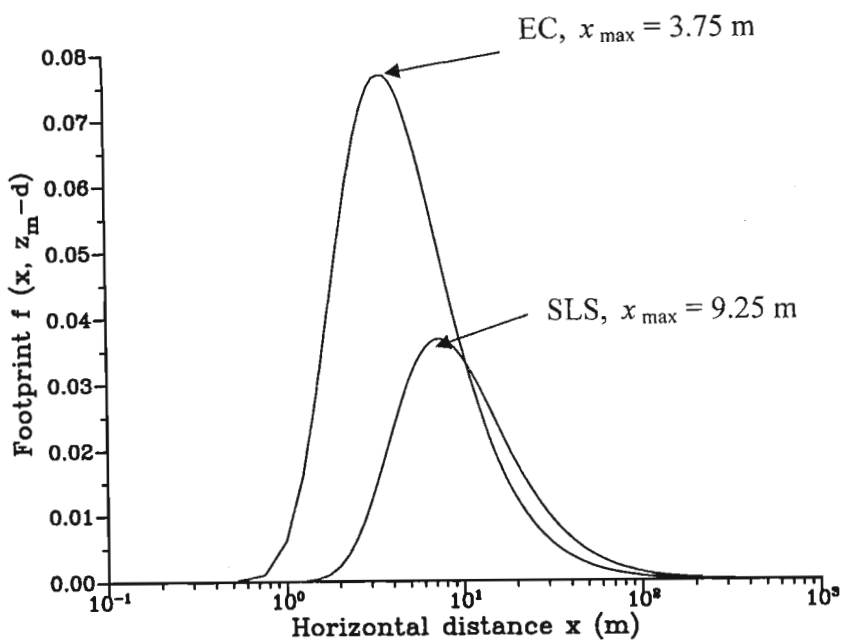


Fig. 5.22 Daytime footprint peak location estimated by the calculations for EC and SLS mid-point beam position for DoY 107, 12h00. On this day the wind direction was random.

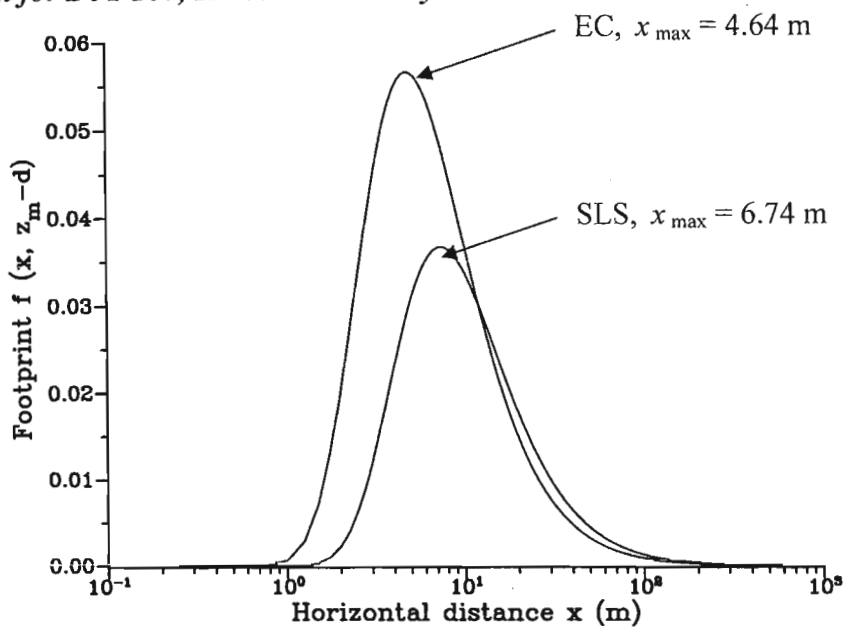


Fig. 5.23 Daytime footprint peak location estimated by the calculations for EC and SLS mid-point beam position for DoY 275, 12h00. For this day the wind speed was nearly perpendicular.

5.5 Conclusions

Measurements of sensible heat flux (F_h) by EC and SLS methods over a mixed grassland experimental site were compared for (i) periods when the SLS beam was set up in a slanting position with the transmitter set at a height of 1.68 m above the ground level while the receiver was at 0.68 m; and (ii) for wind directions approximately perpendicular to the SLS beam path and wind directions either random or approximately parallel to the beam path. There was generally good agreement in the measurements of F_h by the EC at a height of 2 m and SLS measurement methods with the SLS set up in an inclined position with the 30-min data resulting in better agreements.

The findings confirm that the SLS height and slope does not impair its performance in measuring sensible heat flux. This also shows that the SLS method would also work well in non-ideal (heterogeneous) conditions which the inclined optical beam path mimics. In most cases, real field measurements take place under such conditions and hence the importance of testing the SLS for such.

For those days with wind directions approximately perpendicular to the beam, the F_h agreement between the EC and SLS methods was better compared to random wind directions or directions approximately parallel to the SLS beam path. Wind speed also seems to influence the F_h estimates by the two methods since the agreement in the F_h values obtained by the two methods is greater when wind speed is higher compared to times of the day when the wind speed is lower.

The atmospheric stability influences the peak position of footprint. The peak footprint position being further from the measurement position when the atmospheric stability condition is closer to stable as denoted by the Obukhov length of -5 and closer to the measurement point for convectively unstable atmospheric conditions as indicated by the Obukhov length of -30. A larger fetch was also shown to be required when the atmosphere is convectively unstable as indicated by the contours plotted on top of the footprint plots. The footprint for the two methods (EC and SLS) differ more when the wind direction is random compared to when the wind direction is mainly perpendicular to the beam and this may be part of the reason why the sensible heat flux comparisons between the two methods improved for wind directions mainly perpendicular to the SLS beam path than for directions more random or parallel to the beam.

In general, there seems to be very good agreement in the sensible heat flux values obtained by the two methods. Since SLS offers areal-averaged sensible heat flux measurements compared to the EC method which is basically a point measurement method, the correspondence between the sensible heat flux obtained by the two methods is considered very good. The SLS method therefore offers a better alternative for obtaining sensible heat flux from larger and heterogeneous area - although to a limit of 250 m since beyond 250 m, the method suffers from a saturation problem.

Chapter 6: General conclusions and recommendations for further research

6.1 Conclusions

The main aim of this research was to estimate areally-averaged sensible heat flux (F_h) for a mixed grassland community using a surface layer scintillometer with its dual-beam (SLS) and to compare it with the sensible heat flux estimates obtained using the eddy covariance (EC) method. Unlike the SLS method, the EC method does not rely on MOST and its sensible heat estimates do not involve the measurement height or the zero-plane displacement height.

Specifically, the study was designed with the following objectives: to investigate the performance of the SLS for different Bowen ratio values and hence determine the reliability of the SLS method for various atmospheric humidity conditions; to compare the sensible heat flux values obtained by EC and SLS methods for different atmospheric stability conditions and seasons; and finally, to compare the agreement between the sensible heat flux values obtained by the EC and SLS methods for different scintillometer beam heights and orientation and hence verify the reliability of the SLS measurements of sensible heat flux for non-ideal conditions, and also for cases when the prevailing wind direction is approximately parallel, or perpendicular to the beam path.

To meet the first objective, a comparison of the SLS-corrected for the Bowen ratio (β) and SLS-measured C_T^2 (calculated from C_n^2) was carried out, with the results showing very good agreement between the two, indicating that not correcting SLS-measured C_T^2 does not result in statistically significant variations in the resulting C_T^2 values, and hence sensible heat flux. The F_h measurements obtained by the SLS method compared to those obtained by the EC method for different β values show no significant differences. From these findings it can therefore be concluded that the SLS-measured F_h values require no correction (or that both require correction) for β and the SLS method allows for long-term and continuous sensible heat flux measurements since the F_h measurements obtained compare very well with the ones by the EC method which is considered the standard method for surface flux measurements. A sensitivity

analysis of the influence of β on F_h measurements by the SLS method further confirms that there is less influence of β on F_h measurements especially for β values less than 1.0.

The SLS method depends on MOST which in turn depends on the use of semi-empirical similarity functions for estimating the sensible heat flux. A comparison of the various methods for computing the MOST semi-empirical similarity functions was also carried out. The results show a difference in the F_h computed following the various methods suggested by various researchers. The MOST formulation used by Theirman (1992) resulted in better agreement with EC estimates of sensible heat flux. The method used in computing the similarity function should therefore be carefully considered since the different methods lead to differences in the F_h obtained.

To meet the second objective, the SLS-measured sensible heat flux was compared with that from the EC method under various atmospheric stability conditions. There was generally good agreement between the F_h values obtained by the two methods although SLS-measured F_h showed less scatter, especially around midday when the recorded values are greater than the corresponding EC measurements, which appears more scattered around the same time.

Comparisons of the F_h values for different atmospheric stability conditions show that the values are in close agreement when the atmospheric condition is unstable although there is generally good agreement even for the near-neutral atmospheric stability condition.

Better correspondence in F_h measurements by the EC and SLS methods are noticed for the months of June to August whereas in the warmer months of October, November and December, lower agreement in the F_h measured by the two methods was noted most likely due to the stable atmospheric conditions during these periods. The correspondence between the F_h measurements by the EC and SLS methods however appears to be mainly influenced by atmospheric stability conditions.

To test the performance of the SLS system for slanting beam angle position as well as the agreement of the F_h values obtained by the two methods for different wind directions, especially when the wind direction is approximately parallel or perpendicular to the SLS beam path, the scintillometer transmitter and receiver were set up at different heights, with the transmitter at 1.68 m above the ground level while the receiver was set up at 0.68 m above the ground level. This

was done so that the scintillometer measurements of F_h would mimic that of heterogeneous terrain.

The results show that there is generally good agreement in the measurements of F_h by the two methods with the SLS set up in an inclined position with the 30-min data resulting in a better agreement. The findings confirm that the SLS beam orientation does not significantly impair its performance in measuring sensible heat flux. This also shows that the SLS method would work well for heterogeneous terrain conditions which the inclined optical beam path mimics. In most cases, field measurements take place under such conditions and hence the importance of testing the SLS for such.

The atmospheric stability also influences the peak position of footprint with the peak footprint position being further from the measurement point when the atmospheric stability condition is closer to stable as denoted by the Obukhov length of -5 m and closer to the measurement point for convectively unstable atmospheric conditions as shown by the Obukhov length of -30 m.

It was also shown that a larger fetch is required when the atmosphere is convectively unstable as indicated by the contours plotted on top of the footprint plots. The footprint for the two methods (EC and SLS) differ more when the wind direction is random compared to when the wind direction is approximately perpendicular and this may be part of the reason why the sensible heat flux measured by the two methods are more in agreement when wind direction is approximately perpendicular to the SLS beam path than when the direction is more random. The position of the footprint peak may also explain the closer agreement between the two methods (EC and SLS) when the atmospheric condition is unstable since the footprint peak associated with measurements from the two methods are closer when the atmospheric condition is unstable, with the SLS appearing to lose the spatial averaging ability.

In general, there seems to be very good agreement in the sensible heat flux values obtained by the two methods and since the SLS method offers areal-averaged sensible heat flux measurements compared to the EC method which is basically a point measurement method, the SLS method can therefore be considered a better alternative for obtaining sensible heat flux values for a large area - although to a limit of 250 m since beyond that the small aperture scintillometer suffers from the problem of saturation. Scintillometer measurements would also be

more useful than those obtained by EC or other point methods over inhomogeneous terrain as a result of the larger scintillometer source area.

The study has therefore confirmed that the long-term measurements of F_h obtained by the SLS method are reliable since they compare well with those using the EC method which is generally accepted as a standard method for F_h determination. The SLS method however has an advantage of a wider source area and spatial averaging of F_h measurements among others as already mentioned in Chapter 2.

6.2 Recommendations for future research

Studies involving the approximation and measurements of energy flux such as sensible heat and latent energy flux (evapotranspiration) - which is the main process through which water is lost from many land surfaces - are needed in order for more efficient use of water resources and management. Such studies need to cover larger areas e.g. at the scale of whole regions or watersheds. Hence, a combination of scintillometer-derived sensible heat flux with those obtained from satellite remote sensing would be very useful in gaining more understanding of water loss processes from such large areas since satellite images cover wide and even more heterogeneous areas. The scintillometer-derived F_h would therefore be useful in ground truthing and calibrating satellite estimates, and hence information about water lost through evapotranspiration from larger areas which would otherwise be impractical to cover using any point-measurement method would be obtained. Further studies should therefore focus on the combined use of scintillometry and satellite remote sensing to give more insight in water loss processes from watersheds and regions as management of water resources is usually done at such large scales.

Further studies should also be carried out to further test the performance of the SLS under different atmospheric stability conditions since in the current study no conclusive evidence was obtained in this regard due to the problem of a limited data set in some cases as a result of problem with calculations involving friction velocity from the EC datasets. In this study, the performance of the SLS was tested for slanting beam angle to check if the performance of SLS would be impaired by the surface heterogeneity, in terms of terrain profile. It would also be necessary to test the performance of the scintillometer for different surfaces for instance over forests, different agricultural land uses etc. to see how the sensible heat flux measured by SLS

compare with those measured by the EC method under these different surfaces with different surface roughness.

References

- Anandakumar, K. 1999. Sensible heat flux over a wheat canopy: Optical scintillometer measurements and surface renewal analysis estimations. *Agricultural and Forest Meteorology* 96, 145-156.
- Andreas, E. L. 1989. Two-wavelength method of measuring path-averaged turbulent surface heat fluxes. *Journal of Atmospheric and Oceanic Technology* 6, 280-292.
- Andreas, E. L. 1990. Selected papers on turbulence in a refractive medium. SPIE Milestone Series, 25, International Society for Optical Engineering. Bellingham, Washington, USA.
- Andreas, E. L. 2000. Obtaining surface momentum and sensible heat fluxes from crosswind scintillometer. *Journal of Atmospheric and Oceanic Technology* 17, 3-16.
- Arya, S. P. 2001. Introduction to Micrometeorology. Academic Press. London, UK, 420 pp.
- Ashktorab, H., Pruitt, W. O., Paw U, K. T. and George, W. V. 1989. Energy balance determinations close to the soil surface using a micro-Bowen ratio system. *Agricultural and Forest Meteorology* 46, 259-274.
- Baldocchi, D. 2005. Lecture 17, Wind and turbulence, Part 1, Surface boundary layer: theory and principles. Ecosystem Science Division, Department of Environmental Science, Policy and Management. University of California. Berkeley, California, USA.
- Baldocchi, D. D. 1997. Measuring and modelling carbon dioxide and water vapour exchange over a temperate broad-leaved forest during the 1995 summer drought. *Plant, Cell and Environment* 20, 1108-1122.
- Baldocchi, D. D., Falge, E., Gu, L., Olson, R., Hollinger, D., Running, S., Anthoni, P., Bernhofer, C., Davis, K., Evans, R., Fuentes, J., Goldstein, A., Katul, G., Law, B., Lee, X., Malhi, Y., Meyers, T., Munger, W., Oechel, W., Paw U, K. T., Pilegaard, K., Schmid, H. P., Valentini, R., Verma, S., Vesala, T., Wilson, K. and Wolsy, S. 2001. FLUXNET: a new tool to study the temporal and spatial variability of ecosystem scale carbon dioxide, water vapour and energy flux densities. *Bulletin of American Geological Society* 82, 2415-2434.
- Bastiaanssen, W. G. M. 2000. SEBAL-based sensible and latent heat flux measurements in the irrigated Gediz Basin, Turkey. *Journal of Hydrology* 229, 87-100.
- Bausch, W. C. and Bernard, T. M. 1992. Spatial averaging Bowen ratio system: description and lysimeter comparison. *Transactions of the American Society of Agricultural Engineers* 35, 121-129.

- Beljaars, A. C. M. 1982. The derivation of fluxes from profiles in perturbed areas. *Boundary-Layer Meteorology* 24, 35-55.
- Beringer, J., Hurtley, L. B., Tapper, N. J., Coutts, A., Kerley, A. and Grady, P. O. 2003. Fire impacts on surface heat, moisture and carbon fluxes from a tropical savanna in northern Australia. *International Journal of Wildland Fire* 12, 333-340.
- Black, T. 1979. Evapotranspiration from Douglas fir stands exposed to soil water deficits. *Water Resources Research* 15, 164-170.
- Blad, B. L. and Rosenberg, N. J. 1974. Lysimetric calibration of the Bowen ratio-energy balance method for evapotranspiration estimation in the central Great Plains. *Journal of Applied Meteorology* 13, 227-236.
- Bland, W. L., Loew, J. T. and Norman, J. M. 1996. Evaporation from cranberry. *Agricultural and Forest Meteorology* 81, 1-12.
- Böckem, B., Flach, P. Weiss, A. and Hennes, M. 2000. Refraction influence analysis and investigations on automated elimination of refraction effects on geodetic measurements. Paper presented to 16th IMEKO World Congress. Vienna, Austria.
- Bowen, I. S. 1926. The ratio of heat losses by conduction and by evaporation from any water surface. *Physical Review* 27, 779-787.
- Brutsaert, W. H. 1982. *Evaporation into the Atmosphere: Theory, History and Applications*. Reidel, Dordrecht, Holland, 299 pp.
- Cain, J. D., Rosier, P. T. W., Meijninger, W. M. L. and de Bruin, H. A. R. 2001. Spatially averaged sensible heat fluxes measured over barley. *Agricultural and Forest Meteorology* 107, 307-322.
- Cellier, P. and Brunet, Y. 1992. Flux-gradient relationship above tall plant canopies. *Agricultural and Forest Meteorology* 57, 93-117.
- Cellier, P. and Olioso, A. 1993. A simple system for automated long term Bowen ratio measurements. *Agricultural and Forest Meteorology* 66, 81-92.
- Chehbouni, A., Kerr, Y. H., Watts, C., Hartogensis, O., Goodrich, D., Scott, R., Schieldge, J., Lee K., Shuttleworth, W. J., Dedieu, G. and de Bruin, H. A. R. 1999. Estimation of area-averaged sensible heat flux using large aperture scintillometer during the Semi-Arid Lands-Surface-Atmosphere (SALSA) experiment. *Water Resources Research* 35, 2505-2511.
- Clifford, S. F, Ochs, G. R. and Lawrence, R. 1974. Saturation of optical scintillation by strong turbulence. *Journal of Optical Society of America* 64, 148-154.
- Coyle, M. 2005. The gaseous exchange of ozone at terrestrial surfaces: non-stomatal deposition to grassland. PhD Thesis. University of Edinburgh. Edinburgh, UK, 379 pp.

- Daoo, V. J., Panchal, N. S., Faby, S. and Raj, V. V. 2004. Scintillometric measurements of daytime atmospheric turbulent heat and momentum fluxes and their application to atmospheric stability. *Experimental Thermal and Fluid Science* 28, 337-345.
- de Bruin, H. A. R. and Meijninger, W. M. L., Smedman, A. S. and Magnusson, M. 2002. Displaced-beam small aperture scintillometer test. Part I: the WINTEx data-set. *Boundary-Layer Meteorology* 105, 129-148.
- de Bruin, H. A. R., Kohsiek, W. and van den Hurk, B. J. J. M. 1993. A verification of some methods to determine the flux of momentum, sensible heat and water vapour using standard deviation and structure parameter of scalar meteorological quantities. *Boundary-Layer Meteorology* 63, 231-257.
- de Bruin, H. A. R., Kohsiek, W. and van den Hurk, B. J. J. M. 1993. A verification of some methods to determine the fluxes of momentum, sensible heat and water vapour using standard deviation and structure parameter of scalar meteorological quantities. *Boundary-Layer Meteorology* 63, 231-257.
- de Bruin, H. A. R., van den Hurk B. J. J. M. and Kohsiek W. 1995. The scintillometer method tested over a dry vineyard area. *Boundary-Layer Meteorology* 76, 25-40.
- de Bruin, H. A. R., van den Hurk, B. J. J. M. and Kohsiek, W. 1995. The scintillation method tested over dry vineyard area. *Boundary-Layer Meteorology* 76, 25-40.
- de Wekker, S. F. J. 1996. The estimation of areally-averaged sensible heat fluxes over complex terrain with a large-aperture scintillometer. MSc Thesis. Department of Meteorology, Wageningen University. Wageningen, Netherlands, 172 pp.
- Drexler, J. Z., Snyder, R. L., Spano, D. and Paw U, K. T. 2004. A review of models and micrometeorological methods used to estimate wetland evapotranspiration. *Hydrological Processes* 18, 2071-2101.
- Dugas, W. A., Fritschen, L. J., Gay, L. W., Held, A. A., Mathias, A. D., Reicosky, D. C., Steduto P. and Steiner J. L. 1991. Bowen ratio, eddy correlation, and portable chamber measurements of sensible and latent heat flux over irrigated spring wheat. *Agricultural and Forest Meteorology* 56, 1-20.
- Farahani, H. J. and Bausch, W. C. 1995. Performance of evapotranspiration models for maize - bare soil to closed canopy. *Transactions of the American Society of Agricultural Engineers* 38, 1049-1059.
- Finnigan, J. J., Clement, R., Malhi, Y., Leuning, R. and Cleugh, H. A. 2003. A re-evaluation of long-term flux measurement techniques - Part I: Averaging and coordinate rotation. *Boundary-Layer Meteorology* 107, 1-48.
- Foken, T. 2006. 50 years of the Monin-Obukhov Similarity Theory. *Boundary-Layer Meteorology* 119, 431-447.

- Fritschen, L. J. 1966. Evapotranspiration rates of field crops determined by the Bowen ratio method. *Agronomy Journal* 58, 339-342.
- Fritschen, L. J. and Simpson, J. R. 1989. Surface energy balance and radiation systems: general description and improvements. *Journal of Applied Meteorology* 28, 680-689.
- Fuchs, M. and Tanner, C. B. 1970. Error analysis of Bowen ratios measured by differential psychrometry. *Agricultural and Forest Meteorology* 7, 329-334.
- Garratt, J. R. 1992. The Atmospheric Boundary Layer. Cambridge University Press. Cambridge, UK, 334 pp.
- Gash, J. H. C. 1986. A note on estimating the effect of limited fetch on micrometeorological evaporation measurements. *Boundary-Layer Meteorology* 35, 409-413.
- Gash, J. H. C. and Stewart, J. B. 1977. The evaporation from Thetford Forest during 1975. *Journal of Hydrology* 35, 385-396.
- Göckede, M. 2004. Adoption of footprint methods for the quality control of eddy-covariance measurements. PhD Thesis. University of Bayreuth. Bayreuth, Germany.
- Göckede, M., Mauder, M., Markkanen, T., Arnold, K., Jens-Peter, L. and Foken, T. 2005. Approaches to validate footprint models using natural tracer measurements from a field experiment. *Agricultural and Forest Meteorology* 135, 314-325.
- Grant, D. A. and Meinzer, F. C. 1991. Regulation of transpiration in field-grown sugarcane: evaluation of the stomatal response to humidity with the Bowen ratio technique. *Agricultural and Forest Meteorology* 53, 169-183.
- Grant, D. R. 1975. Comparison of evaporation measurements using different methods. *Quarterly Journal of the Royal Meteorological Society* 101, 543-550.
- Green, A. E. 2001. The practical application of scintillometers in determining the surface fluxes of heat, moisture and momentum. PhD Thesis. Wageningen University. Wageningen, Netherlands, 175 pp.
- Green, A. E., Astill, M. S., McAneney, K. J. and Nieveen, J. P. 2001. Path-averaged fluxes determined from infrared and microwave scintillometers. *Agricultural and Forest Meteorology* 109, 233-247.
- Green, A. E., McAneney, K. J. and Astill, M. S. 1994. Surface-layer scintillation measurements of daytime sensible and momentum fluxes. *Boundary-Layer Meteorology* 68, 357-373.
- Green, A. E., McAneney, K. J. and Lagouarde, J. P. 1997. Sensible heat and momentum flux measurement with an optical inner scale meter. *Agricultural and Forest Meteorology* 85, 259-297.

-
- Ham, J. M. and Heilman, J. C. 2003. Experimental test of density and energy-balance corrections on carbon dioxide flux as measured using open-path eddy covariance. *Agronomy Journal*, 195, 1393-1403.
- Hartogensis, O. K., de Bruin, H. A. R. and van de Weil, J. H. 2002. Displacement-beam small aperture scintillometer test. Part II: CASES-99 Stable boundary-layer experiment. *Boundary-Layer Meteorology* 105, 149-176.
- Heilman, J. L., Brittin, C. L. and Neal, C. M. U. 1989. Fetch requirements for Bowen ratio measurements of latent and sensible heat fluxes. *Agricultural and Forest Meteorology* 44, 261-273.
- Hemakumara, H. M., Chandrapala, L. and Moene, A. F. 2003. Evaporation fluxes over mixed vegetation areas measured from large aperture scintillometer. *Agricultural Water Management* 58, 109-122.
- Hill, R. J. 1992. Review of optical scintillation methods of measuring the refractive index spectrum, inner scale and surface fluxes. *Waves in Random Media* 2, 179-201.
- Hill, R. J. 1997. Algorithm for obtaining atmospheric surface-layer fluxes from scintillation measurements. *Journal of Atmospheric and Oceanic Technology* 14, 456-465.
- Hill, R. J. and Clifford, S. F. 1978. Modified spectrum of atmospheric temperature fluctuations and its application to optical propagation. *Journal of Optical Society of America* 68, 330-342.
- Hill, R. J. and Lataitis, R. J. 1989. Effect of refractive dispersion on the bichromatic correlation of irradiances for atmospheric scintillation. *Applied Optics* 28, 4121-4125.
- Hill, R. J., Ochs, J. R. and Wilson, J. J. 1992. Measuring surface layer fluxes of heat and momentum using optical scintillation. *Boundary-Layer Meteorology* 58, 391-408.
- Højstrup, J. 1981. A simple model for the adjustment of velocity spectra in unstable conditions downstream of an abrupt change in roughness and heat flux. *Boundary-Layer Meteorology* 21, 341-356.
- Horst, T. W. and Weil, J. C. 1991. Footprint estimation for scalar flux measurements in the atmospheric surface layer. *Boundary-Layer Meteorology* 59, 279-296.
- Hsieh, C., Katul, G. and Chi, T. 2000. An approximate analytical model for footprint estimation of scalar fluxes in thermally stratified atmospheric flows. *Advances in Water Resources* 23, 765-772.
- Jenkins, F. and White, H. 1976. Fundamentals of Optics. McGraw-Hill. New York, USA, 637 pp.
- Kaimal, J. C. and Finnigan, J. J. 1994. Atmospheric Boundary Layer Flows. Oxford University Press. New York, USA, 289 pp.

- Kaimal, J. C., Wyngard, J. C., Izumi, Y. and Cote, O. R. 1972. Spectral characteristics of surface-layer turbulence. *Quarterly Journal of the Royal Meteorological Society* 98, 563-589.
- Kanda, M., Moriwaki, R., Roth, M. and Oke, T. R. 2002. Area-averaged sensible heat flux and a new method to determine zero-plane displacement length over an urban surface using scintillometry. *Boundary-Layer Meteorology* 105, 177-193.
- Kljun, N., Calanca, P., Rotach, M. W. and Schmid, H. P. 2004. A simple parameterisation for flux footprint predictions. *Boundary-Layer Meteorology* 112, 503-523.
- Kohsiek, W. 1985. A comparison between line-averaged observation of C_n^2 from scintillation of a CO₂ laser beam and time averaged in situ observations. *Journal of Climate and Applied Meteorology* 24, 102-109.
- Kolmogorov, A. N. 1941. The local structure of turbulence in compressible turbulence for very large Reynolds Numbers. *C. R. Akad. Nauk. SSSR* 30, 301-305.
- Lagouarde, J. P., Chehbouni, A., Bonnefond, J. M., Rodriguez, J. C., Kerr, Y. H., Watts, C. and Irvine, M. 2000. Analysis of the limits of the C_T^2 -profile method for sensible heat flux measurements in unstable conditions. *Agricultural and Forest Meteorology* 105, 195-214.
- Leclerc, M. Y. and Thurtell, G. W. 1989. Footprint prediction of scalar fluxes using a Markovian analysis. *Boundary-Layer Meteorology* 52, 247-258.
- Leclerc, M. Y., Karipot, A., Prabha, T., Allwine, G., Lamb, B. and Gholz, H. L. 2003. Impact of non-local advection on flux footprints over a tall forest canopy: a tracer flux experiment. *Agricultural and Forest Meteorology* 115, 19-30.
- Lumley, J. L. and Panofsky, H. A. 1964. The Structure of Atmospheric Turbulence. Interscience Publishers. New York, USA, 239 pp.
- Mahrt, L. 2000 Surface heterogeneity and vertical structure of the boundary layer. *Boundary-Layer Meteorology* 96, 33-62.
- Malek, E., Bingham, G. E. and McCurdy, G. D. 1992. Continuous measurement of aerodynamic and alfalfa canopy resistances using the Bowen ratio-energy balance and Penman-Monteith methods. *Boundary-Layer Meteorology* 59, 187-194.
- McAneney, K. J., Green, A. E. and Astill, M. S. 1995. Large-aperture scintillometry: the homogeneous case. *Agricultural and Forest Meteorology* 76, 149-162.
- Meijninger, W. M. L. 2003. Surface fluxes over natural landscapes using scintillometry. PhD Thesis. Wageningen University. Wageningen, Netherlands, 176 pp.

- Meijninger, W. M. L. and de Bruin, H. A. R. 2000. The sensible heat fluxes over irrigated areas in Western Turkey determined with a large aperture scintillometer. *Journal of Hydrology* 229, 42-49.
- Meijninger, W. M. L., Hartogensis, O. K., Kohsiek, W., Hoedjes, J. C. B., Zuurbier, R. M. and de Bruin, H. A. R. 2002. Determination of area-averaged sensible heat fluxes with large aperture scintillometer over a heterogeneous surface-Flevoland field experiment. *Boundary-Layer Meteorology* 101, 37-62.
- Monin, A. S. and Obukhov, A. M. 1954. Basic laws of turbulent mixing in the atmosphere near the ground. *Academia Nauk* 24, 163-187.
- Moriwaki, R., Suzuki, J., Kanda, M., Mikami, M. and Iwakura, S. 1999. Experiments on the measurement of spatially mean heat flux by using scintillometer. *Annual Hydraulic Engineering* 43, 91-96.
- Nakamura, R. and Mahrt, L. 2001. Similarity theory for local and spatially averaged momentum fluxes. *Agricultural and Forest Meteorology* 108, 265-279.
- Nakaya, K., Chieko, S., Takuya K., Hideshi, I. and Shinji, Y. 2006. Application of a displaced-beam small aperture scintillometer to a deciduous forest under unstable atmospheric conditions. *Agricultural and Forest Meteorology* 136, 45-55.
- National Amendment Water Act 1998 (Chapter 36). Department of Water Affairs and Forestry, Ministry of Environmental Affairs and Tourism. Pretoria, Republic of South Africa.
- Nivolianitou, Z. S., Barbara, M. S. and Aneziris, O. N. 2004. Important meteorological data for use in risk assessment. *Journal of Loss Prevention in the Process Industries* 17, 419-429.
- OriginLab. 2000. Origin Software, Version 6.1. OriginLab Corporation. Nothampton. Massachusetts, USA.
- Panosfsky, H. A. and Dutton, I. A. 1984. Atmospheric Turbulence, Models and Methods for Engineering Applications. John Wiley & Sons. New York, USA, 397 pp.
- Pasquill, F. 1972. Some aspects of boundary layer description. *Quarterly Journal of the Royal Meterological Society* 98, 469-494.
- Paw U, K. T., Qui, J., Su, H. B., Watanabe, T. and Brunet, Y. 1995. Surface renewal analysis: a new method to obtain scalar fluxes without velocity data. *Agricultural and Forest Meteorology* 74, 119-137.
- Pielke, R. A., Avissar, R., Raupach, M., Dolman, A. J., Zeng, X. and Denning, A. S. 1998. Interactions between the atmosphere and terrestrial ecosystems: influence on weather and climate. *Global Change Biology* 4, 461-475.

- Poggio, P. L. 1998. Use of scintillation measurements to determine fluxes in complex terrain. PhD Thesis. Swiss Federal Institute of Technology. Zurich, Switzerland, 156 pp.
- Poggio, P. L., Furger, M., Andre, S. H. P., Graber, K. and Andreas, E. L. 2000. Scintillometer wind measurements over complex terrain. *Journal of Atmospheric and Oceanic Technology* 17, 17-26.
- Prueger, J. H. and Kustas, P. W. 2005. Aerodynamic methods for estimating turbulent fluxes. In: Viney, M. K., Baker, J. M. and Hatfield, J. L. (Eds). *Micrometeorology in Agricultural Systems*. American Society of Agronomy. Madison, Wisconsin, USA, pp 407-436.
- Prueger, J. H., Hatfield, J. L., Aase, J. K. and Pikul, J. L. 1997. Bowen-ratio comparisons with lysimetric evapotranspiration. *Agronomy Journal* 89, 730-736.
- Radiff, A. A. 1999. Integrated water resources management (IWRM): an approach to face the challenges of the next century and to avert future crises. *Desalination* 124, 145-153.
- Rosenberg, N. J., Blad, B. L. and Verma, S. B. 1983. *Microclimate: The Biological Environment*. 2nd ed. John Wiley & Sons. New York, USA, 528 pp.
- Salmond, J. A., Roth, M., Oke, T. R., Satyanarayana, A. N. V., Vogt, R. and Christen, A. 2003. Comparison of turbulent fluxes from roof top versus street canyon locations using scintillometers and eddy covariance techniques. Fifth International Conference on Urban Climate. Lodz, Poland.
- Savage, M. J. 2007. Estimation of evaporation using a dual-beam surface layer scintillometer. Paper revision submitted to *Agricultural and Forest Meteorology*.
- Savage, M. J., Everson, C. S. and Metelerkamp, B. R. 1997. Evaporation measurement above vegetated surfaces using micrometeorological techniques. Water Research Commission (WRC) Report No. 349/1/97, ISBN 1-86845-363-4. WRC, Pretoria, Republic of South Africa, 227 pp.
- Savage, M. J., Everson, C. S., Odhiambo, G. O., Mengistu, M. G. and Jarman, C. 2004. Theory and practice of evapotranspiration measurement, with special focus on surface layer scintillometer (SLS) as an operational tool for the estimation of spatially-averaged evaporation. Water Research Commission (WRC) Report No. 1335/1/04. ISBN 1-77005-247-X. WRC, Pretoria, Republic of South Africa, 204 pp.
- Savage, M. J., McInnes, K. J. and Heilman, J. L. 1995. Placement height of eddy correlation sensors above a short grassland surface. *Agricultural and Forest Meteorology* 74, 195-204.
- Savage, M. J., McInnes, K. J. and Heilman, J. L. 1996. The "footprints" of eddy correlation sensible heat flux density, and other micrometeorological measurements. *South African Journal of Science* 92, 137-142.

- Savage, M. J., Odhiambo, G. O., Mengistu, M. G., Everson, C. S. and Jarman, C. 2005. Theory and practice of evapotranspiration measurement, with special focus on surface layer scintillometer as an operational tool for the estimation of spatially-averaged evaporation. 12th South African National Chapter of the International Association for Hydrological Sciences (SANCIAHS) Symposium. Eskom Convention Centre, Midrand, Republic of South Africa, 9 pp.
- Schmid, H. P. 1997. Experimental design for flux measurements: matching scales of observation and fluxes. *Agricultural and Forest Meteorology* 87, 179-200.
- Schmid, H. P. 2002. Footprint modelling for vegetation atmosphere exchange studies: a review and perspective. *Agricultural and Forest Meteorology* 113, 159-183.
- Scintec. 2000. Surface Layer Scintillometer, SLS20/SLS20-A/SLS40/SLS40-A. User's Manual. Scintec Atmosphärenmesstechnik. Tübingen, Germany
- Scintec. 2006. Surface Layer Scintillometer, SLS20/SLS20-A/SLS40/SLS40-A. User's Manual. Scintec Atmosphärenmesstechnik. Tübingen, Germany.
- Sellers, P. J. and Mintz, Y. 1986. A simple biosphere model (SiB) for use within general circulation models. *Journal of Atmospheric Sciences* 43, 505-530.
- Sinclair, T. R., Allen, L. H. and Lemon, E. R. 1975. An analysis of errors in the calculation of energy flux densities above vegetation by a Bowen ratio profile method. *Boundary-Layer Meteorology* 8, 129-139.
- Smarakoon, D., Chen, A. and Mclean, P. 2000. Estimating daytime latent heat flux and evapotranspiration in Jamaica. *Agricultural and Forest Meteorology* 102, 113-124.
- Spittlehouse, D. A. and Black, T. A. 1980. Evaluation of the Bowen ratio/energy balance method for determining forest evapotranspiration. *Atmosphere-Ocean* 18, 99-116.
- Stanhill, G. 1969. A simple instrument for the field measurement of turbulent diffusion flux. *Journal of Applied Meteorology* 8, 509-513.
- Steduto, P. and Hsiao, T. C. 1998. Maize canopies under two soil water regimes I: Diurnal patterns of energy balance, carbon dioxide flux, and canopy conductance. *Agricultural and Forest Meteorology* 89, 169-184.
- Swinbank, W. C. 1951. The measurement of vertical transfer of heat and water vapour by eddies in the lower atmosphere. *Journal of Meteorology* 8, 135-145.
- Tanner, C. B. 1960. Energy balance approach to evapotranspiration from crops. *Soil Science Society of America Proceedings* 24, 1-9.

- Tanner, C. B. and Pelton, W. L. 1960. Potential of evapotranspiration estimates by the approximate energy balance method of Penman. *Journal of Geophysical Resources* 65, 3391-3413.
- Tatarskii, V. I. 1993. Review of scintillation phenomena. In: Tatarskii V. I. , Ishimaru A. and Zavorotny V.U. (Eds), *Wave Propagation in Random Media (Scintillation)*. Co-published by SPIE-International Society for Optical Engineering and Institute of Physics Publishing. Bellingham, Washington, USA.
- Tatarskii, V. I. 1961. *Wave Propagation in a Turbulent Medium*. Dover Publications. New York.
- Tennekes, H. and Lumley, J. L. 1972. *A First Course in Turbulence*. MIT Press. Cambridge, Massachusetts, USA.
- Thiermann, V. 1992. A displaced-beam scintillometer for line-averaged measurements of surface layer turbulence. Tenth Symposium on Turbulence and Diffusion, American Meteorological Society. Portland, Oregon, USA.
- Thiermann, V. and Grassl, H. 1992. The measurement of turbulent surface-layer fluxes by use of bichromatic scintillation. *Boundary-Layer Meteorology* 58, 367-389.
- Thom, A. S. 1975. Momentum, mass and heat exchange in plant communities. In: Monteith, J. L. (Ed.) *Vegetation and the Atmosphere*. Vol. 1. Principles. Academic Press. London, UK, pp 57-109.
- Todd, R. W. 1996. Latent heat fluxes of a soybean field measured and modelled by energy balance combination models. PhD Thesis. University of Nebraska. Lincoln, Nebraska, USA.
- Tunick, A., Rachele, H., Hansen, F. V., Howell, T. A., Steiner, J. L., Schneider, A. D. and Steve, R. 1994. A cooperative radiation and energy balance field study for imagery and electromagnetic propagation. *Bulletin of American Meteorological Society* 75, 421-430.
- Turnipseed, A. A., Anderson, D. E., Blanken, P. D., Baugh, W. M. and Monson, R. K. 2003. Airflows and turbulent flux measurements in mountainous terrain Part 1. Canopy and local effects. *Agricultural and Forest Meteorology* 119, 1-21.
- Twine, T. E., Kustas, W. P., Norman, J. M., Cook, D. R., Houser, P. R., Meyers, T. P., Prueger, J. H. and Starks, P. J. 2000. Correcting eddy covariance flux underestimates over grassland. *Agricultural and Forest Meteorology* 103, 279-300.
- Wang, T., Ochs, G. R. and Clifford S. F. 1978. A saturation-resistant optical scintillometer to measure C_n^2 . *Journal of Optical Society of America* 68, 334-338.
- Watts, C. J., Chehbouni, A., Rodriguez, J. C., Kerr, Y. H., Hartogensis, O. and de Bruin, H. A. R. 2002. Comparison of sensible heat flux estimates using AVHRR with scintillometer

measurements over semi-arid grassland in northwest Mexico. *Agricultural and Forest Meteorology* 105, 81-89.

- Weather SA. 2006. Climate data for Pietermaritzburg. <http://www.weathersa.co.za/Climat/Climstats/PietermaritzburgStats.jsp>. Accessed on 27th February, 2007.
- Weiss, A. 2002. Determination of thermal stratification and turbulence of the atmospheric surface layer over various types of terrain by optical scintillometry. PhD Thesis. Swiss Federal Institute of Technology. Zurich, Switzerland, 152 pp.
- Wesley, M. L. 1976. A comparison of two optical methods for measuring line averages of thermal exchanges above warm water surfaces. *Journal of Applied Meteorology* 15, 1177-1188.
- Wieringa, J. 1993. Representative roughness parameters for homogeneous terrain. *Boundary-Layer Meteorology* 63, 323-363.
- Wilson, K., Goldstein, A., Falge, E., Aubinet, M., Baldocchi, D., Berbigier, P., Bernhofer, C., Ceulemans, R., Dolman, H., Field, C., Grelle, A., Ibrom, A., Law, B. E., Kowalski, A., Meyers, T., Moncrieff, J., Monson, R., Oechel, W., Tenhunen, J., Valentini, R. and Verma, S. 2002. Energy balance closure at FLUXNET sites. *Agricultural and Forest Meteorology* 113, 223-243.
- Wyngaard, J. C. 1973. On surface-layer turbulence. In: Haugen D. A. (Ed.), Workshop on Meteorology. American Meteorological Society. Boston, Massachusetts, USA, pp 101-149.
- Wyngaard, J. C. 1981. The effects of probe-induced flow distortion on atmospheric turbulence measurements. *Journal of Applied Meteorology* 20, 784-794.
- Wyngaard, J. C. and Clifford, S. F. 1978. Estimating momentum, heat and moisture fluxes from structure parameters. *Journal of Atmospheric Sciences* 35, 1204-1211.
- Wyngaard, J. C. and Cote, O. R. 1971. The budget of turbulent kinetic energy and temperature variance in the atmospheric surface layer. *Journal of Atmospheric Science* 28, 190-201.
- Wyngaard, J. C., Izumi, Y. and Collins, S. A. 1971. Behaviour of the refractive index structure parameter near the ground. *Journal of the Optical Society of America* 61, 1646-1650.
- Xiangun, X. 1996. The combined field experiment for determining evapotranspiration in North China plain. In: Camp, C. R., Sadler, E. J. and Yoder, R. E. (Eds), Evapotranspiration and Irrigation Scheduling, Proceedings of the International Conference, American Society of Agricultural Engineers. St. Joseph, Missouri, USA.